POLITECNICO DI MILANO

Scuola di Ingegneria Industriale e dell'Informazione

Corso di Laurea Magistrale in Energy Engineering

POLITECNICO
MILANO 1863

Battery Energy Storage Systems modeling for robust design of micro grids in Developing Countries

Relatore: Prof. Marco Merlo
Co-relatore: Ing. Claudio Brivio

Tesi di Laurea Magistrale di:
Silvia CORIGLIANO Matricola 853023
Alessia CORTAZZI Matricola 858253

Anno Accademico 2016-2017

"You cannot develop people.
You must allow people to develop themselves."

Julius Nyerere

Ringraziamenti

Desideriamo ringraziare sentitamente le numerose persone che ci sono state di grande aiuto nello sviluppo della nostra tesi.

Un profondo e sincero ringraziamento al Professore Marco Merlo per averci dato la possibilità di svolgere questo lavoro di tesi, esperienza unica di crescita personale. La disponibilità e l'interesse dimostrato nei nostri confronti sono stati fondamentali al raggiungimento di questo traguardo, così come la passione che ci ha trasmesso.
Un grandissimo grazie va a Claudio, guida sicura e amica, che con pazienza, determinazione e preziosi consigli ci ha seguito per questi mesi, regalandoci sempre un sorriso.
Non può mancare un grazie a Matteo per il suo entusiasmo e gioia di vivere che ci hanno accompagnate fino a sotto l'Equatore.

Desideriamo inoltre ringraziare l'ingegnere Michele Liziero e tutto lo staff di Energy Team, per aver collaborato allo sviluppo di questo progetto e averci dedicato tempo prezioso in azienda.

Finally, a huge "Asanteni Sana" to all the beautiful people we met in Ngarenanyuki. Thanks to James, Lilian and their family, who lovely made us feel at home. Thanks to Godfrey, Benson and all the school students for their sincere friendship.

Extended Abstract

Nomenclature

Symbol	*Description*	*Unit*
C	Cell Capacitance	F
I	Current	A
P	Power	W
R	Resistance	Ohm
r	Discount rate	%
V	Voltage	V

Acronym	*Description*
BESS	Battery Energy Storage System
DOD	Depth of Discharge
E4G	Energy for Growing
EIS	Electrochemical Impedance Spectroscopy
LC	Load Consumption
LCOE	Levelized Cost of Energy
LLP	Loss of Load Probability
NPC	Net Present Cost
OCV	Open Circuit Voltage
Poli.NRG	POLItecnico di Milano-Network Robust Design
RMSE	Root Mean Square Error
SOC	State of Charge
SOH	State of Health
SOR	State of Resistance

Introduction

Distributed small scale electricity generation could result nowadays the most convenient solution to address the problem of rural electrification in DCs, where rural areas are widespread and national grid extension costs could be prohibitive [1]. Stand alone systems are mainly constituted of power generation units based on renewable energy sources and a battery energy storage system (BESS). Given the high variability and low reliability of renewable energy sources (RES), BESS are pivotal. Moreover, BESS represent the second major cost in stand alone systems due to their high investment cost and limited life time [2]. A proper battery modeling in off-grid system dimensioning tool is fundamental for decision makers in order to opt for the best investment. The most common battery models used in this kind of applications are the so called empirical or analytical models, which represent BESS with simplified approaches [3].

In such a framework, the scope of the present thesis is to propose a novel approach to model batteries in dimensioning tools. The methodology has been developed starting from a rigorous literature review. As a result, the authors identify, develop and test different methodologies: (i)Empirical models, two options are proposed, a complete model with variable efficiency and a simplified approach with constant parameters; (ii)Equivalent electric circuit model, it is a novel approach in sizing tools applications; the model describes battery in terms of electric quantities. The methodologies are implemented in the software Poli.NRG, a novel Matlab based procedure developed by Energy Department of Politecnico of Milan. The aim is to compare results obtained with the different modeling approaches, in terms of numerical outputs and simulation

times. Simulations are based on a real case study: Ngarenanyuki Secondary school in Tanzania. The authors spent one month in Ngarenanyuki to monitor power consumption, to make an accurate energy assessment of the school and verify battery working conditions.
Finally, the proposed methodology is used to dimension the new school system according to different BESS modeling approaches and different technologies (the emerging Li-ion and the consolidated lead acid [4]). Eventually, results are critically analyzed and discussed in order to compare costs and opportunities.

Review of battery modeling

An accurate modeling of battery behavior is strictly necessary in order to obtain correct simulations. In the literature review, the models have been grouped into four general different approaches:
Electrochemical. Electrochemical modeling is usually based on equations describing electrochemical phenomena of the cell. Besides current and voltage at the external terminals, electrochemical models are able to predict local cell characteristics. Therefore, they tend to be relatively complex and they typically have various parameters to be determined through several experiments [5].
Analytical. They are based on an abstract vision of the electrochemical cell. The battery is described by analytical equations that do not take into account electrochemical processes, but that are empirically fitted. These models usually focus on the evaluation of the SOC of the battery based on energy or current balances [6], [7]. Analytical models' complexity can vary but they are generally quite effective with respect to the computational effort, i.e. they are quite commonly adopted in dimensioning tools[8].
Electrical. Batteries are represented by equivalent electric circuits, that aim to model as accurately as possible operation parameters, e.g. the voltage and current characteristics at the external terminals. Models can be defined with respect to time or frequency domain according to the deployed circuital elements (resistances and capacitances, impedances) [9], [10], [11], [12]. There is a wide range of circuital models, with different degrees of complexity: from circuits composed of few constant circuital elements to circuits constituted by elements that directly reflect electrochemical characteristics of the cell. Given the wide spectra of possible equivalent circuits, these models find application in a broad range of sectors, comprising battery monitoring and design [8]. Electrical models have not been used yet for off grid system design application, although simplified ones could match the required characteristics of short computational time and accuracy, while maintaining a physical basis.
Stochastic. Stochastic models describe charging and discharging phenomena as stochastic Markovian processes, because the complex electrochemical reactions are significantly affected by random variables [13],[14].
Whichever approach is adopted, a proper battery modeling in microgrid design has to be able to estimate together:
State of Charge (SOC). It is necessary to evaluate amount of charge already stored in the battery to compute the amount of energy that cannot be provided to the load (Loss of Load)
State of Health (SOH). Batteries have a limited lifetime due to irreversible degradation processes. Lifetime modeling has to be considered: battery aging can be divided into calendar and cycle aging that cause capacity and power fade. The rate of degradation depends on batteries

operational and floating conditions. A proper evaluation of batteries degradation is necessary to compute replacement's costs.

BESS models investigated

The scope of the present work is to develop a novel procedure to model battery systems in dimensioning tools for off-grid plants; in particular the proposed approaches are integrated in the tool Poli.NRG, a new methodology developed by the Energy Department of Politecnico of Milan for sizing stand alone systems. Poli.NRG is a comprehensive procedure, written in Matlab environment, that allows for a robust dimensioning of a photovoltaic(PV)+BESS plant: it couples the atypical features of rural contexts (i.e. unpredictability of energy sources and load consumption uncertainties) with proper component models, by including estimation errors into the design phase [15].
The software is composed of four building blocks, related to different phases of the design procedure.
1. Data inputs gathering: the information regarding electricity consumption and power generation are collected: users' electric needs, fixed and variable equipment costs and weather data.
2. Inputs processing: the collected input data are processed in order to obtain daily load profiles and power generation profiles. Load profiles are generated with the subroutine LoadProGen which, using a stochastic approach, is able to formulate different daily load profiles starting from field data. Yearly profile is generated by aggregating randomly the daily load profiles and lifetime load profiles are obtained by assuming possible load evolution scenarios.
3. System modeling and simulation: this block includes mathematical models of system's components, namely PV and BESS. Simulations run with a time step of one minute during all the plant lifetime. In this thesis new BESS models have been developed and coded in the Poli.NRG package. At each time step k, the energy required or provided to the batteries is given by an energy balance between load consumption and photovoltaic power generation:

$$E_{user} = E_{PV}(k) - LC(k)/\eta_{inv} \quad (1)$$

Where LC(k) is the load consumption and η_{inv} is the inverter efficiency. Microgrid optimal design is based on performance indexes: Loss of Load Probability (LLP) is the amount of energy not provided to the load during the plant lifetime (LL(k) is the loss of load at each time step k) over the total energy required.

$$LLP = \frac{\sum_{k=1}^{LT} LL(k)}{\sum_{k=1}^{LT} LC_{ns}(k)} \quad (2)$$

Net Present Cost (NPC) is the present value of all the costs of installing and operating the system over the project lifetime.

$$NPC = \sum_{y=1}^{LT} \frac{Inv(y) + O\&M(y)}{(1+r)^y} \quad [\$] \quad (3)$$

Levelized Cost of Energy (LCoE) is an indicator that measures lifetime costs divided by energy production.

$$LCoE = \frac{r(1+r)^{LT}}{(1+r)^{LT}-1} \frac{NPC}{(1-LLP)\sum_{k=1}^{LT} LC_{ns}(k)} \quad [\$/\text{kWh}] \quad (4)$$

4. Output formulation: heuristic and mathematical optimization methods are used to find the most robust design of the systems. An iterative procedure is implemented in order to find the most robust solution for each lifetime load profile LC. The optimization algorithm is divided in two steps: firstly, the searching space is defined, i.e. the ranges of PV and BESS to be investigated; secondly, the optimal combination of PV and BESS is found within the searching space (for more details about the equations see [15]). The second step utilizes an heuristic procedure to find the optimal plant size: the adopted

algorithm is based on the imperialistic competitive algorithm that is an iterative process progressively exploring the searching space. When considering the first load profile, the algorithm tries randomly a fixed number of PV+BESS combinations within the research space; for each of them OpSim tool provides the LLP and NPC [15]. Eventually the optimum solution is found as the combination of PV+BESS having the minimum NPC whilst respecting LLP constraint of 5%. The new load profiles are simulated until a convergence criterion is fulfilled: the new iteration confirms the results of the previous one given a predefined tolerance.

M1-Simplified empirical model

It is the simplest model found in scientific literature [6]. Battery is characterized by a constant efficiency that represents energy losses during charge and discharge. The energy flows entering ($E_{charge(k)}$) or exiting ($E_{discharge(k)}$) at each time step are computed as follows:

$$\begin{aligned} E_{charge(k)} &= E_{user} \cdot \eta \\ E_{discharge(k)} &= E_{user}/\eta \end{aligned} \tag{5}$$

where $E_{user} = E_{PV} - E_{load}$ is the energy balance between energy production and consumption, i.e. the energy withdrawn or injected in the battery by users.

SOC of the battery at each time step is computed as:

$$SOC(k) = SOC(k-1) + \frac{E_{charge(k)/discharge(k)}}{E_{BESS}} \tag{6}$$

E_BESS is the nominal battery energy. The model is subject to constraints that define the BESS performance:

-a maximum value for the power to energy ratio PE_{ratio}, which is the maximum power output with respect to the rated capacity of the batteries; E_{max} is defined as

$$E_{max} = PE_{ratio} \cdot \Delta k \cdot E_{BESS} \tag{7}$$

-minimum and maximum value for SOC that will prevent permanent damage to battery. As a consequence, the eventual loss of energy required by the loads that the system is not able to supply is evaluated as a loss of load LL:

$$\begin{aligned} &LL(k) = LL(k-1) + (E_{max} - E_{user}(k))\eta_{inv} \\ &\quad \text{if } E_{user}(k) \leq -E_{max} \\ &LL(k) = LL(k-1) + (SOC_{min} - SOC(k)) \cdot E_{BESS}\eta_{inv}\eta \\ &\quad \text{if } SOC(k) \leq SOC_{min} \end{aligned} \tag{8}$$

SOH is not estimated by the model. To account for degradation, some constraints are imposed to the battery:

-Max number of cycles before replacement, to account for cycle aging. The equivalent cycle linked to the single time step is calculated as:

$$Eq_{cycle}(k) = \left| \frac{SOC(k) - SOC(k-1)}{2} \right| \tag{9}$$

Then, the amount of equivalent cycles are computed as follows:

$$Eq_{cycles}(k) = Eq_{cycles}(k-1) + Eq_{cycle}(k) \tag{10}$$

-Max number of years before replacement, to account for calendar aging.

M2-Empirical model

The model is an improved class of the model previously described. Given the evidence that battery efficiency depends on E-rate [16], which is defined as the ratio of power to rated energy:

$$E_{rate}(k) = P(k)/E_{BESS} \tag{11}$$

a cubic correlation has been adopted: $\eta(k) = aE_{rate}^3 + bE_{rate}^2 + cE_{rate} + d$, to properly model efficiency degradation at higher E-rate.

Also cycle aging is taken into account with a decrease of SOH during lifetime as follows:

$$SOH(k) = SOH(k-1) - Eq_{cycle}(k)cf(k) \tag{12}$$

SOH decrease is proportional to the number of cycles and to the capacity fade index cf which differs according to the technology. cf is an increasing function of E-rate when considering lithium ion batteries and an increasing function of DOD when considering

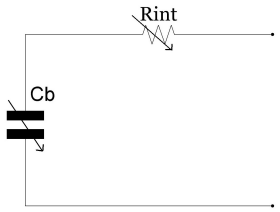

Figure 1: Equivalent circuit model

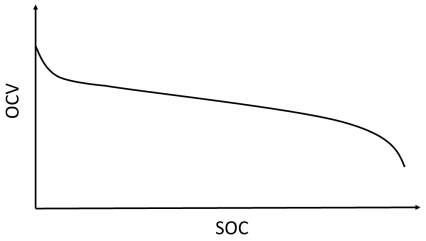

Figure 2: Open circuit voltage vs SOC

lead acid batteries.
In the model proposed the constraints that limit battery life are:
-Min SOH value before replacement, to account for cycle aging.
-Max n. years before replacement to account for calendar aging.
SOC at each time step is computed as follows to take into account capacity fade:

$$SOC(k) = SOC(k-1) + \frac{E_{charge(k)/discharge(k)}}{E_{BESS} SOH(k)} \quad (13)$$

M3-Electrical model

A simplified electric equivalent circuit model is proposed as a valid alternative to the more widespread analytical models. The proposed circuit (fig. 1) is a passive model. It is composed of a capacitance, Cb that represents battery equilibrium condition, in series with a resistance Rint to account for losses during operation; both the parameters depend on SOC and aging conditions. Voltage across Cb is the OCV voltage while voltage drop across Rint is the overpotential of the cell. The proposed approach to set the internal resistance-SOC relation is based on EIS: laboratory testing has to be performed at different battery SOC to define the resistance as the real part of impedance at a specific frequency. Reference frequency is related to the load input profile; while Cb, as a function of OCV (fig. 3) is determined from the cell discharge curve (fig. 2) (OCV vs SOC) by applying the capacitor's constituent equation.

The following equations characterize the

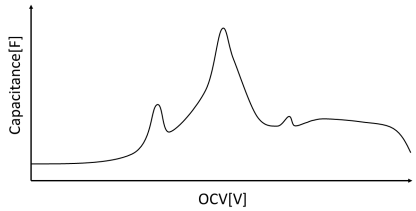

Figure 3: Intercalation capacitance vs SOC

cell:

$$\begin{cases} I = P/V \\ I = C(OCV)\frac{dOCV}{dt} \\ V = OCV(SOC) + R(SOC)I \end{cases} \quad (14)$$

In order to be implemented in Poli.NRG, they have to be solved numerically.
The power flowing in each cell is defined as:

$$P(k)_{user} = \frac{E_{user}}{\Delta t N_{cells}} \quad (15)$$

The number of cells N_{cells} is equal to the size of the BESS divided by the capacity of the cell.
Therefore, the current I(k) can be computed as:

$$I(k) = P(k)/V(k-1) \quad (16)$$

OCV(k) and V(k) are updated accounting for Cb and Rint at the previous time step.

$$OCV(k) = OCV(k-1) + \frac{I(k)}{C(k, OCV(k-1))}\Delta t \quad (17)$$

$$V(k) = OCV(k) + R(k, SOC(k-1))I(k) \quad (18)$$

The constraints are: i) maximum value for the power to energy ratio PE_{ratio}; ii) maximum and minimum voltage. Cycle aging is taken into account with SOH and SOR (State of Resistance) indicators. SOH vari-

ation during lifetime is the same as for empirical model; SOR accounts for resistance growth and increases with number of cycles for lead acid cell and number of cycles and C-rate in lithium ion. The capacity Cb and the resistance Rint are updated during simulations to take into account degradation :

$$Cb(k) = Cb(0) \cdot SOH(k) \tag{19}$$

$$Rint(k) = Rint(0) \cdot SOR(k) \tag{20}$$

The loss of load of the system is computed as

$$\begin{aligned} &LL(k) = LL(k-1) + (E_{max} - E_{user}(k))\eta_{inv} \\ &\quad \text{if } E_{user}(k) \leq -E_{max} \\ &LL(k) = LL(k-1) - E_{user}(k)\eta_{inv} \\ &\quad \text{if } V(k) \leq V_{min} \end{aligned} \tag{21}$$

Battery is replaced when either SOH has reached the minimum value (cycle aging) or the battery has reached the maximum number of years (calendar aging).

The three models have been parametrized for a lithium and lead acid cell with data taken from literature, datasheets, and experimental measurements. The electric model for a lithium ion cell has been validated with measures taken the at the Energy Storage Research Center (ESReC) located in Nidau(CH). The measurement were carried out within the framework of the collaboration between Politecnico of Milan (DoE) and CSEM-PV Center (Swiss Center for Electronics and Microtechnology). The tested cell is the Lithium Nickel Cobalt Oxide(LNCO) cell BostonPower-Swing5300. Detailed description about laboratory testing is reported in [17]. A square current profile at different current values and SOC=50 % has been applied to the cell to test the proposed model. The resulting measured and simulated voltages are shown in fig. 4. The rmse error between measured and simulated voltage is 0.08V both with Euler method and the more accurate adaptive step size method Runge Kutta (ODE 15s in matlab). The small error confirms the validity of the model and of the chosen numerical approach.

Simulations and results

A real life case study has been taken into consideration: Ngarenanyuki secondary school, in Tanzania. The energy consumption in the school has been monitored by Politecnico of Milan since 2015, when a hybrid stand alone system was deployed. The recent connection to the national grid has lead the school to increase number of loads and power consumption. The authors spent one month at Ngarenanyuki school with three different purposes:

1. Perform a field survey in order to assess school's loads and generation units. Design a microgrid (PV+BESS) capable to properly feed the school.
2. With respect to the small-size microgrid already in place, BESS characterization and cells internal resistance measure has been performed. Lead acid batteries installed in the school are subject to long periods at low SOC, high current levels and almost never complete charges. Moreover, data collected from Italy are affected by many errors and uncertainties due to non controllable external conditions.
3. In order to improve the "already in place" microgrid monitor, a new monitoring system (donated by the company Energy Team S.p.A.) has been deployed. School loads are supplied both by the national grid "Tanesco" and by the existing microgrid: with the new monitoring system, school consumption is entirely controlled by merging data of the two systems.

The above mentioned activities, in particular the first two point of the list, were aimed to set up Poli.NRG simulations. Data collected through field survey were used to generate realistic load profiles in input to

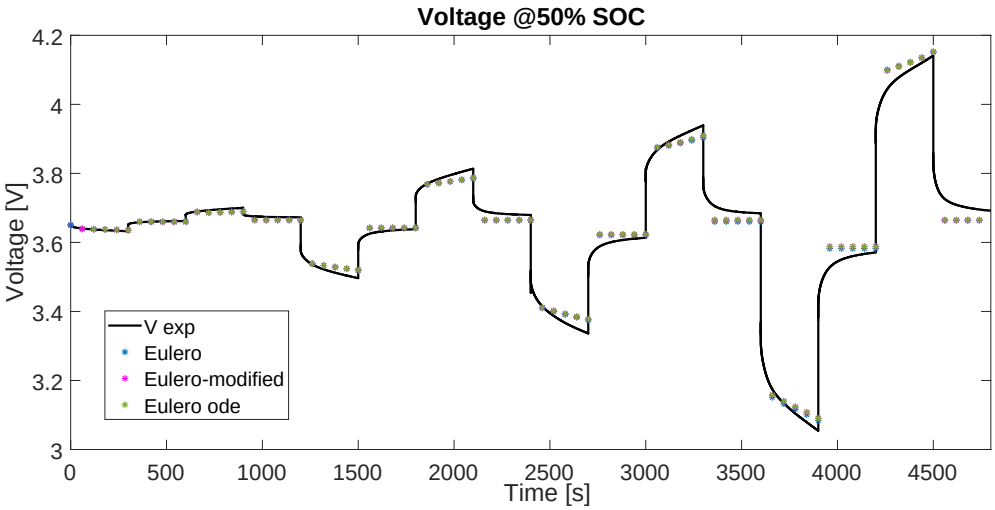

Figure 4: Simulated and measured voltage of BOSTON POWER SWING5300 cell when cycled with a square current profile at 50%SOC

Poli.NRG; the second activity was instead aimed to the parametrization of BESS models in the tool. However, the data resulting from the experimental procedure did not have the necessary characteristics of repeatability and reproducibility, hence they have not been used for BESS models' parametrization in Poli.NRG, where laboratory data and manufacturer's data were preferred.

Simulations' set up

The data collected through the field survey were classified in daily loads (e.g classroom lights, household appliances, water pump) and occasional three phase loads, mainly a mill machine. They were used to generate stochastic load profiles with Poli.NRG-LoadProGen subroutine; figure 5 shows 20 days of simulated load profile compared with 20 days of measured load profile. Yearly load profile has been extended over the entire plant lifetime (20 years) considering a constant load consumption. Cost information about PV modules, batteries, and off-grid inverters are collected from a survey among Tanzanian local suppliers, while O&M, other investment costs and modeling parameters have been estimated based on experience. Several simulations have been carried out over the system lifetime to size the new theoretical microgrid constituted by PV+BESS for the school, which could cover the whole energy needs and substitute the already present "small" stand alone system. In particular, empirical simplified, empirical and electrical battery models have been implemented with the two driving technologies Li-ion and lead acid and eventually they are compared in terms of sizing results, costs and simulation time. The tables 1 and 2 summarize the BESS parameters in input to Poli.NRG.

Results and discussion

Figures 6 and 7 display the map of solutions of the simulations with the three BESS models (electrical, empirical, empirical simplified) for lead acid and lithium ion technology. The map of solutions is composed of different areas of solutions that are related to the specific BESS model adopted in the simulation. Each area of solutions represents with contour lines the resulting optimal combinations of PV and BESS size among the N simulated lifetime profiles LC.

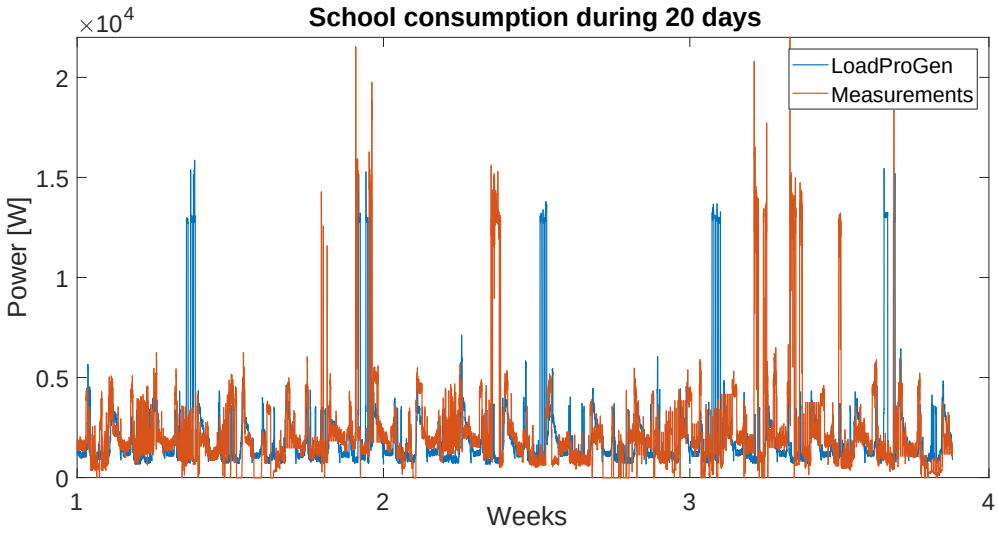

Figure 5: Measured and simulated load profile over 20 days

	Lithium ion		
	M1	**M2**	**M3**
SOC initial	1	1	1
SOC min	0	0	-
PE ratio [kW/kWh]	2	2	2
SOH min	-	0.8	0.8
Calendar life [years]	12	10	10
Cycle life [n cycles]	2000	f(E-rate)	f(C-rate)
Charge efficiency %	97.5	f(E-rate)	-
Discharge efficiency %	97.5	f(E-rate)	-
Cell capacity [Ah]	-	-	5.3
Max voltage [V]	-	-	4.2
Min voltage [V]	-	-	2.75

Table 1: Lithium ion battery specifications

	Lead acid		
	M1	**M2**	**M3**
SOC initial	1	1	1
SOC min	0.5	0.5	-
PE ratio [kW/kWh]	0.25	0.25	0.25
SOH min	-	0.8	0.8
Calendar life [years]	8	8	8
Cycle life [n cycles]	1500	f(DOD)	f(DOD)
Charge efficiency %	90	f(E-rate)	-
Discharge efficiency %	90	f(E-rate)	-
Cell capacity [Ah]	-	-	10
Max voltage [V]	-	-	2.17
Min voltage [V]	-	-	2

Table 2: Lead acid battery specifications

The contour line of the optimal combinations is a curve along which specific combinations have appeared with the same frequency (i.e., it represents isolines). The frequency ranges between 0 and 1 since it has been normalized according to the most frequent combination in the considered BESS model. The isolines are concentric, the most external is the one with the lowest frequency of occurrence.

The table 3 shows the robust design solutions of six BESS model simulations. The robust design (optimal BESS size $BESS_{opt}$;optimal PV size PV_{opt}) is evaluated as the optimal combination result with the highest frequency (i.e, 1). The NPC, LCOE and LLP of the robust design are evaluated as the mean value of each solution in which appears $BESS_{opt}$ and PV_{opt}. Frequency of occurrence F_{opt} is the number of

BESS technology	**BESS model**	PV_{opt} **[kW]**	$BESS_{opt}$ **[kWh]**	**NPC [k$]**	**LCOE [$/kWh]**	**LLP [%]**	**Single LC simulation time [min]**	LC_{opt}	F_{opt}
Lead acid	Empirical simplified	14.2	105	119.82	0.644	4.99	8	114	4
	Empirical	12.9	112	118.66	0.637	4.99	45	124	7
	Electric	12.35	94.5	114.85	0.617	4.99	67	114	8
Li-ion	Empirical simplified	11.9	60.6	120.50	0.648	4.90	7	101	12
	Empirical	12.9	48.6	116.28	0.625	4.99	45	108	5
	Electric	12.8	49.1	116.22	0.624	5	140	98	4

Table 3: Results of PoliNRG simulations with different battery technologies and modeling approaches

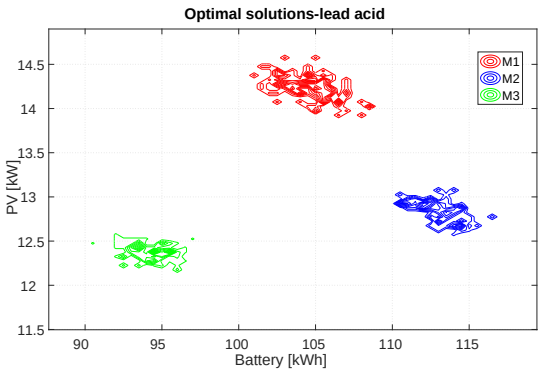

Figure 6: Sizing results of Poli. NRG with lead-acid BESS systems

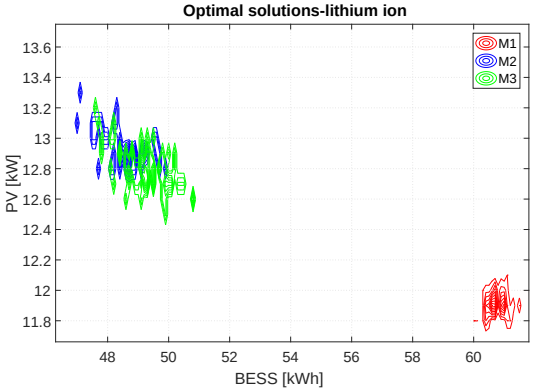

Figure 7: Sizing results of Poli. NRG with Li-ion BESS systems

times the optimal solution appears in simulation's results. The parameter LC_{opt} represents the number of simulated load profiles until convergence. Every simulation provides a robust solution, since the dispersion of the optimum around the identified design is very limited. Regarding lead acid technology, the empirical model tends to overestimate system size (+18%) with respect to robust design using electrical model, as can be seen from table 3. The overestimation, can be caused both by the different estimation of SOC and SOH and by the different parametrization of M2 and M3: for M2 the manufacturer's data have been used, while for M3 experimental data were available. As a consequence, the NPC is 4000$ higher when sizing the system using empirical model. The BESS size in the simulation with the simplified empirical model is an intermediate value between the other two models and PV size noticeably bigger than M2 PV_{opt}, due to the fact that battery operates meanly with a lower efficiency in M1 with respect to M2. This implies that even if the parameters in input to the simplified empirical model (efficiency and maximum number of cycles) are correctly estimated, simulation results could not resemble the ones of more sophisticated approaches.

Considering Li-Ion technology simulations, electric and empirical model result to have very similar system sizes while the simplified empirical model shows a non negligible difference. The resulting NPC is very sim-

ilar between electric and empirical methodologies while it is 4000 $ higher when using the more simplified approach. The results' similarity among M2 and M3 for lithium ion is likely due to models' parametrization: the values of the variable parameters of the different BESS models and degradation curves have been computed from experimental measurements. As reported in the last column of the table 3, computational times for simulating one lifetime load profile LC strongly varies with the BESS modeling approach adopted; notice that single profile simulation time depends on the calculator processor (specifically to the present thesis, an "Intel i7 4700k-16 Gb has been used). Empirical model takes almost 6 times the simulation time needed for simplified empirical model, both for lead acid and lithium ion technologies; electrical lead acid model computational effort is 8 times higher than the simplest model, while for lithium ion batteries is even 18 times higher. The conclusion is that accuracy works at the expense of higher computational effort. It is worthwhile to highlight that Li-ion batteries constitute the 26 % of the total capital investment cost while lead acid batteries only the 21%. Nevertheless, it is necessary to account also for batteries' replacement costs for a proper analysis of the costs associated to each technology; in fact, lead acid batteries have to be replaced three times during plant lifetime while lithium ion batteries only one. For this reason NPC of the plant with lithium ion batteries is only 2000 $ higher than with lead. Moreover, the LCOE of the two technological options are considerably similar: Li-ion batteries are nowadays competitive with respect to lead acid batteries and they can even be a better solution for off grid systems.

Conclusions

The scope of the present thesis is to develop a new methodology for modeling battery storage systems, to be integrated in tools for sizing off-grid plants. The proposed novel model represents the battery as an equivalent electric circuit, as a capacitance is series with a resistance. Parameters values depend on SOC and SOH. This approach for BESS modeling is commonly found in literature for online applications, but no examples of implementation in sizing softwares have been found. In addition to the novel approach, 2 empirical models have been proposed: the simplified model with constant efficiency and the more advance one with efficiency and lifetime modeling depending on working conditions. The proposed models have been implemented in the dimensioning tool to design a PV+BESS system for Ngarenanyuki school in Tanzania. The three modeling approaches have been parametrized both for lithium and lead acid technologies and compared in terms of results and computational time. The models differ greatly in terms of computational effort: the higher the model's complexity, the higher the time. The empirical simplified model leads to an oversizing of the plant with consequent overestimation of investment costs. Empirical and electric models are instead comparable when data are taken from laboratory measurements. In conclusion, this thesis highlights the necessity of a proper and smart BESS modeling when facing the design of off−grid systems. By using Poli.NRG, investors will be given the opportunity to choose between different BESS modeling, according to their needs. Finally, the output of the tool can help investors decide whether to invest in lead acid or lithium ion battery technologies; Li-ion battery costs are nowadays competitive with respect to lead acid and they also have better performances.

Bibliography

[1] World Bank Group. The World Bank. http://www.worldbank.org.

[2] International Renewable Energy Agency. *Solar Pv in Africa: Costs and Markets*. Number September. 2016.

[3] Geoffrey T Klise and Joshua S Stein. Models Used to Assess the Performance of Photovoltaic Systems. 2009.

[4] International Renewable Energy Agency. *Electricity storage and renewables: Costs and markets to 2030*. Number October. 2017.

[5] Dennis W. Dees, Vincent S. Battaglia, and André Bélanger. Electrochemical modeling of lithium polymer batteries. *Journal of Power Sources*, 110(2):310–320, 2002.

[6] Nicholas Etherden and Math H J Bollen. Dimensioning of energy storage for increased integration of wind power. *IEEE Transactions on Sustainable Energy*, 4(3):546–553, 2013.

[7] James F. Manwell and Jon G. McGowan. Lead acid battery storage model for hybrid energy systems. *Solar Energy*, 50(5):399–405, 1993.

[8] M.R. Jongerden and B.R. Haverkort. Which battery model to use? *IET Software*, 3(6):445, 2009.

[9] S M G Mousavi and M Nikdel. Various battery models for various simulation studies and applications. *Renewable and Sustainable Energy Reviews*, 32:477–485, 2014.

[10] Lijun Gao, Shengyi Liu, Roger A Dougal, and Senior Member. Dynamic Lithium-Ion Battery Model for System Simulation. *IEEE Transactions on Components and Packaging Technologies*, 25(3):495–505, 2002.

[11] V Johnson. Battery performance models in ADVISOR. *Journal of Power Sources*, 110(2):321–329, 2002.

[12] Luiz Carlos Stevanatto, Valner Joao Brusamarello, and Stanislav Tairov. Parameter identification and analysis of uncertainties in measurements of lead-acid batteries. *IEEE Transactions on Instrumentation and Measurement*, 63(4):761–768, 2014.

[13] Laifa Tao, Jian Ma, Yujie Cheng, Azadeh Noktehdan, Jin Chong, and Chen Lu. A review of stochastic battery models and health management. *Renewable and Sustainable Energy Reviews*, 80(July 2016):716–732, 2017.

[14] CF Chiasserini and R.R. Rao. Pulsed Battery Discharge in Communication Devices. 1999.

[15] Claudio Brivio, Matteo Moncecchi, Stefano Mandelli, and Marco Merlo. A novel software package for the robust design of off-grid power systems. *Journal of Cleaner Production*, 166:668–679, 2017.

[16] Massoud Pedram and Qing Wu. Battery-powered digital CMOS design. *Proceedings -Design, Automation and*

Test in Europe, DATE, 10(5):72–76, 1999.

[17] Claudio Brivio. *Battery Energy Storage Systems: Modelling, Applications and Design Criteria*. PhD thesis, Politecnico di Milano, 2017.

Contents

Abstract

During the past years, Battery Energy Storage Systems (BESS) have gained importance in several contexts, especially in off-grid systems applications. Power production in stand alone systems is often based on highly variable and non reliable renewable energy sources: BESS are fundamental in this context to balance sources variability and satisfy load demand. Nevertheless, batteries represent one of the major costs in mini grids due to their high investment cost and limited life time. Hence, it is important to introduce in design tools of off-grid systems an adequate BESS model that allows to account for system reliability and costs.
The present thesis work is devoted to develop a new methodology for modeling battery storage systems, and to implement it in microgrid design tools.
The authors rigorously review the majority of the approaches found in literature, with the purpose of classifying the models according to diverse methodologies; models are analyzed in terms of accuracy and computational effort.
A novel approach is then proposed, the goal is to accurately represent battery performance. The chosen model represents the battery as an equivalent electric circuit constituted by a variable capacitance (i.e. stored energy) and a variable resistance (i.e. battery losses). In addition, two empirical models are proposed; they are simpler and represent a classical approach in off-grid sizing tools, requiring little computational effort. A comparison between the different models is proposed in order to point out pros and cons of each one. The models are parametrized with data of both lead acid and lithium ion batteries as far as they are the two technologies that will likely compete in the future in off-grid applications.
The methodologies are implemented in the novel dimensioning tool Poli.NRG developed by a research Team in Politecnico. Eventually the tool is validated in a real life scenario: the experimental microgrid in place at Ngarenanyuki school, Tanzania. Data regarding school consumption are collected by on field survey performed by the authors during one month spent there. Results obtained with the different model methodologies are compared and discussed.

Keywords: *BESS, off-grid systems, dimensioning tools, battery modeling, equivalent circuit models, Tanzania*

Sommario

I sistemi di accumulo di energia a batterie (BESS) hanno acquisito negli ultimi anni molta importanza in diversi contesti, specialmente nelle applicazioni in sistemi "Off Grid". I sistemi ad isola si basano su fonti di energia rinnovabile altamente variabili e inaffidabili: i sistemi di accumulo a batterie sono fondamentali in questo campo per bilanciare la variabilità delle risorse e per soddisfare la domanda di carico. Di conseguenza, è importante introdurre nei software di dimensionamento per sistemi Off-Grid un modello adeguato di BESS che permetta di considerare i costi e l'affidabilità del sistema.
Il presente lavoro di tesi ha lo scopo di sviluppare una nuova metodologia per i modelli BESS da implementatare in strumenti di dimensionamento di "Microgrid". La maggioranza degli approcci presente in letteratura è analizzata rigorosamente dagli autori, ai fini di classificare gli approcci di modellazione in base all'accuratezza e all'onere computazionale. Successivamente viene proposto un approccio innovativo: l'obiettivo è di rappresentare accuratamente le prestazioni della batteria. Il modello prescelto rappresenta la batteria come un circuito elettrico equivalente costituito da una capacità variabile e da una resistenza variabile. Inoltre, sono proposti due modelli empirici, che rappresentano un semplice e classico approccio usato nei software di dimensionamento e che richiedono uno sforzo computazionale inferiore. Un confronto tra i differenti modelli è proposto con l'obiettivo di evidenziare vantaggi e svantaggi di ognuno di essi. I modelli sono parametrizzati con dati sia di batterie al piombo che di batterie al litio, dal momento che sono le due tecnologie che più probabilmente competerranno nel futuro delle applicazioni "Off Grid". Le metodologie sono implementate in Poli.NRG, uno strumento innovativo per il dimensionamento sviluppato da un gruppo di ricerca in Politecnico. Infine, il software è validato in uno scenario reale: la microgrid sperimentale situata nella scuola di Ngarenanyuki, Tanzania. I dati riguardanti i consumi della scuola sono raccolti attraverso un sondaggio effettuato sul campo dagli autori durante il mese vissuto nella scuola. I risultati ottenuti utilizzando le diverse metodologie di modellazione sono confrontati e discussi.

Parole chiave: *BESS, sistemi off-grid, software di dimensionamento, modellazione di batteria, modelli elettrici con circuito equivalente, Tanzania*

List of Figures

List of Tables

List of Acronyms

Acronym	*Description*
ADVISOR	Advanced Vehicle SimulatOR
BESS	Battery Energy Storage System
BMS	Battery Management Systems
BOL	Begin of Life
DAE	Differential Algebraic Equation
DC	Developing Country
DOD	Depth of Discharge
DP	Dynamic Programming
E4G	Energy for Growing
EIS	Electrochemical Impedance Spectroscopy
EOL	End of Life
EV	Electric Vehicle
FDM	Finite Difference Method
FVM	Finite Volume Method
HEV	Hybrid Electric Vehicle
HFR	High Frequency Resistance
HPPC	Hybrid Pulse Power Characterization
KiBam	Kinetic Battery model
LCO	Lithium cobalt oxide
LCOE	Levelized Cost of Energy
LFP	Lithium iron phosphate
Li-ion	Lithium ion
LLP	Loass of Load Probability
LMO	Lithium manganese oxide
LPM	Linear Programming Model
LTO	Lithium titanium oxide
MILP	Multi-Input Linear Programming
MOEA	Multi-Objective goal Programming
MOP	Multi-Objective Programming

Acronym	*Description*
NCA	Lithium nickel cobalt aluminium oxide
NLP	Non-Linear Programming
NMC	Lithium nickel manganese cobalt oxide
NPC	Net Present Cost
O&M	Operation and Maintenance
OCV	Open Circuit Voltage
ODE	Ordinary Differential Equation
P2D	Pseudo two Dimensional
PLC	Programmable Logic Controller
Poli.NRG	POLItecnico di Milano-Network Robust Design
PV	Photovoltaic
RERL	Renewable Energy Research Laboratory
RES	Renewable Energy Source
RMSE	Root Mean Square Error
SEI	Solid Electrolyte Interface
SHS	Solar Home System
SOC	State of Charge
SOH	State of Health
SOR	State of Resistance
SP	Single Particle
VRLA	Valve Regulated Lead Acid

Introduction

The issue of access to energy has a high priority on the global agenda. Sustainable energy is the seventh goal of the 17 UN Development Goals. The target is to ensure by 2030 "access to affordable, reliable, sustainable and modern energy for all". [1] Sustainable Development Agenda refers to energy in its broad dimension, comprising access to electricity as well as clean fuels for cooking and heating, each of them contributing to satisfy basic needs. Electricity is yet one of the most important factors that can drive development. In 2014, 1.06 billions people still lived without access to electricity, ca 15% of the global population. Among these, 609 millions of people lived in Sub-Saharian Africa, where electricity access deficit hits the 62.5% of the population. Majority of these people live in remote rural areas, where deployment costs of the national electric grid are prohibitive [2].
To address the problem of rural electrification, different strategies can be employed [3]:

- Extend the national established grid to sparsely populated area. Cost of energy would be low but investment costs as well as technical losses due to long distances could be very high.

- Off grid systems: distributed generation, small scale electricity production could be an effective solution in remote areas, though requiring a high investment cost. Stand alone systems can range from home based systems relying on a single source to mini grids integrating more than one source of energy.

- Integrated microgrids: they can be defined as an aggregation of loads and micro-resources operating as single system providing both power and heat, integrated to national grid or not. They have their internal control and optimization scheme and could operate in connection with the main grid.

Although a centralized approach would be more cost-effective in a long term perspective, it is accepted that off-grid systems represent the most effective solution for the near future [3].
An example of stand alone system is depicted in figure 1. The main components by which the system can be constituted are:

- One or more primary electricity generation technologies, bases on unreliable renewable energy sources-Solar Photovoltaic, Small Wind Turbines, Small Hydropower Turbine; when more than one energy source is present, the system is called Hybrid System.
- Secondary electricity generation technologies, typically a diesel generator. Hydro power plants are considered as secondary when the electricity generation is continuous and it cannot be interrupted by uncontrollable causes (e.g., when the river is shared for irrigation or other basic purposes).
- A storage system-a number of technologies based on different principles are available (fuel cell, supercapacitors, flywheel...) but for small scale systems, up to some MW, batteries are the most common device, especially lead acid batteries.
- Inverter and charge controller.
- Other electric material (cables, wires...).

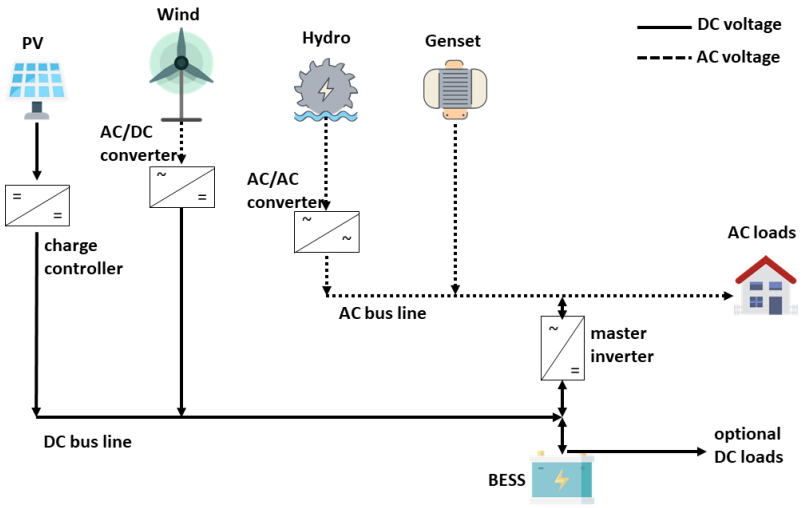

Figure 1: AC/DC bus lines Hybrid System

Due to the high variability and low reliability of renewable energy sources (RES), storage systems are of fundamental importance in mini-grids. They allow to increase efficiency in energy usage, storing energy when there is excess in production (e.g. during the day in the case of solar energy) and releasing it during peak hours (e.g. during evening hours), avoiding loss of energy demand. Battery Energy Storage Systems (BESS) can help the diffusion of RES as opposed to expensive and polluting traditional energy sources (diesel or kerosene), allowing a major energy independence and development of communities.

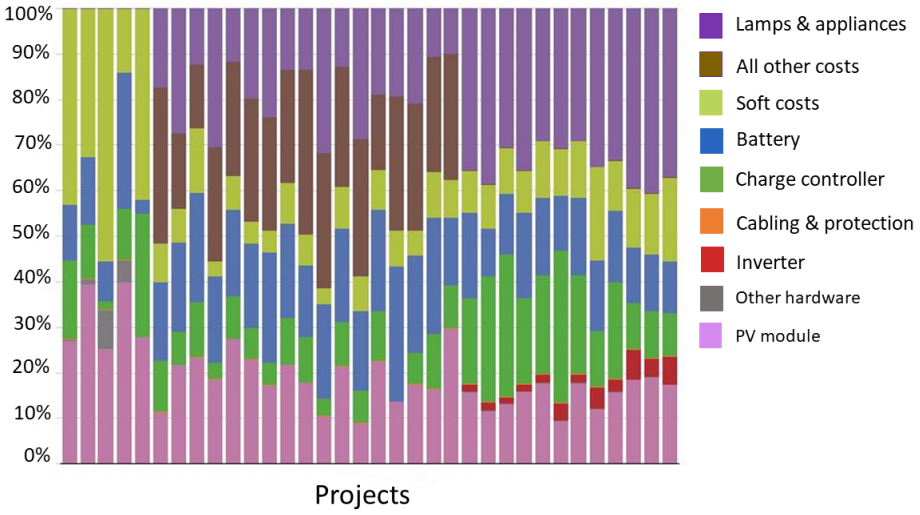

Figure 2: Solar Home System (>1kW) cost breakdown shares, 2013-2014 [4]

Batteries represent one of the major costs in stand alone systems due to their high investment cost and limited life time. In figure 2 solar home-based system investment cost breakdown of different projects is reported: each column is related to a specific project. The columns in the right part of the graph are related to installations smaller than 2kW: in those cases, systems are sold with lamps and appliances, which increase the total installed cost of these SHS by 11% to 68% depending on the system. However, batteries and PV represent the second large share of the cost, on average 18% and 19%.
Due to unavoidable irreversible phenomena happening inside electrochemical cells, nowadays batteries become heavily degraded after less than 10 years, which is lower than the plant lifetime. Decision making process by investors' is hence not an easy task: not only the immediate investment cost but also battery replacement's cost need to be taken into account. Two aspect need mainly to be considered when choosing the optimal BESS system:

- BESS size: the bigger the size of batteries and the initial investment cost, the lower the stress level that batteries experience during operation and the longer is their lifetime. Moreover, the smaller batteries are, the higher will be the energy not provided to the load.
- BESS technology: many different battery technologies exist nowadays, with different chemistries, costs and operational characteristics. Lead acid batteries are nowadays the most mature and diffuse technology in stand alone energy systems due to their low cost and great availability; lithium batteries, more expensive but more efficient, will likely diffuse in the next future.

Some dimensioning tools that help in the optimal investment choice for stand alone

systems are commercially available (e.g. HOMER [5], HybSim [6], Hybrid2 [7], Hoga [8], Trnsys [9]). They are based on algorithms that allow to find the economic optimal size of generators and storage systems. These softwares have to take into account many aspects of the off-grid system (e.g. load profiles, modeling of generation units, RES power production) and BESS are often modeled in a very simplified manner. The most common battery models used in this sector are the so called empirical or analytical models: they are based on an abstract vision of the electrochemical cell. Battery is described by mathematical equations, empirically or analytically derived, which aim to reproduce its energetic behavior without focusing on the real physics. These models entail strong simplifications that allow for short computational time at the expense of accuracy. The risk, when not enough physical aspects are taken into account, is that the output of the software is not reliable. Errors in dimensioning stand alone systems could have severe consequences on the costs and lifetime of the plant. For this reason it could be worthwhile to study and analyze possible alternative options.
Other modeling approaches can be found in literature applied to other contexts: they range from the most accurate electrochemical models which describe batteries with physical laws, to stochastic abstract models. Battery can also be seen as an equivalent electric circuit, when considering its voltage and current characteristic: electrical models are widely adopted for the modeling of batteries in particular in automotive applications.

The scope of this thesis work is to propose a novel approach to model batteries in microgrid dimensioning tools. It has to be simple to allow for viable computational time but accurate enough to provide reliable cost estimation. Development of the model is divided into two parts:

1. State of Charge estimation: it is necessary to model battery behavior during operation, to evaluate amount of charge already stored in the battery and compute the amount of energy that cannot be provided to the load (Loss of Load).

2. State of Health estimation: a correct evaluation of battery degradation, which is strongly dependent on cycling conditions,allows to forecast the battery lifetime and the consequent replacement's cost.

The methodology has been developed starting from a rigorous literature review that allowed to understand strengths and weaknesses of each modeling approach. As a result, the authors proposed two different models:

- Empirical model: it constitutes a classic approach, that describes battery in terms of its energetic behavior. Two versions of the model, of different complexity are proposed.

- Equivalent electric circuit model: it is a novel approach in sizing tools applications. The model describes battery in terms of electric quantities: it can accurately estimate current voltage characteristic as well as the state of charge. It represents a good compromise among all battery approaches in terms of accuracy and computational time.

The methodologies have been implemented in the package Poli.NRG, a novel Matlab based procedure developed by Energy Department of Politecnico of Milan. The aim is to compare results obtained with different modeling approaches, in terms of numerical outputs and simulation times. The novel electrical approach requires a greater computational effort; if the results in terms of optimal size of the systems were noticeably different among the methodologies, it could make sense to use the most accurate. In other words, if simplified BESS models lead to relevant errors in simulations, there could be an over or under sizing of the off-grid system with consequent costs; in this context, a longer simulation with an accurate model that leads to a correct dimensioning would be preferable.
In order to test the realistic approach conditions, Poli.NRG optimization process is applied to the real case study of Ngarenanyuki Secondary school in Tanzania, in the framework of a long term collaboration with Politecnico of Milan. The scope is to size a new theoretical PV+storage system for the school that could cover the whole energy needs and substitute the already present undersized stand alone system. The authors spent one month in Ngarenanyuki: they monitored power consumption and made an accurate energy assessment of the school, taking into account also the recent arrival of the national electric grid managed by Tanesco. As a conclusion, dimensioning of the new school system is performed checking both different BESS modeling approaches and different technologies (lithium and lead acid), to compare costs and opportunities: the results are critically analyzed and discussed.

The structure of the thesis is the following:
Chapter 1 reports a general overview of batteries' technologies and applications. Subsequently, the physical laws governing operation of an electrochemical cell are described and the chemistry of the two most common type of batteries for off grid applications, Lithium and Lead Acid as well as their degradation process are reported. Finally, the most important operational characteristics, which have to be taken into account when modeling batteries, are described.
Chapter 2 comprises a rigorous and detailed literature review regarding battery modeling. Four different approaches: electrochemical, analytical, electrical and stochastic are studied.
The process of battery modeling is divided into two sections, SOC estimation and SOH estimation. At the end of the chapter, a comparison of the four modeling methods is reported, with possible applications for each category.

In Chapter 3 the state of the art of off-grid sizing methodologies present in scientific literature is reported. Subsequently, the structure of Poli.NRG modeling tool, and its main features are described.
In Chapter 4 two methodologies for BESS modeling, to be applied in Poli.NRG, are proposed. Firstly, the authors present a classical approach: they propose an empirical battery model with constant efficiency and a more advanced one which accounts for variable efficiency and degradation. Subsequently, the novel approach, the electrical battery model, is proposed and it is moreover validated with experimental data. Parametrization of the models is done both for lithium and lead acid technologies
Chapter 5 presents the case study of Ngarenanyuki school. Poli.NRG methodology, with the novel proposed BESS approaches is applied to the school, in order to size an optimal theoretical new PV+BESS system which can cover the present needs. Firstly, the energy assessment of the school, performed during the month spent by the authors in Tanzania is reported; results of the field survey have been used to generate the school yearly load profile with NRG procedure. Secondly, simulations with Poli.NRG are set up: the proposed BESS modeling methodologies, implemented with both lithium ion and lead acid technologies, are used to simulate 20 years of plant life.
In Chapter 6 the results of the simulations are reported. Firstly, a qualitative analysis of school load profiles generated with the tool LoadProGen is reported, moreover a comparison with real measured data is shown. Subsequently, the proposed BESS models have been simulated adopting the procedures developed in the thesis project. The diverse BESS modeling approaches and technologies are compared in terms of optimal PV and BESS size, costs and simulation time.

Chapter 1

Battery basics

1.1 Overview of applications and technologies

Global energy storage market is growing exponentially to an annual installation size of 6 gigawatts (GW) in 2017 and over 40 GW by 2022, from an initial base of only 0.34 GW installed in 2012 and 2013 [10]. Among all the different type of energy storage systems, electrochemical energy storage is one of the most rapidly growing market segments, even though operational installed battery storage power capacity is still only 1.9GW, small when compared to the other thermal or pumped hydro storage (more than 150GW installed) [11]. The figure 1.1, shows the exponential increase of global installations of electrochemical storage systems in the past 20 years, thanks to decreasing costs and performance improvements. Electrochemical

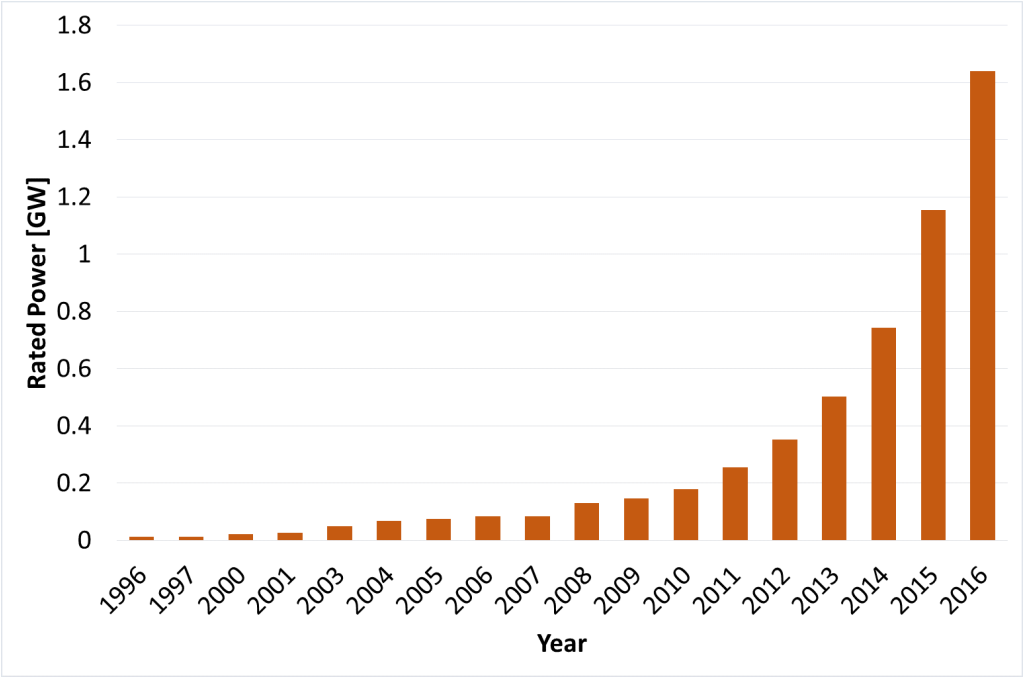

Figure 1.1: Global electrochemical storage capacity, 1996 – 2016*[11]*

batteries are an important power source in all cases where very high power is not needed. A first general classification distinguishes batteries in **primary batteries** and **secondary batteries**, where the former correspond to non-rechargeable batteries and the latter correspond to rechargeable batteries [12].
Primary batteries are typically used from low to moderate power applications, such as in industrial applications and in some electronic devices (e.g. watch, radio, calculator ...). Secondary batteries are commonly used as Energy Storage System (BESS) and nowadays they are used in a wide range of applications:

- Stationary applications: off grid energy storage, uninterruptible power supplies, emergency power, load leveling, peak shaving, load shifting, dispatchability of non-programmable renewable energy plants;
- Automotive sector, in electric and hybrid vehicles;
- Portable devices: laptops, mobile phones, cordless devices;

It is worth noticing the important role that batteries play in off-grid energy systems. Approximately 1.06 billion people in the world do not have access to electricity grids. They often used to rely on expensive and polluting diesel generators to supply to power needs. In the last decade, stand alone systems based on renewable energy sources (RES) began to diffuse in remote and rural areas of developing countries. RES are by nature highly unreliable and unpredictable; BESS are be useful in order to store and provide energy according to the needs, and assure continuous power supply. Their usage could increase the implementable amount of renewable energies in off-grid systems up to 100%, allowing for clean and sustainable energy supply.
There are many types of batteries, suited to different applications, their principal characteristics are reported in the table 1.1. Lead acid batteries are the most widely used technology as energy storage systems in off grid applications. VRLA (Valve

Specifications	**Lead acid**	**Li-ion**	**Ni based**	**Na based**
Energy density [Wh/kg]	25-50	60-260	30-80	90-120
Power density [W/kg]	60-180	500-3000	150-1000	150-160 [W/l]
Cycle life	300-2000	700-7000	500-2500	2500-3000
Cell nominal voltage V	2	3.3	1.2	2-2.6
Initial cost [$/kWh]	100-200	350-1150	150-750	100-300

Table 1.1: Characteristics of different BESS technologies. Costs refer to year 2015 [13], [14]

Regulated Lead Acid) batteries in particular are widespread due to their low initial costs, high availability even in developing countries, safety reasons and disposal possibility. The characteristic features of off-grid renewable energy, though, such as high variable charging and discharging power, deep cycles, low periods without fully charging batteries and extreme temperatures are known factors that influence negatively lead battery lifetime [15]. For this reason, researchers are starting evaluating other solutions suitable to application in disadvantaged contexts.
Lithium ion batteries have a high energy density together with high efficiency both during charge and discharge, as can be seen from the table 1.1. Their cycle lifetime is longer than lead acid batteries and they can withstand higher temperatures. All this positive characteristics come at the expense of higher capital costs [16].
Nowadays, Li-ion batteries are yet expensive and their light weight and high power densities could be not enough to motivate their exploitation in stationary storage systems [17]. Nevertheless, lithium battery sector is expanding, and research and development in automotive sector will eventually lead to a substantial decrease in their manufacturing cost. The forecast is that they will become competitive in a near future even in off grid applications (according to a report by IRENA their cost will fall below 200$/kWh by 2030 for stationary applications), where their longer lifetime, no need for maintenance and resistance to extreme conditions will represent economical advantages.
In order to make the most convenient choice in off-grid contexts, not only the initial investment cost, but also battery lifespan, maintenance and replacement costs need to be evaluated. Battery performance and their ability to satisfy load demand need also to be taken into account. Many sizing tools that help in the optimal plant dimensioning are commercially available (see chapter 3). Most of them rely on battery mathematical models quite far from the real battery physics.
Properly modeling a battery, signifies being able to reproduce its behavior as seen externally, in terms of energy absorbed and provided as well as voltage and current characteristics. In the following sections, the physical laws governing electrochemical cell operation are reported, followed by a description of lithium and lead acid batteries. The starting point to model batteries is in fact the deep understanding of electrochemistry together with the specific chemistry of the type of batteries taken into consideration. Lead acid batteries, as previously said, are the most diffuse technology for off-grid applications while lithium batteries represent a likely alternative for the future. Finally, battery operational characteristic is reported: each physical phenomenon happening in the cell is linked to peculiarity in battery behavior at external terminals, which is important to observe and describe.

1.2 Electrochemical cell

The cell is the basic electrochemical energy device that converts electrochemical energy released by a red-ox reaction into electricity (and vice versa). A battery is composed by one or more cells that are connected in series or parallel according to the operational voltage and current required, and other secondary devices like diodes, fuse etc. The cell consists of three major components:

1. The anode, which is the electrode where the oxidation reaction ($red \rightarrow ox + ne^-$) occurs; the electrons are free to flow through the external electric circuit.

2. The cathode, which is the electrode where the reduction reaction ($ox' + n'e^- \rightarrow red'$) occurs; it withdraws electrons from the external electric circuit.

3. The electrolyte is a substance (liquid, solid...) that allows the ions transport between the two electrodes.

The energy and power characteristics of a cell follow directly from the electrochemical reactions and principles that are synthetically described as follow. It is worth to notice that the following section generally describes electrochemical energy conversion device, either a fuel cell and a battery.

Thermodynamics

For a general evaluation of an electrochemical cell, the thermodynamic principles have to be investigated. The two half-cell reactions that take place at the electrodes can be added together leading to the overall reaction of the cell. The basic thermodynamic equation for a reversible transformation is

$$\Delta G = \Delta H - T\Delta S \quad \text{and} \quad \Delta G^\circ = \Delta H^\circ - T\Delta S^\circ \tag{1.1}$$

where G is the Gibb's free energy of reaction, H is the enthalpy, T the absolute temperature and S is the entropy; the apex $^\circ$ stands for standard condition at T=25° and unit activity. Moreover, the Euler equation states that G is also equal to the sum of the chemical potential of the species in a system. This equation can be used also for the electrochemical potential

$$\tilde{\mu} = \mu_i + z_i F \varphi_i \tag{1.2}$$

(z=charge of component i, F=Faraday's constant, φ=electrical potential). It is possible to demonstrate that the maximum work achievable through a reversible transformation is

$$W = -\Delta G_{reaction} \tag{1.3}$$

When the cell is at the electrochemical equilibrium (but it in chemical disequilibrium, because at the two electrodes there are different species), i.e. when the circuit is open

$$d\tilde{G} = \sum_{i=1}^{M} \tilde{\mu}_i dN_i \tag{1.4}$$

becomes equal to zero and it is valid for both electrodes, leading to the expression for the Equilibrium Potential Difference between the two electrodes:

$$\varphi_{electrode+} - \varphi_{electrode-} = \frac{-\Delta G_{reaction}}{n_e F} = E_{eq} \tag{1.5}$$

Where n_e is the number of electrons involved in the overall red-ox reaction. The combination of 1.1 b and 1.2

$$W = E_{eq} n_e F = -\Delta G_{reaction} \tag{1.6}$$

proves that and ideal cell in electrochemical equilibrium extracts the maximum work, which is the net available electric energy, from chemical disequilibrium. When conditions are other than in the standard state, the Nernst law gives the Equilibrium Potential Difference

$$E_{eq} = E_{+}^{\circ} - E_{-}^{\circ} + \frac{RT}{n_e F} ln \prod_{i=1}^{M} a_i^{\nu} \tag{1.7}$$

Where a_i represents the activity coefficient of the species i, raised at its stoichiometric coefficient. E_{+}° and E_{-}° are the equilibrium electrode potential measured with respect to a reference electrode that by convention is the hydrogen one, that has "zero" potential.

Kinetics

Thermodynamics describe reactions at equilibrium and the maximum energy release for a given reaction [12]. Once the current is drawn from (or injected into) the cell, non-equilibrium conditions at electrodes and in electrolyte are set. Non-equilibrium oxidation and reduction affect the equilibrium electrode potential by a term η called "overpotential", negative for reduction and positive for oxidation. For example, when a battery is discharging, the operational voltage externally seen is lower than the ideal one (the Equilibrium Potential Difference).
This section will analyze the effect of the kinetics on overpotential governing the half-cell reactions occurring at the interface electrode/electrolyte. Each electrode does not react directly with charged species, but through a catalyst that enhances the reaction. According to catalysis' theories, a generic surface reaction $A\sigma + B\sigma \rightarrow P\sigma + Q\sigma$ is the rate determining step, thus the reaction that mostly affects the kinetic of the whole process. Considering the specific case of electro-oxidation (or reduction) of one electrode, transition state theory is used to described this type

of kinetic. In these treatments, the reaction proceeds towards a path involving an activated complex, where the rate determining step is the dissociation of the activated complex

$$ox * M \leftrightarrow red + M + e^{-} \tag{1.8}$$

where M is the catalyst molecule. The backward and forward reactions are considered. The forward and backward reactions can be described by heterogeneous rate constants kf and kb, respectively[2]. The rate of reaction is defined according to transition state theory:

$$\vec{r_f} = k_f e^{\frac{-\Delta G^f}{RT}} \qquad \vec{r_b} = k_b e^{\frac{-\Delta G^b}{RT}} \tag{1.9}$$

This equation is a more accurate version of the well known Arrhenius' law. The Gibbs free energy variation can be substituted with electrochemical potential, of reactants, products and activated complex using equation1.4. The role of electrons in the process is established by assuming that a fraction $\beta + E$ of the electrode potential represents the electrical potential of the activated complex for the forward reaction, while another fraction $\beta - E$ goes for the backward reaction[2]. β is called "symmetry factor": it is always greater than zero and it depends on the number of electrons involved in the red-ox reaction steps. For convenience, the reaction rates can be written in terms of net current density $i = F(\vec{r_f} - \vec{r_b})$ and with further mathematical steps, that are neglected in this treatment:

$$i = n_s F(K_o a_o^{\nu_o} e^{\frac{\beta_o F(E+\eta)}{RT}} - K_r a_r^{\nu_r} e^{\frac{\beta_r F(E+\eta)}{RT}}) \tag{1.10}$$

where n_s is the number of non-repeated electrochemical steps. Eq 1.10 is the well-known "Butler-Volmer equation", in which the exchange current density is directly related to the reaction rate constant, to the activities of reactants and products, and to the potential gradient through the double layer. When an electrode, which is a metal surface, is submerged in an electrolyte, the electronic charge on the metal attracts ions of opposite charge and orients the solvent dipoles, creating a layer of charge on the metal surface and another layer of opposite charge in the electrolyte. This charge separation establishes what is commonly known as the "double layer" [2] that induces an electrical field and behaves as a capacitor. When the exchange current is quite higher or lower than zero, hence far from the equilibrium, the Butler Volmer equation can be approximated with the "Tafel equation" for oxidation and reduction respectively:

$$i_\circ = n_s F(K_o a_o^{\nu_o} e^{\frac{\beta_o F(E+\eta)}{RT}}) \qquad i_r = n_s F(K_r a_r^{\nu_r} e^{\frac{\beta_r F(E+\eta)}{RT}}) \tag{1.11}$$

In many studies the loss for overpotential associated to kinetics of reactions at the interface electrode/electrolyte is called "activation polarization", as in [2] and [12].

Mass transport

In the previous section, the effect of kinetics of electrode's process on the overpotential has been investigated. Nevertheless, another important phenomenon for evaluating losses in a cell is the mass transport process to and from electrode surfaces. Mass transport of charged species and reactants follows the Nernst-Planck equation (the mathematical demonstration is not reported here):

$$N_i = -D_i^* grad C_i - z_i \frac{F}{RT} D_i C_i grad\varphi + C_i\omega \tag{1.12}$$

Where N is the molar flow, D is the corrected diffusivity, C is the concentration and z is the charge (0 or -1 or 1) of the species i, ω is the absolute velocity. This equation means that mass transport to or from an electrode can occur by three processes: (1) diffusion in a concentration gradient, (2) electrical migration and (3) convection, usually negligible. The molar flow of the Nernst-Planck equation is related to the current by the Faraday's law:

$$\begin{aligned} &j = n_i F N_i \text{ for reactant, } n_i \text{ is the number of electrons per mole of reactant} \\ &j = z_i F N_i \text{ for charged species} \end{aligned} \tag{1.13}$$

The combination of 1.12 and 1.13 underlines the influence of reactants transport on the overpotential that appears in Butler Volmer equation, since an expression of j as a function of the activity is obtained

$$\frac{j}{n_s F} \propto D_i(a_{i,bulk} - a_i) \tag{1.14}$$

Decreasing the local activity of reactants, the current increases and so does the flux. The difference in concentration existing between the electrode surface and the bulk of the electrolyte results in a concentration polarization. This is clear if the Tafel equation is reformulated as (for example during discharge)

$$\begin{aligned} E^+ + \eta^+ &= -b_r ln(-\frac{i_r}{n_r F K_r}) + b_r \nu_r ln a_r \\ E^- + \eta^- &= -b_o ln(-\frac{i_o}{n_o F K_o}) + b_o \nu_o ln a_o \end{aligned} \tag{1.15}$$

There exists a limiting current j_{lim} proportional to the bulk activity, because as the local activity approaches to zero, the overpotential theoretically increase to an infinite value. Concentration losses arises for high value of current, mainly determined by limited diffusion of active species to and from electrode surface to sustain the reaction, that is consuming reactants. Moreover, the electrolyte resistance to ion transport must be considered, that causes a linearly variable electrical potential of the electrolyte from anode to cathode. The expression for this loss can be generically written as:

$$\eta_{el} = \varphi_{el}^- - \varphi_{el}^+ \tag{1.16}$$

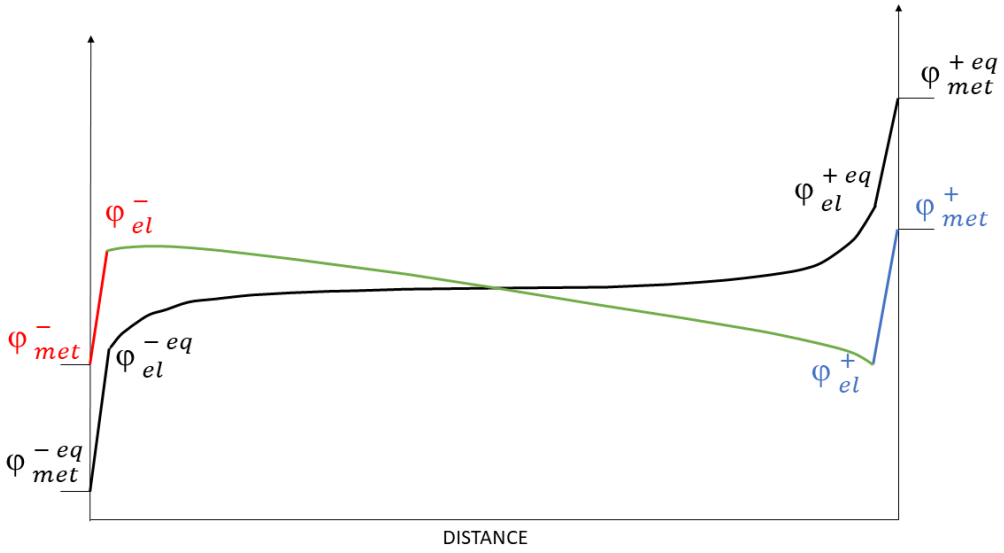

Figure 1.2: Variation of the electrical potential inside a generic electrochemical cell. [18]

It can be represented as an ohmic loss:

$$\eta_{el} = RI \tag{1.17}$$

The conductive diluent, and materials of construction of the electrodes, current collectors, terminals, and contact between particles of the active mass and conductive diluent or from a resistive film on the surface of the electrode [12] also contribute to the definition of the Ohmic resistance R.
Finally, the cell voltage during operation can be expressed as

$$\Delta V = E^{+} + \eta^{+} - E^{-} - \eta^{-} - \eta_{el} \tag{1.18}$$

and it can be represented on the polarization curve.

1.3 Lead acid and lithium ion batteries

Chemistry of lead acid batteries

The positive electrode of lead acid batteries is composed of lead dioxide, the active material of the negative electrode is metallic lead and the electrolyte is typically sulfuric acid dissolved in water. Chemical reactions occurring during charge and discharge are the following:

$$\begin{array}{lll} \text{Negative electrode} & Pb \rightleftharpoons Pb^{2+} + 2e \qquad Pb^{2+} + SO_4^{2-} \rightleftharpoons PbSO_4 \\ \text{Positive electrode} & PbO_2 + 4H^{+} + 2e \rightleftharpoons Pb^{2+} + 2H_2O \qquad Pb^{2+} + SO_4^{2-} \rightleftharpoons PbSO_4 \\ \text{Overall reaction} & Pb + PbO_2 + 2H_2SO_4 \rightleftharpoons 2PbSO_4 + 2H_2O \end{array} \tag{1.19}$$

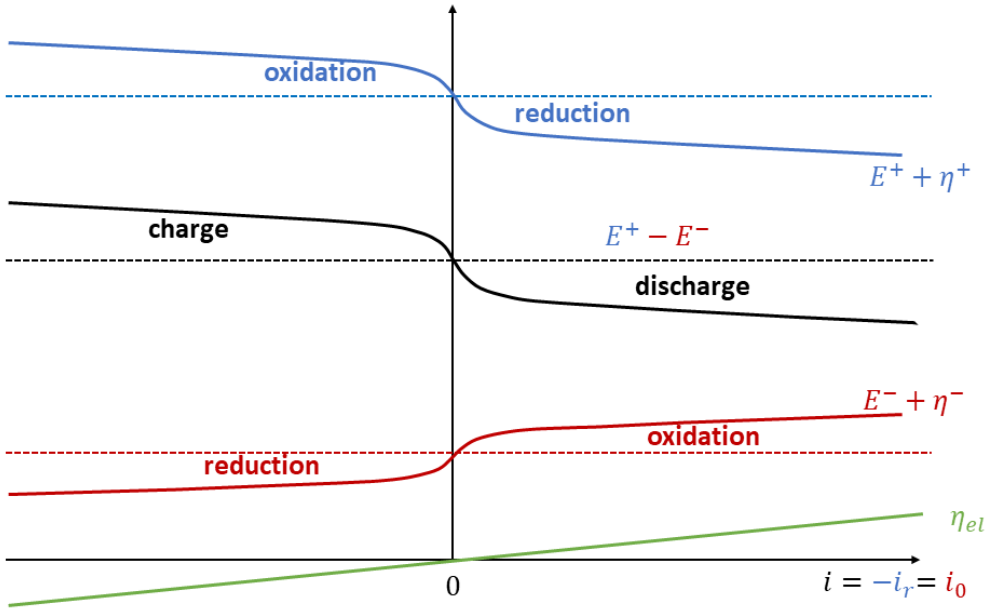

Figure 1.3: Polarization curve for a generic electrochemical cell. [18]

Internal chemistry is the same in all lead- acid batteries but they can be divided into two categories according to design considerations:

1. Flooded lead acid batteries contain liquid water that can eventually evaporate. They must be kept in upright position and regular maintenance is needed in order to assure the right amount of liquid is present in the electrolyte.

2. In valve regulated lead acid batteries, also called sealed batteries instead, electrolyte is completely absorbed in the separator and can be contained in two different ways. Gel batteries utilize a substance that transforms electrolyte into a gel, while Absorbed Glass Matrix use a glass matrix to contain the liquid electrolyte. These batteries are maintenance free and often used in off grid power systems, in combination with PV or wind turbines.

During lifetime lead acid batteries are subjected to some degradation phenomena that alter the chemical characteristics and the performances of the battery itself.

Degradation of lead acid batteries

The main degradation mechanisms occurring in lead acid batteries are listed in the following [19], [20].

- Corrosion: it mostly affects positive electrode and it is practically unavoidable because metallic lead in the positive plate grid is thermodynamically unstable. It is accelerated by overcharging and high temperature. In case of valve regulated lead acid batteries, corrosion can be a problem also for the negative

plate, in particular in lugs, straps and posts. To avoid this last issue, batteries are kept at high float voltage, which has adverse effect on grid corrosion.

- Positive active mass degradation and loss of adherence to the grid: during cycling, there can be a morphological shape change of the active mass. Loss of contact between grid and active mass leads to an increase of conduction resistance. Charging at high currents and high temperature can reduce this phenomenon.
- Sulfation: battery plates' active material, lead and lead dioxide react with the electrolyte during discharge, forming crystalline lead sulfate. If the battery is kept for a long time in discharged state, the crystals can grow and the process becomes irreversible. The consequence is a loss of active mass and hence loss of capacity in the battery. Moreover, lead sulfate deposits on battery plates, causing an increase of battery resistance to diffusion. Sulfation is enhanced when batteries are not being charged sufficiently or not frequently enough. High temperature could increase sulfation during rest periods while it could diminish it during cycling.
- Stratification: during cycle life, electrolyte tends to become non uniform. Ions, which are heavier than water tend to accumulate on the bottom of the battery, creating a stratification. Battery reaction are in this way possible only on specific parts of the battery and this leads to a decrease in capacity. It is enhanced by long periods of low SOC and non complete charges.
- Short circuits: they could happen across the separator at prolonged deep discharge. In this case acid concentration is really low and lead sulfate could precipitate forming metallic lead on the separator ("metallization"). Short circuits could also be provoked on positive plate by active mass degradation. They cause insufficient charge of the battery and consequent sulfatation
- Gassing: when the cell voltage is really high, hydrogen could form at the negative electrode and oxygen at the positive. This is one of the most important side reaction in lead acid batteries. Hydrogen must be vented away causing loss of water. This leads to an increase in acid concentration in the electrolyte that enhances the previously described degradation mechanisms.

Chemistry of lithium ion batteries

Negative electrode active material is composed in the majority of cases of lithiated carbon with layered structure similar to graphite. Positive electrode is instead made of lithium metal oxide; Li ions must be able to freely diffuse through their crystals. There is a great variety of chemistries, especially due to the different possible materials of positive electrode, while negative electrode is constituted mainly by graphite.

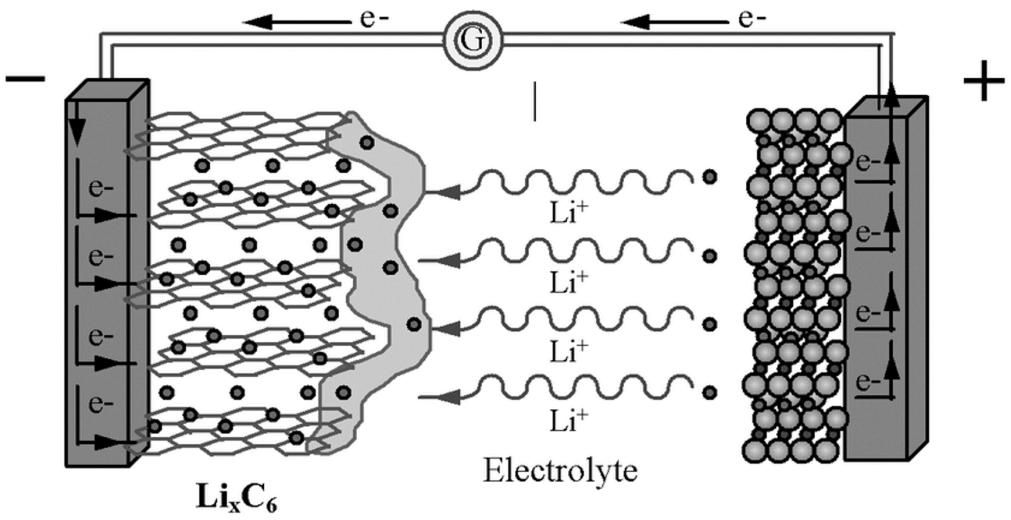

Figure 1.4: Schematic representation of a lithium ion battery [21]

Electrolyte can be composed either by a lithium salt dissolved in an organic solvent (Liquid Organic Electrolyte Batteries) or it can be made of a solid polymeric matrix (Polymer Electrolyte Batteries). The latter provides a higher safety in spite of lower conductivity, but the former still represents the most used technology in off-grid applications.

Lithium ion batteries are based on intercalation reactions involving Li ions, which move between positive and negative electrode during charge and discharge. Intercalation process is composed of three steps: migration of solvated Li_+ ions, desolvation and injection of Li_+ ions into the vacancy structure, diffusion of Li_+ ions into the host structure.

In case of Lithium cobalt oxide cell, negative and positive electrode reactions are respectively:

$$\begin{aligned} &\text{Negative electrode} \quad Li_xC_6 \rightleftharpoons xLi^+ + 6C + xe \\ &\text{Positive electrode} \quad xLi^+ + Li_{1-x}CoO_2 + xe \rightleftharpoons LiCoO_2 \end{aligned} \tag{1.20}$$

For a lithium iron phosphate the electrochemical reactions are:

$$\begin{aligned} &\text{Negative electrode} \quad Li_xC_6 \rightleftharpoons xLi^+ + 6C + xe \\ &\text{Positive electrode} \quad xLi^+ + Li_{1-x}FePO_4 + xe \rightleftharpoons LiFePO_4 \end{aligned} \tag{1.21}$$

The negative electrode reaction is the same for both lithium cobalt and lithium phosphate since the negative electrode is made with the same material.

In table 1.2 are reported the different types of lithium ion technologies. Lithium cobalt oxide batteries are well developed and well known but they are not commonly used in stationary application; lithium nickel cobalt aluminum cells and lithium titanium oxide cells are not suitable for off-grid applications, especially in DCs, due to the very expensive catalyst's materials. Lithium manganese oxide technology has

low cost due to manganese abundance, very good thermal stability and high power capability; nevertheless, its moderate cycle life and low energy performance are insufficient for off-grid applications [11]. Lithium iron phosphate batteries present very good thermal stability, very long cycle life and calendar life, very good power capability, low costs, and low degradation in RES applications [11]; this technology could be especially suited for off-grid renewable applications [15].
Equally to lead acid batteries, also lithium ion batteries face during their lifetime degradation phenomena, but they are different from lead acid batteries due to the dissimilar chemical composition.

Degradation of lithium ion batteries

Aging phenomena occur mainly at the electrodes, with different characteristics on anode and on cathode [24].

Negative electrode degradation

- Formation of passivated surface layer: when the battery is in the charged state, the potential of the negative electrode is low, at a voltage that is outside the electrochemical stability window of electrolyte components. Hence, reduction reactions of electrolyte components take place at the electrolyte/electrode interface. These reactions consume lithium ions, and at the same time produce products that accumulate on electrode surface, building up a protective layer, called Solid Electrolyte Interface (SEI). SEI formation takes place mainly in the first few charge/discharge cycles, leading to a rapid decrease in battery capacity at the beginning of its life. The layer partly protects the anode from further oxidation, but it continues to stabilize and grow during all the life of the battery, playing a major role on the resistance increase and decrease in nominal capacity. In particular, when battery is subject to high stresses due for

Specifications	**LCO**	**LMO**	**NMC**	**LFP**	**NCA**	**LTO**
Cathode material	$LiCoO_2$	$LiMn_2O_4$	$LiNiMnCoO_2$	$LiFePO_4$	$LiNiCoAlO_2$	Various
Anode material	Graphite	Graphite	Graphite	Graphite	Graphite	$Li_4Ti_5O_{12}$
Energy density [Wh/kg]	110-190	100-120	150-220	90-120	200-260	60-80
Power density [W/kg]	600	1000	500-3000	1400-2400	1500-1900	750
Cycle life	500-1000	700-1000	2000-3000	> 3000	> 1000	3000-7000
Cell nominal voltage V	3.7	3.8	3.6	3.3	3.6	2.4
Initial cost [$/kWh]	200-400	300-850	450-850	350-1150	250-950	550-1900

Table 1.2: Characteristics of different chemistries of Li ion batteries. Costs refer to cell prices for utility scale applications [22], [23]

example to high currents, cracks can propagate through the SEI layer, leading to its decomposition and a successive reforming.

- Metallic lithium plating and lithium dendrite growth: it might occur at low temperature and high discharging rate. What happens is that lithium, due to low diffusion, deposits on the surface of graphite layer instead of intercalating into the lattice of the carbon. Li metal will subsequently react with electrolyte accelerating the degradation of useful lithium for evaluating capacity of the battery.

- Graphite exfoliation and cracking: caused by solvent co-intercalation, electrolyte reduction inside graphite and gas evolution. The consequent loss of active material and of lithium leads to a capacity decrease. It is enhanced by high state of charge.

- Contact loss of active material particles and change in porosity: volume changes of active material during charge and discharge cycles affect the mechanical structure of the composite electrode. High current rate associated with high cycle depth and high state of charge enhance the phenomenon leading to resistance rise and capacity decrease.

- Current collector corrosion: there might be reactions between current collector and electrolyte that lead to loss of contact between current collector and other electrode components. This phenomenon is enhanced at low state of charge, when the potential of the anode is high, and leads to an increase of the resistance.

- Binder decomposition: increased by high temperatures and high state of charge.

Positive electrode degradation

- Lithium metal oxide structural disordering.

- Metal dissolution: typical in lithium manganese spinel, at elevated temperature manganese dissolves in the electrolyte, leading to capacity fade. Also, when dissolved manganese ions arrive to the anode, they promote the formation of SEI layer leading to further electrolyte decomposition. It can happen at both high or low potentials, i.e. extreme SOC values.

- Formation of surface layer: electrolyte oxidation reactions with consequent formation of surface layers are seen to occur in lithium nickel cobalt oxide cathodes. They are enhanced by high temperatures and high SOC and induce an increase of the resistance.

- Conductive agent oxidation.

- Current collector corrosion.
- Binder decomposition.

The last three phenomena entail loss of contact and resistance increase.

1.4 Battery operational characteristics

Regardless from the technology, it is necessary to know battery external terminal characteristics to reproduce as accurately as possible BESS operational behavior in a simulation model. In the next paragraphs a list and description of the most important characteristics is reported.

Capacity

Capacity represents the specific energy of a battery and it is expressed in ampere-hours [Ah]. Ah is the discharge/charge current a battery can deliver over time. Commonly, on battery datasheet it is written the nominal capacity, which represents the maximum capacity that is possible to store or discharge with a given current, reaching the voltage limits of the battery. However, during operation the final capacity depends on the current, or more precisely on the C-rate.

C-rate

The C-rate specifies the speed a battery is charged or discharged.

$$C_{rate} = \frac{i}{C_n} = [\frac{1}{(h)}] \tag{1.22}$$

At 1C, the battery charges and discharges the nominal capacity in 1 hour time. At 0.5C, the current is half and the time is doubled, and at 0.1C the current is one-tenth and the time is 10-fold.

State of charge (SOC)

The state of charge SOC is usually expressed as a fraction (or percentage) and defined as

$$SOC = SOC(0) - \frac{1}{C_{ref}} \int_0^t I dt \tag{1.23}$$

or equally, if the battery is completely charged when the the discharging process begins

$$SOC = 1 - \frac{C}{C_{ref}} \tag{1.24}$$

According to these definition, it represents an abstract relative characteristic, defined with respect to a reference capacity in Ah. The current I indeed is expressed in

amperes. The reference capacity is usually the nominal capacity of the cell; however, another option is to use as reference capacity the effective dischargeable capacity at specific operating conditions.
From a strictly chemical point of view, the SOC is equivalent to the activities of reactants and products of the electrochemical reactions. The problem with this definition is that, for a battery, it is not possible to know precisely the whole chemistry, because it is a secret of each battery producers.
Another quantity is commonly utilized, namely the Depth of Discharge (DOD). It is defined by international standards as SOC variation during cycling: $DOD = \Delta SOC$ Some authors, instead, define it as the 1's complement to the SOC: $DOD = 1 - SOC$ [25].

Open Circuit Voltage (OCV)

The voltage, measurable at the external terminals when the cell is at open circuit (OCV, Open Circuit Voltage) and when it is in thermal and electrical stability, is given by the Nernst law 1.7. It depends on chemistry, on SOC and on the number of cells connected in series; it shows a non-linear trend as function of SOC.
Two examples of discharge curves (OCV as a function of SOC) are reported in figure 1.5(a) and figure 1.5(b): they refer respectively to the lithium ion cell and the lead acid cell that have been examined for the models proposed in chapter 4. Notice that the lithium OCV is much more non-linear than the lead one.

Voltage

Batteries are marked with nominal voltage which is 5-7 % lower than the open circuit voltage (OCV) of a fully charged battery [26]. The closed circuit voltage (CCV) is the operating voltage, described in equation 1.18. As already explained, the voltage at the external terminals strictly depends on the operational current (the higher the current, the lower the voltage and the capacity that can be discharged) and on the state of charge. Batteries have a maximum and a minimum voltage that is possible to reach in order to prevent permanent damage to them. Voltage limits are different according to the specific chemistry of the battery.

Non-linearities

Modeling the behavior of batteries is complex, because of non-linear effects during operation. In the ideal case, the voltage remains constant until all the stored energy is consumed and after that the voltage instantly goes to zero. The ideal capacity of a battery would be constant for all currents and state of charge, and all energy stored in the battery would be provided to the load. However, for a real battery the voltage and the capacity are not constant [27].

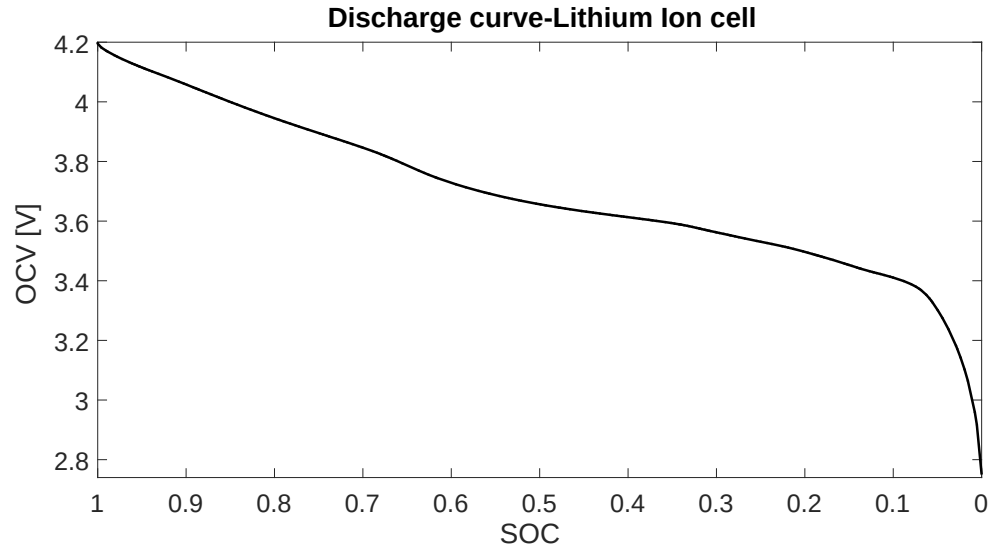

(a)

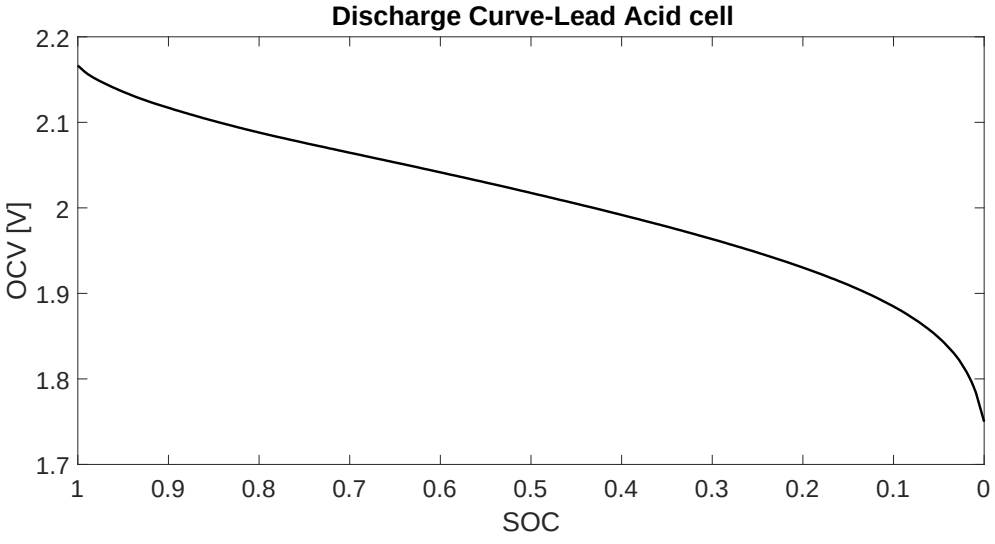

(b)

Figure 1.5: OCV of lithium ion cell(a) and lead acid cell(b)

1. **Rate capacity effect**

   The effective capacity that can be discharged from a cell, with the same

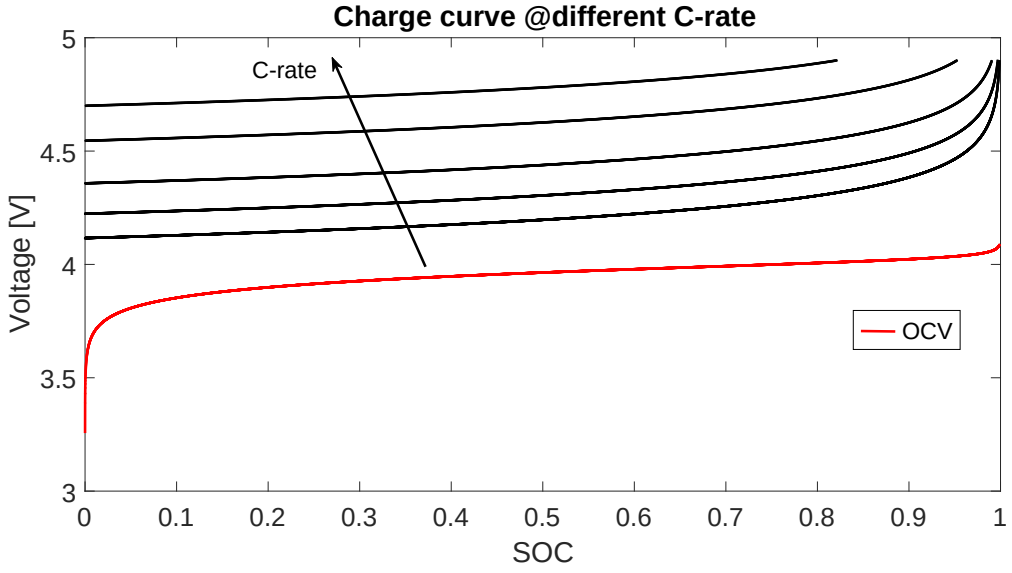

(a)

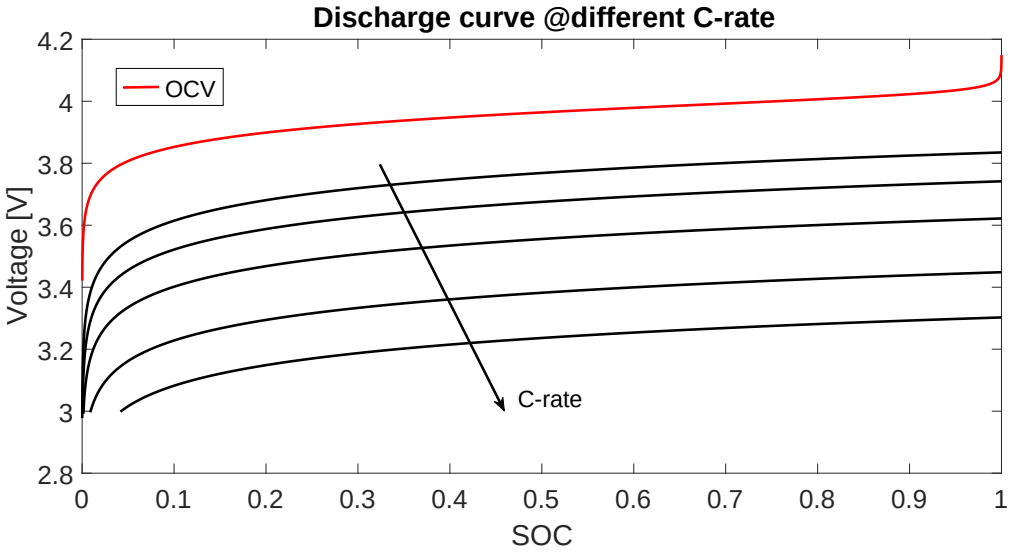

(b)

Figure 1.6: Charge curves at different C-rates(a) and discharge curves at different C-rates(b)

initial conditions, depends non linearly on the value of the applied current. The voltage slowly drops during discharge and the higher the current rate the lower is the effective capacity, meaning that the voltage limits are reached earlier [27].

The figures 1.6(a) and 1.6(b) show the evolution of the voltage over time at different C-rates; notice that for high C-rate the voltage reaches the limiting value without completely charging/discharging.

2. **Recovery effect**
   During idle periods or very low discharge, batteries can recover to a certain extent the capacity that has not been exploited during periods of very high discharge rates. Indeed, a cell, at same initial conditions and with the same value of current, allows to withdraw a higher capacity if the discharge process is an intermittent one with respect to a continuous discharge. Moreover, during idle periods it is possible to see in the discharge curve that the voltage measured at the external terminals tends to reach the value of the OCV corresponding to the actual SOC, provided that the resting time is long enough. The resting time depends on the type of the battery (chemistry, materials,...) and on its age. In this way, the effective capacity is increased and the battery lifetime is lengthened [27] .

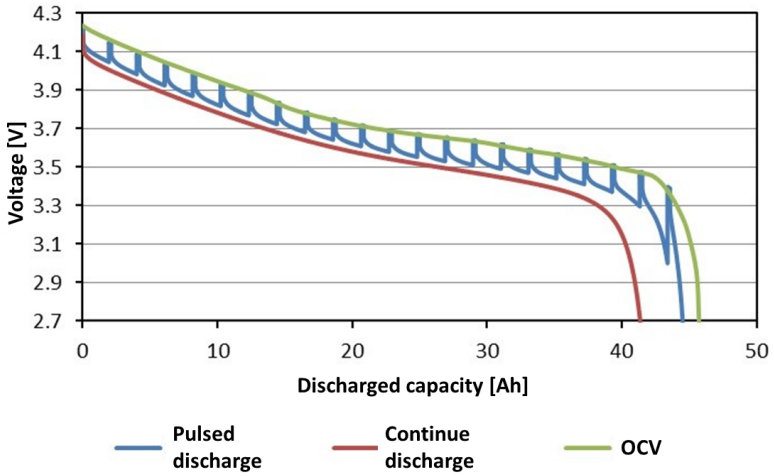

Figure 1.7: Recovery effect [28]

3. **Ohmic voltage drop**
   If the battery stays at open circuit for a sufficient time, it reaches the open circuit voltage. Starting from this conditions, when a load is applied to the battery it is possible to observe a sudden voltage drop in the first seconds of the discharge. This variation cannot be caused by the change in the SOC, since the transient response of the battery needs more than few seconds to change its SOC. Moreover, the higher the current the higher this voltage drop is; as long as the behavior resembles a resistance the phenomenon is called Ohmic voltage drop. The same consideration can be done in charge case.

   For all types of batteries these effects occur. However, the extent to which they are exhibited depends on the battery type.

4. **Self-discharge effect**
   The effect of self-discharge mainly appears in lead acid batteries, while in

lithium ion batteries it is much less relevant.
If a charged battery is not used for long period of time, it will lose part of its initial capacity even if no load is applied. This phenomenon is known as self-discharge. Nevertheless, according to how much the battery has been stressed during its lifetime (i.e., high c−rates), self−discharge can be higher or lower for the same type of battery. The extent of the capacity lost due to selfdischarge depends also on the ambient temperature: a battery kept in a cold environment faces a lower self-discharge effect [29].

What appears with evidence from the previous analysis, is that batteries are complex systems, with strong non linearities and time dependent behavior. Accurate models are needed in order to predict their cycling and lifetime characteristics and compute their costs. However, when one wants to take into account all the different phenomena, models risk to become too detailed and not easily viable with short enough computational time. Some approximations are needed, especially when battery models are used to dimension off grid power systems, where the focus is on the optimization of the whole plant. In the following section a detailed review of batteries' modeling approaches is reported.

Chapter 2

Review of battery modeling

2.1 Introduction

To predict and analyze battery behavior in many different operational conditions, it is often required the aid of the calculator's simulations, because an "in situ" diagnosis and analysis result in a very time-consuming and expensive operation. With this perspective, an accurate modeling of battery behavior is strictly necessary in order to obtain correct simulations. In the literature review, the models have been grouped into four general different approaches:

1. Electrochemical: electrochemical modeling is usually based on equations for mass, energy and momentum transport of each species for each phase and component of the cell. It typically involves a system of coupled partial differential equations that must be solved in time and spatial dimensions. Electrochemical models are able to predict local distribution of concentration, electrical potential, current and temperature inside the cell, besides current and voltage at the external terminals. Therefore, they tend to be relatively complex and they typically have various parameters to determine through several experiments [30].

2. Analytical: they are based on an abstract vision of the electrochemical cell behavior. The battery is described by analytical equations that do not take into account electrochemical processes, but that are empirically fitted. These models usually focus on the evaluation of the SOC of the battery based on energy or current balances. Voltage characteristic of the battery is normally neglected. Analytical models' complexity can vary but they are in general simpler than other model categories: for this reason they are often used in dimensioning tools. [31]

3. Electrical: batteries can be represented by equivalent electric circuits, that aim to model as accurately as possible battery operation, especially the voltage and

current characteristics at the external terminals. These models could be very simple, comprising few circuital elements (e.g. voltage source to represent energy stored and a resistance in series to take into account losses), or more complex, with each circuital element related to a precise physical phenomena occurring in the cell. Due to the wide spectra of possible equivalent circuits, these models find application in a broad range of sectors, comprising battery monitoring and design. [31]

4. Stochastic: stochastic models describe charging and discharging phenomena as stochastic Markovian processes, because the complex electrochemical reactions are significantly affected by random variables as ambient temperature and usage profile [32]. The battery is represented by a Markov chain with N+1 states of charge, enumerated from 0 to N. The number of the battery's state is linked to the number of units of charge available in the battery [33].

When modeling a battery, whatever approach is followed, two aspects have to be taken into consideration:

- State of Charge (SOC): a correct estimation of battery SOC allows to understand the amount of charge and hence energy that can be stored or provided by the battery. In the framework of BESS modeling for off-grid dimensioning tools applications, it is useful to predict the amount of energy not provided to the load, i.e. the loss of load.

- State of Health (SOH): as explained in chapter 1, batteries have a limited lifetime due to irreversible degradation processes happening inside the cells. The rate of degradation depends on batteries operational and floating conditions. An accurate evaluation of batteries' SOH allows to account for BESS replacement costs which, when speaking as an example about stand alone sizing tools, contributes to the total plant cost.

In the following sections, the models found in scientific literature for estimating batteries' SOC and SOH are reported, divided into the four approaches listed at the beginning of the chapter.

2.2 Battery Models comparative analysis: SOC estimation

In the present section, different battery models are reported, classified into the methodologies previously described. The focus is placed on the approaches followed to predict battery SOC and on their effectiveness.

Electrochemical models

The starting point of this typology of models is the accurate description of a battery through its electrochemical governing equations (see section 1.2).
A problem consisting of a system of partial differential equation, to be solved in time and space domain, is set. The independent variables are numerous, comprising concentration of species and potential across the cell. State of Charge of the cell is strictly related to concentration of reactants, and its evolution in time can hence be determined, solving the problem for a given load profile.
In order to make the system numerically solvable the structure of the cell needs to be simplified. The most common approaches, utilized in particular to model lithium-ion cells are the following:

- **Pseudo two dimensional model (P2D)** Electrodes are assumed to be composed of a lattice of identical spherical particles. Li ions can move through two spatial coordinates: a radial coordinate r, across the spherical particles of active materials in the electrodes and a linear coordinate x, going across the cell from the negative to the positive electrode. It is called pseudo 2D model since the radial coordinate does not represent a physically new dimension.
  Doyle, Fuller and Newman where among the first authors to conceive a model based on these assumptions[34]. They developed Dualfoil [35], which is a Fortran program based on their electrochemical model. It is widely used in order to simulate battery response to a certain load profile (power/current) and to check the accuracy of new simplified models.

- **Single particle model (SP)** Electrodes are assumed to be composed of one single spherical particle whose area is equivalent to the surface area of solid active material in porous electrode. Porosity is neglected and lithium ions surface concentration is assumed constant along the x-axis of the electrode. Solid phase potential is hence only a function of time t. The solving process is much faster than P2D model but the model is less accurate.

In [36] and [37] the authors compare the 2 models in order to assess accuracy and time requirements. SP results less time consuming but not really accurate at high discharge or charge currents.
Finite element, partial differential equation solvers are needed in order to simulate battery cycling. The main methods found in literature for simulations can be categorized as [38]:

- DUALFOIL, based on the Newman's BAND subroutine developed in FORTRAN. This is a finite-difference method.[35]

- Finite volume method (FVM) that discretizes time with various schemes.

- COMSOL Inc. Multiphysics [39],[40]. They employ respectively a finite element method(FEM) and a finite difference method (FDM) and they offer an implementation for the P2D model.
- Finite difference method (FDM) or reformulation schemes in spatial coordinates using adaptive solver such as FlexPDE [41]and DASSL [42] in time.

Electrochemical models need the determination of a large set of cell parameters, that can be derived with various techniques, as for instance Electrochemical Impedance Spectroscopy. Their complexity makes electrochemical models not suitable for real time monitoring and for dimensioning tools, in which a balanced compromise between accuracy and fast simulations is required. They are usually employed for cell design simulation, in order to enhance cell geometry and material. Moreover, they can be used as a reference in order to validate the accuracy of more simplified models.
In the following subsection, an example of pseudo-two-dimensional model is reported since it is the most common approach found in literature.

Pseudo-two dimensional model
The model proposed by Doyle et al [34] is here analyzed, since it is one of the very first works that adequately models the electrochemical cell and many subsequently developed models are based on it.
It has been developed for a lithium polymer cell, but in literature this kind of model can be found also for other types of batteries [43].
The active materials are polymer electrolyte, metallic lithium negative electrode and a porous positive electrode.
The assumptions made by the authors are:

- The diffusion coefficient for the lithium ions in the positive electrode active material is constant. This assumption allow the authors to use a superposition integral for solving, being mathematically advantageous. In the model developed by Dees et al. [30], the authors base their work on the model of Doyle et al., but they improve it by changing this assumption: in their model, the diffusion coefficient for the lithium ions in the positive electrode active material depends on its concentration.
  The distance across the cell is the first dimension and the radial distance of the assumed spherical particles is the second.
- For the polymer electrolyte and the cell in general, the all solid-state system and assumption of isothermal operation allows the momentum and thermal transport effects to be neglected.

The transport equations for the electrolyte are mass transfer expressions for each species and electroneutrality, employing the Nernst-Planck equation (eq 1.12) that

can be related to current density by the Faraday's law.
A material balance on the salt in the separator is set and also the equation for conservation of charged species.
The positive electrode is composed of the polymer electrolyte, a conducting material and the catalyst's particles. These phases are treated as superimposed continua, so that the material balance on the lithium in the polymer/salt can be easily established.
Transport of lithium through the active positive electrode material (spherical particle) is a diffusion mechanism that follows Fick's law (eq. 2.11).
The current flowing inside the electrolyte and electrodes follows the ohm's law. The electrodes' processes are described by Butler-Volmer kinetics (eq. 1.10). In addition, the variation of current with solid and solution phase concentrations is accounted for by using a concentration-dependent exchange current density.
The open circuit potential of electrodes changes with the amount of lithium inserted and is expressed as

$$U_{OCV} = U^0 - U^0_{ref} + \frac{RT}{F}(ln(\frac{c_{max} - c_s}{c_s}) + \beta c_{max} + \varsigma) \tag{2.1}$$

which is coherent with the Nernst law (eq 1.7). This is similar to the expression proposed by West et al. [44]. c is lithium ions concentration and the parameters β and ς represent activity corrections and are taken to be constants. They can be fit from experimental data on open-circuit potential versus state of charge.
Boundary conditions are necessary to solve partial differential equations.
The dependent variables of concentration, potential, reaction rate, and current density appear in more than one equation, and therefore they must be solved simultaneously. In addition, material properties often vary considerably with concentration. The result is a system of coupled partial differential equation that cannot be solved analytically. Thanks to the first assumption of [34], mathematically speaking the equations result in a single-dimension problem. On the contrary, the hypothesis of variable diffusion coefficient in [30] makes the system a pseudo two-dimensional problem, which is more difficult to be solved but also more accurate for a wider range of cell types. There are many options for numerically solving a pseudo two-dimensional problem.
The most common used technique is the finite-difference method. The model can be discretized with a determined number of nodes in the spatial direction for each variable. The active positive electrode particles were radially discretized using a finite difference form of the differential diffusion equation. Two different solvers have been used to solve partial differential equation in time and space: the first one is a finite-different based one dimensional solver developed by Verbruggee and Gu [45] and the other one is FlexPDE. The advantage of using adaptive solvers is the increase in simulation speed compared to fixed-time schemes.

Multiscale, multidimensional, and multiphysics electrochemical-thermal coupled models enable to add more accuracy for describing all the phenomena occurring inside a cell [38]. For instance, the model proposed by Parthasarathy M. Gomadam et al. [43] for a lithium ion battery is based on the previously described governing equations, including also an energy balance for temperature variation inside the cell. Moreover, the authors tried to evaluate the dependency on concentration of the diffusivity with algebraic equation.

Analytical models

Few simple equations are used in order to describe battery behavior. Values of parameters can be empirically found by experimental data or by manufacturers' datasheet. In the majority of cases there is no direct reference to the voltage variation of the battery, and the SOC is computed through charge or energy balances.
Due to the simplicity of these models, they are the ones more often employed in dimensioning tools [46], [47]. Their simplicity comes however at the expenses of accuracy and errors in predicting battery performance could be relatively high. In the following paragraphs, four different approaches of growing complexity are presented.

Empirical model-battery efficiency
The simplest approach, is to describe the battery as a system that, due to non-ideal behavior, dissipates some energy. A round trip efficiency can be defined as the ratio of energy provided by the battery during discharge over energy absorbed during charge, at a given C-rate and SOC variation.
Knowing the total power required or provided by users to the battery, energy actually entering or exiting the batteries depends on the efficiency. In particular, energy entering or exiting the batteries is the integral of power over time and it has to be multiplied by the efficiency when power is provided to the battery and divided by the efficiency when released. SOC can be calculated as the energy accumulated over the maximum storable energy (given by manufacturers).
Efficiency can be considered constant, as in [48] or a decreasing function of charge or discharge power or analogously current. Massoud Pedram and Qing Wu in [49] wrote the battery efficiency as a linear or quadratic function of the load current:

$$\begin{aligned} \eta &= 1 - \beta * I \\ \eta &= 1 - \gamma * I^2 \end{aligned} \tag{2.2}$$

Describing battery behavior by simply utilizing an efficiency, is a way to estimate energy providable by the battery utilizing data given in battery datasheet. No complex experimental parameters evaluations are required. However, battery dynamic response, as well as voltage characteristics are totally ignored.

Peukert's Law
It was developed in order to model the change in capacity of lead-acid batteries at different discharge rates.[31]
The time to discharge a battery is given by:

$$t = \frac{C}{I^k} \tag{2.3}$$

I is the discharge current, and C is a constant, empirically found and similar to battery nominal capacity [Ah]. K is the Peukert coefficient, it would be = 1 in case of an ideal battery, whose capacity is independent on the current. It is instead > 1 for real batteries. K varies with temperature and aging, increasing with the life of the battery. So, the higher the current and the higher k, the shortest the time to arrive at complete battery discharge and hence the smaller the actual discharged capacity: $C_{dis} = I * t$. The output of Peukert's law is hence similar to the variable efficiency described in the previous subsection (higher current leads to lower discharged energy). The difference is that the emphasis is on accumulated charge instead of stored energy. In the case of variable current, an average value of current during the time frame can be computed. To estimate SOC of a battery during discharge, Peukert's law could be coupled with the Coulomb Counting method:

$$SOC = \frac{\int Idt}{C_{ref}} \tag{2.4}$$

C_{ref} is the reference battery capacity, it could be the nominal battery capacity or the actual maximum dischargeable capacity, calculated by Peukert's law at the given charge or discharge current.

Shepherd model
The model presented in [50] describes the battery through the equation

$$y_k = E_0 - Ri_k - \frac{\mu}{SOC_k} \tag{2.5}$$

where y_k is is the battery voltage, k is the time index, E_0 is the battery constant voltage, R represents the internal resistance of the cell, i_k is the cell current and μ is a parameter for fitting. This equation is valid both during charge and discharge. Despite using electric quantities, this model does not represent battery as an equivalent electric circuit. In fact, it tries to follow the voltage characteristic of the cell via an analytical expression.
This model is particularly suitable for simulating lead acid batteries in stand-alone PV systems [51]. It has also been used for battery management systems of lithium batteries in hybrid electric vehicles [52]. Copetti et al. in [53] tested Shepherd model with lead acid battery and the results showed an adequate reproduction of battery behavior during discharge while it presented significant errors during charge

and overcharge. Hence, the authors proposed an improvement of Shepherd model in order to employ it for PV system simulation. The main changes were a correction factor for temperature variation, an expression for overcharge and an expression for resistance variation with current and SOC.
Hybsim [6], the software tool for cost-benefits analysis of remotely located hybrid systems, models energy storage via a modification of Copetti and Shepherd equations [54]. For more details about the software see chapter 3.
Trembley et al.proposed in [55] a parametric model, as an improvement of Shepherd model to avoid simulation instability.
The authors developed an equation, aimed to accurately model battery open circuit voltage.

$$E(Qi) = E_0 - K\frac{Q}{Q - Qi} + Ae^{-BQi} \tag{2.6}$$

where E is the open circuit voltage that depends on battery capacity Q[Ah], Qi is the actual battery charge [Ah] (integral of current over time), A is the amplitude of the discharge curve exponential zone and B $[Ah^{-1}]$ is the time constant inverse of the exponential zone. The terms are related to the shape of the discharge curve (see fig. 2.1).

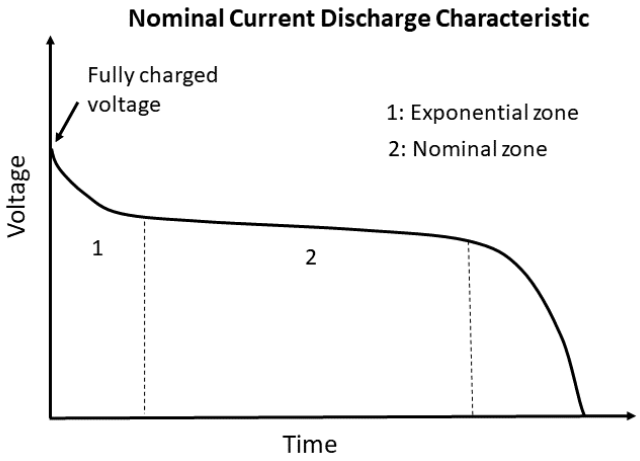

Figure 2.1: Discharge curve [55]

The model is integrated in Matlab-Simulink Sim-PowerSystems library and it is utilized for hybrid electric vehicle simulations as it can accurately represent battery behaviour.

KiBam model
The authors represent the battery with a hydraulic model [56].
The charge stored in the battery is split in two tanks, one containing the available charge (q1), and the other the bound charge (q2). The first one is the charge immediately accessible by the load, while the second one is the charge chemically

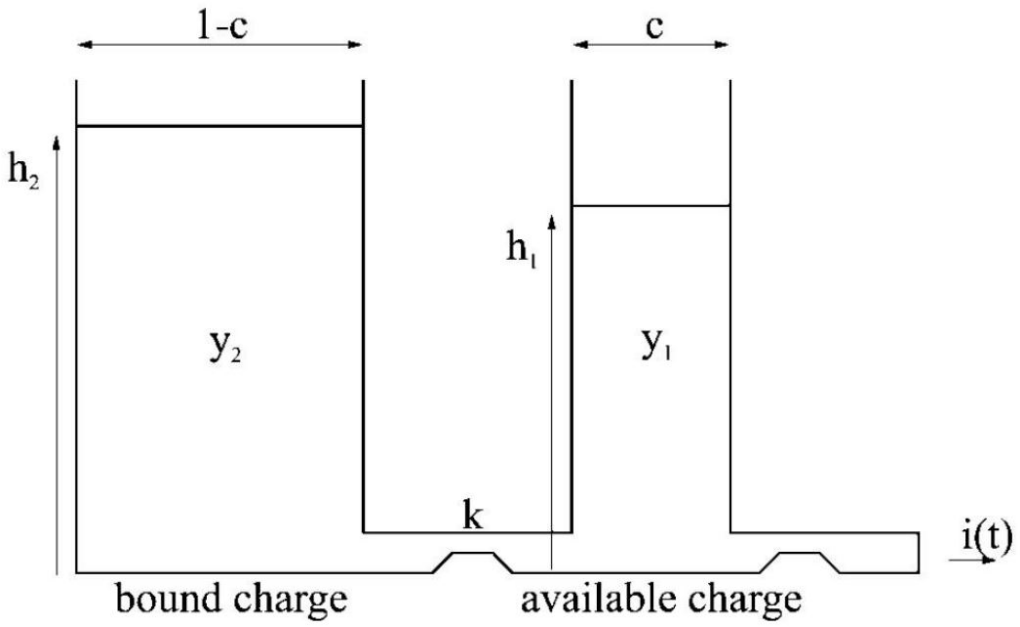

Figure 2.2: KiBam model [31]

bound. Battery is considered totally discharged when q1=0. The tanks are divided by a valve with a fixed conductance k', by which the bound charge becomes available. k' accounts for the rate constant of the cell's electrochemical reaction and the rate of diffusion processes: for this reason, the model is called kinetic battery model (KiBaM).
Bound charge becomes available at a rate which is proportional to the difference in head of the two tanks.
The depth of each tank is set equal to 1, the volume is equal to the charge stored (maximum total volume =qmax) and the widths are c for available charge tank and 1-c for the other one. Total area is hence 1.
Given a constant charge/discharge current, the equations describing the battery dynamic behavior are the following:

$$\begin{cases} \frac{dq1}{dt} = -I - k'(h1 - h2) \\ \frac{dq2}{dt} = k'(h1 - h2) \end{cases} \tag{2.7}$$

$$\begin{cases} h1 = q1/c \\ h2 = q2/(1-c) \end{cases} \tag{2.8}$$

A new rate constant k is defined: $k = k'/(c * (1-c))$. Solving the differential equations, available charge as a function of time can be found.

$$q1 = q1_0 e^{-kt} + \frac{(q_0 kc - I)(1 - e^{-kt})}{k} - \frac{Ic(kt - 1 + e^{-kt})}{k} \tag{2.9}$$

$q1_0$ and q_0 are are the amount of available and total charge at the beginning.
SOC of the battery can be computed as q1/qmax being qmax the maximum charge

providable by the battery.
The parameters that need to be found are qmax, the maximum capacity of the battery, c, the available fraction and k the rate constant. Variation over time of open circuit voltage (E) can be computed as a linear function of the state of charge:

$$E = E_{min} + (E_{max} - E_{min}) * \left| \frac{q1}{q1max} \right| \tag{2.10}$$

It is worthwhile to mention that the important part of this work is related to variation of charge with time and the voltage variations are just accounted for with a linear relationship, not derived by physical laws or experimental data.
The battery model assumes explicitly that charge is conserved under charge and discharge. Energy, however, is not conserved. When a load is applied to the battery, the available charge reduces, and the height difference between the two tanks grows. When the load is removed, charge flows from the bound-charge tank to the available-charge tank until h1 and h2 are equal again. So, during an idle period, more charge becomes available and the battery lasts longer than when the load is applied continuously. In this way the recovery effect is taken into account. Also, the rate capacity effect is covered, since for a higher discharge current the available charge well will be drained faster, less time will be available for the bound charge to flow to the available charge. Therefore, more charge will remain unused, and the effective capacity is lower. This model was proposed by the authors as a valid substitute of circuital models, its advantages being the small amount of parameters required, often derived simply by manufactures' data. One of the main drawbacks is that it is mostly applicable to lead acid batteries. HOMER [5] and Hybrid2 [7] , software tools for microgrid design, represent the battery through a KiBam model.

Diffusion model
This model was proposed by Rakhmatov and Vrudhula in [57], [58] and is based on the diffusion of the ions in the electrolyte. It was validated with data of lithium-ion batteries.
The authors describe the evolution of the concentration of active species in the electrolyte during battery discharge. Battery discharge time under a given load is predicted. Processes occurring at the electrodes are assumed to be identical and the symmetry of the battery allows to take into account only one electrode. The picture shows the steps occurring in the semi-cell during discharge. At first the battery is full charged and the concentration of electroactive species is constant. When a load is applied, the chemical reaction occurring at the electrode starts consuming species near to its surface. A gradient is hence created across the electrolyte and this allows ions to move by diffusion. When the load is removed, battery has time to recover part of the charge by redistribution of electroactive species in the electrolyte. The battery is considered completely discharged when the concentration at the electrode

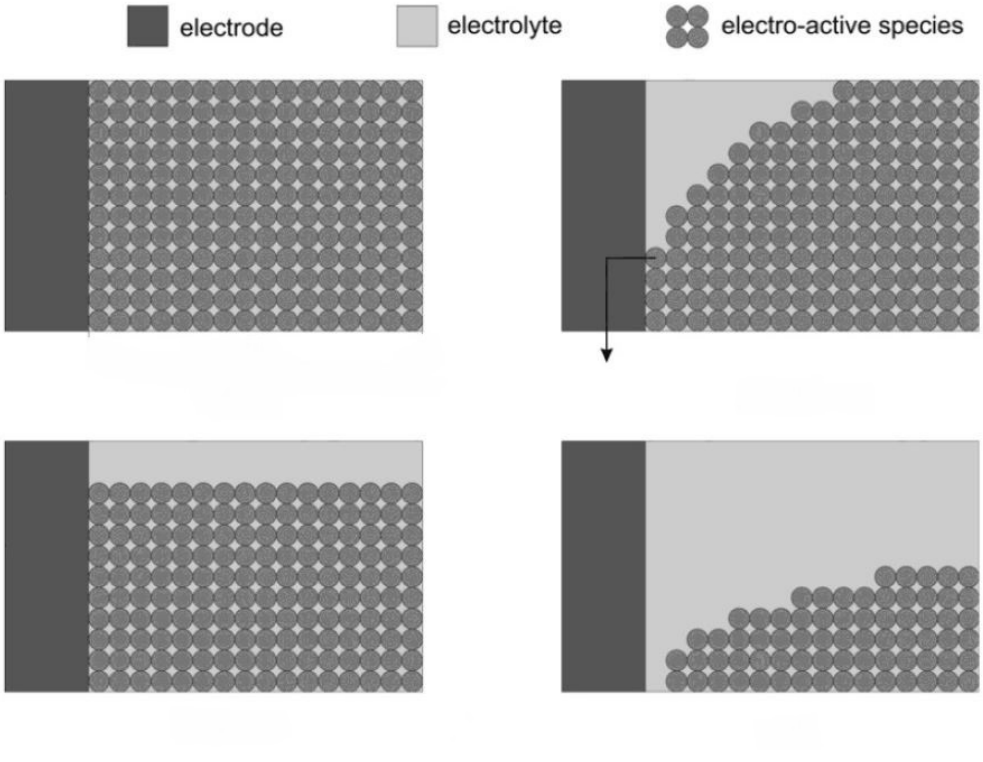

Figure 2.3: Diffusion model [31]

drops below a certain level (C cut off) and hence the reaction can no longer be sustained.
The concentration of the electro-active species at time t and distance x is denoted by C(x,t). The maximum length is w. When the battery is completely charged, concentration is constant over the length of the electrolyte: C(x,0)=C*. The battery is considered empty when C(0,t) drops below the cutoff level Ccutoff.
Diffusion of active species can be described by Fick's law:

$$\begin{cases} -J(x,t) = D\frac{\partial C(x,t)}{\partial x} \\ \frac{\partial C(x,t)}{\partial t} = D\frac{\partial^2 C(x,t)}{\partial x^2} \end{cases} \tag{2.11}$$

Where J is the flux of the electro-active and D is the diffusion constant. The flux at the electrode surface (x=0) is proportional to the current [i(t)], according to Faraday's law (eq. 1.13). The flux on the other side of the diffusion region (x=w) equals zero.
Solving the equation, an expression for σ, the apparent charge lost until time t, is found:

$$\sigma(t) = \int_0^t i(\tau)d\tau + u(t) \tag{2.12}$$

The apparent charge lost can be separated in two parts: the charge lost to the load [l(t)], which is simply the integral of current over time, and the unavailable charge [u(t)]. The first is the charge used by the device, effectively gone out from

the battery, the second is charge which remains unused in the battery. This result, with the concept of available and bound charge is the one already discussed in the KiBam model. KiBam model can be in fact thought of as a discretization of the diffusion model. Recovery effect is modeled as well as rate capacity effect. Battery charge lost during battery lifetime ($\sigma(L)$) is equal to battery capacity α. When t=L the battery is considered fully discharged. The authors refer in this case to non rechargeable batteries, whose lifetime corresponds to the time to arrive to full discharge.
During idle periods the unavailable charge will decrease and will be available again for the load. This model has the advantage of being physically justified, being developed starting from physical laws describing processes occurring in the cell. However, it is simplified with respect to electrochemical, low level models, entails less equation and a much shorter computational time. A drawback of the model is that it does not give information about voltage profile of the battery. It can instead be used to compute battery discharge time, as a substitute of Peukert's law, to optimize battery management systems.
In [31], the authors compare Peukert's law, Kibam model, diffusion and Dualfoil model in order to predict battery lifetime. As expected, Peukert's law results the less accurate model, having the bigger error with respect to Dualfoil. Kibam and diffusion model appear instead to have very similar results, that match well the electrochemical model.

Electric models

Batteries can be represented by equivalent electric circuits that, to an external observer, exhibit their same characteristic of voltage and current.
There is a wide range of circuital models, with different degree of complexity. The simplest ones, with few, constant circuital elements, are far from describing the real physics of the battery, and they could be compared with empirical models, as long as they entail a high degree of abstraction. On the contrary, the most advanced models, are composed of circuital elements that directly reflect electrochemical characteristics of the cell; they could be really accurate, even almost as electrochemical models, but they require the determination of many parameters and time consuming simulation.
As a general rule, electric circuits, need to be composed of two different parts, in order to properly model battery behavior:

1. The first part of the circuit represents the equilibrium voltage of the cell. This is directly related to the energy content of the cell, hence the SOC. In literature, OCV is found to be represented in two different ways and two categories of models are defined [59], [60]:

- **Active models**: OCV is represented by an ideal voltage source, with voltage varying according to SOC. This kind of models are called active models, as long as the voltage generator is an active element.
- **Passive models**: open circuit voltage can be thought of as the voltage drop across a capacitor. The capacitance (called incremental [61], intercalation capacitance [62]...), is the passive element that represents the charge stored in the cell. Capacity and voltage drop across the capacitor vary with SOC.

2. The second section of the circuits is composed of elements that have to represent the overpotential with respect to equilibrium condition (see sec. 1.2). The elements can be represented in time or frequency domain. [63],[64]

   - **Time domain**: Circuits are constructed utilizing serial and parallel networks of resistances and capacitances. They are lumped element models. The value of circuital elements is often found by fitting of discharge curves. [65].
   - **Frequency domain**: circuits utilize impedances that remain expressed in the frequency domain, not being directly representable by resistances or capacitances. When passing from frequency to time domain, some approximations are needed. They are distributed element models. They often utilize Electrochemical Impedance Spectroscopy (EIS) in order to give each element a precise physical meaning and to estimate the value of parameters [65]. Constant Phase Element, Warburg impedance and ZARC impedance are typical elements utilized in this category of models and they are associated with particular shapes in EIS diagram [66]. In annex A are reported details about EIS and impedances.

Electric circuit modeling is one of the most common approach utilized nowadays. Thanks to the flexibility, relative simplicity when compared to electrochemical models but high accuracy, electric circuit models can cover a wide range of applications. They are in particular used in real-time applications, such as in electric vehicles, in order to predict the state of batteries [63],[67],[68].
Equivalent circuit models are often coupled to Coulomb Counting Method (eq. 2.4) in order to estimate SOC of the battery during operation [69],[70]. Coulomb Counting method, based on computation of the integral of the current over time, is often subject to mistakes, due to systematic errors in current measurement. To check the accuracy of SOC estimation, predicted voltage of the circuit at the computed SOC is calculated and compared to the measured one, in what are called closed loop algorithms.
If models want to represent battery behavior with a high level of accuracy, parameters need to be experimentally estimated taking into account the various possible

different operating conditions. Data of parameters varying with temperature, SOC, SOH are needed. The easiest but time consuming strategy is the offline estimation, with creation of lookup tables or polynomial function. It is also possible to estimate parameters online in case of adaptive models. [71]
The most used techniques for battery parametrization are the following.

- **Electrochemical Impedance Spectroscopy (EIS)**: as previously said, one of the most efficient way to estimate battery parameters is through EIS.The frequency of each section of the Nyquist plot can be related to the characteristic frequency of phenomena happening inside the cell. Once having related each part of the graph to real phenomena occurring in the cell, it is possible to estrapolate an equivalent electric circuit (further details in annexA). Values of parameters are found by fitting of EIS curves at various SOC, temperature and aging conditions.

- **Hybrid Pulse Power Characterization (HPPC)**: as an alternative to EIS, a Hybrid Pulse Power characterization test could be made in order to analyze battery dynamic behavior and estimate values of parameters. It consists of a series of discharge and charge pulses alternated by pauses. It can be realized at various SOC and levels of current. Ohmic resistance and polarization resistance can be determined analyzing voltage-current response of the battery. Moreover, OCV characteristic as a function of SOC can be derived. More details about the standard test procedure for hybrid electric vehicles are reported in [63].

- **Static capacity test and constant power discharge test**: These are other standardized procedures that allow to determine battery capacity at constant current and power [63].

Active models
As explained before, what characterizes these models is the presence of an ideal voltage source to represent the charge stored in the battery. This could ideally provide an infinite amount of energy, hence it is not representative of the real battery physics.

Time domain
The electrical circuits of the three principal models in time domain are depicted in figure 2.4.
R int (fig. 2.4(a)). The simplest battery model present in literature is constituted by a voltage source and an internal resistance. This model does not take into account the transient response of the battery.
The difficult part of the model is to find a value of R int that properly models the behavior of the battery. In [72], a critical review of the possible ways in which R int could be determined is made. They mainly distinguish three methods: pulse power

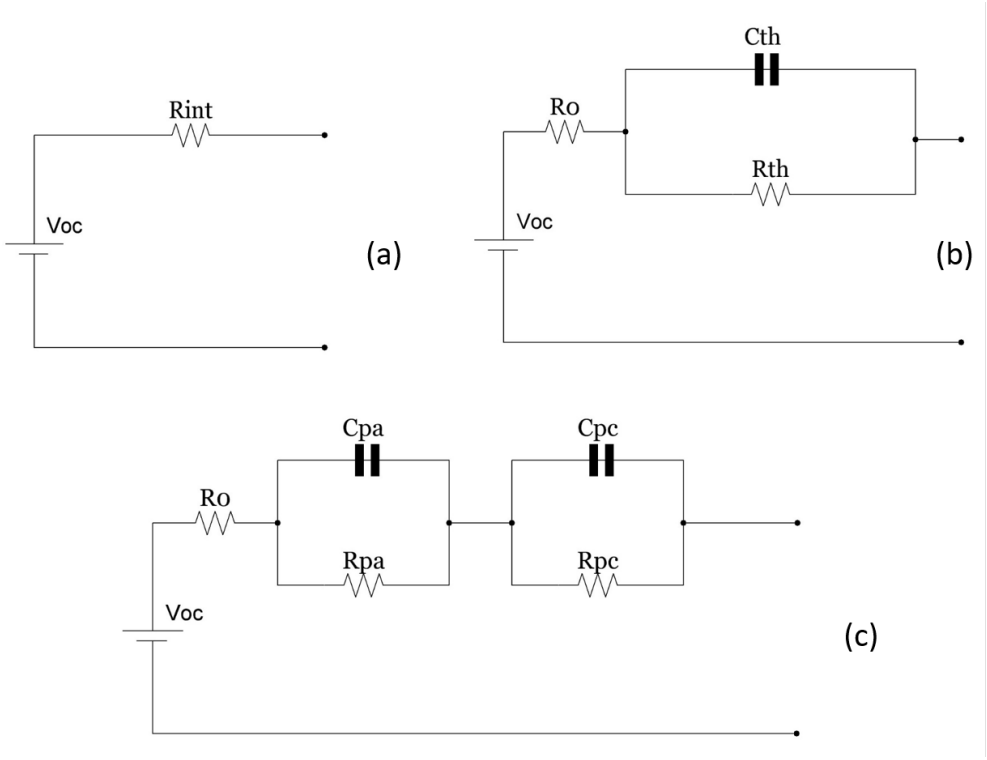

Figure 2.4: Active models in time domain: Rint(a), Thevenin(b), Double polarization(c)

characterization (fig. 2.5), EIS, and thermal methods that account for Joule losses. When EIS method is utilized, according to the specific application of the model,

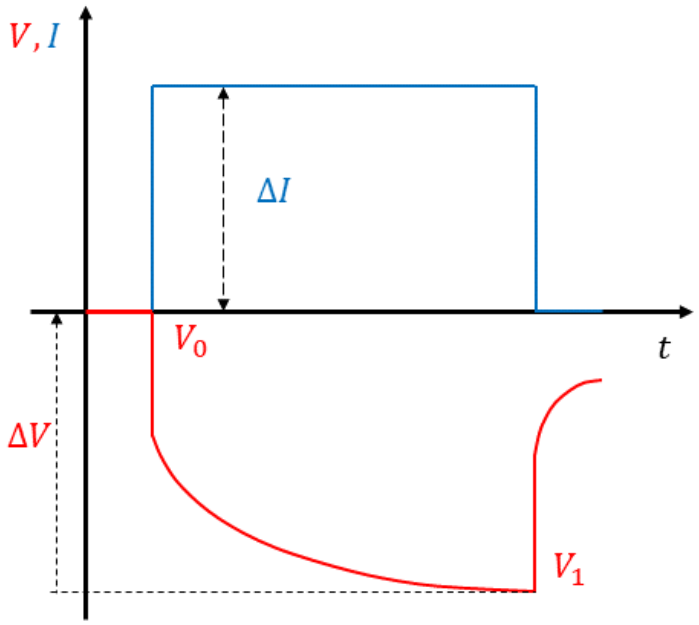

Figure 2.5: HPPC test

and the typical periods of the discharge charge cycles of the battery, an internal

resistance corresponding to different frequencies could be taken into account.
Accuracy of the model can increase when parameters vary according to temperature, SOC and SOH [59] [73]. It has been used to model lead acid batteries applied in uninterruptible power supply or traction vehicles [73]. R int model is validated by the National Renewable Energy Laboratory (NREL), which is part of the US Department of Energy. The model is tested in order to be used it in the Advanced Vehicle Simulator (ADVISOR), for simulation of high power lithium ion batteries of hybrid electric vehicles [74].

Thevenin (fig. 2.4(b)). This model is mainly composed of three parts including open-circuit voltage Voc, internal resistances and equivalent capacitances. The internal resistances include the ohmic resistance Ro, comprising losses in electrolyte and conductors and the polarization resistance R_{th}. The latter is the one associated to the electrochemical reaction. The equivalent capacitance C_{Th} is used to describe the transient response during charging and discharging. All the transient effects, arising mainly from double layer formation and diffusion phenomena, are accounted for by a single RC branch, and hence by a single time constant.The parameters are assumed in the first version of the model to be constant.
In subsequent works, the dependence of the parameters on SOC, T, SOH and C-rate is considered[75]. These dependencies can be experimentally determined and then taken into account via look-up tables.
Applications of this model in PV systems, virtual prototyping of portable battery-powered systems, and real time simulation of hybrid and electric vehicles are found in literature [73].

Double Polarization (fig. 2.4(c)). The model called double polarization is similar to Thevenin model, with an additional RC group. This last element is added in order to make a distinction among transient phenomena occurring in the battery. The first RC group, with a smaller time constant, is related to electrochemical polarization. The second RC group has a larger time constant and it characterizes the diffusion processes occurring inside the cell. This kind of polarization is called concentration polarization [76].
This model is more accurate than Thevenin and can more rigorously simulate battery behavior, especially in the moments at the end of charge or discharge. It is worth to mention that the higher the number of RC groups in series, the more accurately the model reflects the transient behavior of the battery (models with more than two RC groups are found in literature); part of them represent the diffusion occurring in the battery and other part charge transfer and double layer [77]. The more sophisticated the model is, however, the higher the computational effort. For this reason, Double Polarization model is more often preferred and it can find ap-

plication in electric/hybrid vehicles.

Frequency domain
In this section, the most significant active models in frequency domain are explained and their equivalent electric circuits are shown in figure 2.6.

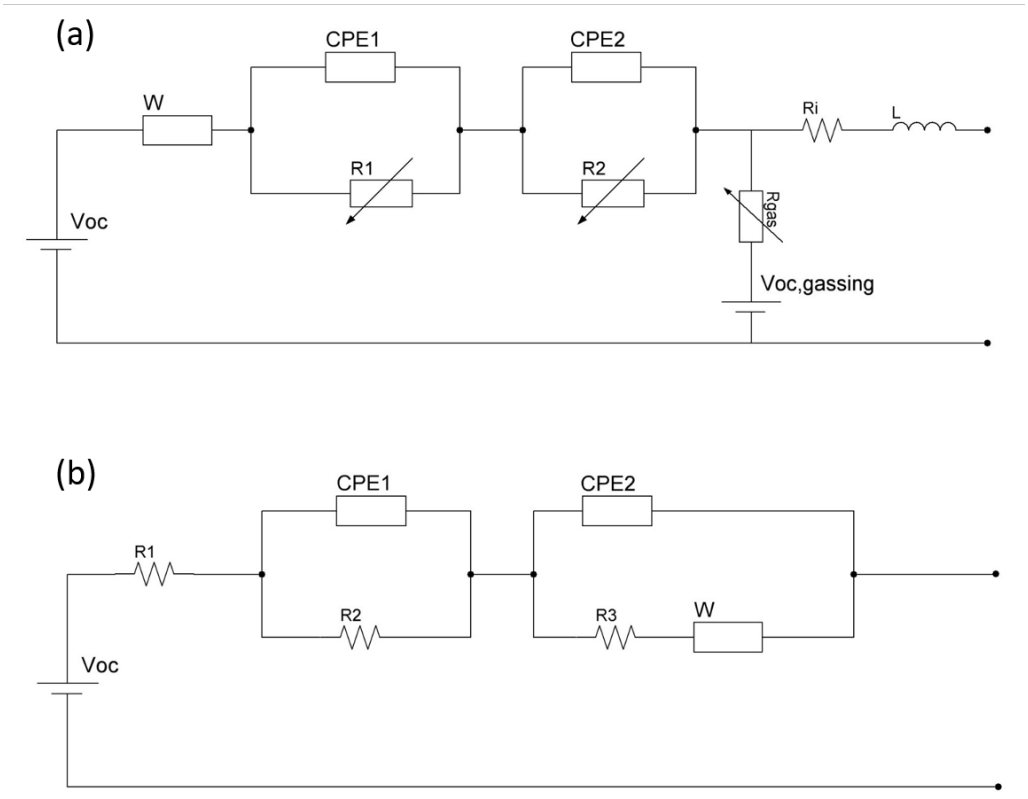

Figure 2.6: Active models in frequency domain: Lead acid active model(a) and Li-ion active model(b)

Lead battery model (fig. 2.6(a)). The idea of the authors that proposed the model [78], was to put in series two Randles circuits (see later in the chapter for more details) and to apply some modifications, typical of lead-acid batteries. R1, R2 and Rgas are non linear resistances. The 2 constant phase elements have been used instead of capacitances to represent depression. A parallel branch has been inserted to take into account the losses associated to the phenomenon of gassing, typical of lead-acid batteries. Only one diffusion element, the Warburg impedance W, is utilized to describe diffusion in the two half cells. This is an approximation that simplifies the implementation of the model. Finally, an ideal voltage source is used to represent OCV. Parameters are found through EIS.
The model, implemented in Matlab/Simulink, according to the authors, allows to represent the behavior of lead acid batteries for the automotive sector. It could be used to simulate the voltage response of automotive power sources.

Lithium battery model (fig. 2.6(b)). The model structure was empirically found by fitting of EIS curves of a lithium-ion battery. The parameters were found in the frequency domain. R1 represents ohmic losses, W is the Warburg impedance to account for diffusion and the other parts account for charge transfer in the two electrodes.
In the work [79], an approximation has also been done, in order to simplify the model and pass to the time domain form. This model is able to predict the output voltage. All the parameters depend on SOC and temperature. SOC can be computed by coulomb counting method.
This model has been proposed as an improvement to Thevenin and R-int model in order to be utilized in real-time electric vehicle battery management systems. In the paper, in order to validate the model, the simulation results are compared to experimental curves obtained by HPPC tests. The error of the proposed model is smaller than the simplified previously mentioned models and hence it could be used to predict accurately battery behavior avoiding time consuming performance tests.

Passive models
This typology of models, employ a capacitance in order to represent energy storage. Charge stored in the capacitor is in fact equivalent to the charge stored in the battery. Value of the capacitance, which represents the battery regime condition, could be constant or variable according to SOC. Its value can be derived from the discharge curve, as the derivative of voltage with respect to charge at constant current. In [61], [80], [81], [82] the capacitance is called incremental capacitance to underline its mathematical derivation. In [62] it is named intercalation capacitance because it describes the accumulation and depletion of Li ions within the electrode.

Time domain
The main passive models in time domain are listed in the following.
R int based model (fig.2.7). The simplest passive battery model is composed by a capacitance in series with a resistance. C_b is the bulk capacitance of the cell and R int is the internal resistance. It is not a model commonly found in literature, but as stated in [73], RC groups can be simplified by a single resistance when a high degree of accuracy is not needed. Starting from the Thevenin based battery model later described, it is hence possible to arrive to the model shown in the picture.
As for the R int active model, value of resistance can be found via different techniques, among which it is relevant to mention EIS.

Thevenin based model (fig.2.8). This model is very similar to the Thevenin model ([83],[60]). The only difference is that OCV is represented by a capacitance, instead than a voltage source (fig.2.8). It is hence a passive model with a resistance to

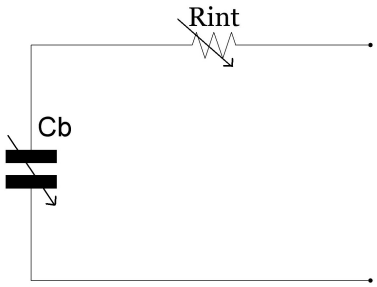

Figure 2.7: Rint passive model

account for ohmic losses, a RC group to represent the transient behavior. It was not derived by impedance spectroscopy but only by discharge curves. The capacitance is a function of voltage and current and it is computed as the ratio of charge exchanged over voltage.
To improve the accuracy of passive models, as in active models, it is possible to increase the number of series RC groups [64].

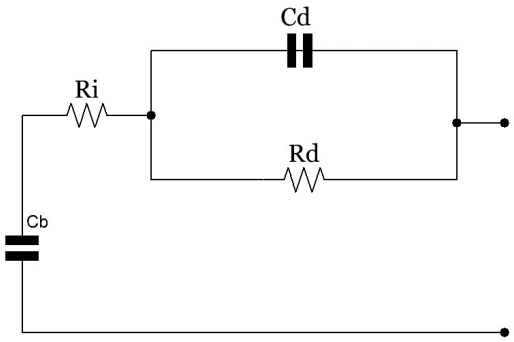

Figure 2.8: Thevenin based passive model

Lead battery model (fig.2.9). In [84], the authors proposed a dynamic model for lead-acid batteries. It was in particular developed for batteries belonging to a buffer/storage device of a domestic CHP.
Even if the model is developed for different purposes, it has, similarly to the previous model, just one RC group. It has however some additional elements:

1. Rp is the self discharge resistance. It is a big resistance that takes into account the fact that battery has a small self discharge leakage current even when it is disconnected. It is function of OCV.

2. There are two couples of resistances, ohmic and charge transfer, and they

are in series with diodes. The reason is that, typically in lead acid batteries, resistance is different during charge and discharge.

All the circuit elements depend on OCV and the relationships are obtained by curve fitting process. Capacitance, in particular, is described as a parabolic function of voltage.

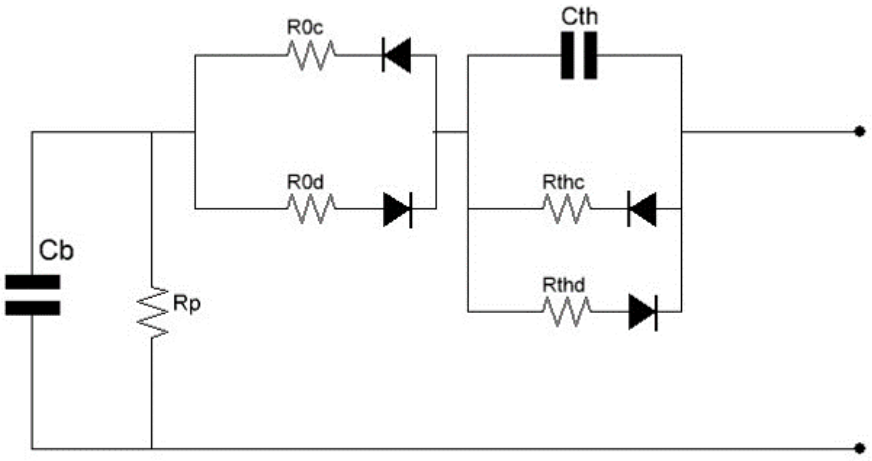

Figure 2.9: Lead acid battery passive model

RC model (fig.2.10). The model was developed by Saft company and used by National Renewable Energy Laboratory (NREL) in the vehicle simulation tool ADVISOR [85],[86]. It is named resistance capacitance battery model, as long as it is composed of two capacitors and three resistors. Cb is the bulk capacitance, representing charge chemically stored in the battery, Cc is a smaller capacitance that accounts for the surface effects of the cell, diffusion of material and chemical reactions. The resistors represent losses associated to various part of the cell.
Parameters depend on temperature and SOC and their value is found through HPPC tests. Battery SOC is predicted using the voltage across the larger capacitor C_b and battery OCV SOC characteristic. Also the voltage across the smaller capacitor influences, in minimal part, the SOC estimation. The model has been adapted to various batteries' chemistry. When implemented in ADVISOR to simulate lithium ion batteries, it showed a better performance than the previously utilized R int model.

Frequency domain
The first models ("Randles models") presented in this subsection mainly focus on

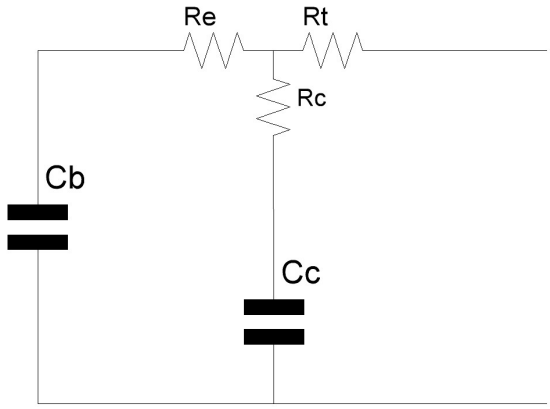

Figure 2.10: RC model

the representation of the impedance of the cell, not considering the equilibrium condition. Impedance allows to compute the overpotential, to which, in order to obtain battery terminal voltage, it is necessary to sum up the open circuit voltage. They utilize open circuit voltage characteristics given by discharge curves in order to find OCV related to SOC.
The last two models presented, have instead a bulk capacitance to take into account charge storage and SOC. Firstly, equivalent electric circuits of Randles models are represented in figure 2.11.

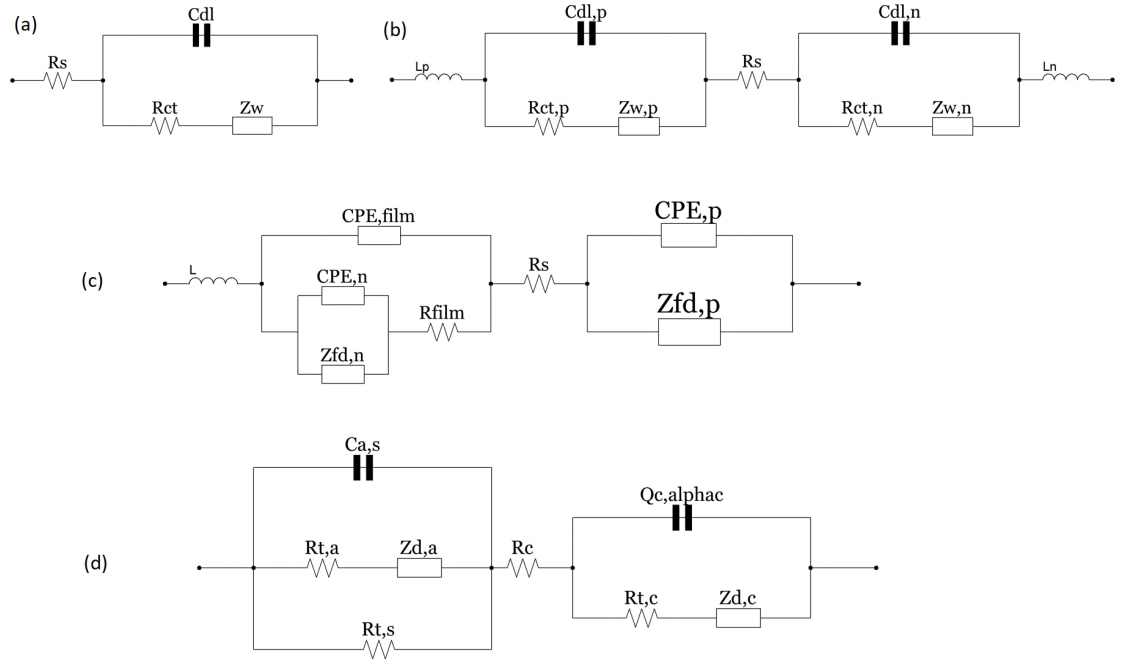

Figure 2.11: Passive models in frequency domain based on Randles circuit:Randles circuit(a), Randles model for the cell(b), modified Randles models for Li-ion cell(c)(d)

Randles model (fig.2.11(a)).The oldest model of this category, and also the one that is taken as a reference in more recent works, is the Randles equivalent circuit [87]. John Edward Brough Randles, in 1947 modeled interfacial electrochemical reactions in presence of semi-infinite linear diffusion of electroactive particles to flat electrodes. The circuit well represents the behavior of half battery cell.

- Zw is the Warburg diffusion element that models diffusion processes occurring at electrodes.
- Rct is the charge transfer resistance at the electrodes.
- Cdl is the double layer capacitance.
- Rs represents ohmic losses in wires, electrodes and electrolyte.

Ideally the cell is composed of two identical half cells, with the same Randles structure but different parameters' value. Inductances show their effect only at high frequencies and are due to battery current collectors and cables. In the picture 2.11(b), the impedance of the whole cell is represented. However, in practice, it is impossible to separate the impedance measurement of the negative and the positive electrode for sealed battery cells. Therefore, the original Randles model (see figure 2.11(a)) is widely used as a representative lumped model of the electrochemical battery cell.

Modified Randles model-1 (fig.2.11(c)). A modified Randles model, applicable in particular to Li-Ion cells is presented in [88]. The authors described each process occurring in the cell via the physical governing equations and arrived to define the impedances that form their proposed model. It has hence a strong physical basis and what is noticeable is that it is really similar to Randles circuit.
The model presents an anode impedance and a cathode impedance connected in series, a resistance R0 to represent the ohmic losses and an inductance L that as said previously represents the inductive behaviour at high frequencies.
Zfd is the faradaic impedance present at both anode and cathode. It can be derived from electrochemistry using Butler-Volmers equations (eq. 1.10) and Fick's law of diffusion (eq.2.11). It is composed by 2 terms: the charge transfer resistance and the impedance caused by solid-phase diffusion.
Besides the Faradaic impedance, the negative electrode impedance includes the effects of double layer and SEI (solid electrolyte interface) film at anode. Details about SEI film formation are reported in section 1.3.
The porous electrodes have rough electrode surface which leads to double layer effect with capacitance dispersion, rather than behaving like an ideal capacitor. A constant phase element (CPE) is used to describe this dispersed capacitance. The

CPE is used for both double layer capacitance and SEI film.

Modified Randles model-2 (fig.2.11(d)). In this model, it is made another modification of Randles circuit, in order to take into account electrode porosity and SEI layer [89].
The anode part of the circuit slightly differs from Randles model.
The desired intercalation reaction of lithium at the anode, and the reaction of lithium with electrolyte's components that forms the SEI, happen in parallel. For this reason, the impedance associated with SEI formation and the one associated with lithium intercalation are in parallel. The first one is composed by a charge transfer resistance and a capacitance ($R_{t,s}$, $C_{a,s}$) and the second one a charge transfer resistance in series with a diffusion impedance ($R_{t,a}$, $Z_{d,a}$).
The ohmic resistance Rc is the analogous of other models.
Through EIS measurements, cathode impedance seems not to correspond exactly to a Warburg impedance. Anomalous diffusion in the cathode, that does not obey to Fick's law, is assumed. The impedance is expressed as follows:

$$Z_d(\omega) = \frac{Z_d(0)}{\tau^{\gamma/2}} coth[(j\omega\tau)^{\gamma/2}] \tag{2.13}$$

where Zd(0) is the zero-frequency asymptote for the real part of the diffusion impedance, and τ is the time constant.

EIS based models (fig.2.12). These models differ from the previous ones due to diverse characterization of the parameters; particularly, they derive directly from EIS measurements [90]. However, they still lacks to represent a bulk capacitance to show storable energy of the battery and relate it to SOC.
Andre et al. gave a physical interpretation of the sections of Nyquist plot [91], then they proposed an equivalent electric circuit model (see fig.2.12(a)).
The inductance represents the behavior of cables at high frequencies, then there is R1, a ohmic resistance and 3 RC groups to represent SEI, intercalation at electrodes, double layer capacitance and charge transfer resistance and diffusion.
The authors proposed also a more accurate model, depicted in figure 2.12(b), in frequency domain; the meaning of the various parts of the circuit is the same. SOC is found in both the models by an integration of the current. With a lookup table, the open circuit voltage is found. The output voltage is then given by the sum of the potential drop over each element at each current.
The models were validated and resulted performing well for the prediction of battery voltage; they were proposed to be utilized for electric vehicles simulations.

Finally, the two models that include also the bulk capacitance are represented in figure 2.13.

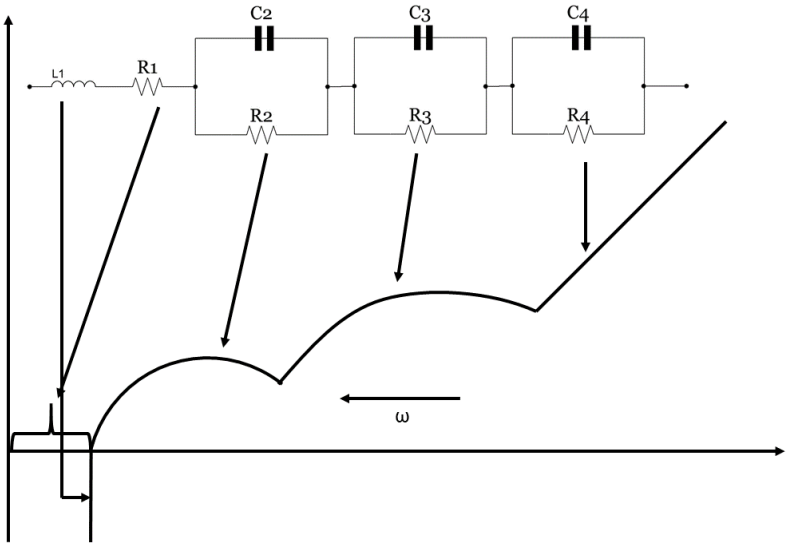

(a)

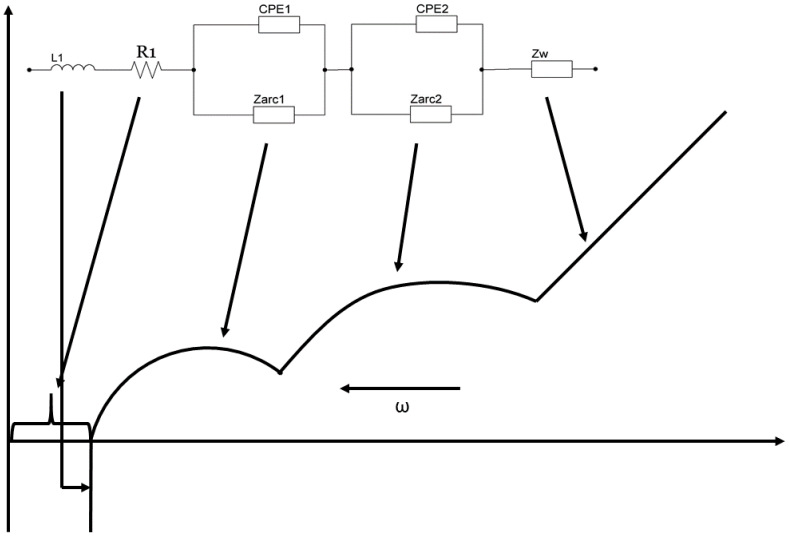

(b)

Figure 2.12: Electric circuits of two EIS-based models and their respective Nyquist plots: EIS-based model with lumped parameters(a) and EIS-based model in frequency domain(b)

Energetic model (fig.2.13(a)). The authors derive an electric model starting from Fick's law of diffusion (eq. 2.11) [92]. The strong physical basis of this model, makes it accurate and comparable to electrochemical models.
Differently from Randles model, it focuses on the electrochemical energy storage, represented by the storage capacitance Cs, which is related to the SOC (see fig.2.13(a)). Moreover, it includes a relaxation branch, composed by C_r and Rr, that takes into account the phenomenon of relaxation, happening at really low frequencies. This phenomenon is rarely represented by circuital models. R_{hf} is the ohmic resistance representing ohmic losses in electrolyte and electrodes.
C_{dl} is the double layer capacitance. Z_t is the Faradaic impedance that consist of a charge transfer resistance in series with a concentration impedance. Z_p is the impedance representing diffusion in porous electrodes.

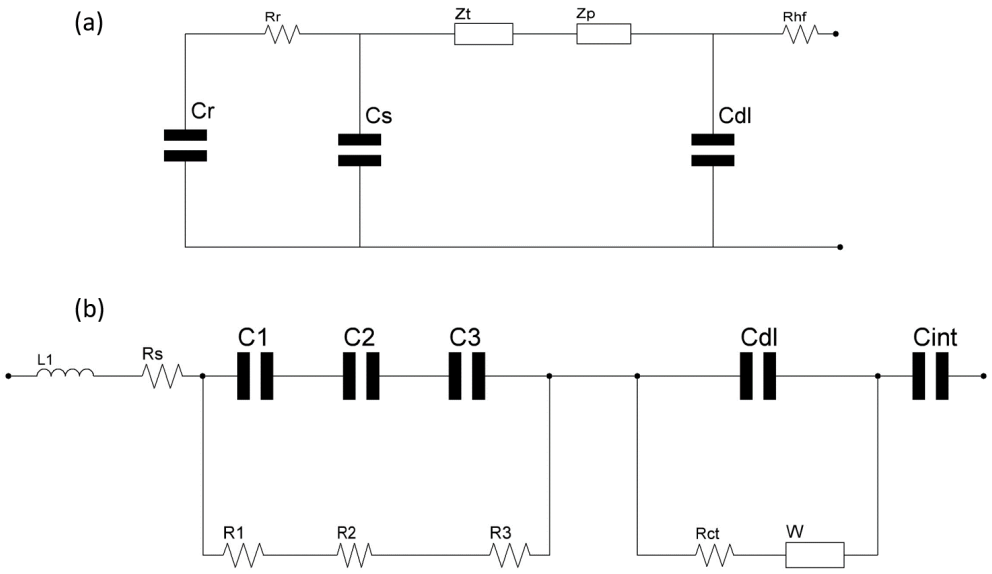

Figure 2.13: Passive models based on EIS with bulk capacitance: Energetical passive model(a) and Li-ion EIS-based model-2(b)

ECM with bulk Capacitance (fig.2.13(b)). The authors developed an equivalent circuit model with the aim of improving battery control techniques [62]. The parameters were evaluated with EIS, at various SOC and temperatures. Authors give to each part of Nyquist plot a physical meaning.
The low frequency portion represents the solid-state diffusion of lithium ions into the porous electrode matrix; extremely low frequencies signify the differential intercalation capacitance of the electrode, which describes the accumulation of lithium ions within the host material. The intercalation capacitance C_{int} included in this model shows the variation of open circuit potential with SOC.

Inductance L1 is used to incorporate the inductive behavior due to electrical energy storage and the geometry of the electrodes. Rs is solution resistance to represent ohmic losses.
R-C circuits (R_n and C_n, with n=1, 2, 3) in parallel denote the slow migration of Li-ions through surface films of the electrode. There are also a charge transfer resistance (R_{ct}), a double layer capacitance (C_{dl}) of electrodes and the diffusion impedance of the anode and cathode also known as Warburg impedance.

Stochastic models

Stochastic models describe battery system as a whole, modeling not only battery behavior but also the stochastic nature of random use profile. They describe battery in mathematical terms, employing a high degree of abstraction.
Chiasserini and Rao were among the first authors to develop and improve a stochastic model for batteries. In their papers, [33], [93], SOC of the battery is predicted utilizing the theory of Markov chains. They modeled in their analysis non rechargeable batteries. Other authors adapted their model in order to apply it to rechargeable ones [32].
The models entail few parameters that can be experimentally found and they are able to predict battery behavior with a particular focus on the recovery effect, once given the usage pattern.
The models are suitable to be used in real time battery management systems, due to low time consumption and high accuracy: [94] and [93] give some examples of the way in which a stochastic model could be used to improve battery utilization pattern. In particular, these models are able to simulate the improvement of battery lifetime through proper regulation of pulsed discharge. One of the used strategies, could be to balance the load applied to batteries by switching among them over time in order to allow charge recovery.
Stochastic models could be integrated with electrical or analytical models in order to describe the necessary battery characteristics.

Basic stochastic model
The amount of charge available in a battery is divided into N states of a Markov chain [33]. When the battery is in the state 0, it means that SOC=0 and that the battery is completely discharged. When, instead the state of the battery is N, the battery is completely charged.
Notice that SOC is considered in this section in relative terms, related to the actual maximum capacity, not the theoretical one. The basic unit of this model is the charge unit, that is the amount of charge necessary to transmit a data packet, typical in the telecommunication world. During each time step, each charge unit has a probability a1=q to be consumed, hence leading the battery to a lower state of charge and

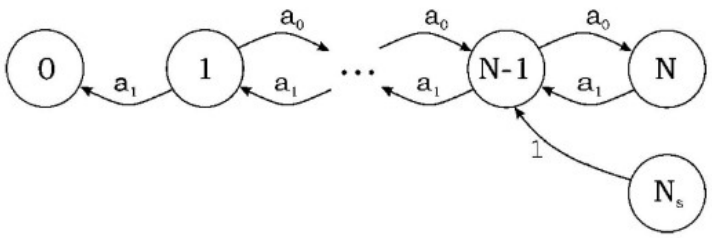

Figure 2.14: Markov chain

a0=1-q to be recovered. End of discharge is reached when the battery arrives to the state 0 or when the total amount of theoretical capacity (T) is exhausted. N is in fact the amount of charge recoverable with continuous discharge, and it can differ from the charge obtained via pulsed discharge, due to the advantages of recovery effect.
The major findings of the work are two parameters:

1. mp that is the predicted amount of transmitted charge units.
2. G that is the gain, defined as mp/N

G is equal to one for continuous discharge and greater than one for pulsed discharge, reaching a maximum value of T/N.

General stochastic model
Chiasserini and Rao, proposed later more advanced models, able to predict battery behavior also in more complex situations.

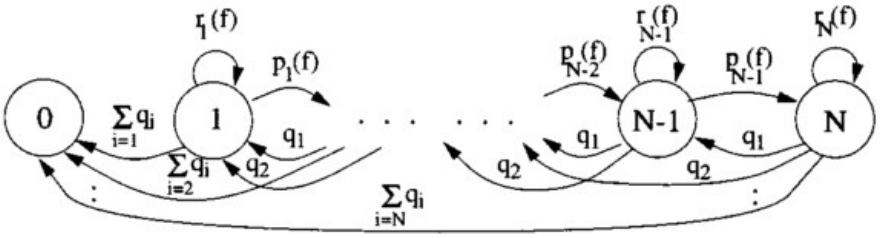

Figure 2.15: Markov chain of general stochastic model

The first change, applied in [33], consists on considering the possibility that in each time frame more than one packet can be transmitted arriving to a maximum number of packets of $M \leq N$. This allows taking into account the discharge at high currents.
In a subsequent work [93] it was considered that the probability to recover is not constant but a decreasing exponential function of SOC, depending also on the total discharged capacity. SOC is represented by the state j of the system, while the discharged capacity is taken into account via the number of phases f. The higher f, the

higher the amount of consumed charge units and the lower the recover capability. The battery has also a non zero probability ($r_j(f)$) of remaining in its same state, without neither charge recovery nor discharge. By changing the value of transition probabilities, different load profiles can be simulated.
In [93], the stochastic battery model previously described, is compared to Dualfoil electrochemical model (see section about Electrochemical models) of a lithium-ion cell. The aim is to utilize the battery model in order to optimize charge recovery mechanism and hence prolong battery lifetime. Curves representing the gain G as a function of discharge demand rate closely match in the two models. The conclusion is that the stochastic model, thanks to its simplicity and low computational time, could be used for real time applications such as battery management techniques.

Kibam-based stochastic model

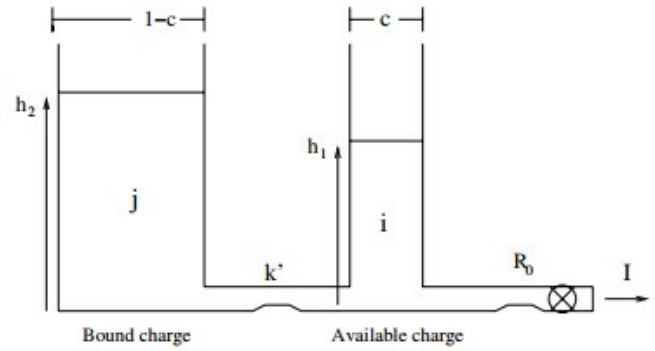

Figure 2.16: Hydraulic circuit of the Kibam-based stochastic model

The authors in [58], coupled a stochastic model with the previously described KiBaM model (see fig. 2.2). The idea was to model in this way both the statistical nature of the work load and the behavior of the battery in a more accurate way than with a simple stochastic model. During idle period, the battery has a certain recovery probability, dependent on the state of charge. Considering that at time t the bound

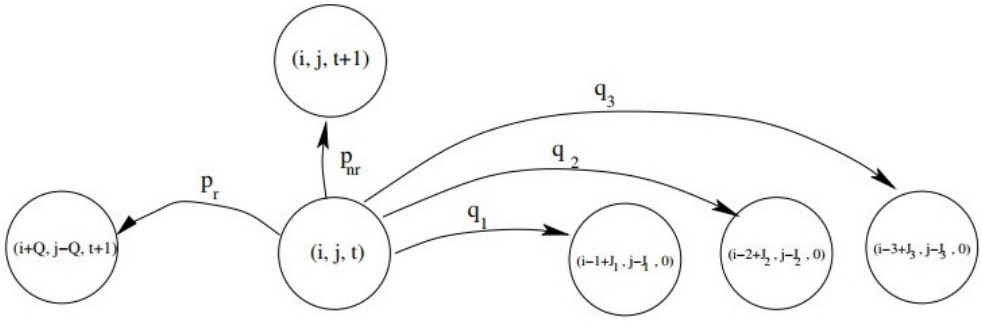

Figure 2.17: Markov chain of the Kibam-based stochastic model

charge is j and the available charge is i, the battery can change its state according to probabilistic laws. The discharge process can go on until the amount of available charge is equal to 0, $(i = 0)$.
Battery behavior is described by a Markov process. Each state of the Markov chain is described by the 3 parameters: i,j,t and the battery can experience 3 possible transitions, each of them with a certain probability:

- Charge recovery during idle period. An amount Q of charge is transferred from bound to available charge and no current is extracted.
- The idle period during which the battery does not recover charge.
- Charge drained from the battery, when a current is applied. In this case, the charge transferred from one well to the other is given by the equation: $J = k' * h2 * (h2 - h1)$.

When the load profile is given or deterministic, the average current over each time step can be computed and it can be converted into the corresponding number of charge units I. The probability that I charge units are drawn from the battery is hence qI=1, while the recovery during idle slot remains probabilistic.

2.3 SOH estimation

Life of batteries is limited due to aging mechanisms occurring inside the cell as explained in chapter 1.
Batteries, during time, experience two phenomena:

- Capacity fade, that is a decrease in the amount of storable energy. It is caused by loss of cyclable ions or by loss of electrode active material.
- Power fade, which means a worsening in the operational performance of the battery, or symmetrically a decrease in its efficiency. It is caused by increased resistance to conduction and diffusion at the electrodes i.e., when using the electric analogy, by an impedance rise.

Battery aging can be divided into:

- Calendar aging, occurring during storage of the battery, when it is at open circuit.
- Cycle aging, taking part during battery utilization.

The most used indicator in order to evaluate battery degradation is the State Of Health(SOH). It can be calculated in various ways, the most common being:

$$SOH = \frac{C(t)}{C_{nom}}\% \tag{2.14}$$

Where C(t) is the battery capacity at time t and C_{nom} is the nominal capacity at the beginning of life. Another indicator is the one that represents the increase in internal resistance. It is here defined as SOH_R. It is the ratio of high frequency resistance (HFR) at the beginning of life (BoL)and at the end of life (EoL).

$$SOH_R = \frac{HFR(BoL)}{HFR(EoL)}\% \tag{2.15}$$

This indicator is particularly relevant for hybrid electric vehicles where the most important battery characteristic is the ability to deliver power [95].
Battery end of life is usually defined as the status in which remaining capacity of the battery is 80% of the initial capacity, i.e. SOH=80%.
Aging mechanisms could differ substantially among different batteries' technologies due to diverse chemical elements present in the cells (chap. 1). Calendar aging in lithium ion batteries depends on lifetime, temperature and SOC (being faster at high T and SOC). Cycle aging increases with increasing the number of cycles[1], the average SOC of each cycle, SOC variation during each cycle, current rate and temperature. Aging in lead acid batteries is in literature rarely divided into cycle and calendar one. The aging mechanisms, taking into account both phenomena, is accelerated at low levels of SOC and prolonged periods of non complete charge.
Modeling of battery degradation processes is becoming more and more important nowadays, especially in electric vehicles application. Monitoring and estimating change of performance of batteries during operation, can improve battery management systems and improve vehicle security [96]. For this reason, most of the literature related to battery degradation models concerns automotive sector, rather than tools for dimensioning of microgrid systems. In literature, many different approaches have been used to model ageing mechanisms and estimate battery state of health [96], [97]. In the following subsections, degradation modeling is described in accordance with the previously utilized models' classification.

Electrochemical models

Electrochemical modeling aims at describing various degradation phenomena through equations based on electrochemical principles. This set of equations are usually connected as subsystem to the governing equations of the electrochemical battery model, through some variables like intercalation current or potential. Electrochemical models for degradation usually refer to lithium technology.
Ex situ techniques (X-ray diffraction, scanning electron microscopy, transmission electron microscopy, x-ray photoelectron spectroscopy, Atomic force microscopy) can get insight into the operation and degradation process. From this analysis, it is

[1]Battery has experienced a charge-discharge cycle when the throughput Ah are equal to the double of the battery capacity: $N_{cycles} = \int \frac{abs(I(t))dt}{2C_{nom}}$

possible to obtain information about the structural change and parameters variation of materials[98]. However, this kind of techniques must be performed on samples that have been disassembled and cannot operate anymore. Hence, developing degradation model using these detailed data is particularly laborious.
Moreover, EIS technique can be used for electrochemical model parametrization, since parameters change along battery lifetime due to degradation [99].

Lithium ion: capacity fade due to corrosion
The model of Broussely et al.[100] attempts to describe the cell calendar aging of a LiCo oxide and LiNi oxide cells referring only to the lithium corrosion phenomenon at the porous carbon negative electrode(capacity loss), which is related to side reactions occurring between electrolyte and lithium. Corrosion rate is limited by electronic conductance of SEI for Li. The insoluble products of corrosion trap in the $Li+$, causing irreversible capacity loss. The model fits with experimental data analyzed in this work. The effect of temperature is considered using Arrhenius law (eq. 1.9) and a general equation to calculate lithium corrosion curves as a function of time and temperature is found

$$t = e^{a/T-b} \cdot x^2 + e^{a/T-c} \cdot x \tag{2.16}$$

where t is the time, x is the number of lithium moles having reacted, T is the temperature and a,b and c are parameters experimentally determined. Notice that lithium corrosion depends on the square root of time, a result that is often found in literature.
If a new chemistry is adopted, then the storage experiments have to be performed again to deduce the new rate coefficients.
It is worth noticing that this equation is only used to forecast capacity fade, but it is not added to a general electrochemical battery model.

Lithium ion: capacity and power fade due to cathode degradation
The work proposed by Schimdt et al [101] slightly differs from the previous one. Indeed, it only considers degradation phenomenon for cathode as the most crucial one, whereas the aging effect at the anode is neglected for simplicity.
In the model, the actual capacity is expressed by the parameter cathode porosity: during operation, some particles will be isolated from the conductive area or will crack, reducing cathode effective porosity. Thus, the capacity fade is modeled as reduced cathodic porosity and loss of active insertion material.
Moreover, due to aging effects, especially cycle aging, an increase in overpotential of the cell is observed. Within this model the issue is addressed by a decrease in electrolyte conductivity, meaning that the power fade is estimated through the model parameter electrolyte conductivity.

The algorithm used for estimation of parameters and state of health is an Unscented Kalman Filter, that allows to monitor of the capacity and power fade of the cell without a parameter update of the model during battery lifetime.

Lithium ion: capacity fade due to SEI formation
The model proposed by Ramadass et al.in [102] for a LiCo oxide cell focuses on the side reactions occurring at anode of lithium-ion batteries responsible of SEI formation. Specifically, they take into account the reaction of electrolyte solvent with lithium ions. Degradation modeling is included in a P2D electrochemical cell model (sec. 2.2), in order to asses change of battery operating performance. Butler Volmers' kinetics was defined separately for Li-ion intercalation reaction and for the solvent reduction reaction. The total current at the anode (J_{tot})is given by the sum of intercalation current (J_n)and solvent side reaction current(J_{sd}).

$$J_{tot} = J_n + J_{sd} \tag{2.17}$$

SEI development leads to the formation of an additional resistance, whose value is dependent on SEI film thickness, varying with time. Overpotential at the anode is changed by the film resistance as shown by the following formula:

$$\eta_j = \phi 1 - \phi 2 - U_{j,ref} - \frac{J}{a_n} R_{film} \tag{2.18}$$

Where $U_{j,ref}$ is the equilibrium potential, J is the total current density and ϕ are the local potentials. Applying a modification to the boundary condition at the surface of negative electrode, the authors were able to incorporate solvent reduction reaction to the initial electrochemical model: this represents an advantage with respect to previously described approaches. Capacity loss due to SEI formation during cycling is given by the integral of side reaction's current over time.
The model, comprising a total of eight variables (including currents and potentials), was simulated with FemLab software [103]. The model is quite accurate but it considers only one degradation mechanism; a possible improvement could consider making a comprehensive analysis of the whole battery aging process.

Analytical models

These models are based on cycling test procedures or accelerated stress tests. Part of them propose equations derived by purely data fitting, others seek to relate observed trends with physical laws. Therefore, it is possible to distinguish empirical and semi-empirical models.
Analytical models correlate capacity and power fading rate with a combination of stress factors (like temperature, SOC, number of cycles...) that were seen to have a great influence on battery lifetime. They can deal separately with calendar and

cycle ageing (distinction typically found for lithium-ion batteries) or they can take into account the life of the battery as a whole in what are called cycle life models. Moreover, two different general approaches can be highlighted:

- Some models evaluate capacity fade and power fade indicator updating parameters, e.g. reducing the battery capacity or the efficiency; consequently battery operational characteristics change during lifetime.
- Other models simply evaluate battery residual lifetime by assessing cycle and calendar degradation but do not update battery parameters, e.g. they calculate the number of cycles to failure. Consequently battery behavior does not change during lifetime and end of life is defined at a minimum SOH value.

Some of the models present in literature are here reported.

Equivalent full cycles to failure
This method is the simplest approach to predict battery lifetime [46]. It estimates the number of full charge-discharge cycles until the battery reaches a defined maximum number of cycles, that represent the end of the life. The maximum number of cycles can be set from datasheet or reference literature. This method entails a strong simplification, because there is no dependence on the characteristic of each cycle. It is commonly used for simulation and optimization tools due to its simplicity [104]. Greenleaf et al. in [105] apply this method to predict the state of health of the battery for residential PV system sizing. Given the maximum amount of cycles the battery can experience, SOH is written as a linear function of the number of cycles:

$$SOH_{cyc} = SOH_{BoL} - \frac{SOH_{BoL} - SOH_{EoL}}{N_{max}} * (N_{cycles}) \tag{2.19}$$

SOH_{BoL} and $SOH_{EoL}$are the values of SOH corresponding respectively to the beginning and end of life and N_{max} is the maximum number of cycles. Actually, this model does not consider the decrease of capacity and power in time and the resultant change in battery operation.

Empirical models
Empirical models derive mathematical expressions for capacity and power fade using the least square fitting method from measurements. These equations are easy to use but they are strongly dependent on the specific battery technology, due to the lack of physical background. Moreover, they typically entail long testing periods for parametrization.

- *Improved equivalent full cycles to failure*
  In [106] the authors describe the cycle life of a LiFePO4 Li-ion battery as dependent on various parameters, such as temperature, DOD and current.

The model evaluates the number of cycles to failure, which vary according to different operating conditions. This model improves the simple "equivalent full cycles to failure" model but it does not predict the power and capacity fade yet. Moreover, the authors analyze the increase of Peukert's coefficient (see Peukert model in sec. 2.2) with cycles at different current rates.

- *Lithium ion: power fade during calendar aging*
  In this study of a LiNiCoAl oxide lithium ion battery [107], power fade is assessed through HPPC tests: given a predetermined amount of discharged energy, the maximum power that the battery can provide decreases with time. Power fade during calendar aging is estimated through the following equation:

$$Y(t,T,SOC) = \frac{exp(a_0 + a_1(1/T)}{1 + exp(a_0 + a_1(1/T)} - exp(b_0 + b_1(1/T) + b_2 SOC)t^{3/2} \quad (2.20)$$

  where Y is the relative power compared to the initial value of the cell. It depends on the temperature T, on SOC and on time t. a0,a1,b0,b1,b2 are parameters empirically determined. Two degradation processes contribute to the power fade: the first term of the equation is related to the faster process and it is strongly enhanced by high temperature. The second term represents the less rapid degradation process and its kinetic depends on the square root of the time at the power of three.
  This model has been developed for HEVs applications.

- *Lithium ion: capacity and power fade during calendar and cycle aging*
  Swierczynski et al. in two separate works, [108] and [109], derive equations for both capacity and power fade during calendar and cycle aging of nanophosphate LiFePO4/C Li-ion chemistry. Calendar aging depends on time, temperature and SOC, while cycle aging depends on the number of cycles, temperature and cycles' depth ΔSOC. Two equations of [108], are here reported, specifically power fade (i.e. decrease in power pulse capability) during calendar and cycle aging:

$$\begin{aligned} P_{fade} &= \frac{a \cdot SOC + b}{c} \cdot d \cdot exp^{e \cdot T} \cdot t \quad \text{Calendar aging} \\ P_{fade} &= 1/3(a \cdot exp^{b \cdot T} + c) \cdot exp^{d \cdot \Delta SOC} \cdot N_{cycles}^{(e \cdot T - f \cdot \Delta SOC - g)} \text{ Cycle aging} \end{aligned} \quad (2.21)$$

  To provide a lifetime model, the two aging mechanisms have to be combined. Cycle aging equations are used when battery is working while calendar aging relationships are employed during battery rest periods. The authors also analyzed in [109] the increase of internal resistance with an approach that will be discussed in paragraphs related to equivalent circuits models.

This model can be used for analyzing different driving profiles and HEVs operational scenarios[108]. The model in [109] has been developed for lifetime estimation of a lithium ion battery used in augmented wind power plants.

- *Lead acid: capacity fade*
  Cherif et al.[51]measure capacity fade of lead acid batteries starting from Shepherd model (see section 2.2). They tested battery degradation during different stages of aging, through charge/discharge measurements at different applied constant currents. Therefore, they estimated the evolution in time of the model parameters. The authors empirically developed equations for the aging of a total of 9 parameters, among which battery capacity, resistance and voltage characteristics. The parameters change according to exponential, logarithmic or linear laws, capacity is the most sensitive to aging. Each parameter is updated at every iteration, so it is possible to monitor changes in battery power capability and capacity. Moreover, they separately assessed the reduction of lifetime through an equation dependent on number of cycles and depth of discharge. This model can be used for optimal monitoring management of a PV plant in order protect battery from deep discharge.

Semi-Empirical models

Semi-empirical models are based on a physical description of battery degradation. The modeling approach consists on the establishment of analytical equations and on a subsequent parameter estimation through data fitting.
The majority of the works considers that the reaction rate of parasitic, unwanted reactions occurring inside the cell (e.g. electrolyte decomposition and SEI formation) exponentially increases with temperature according to Arrhenius law (eq 1.9). Moreover, many studies use a correlation between capacity fade and $\sqrt{time}$. A possible explanation for this is that corrosion rate at the anode, limited by diffusion in the passivated layer (electron or electrolyte components), is dependent on $t^{1/2}$(see also the previous subsection about degradation in electrochemical models).

- *Lithium ion-capacity fade*
  Wang et al. in [110] and[111] developed 2 semi-empirical models for LiFePO4 cell and NiCoMn oxide lithium ion battery. In their first work, no distinction between calendar and cyclic aging is made. They found out that DOD influence on capacity fading was negligible. Starting from Arrhenius law they proposed a power law equation for the capacity loss, depending on T, C-rate and time:

$$C_{loss}(\%) = a * exp[-\frac{b + c \cdot C_{rate}}{RT}] \cdot (Ah)^{0.55} \tag{2.22}$$

  a,b and c are constants. Very low temperatures were not taken into account, in that case, degradation mechanisms are different and a different model might be

necessary. The authors found an empirical relation between activation energy and C-rate that suggests that higher currents induce higher stresses accelerating chemical processes involving lithium consumption.
In the subsequent work, Wang et al. made a step further. They considered separately calendar and cycle aging. In the following equation the total capacity loss during battery life is reported as the sum of cycle and calendar degradation.

$$C_{loss}(\%) = (aT^2+bT+c)exp[(dT+e)\cdot C_{rate}]\cdot Ah + f*t^{0.5}exp[-E_a/RT] \quad (2.23)$$

a,b,c,d,e,f are parameters experimentally determined. It is noticeable that calendar aging depends on the square root of time and on temperature via Arrhenius law.

- *Lithium ion-Stress factors' model*
  Bolun Xu et al. [112] building on the basis of Millner's work[113], propose a semi empirical model, useful to predict lithium manganese oxide battery end of life and utilizable in a wide operating region.

$$fd(t, \Delta SOC, SOC, T) = ft(t, \bar{SOC}, \bar{T}) + \sum_{i}^{N} n_i fc(SOC_i, \Delta SOC_i, T_i) \quad (2.24)$$

$$L = 1 - \alpha_{SEI} \cdot e^{-\beta_{SEI} fd} - (1 - \alpha_{SEI}) \cdot e^{-fd} \quad (2.25)$$

  L is the overall normalized life loss. It is conceptually similar to SOH and numerically its 1's complement: L is equal to 0 at the beginning of life and equal to 0.2 at the end. fd is the degradation function, given by the sum of calendar and cycle aging. The second equation takes into account the fact that degradation rate is higher in the first cycles due to SEI formation and in the last cycles due to low availability of lithium ions. α_{SEI} is the percentage of lithium loss due to SEI formation. Once SEI parameters are evaluated, it is important to estimate the degradation function, fd which is evaluated through stress factors models. Cycle aging (fc) depends on stress factors which are DOD, average SOC and Temperature. Calendar aging (ft) depends instead on time, SOC and T. Note that in this case DOD is defined as equal to 2 times the cycle amplitude, i.e. equal to ΔSOC. A great number of parameters must be determined, making the model quite accurate in predicting lifetime of lithium-ion batteries.
  The model has been proposed to evaluate battery capacity fading in the context of grid services such as frequency control in regulation market.

- *Lead acid-Weighted Ah aging model*
  One of the most accurate analytical models present in literature is the Weighted

Ah aging model developed by Schiffer et al in [25].They proposed an heuristic model aimed to predict lead acid batteries lifetime in applications with irregular operating conditions. Aging of the battery depends on the number of cycles and on operating conditions: each Ah throughput of a battery is multiplied by a factor that represents the conditions to which the battery is subject during cycling. The more severe operating conditions are, the more the weighting factor is high. Aging depends on the depth of discharge, current rate, acid stratification and the time since last full charging. Capacity fade is divided into capacity loss by corrosion of positive grid and degradation of active mass. The model is based on several parameters that can be obtained from batteries datasheets, literature or experimental evaluations. The effects are taken into account starting from a physical analysis of battery behavior; the strong electrochemical background makes it quite accurate even though it remains easy to use.
The model is particularly suitable for design tools and system simulations.

Electrical models

Once an electrical equivalent battery circuit is proposed, degradation phenomena of the battery can be assessed by analyzing how the parameters of the model vary during life time.

- Capacity fade: many authors estimate it by looking at discharge curves, especially in case of active models. Another possibility would be to look at the variation of the intercalation capacitance over time (see ref. [82], [81], [80]) when passive models are taken into account.

- Power fade: it is related to an increase of the impedance of the cell. One of the adopted techniques to evaluate power fade is EIS: by looking at the variation of curves in Nyquist plot, in fact many authors were able to write empirical relationships in order to model impedance rise over time. Some authors take into account the increase of a single internal resistance, while others look at the variation of all the circuital elements. Other utilized techniques are fitting of discharge curves or HPPC tests.

Moreover, EIS studies on degradation can help to understand the accuracy of electric models. Correlating in fact the change of Nyquist plot with time with real phenomena happening in the cell, it is possible to better understand which phenomenon can be linked to which part of the diagram [114] [115].
Most of the literature related to this topic, focuses on degradation of lithium-ion batteries. Circuital elements vary with time according to the same stress factors described in the subsection about analytical models. Even in this category of models,

aging equations could be totally empirical or based on some physical considerations. In order to experimentally evaluate battery aging, batteries are typically subject to accelerated aging conditions (high temperature and SOC) and to reference performance tests after determined time periods[107].

SOH estimation in Single Resistance model
In literature, different studies, ([114], [116] [117]) evaluate the increase of battery internal resistance during lifetime. They do not associate it to an equivalent electric circuit even though the most obvious application is to relate it to the variation of R int in the previously described model (fig. 2.7).
Resistance measurements are done through HPPC tests or EIS. The resistance is computed as the ratio of $\Delta V/\Delta I$, applying a current pulse of predefined length. An example of the results found in the first paper is reported:

$$Rint_{increase}(t, T, SOC) = (a \cdot e^{b \cdot T})(c \cdot e^{d\dot{S}OC} \cdot t^{0.8}) \tag{2.26}$$

Calendar aging is investigated. The exponential dependence on temperature and the dependence on time are in accordance with physical laws explained in the previous subsections.

SOH estimation in Thevenin model
Liaw et al. in [118], and Einhorn et al. in[119],started from the Thevenin model (fig. 2.4(b)) to model degradation of LiNiCoAl oxide Li-ion cells. The first study focuses only on R_{th} change with time considering ohmic resistance and OCV as constant. The authors state that these two parameters are intrinsic of the cell and hence do not vary with thermal aging.
All the relationships in this work are totally empirical and found by fitting of discharge curves. This work has also been utilized by the italian research center RSE (Ricerca Sistema Energetico) in their report about the estimation of SOC and SOH in lithium ion batteries [120].
The second study instead, derives an expression for both capacity fade during cycling and R_o resistance increase. They are both linear functions of the number of cycles:

$$\begin{aligned} C_N(Ncycles) &= C_{N,0} + k_C \cdot N_{cycles} \\ R_o(Ncycles, SOC) &= R_{o,0} + k_{Ro,N} \cdot N_{cycles} + k_{Ro,SOC} \cdot SOC \end{aligned} \tag{2.27}$$

Where k's are coefficients that can be extracted by manufacturer's data-sheet or experimentally determined.
Nominal capacity is used to estimate SOC and hence OCV through Coulomb Counting method. Its value, together with resistance value is updated during battery lifetime.

The model is proposed to be utilized in dynamic system simulations of electric vehicles.

SOH estimation in Active and Passive models-frequency domain

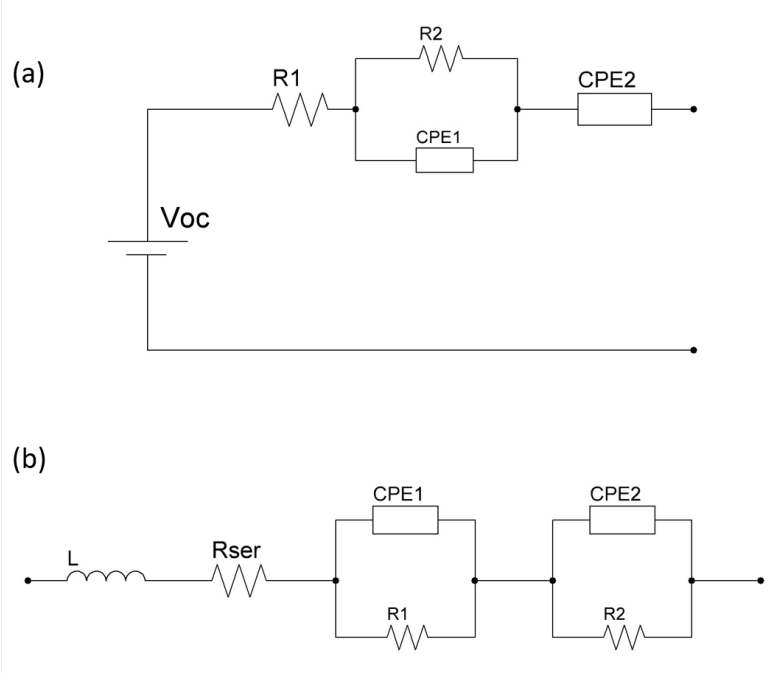

Figure 2.18: Active model(a) and Passive model(b) in frequency domain for SOH estimation

After proposing an active battery model in the frequency domain (fig.2.18(a)), a model to predict remaining useful life during calendar aging is developed for a high-power LiCOMnNi oxide Li-ion cell [121].
In this work the attention was focused on the increase of impedance at low frequency value, because it was experimentally seen, it was the one mostly contributing to degradation. With the help of EIS, the value of impedance real part at low frequency, (0.1Hz) is analyzed and described by an empirical equations:

$$\begin{aligned} Re(t,T,SOC) &= A(T,SOC)\cdot H(t) + B(T,SOC) \qquad H(t) = t^{1/2} \\ A(T,SOC) &= a1\cdot SOC + a2\cdot T + a3\cdot T\cdot SOC \\ B(T,SOC) &= b1\cdot SOC + b2\cdot T + b3\cdot T\cdot SOC \end{aligned} \tag{2.28}$$

The equation, as it was described for semi-empirical models has a physical background: the square root of time is in fact related to the SEI growing process. The model was suggested for prediction of battery remaining life in electric vehicles' applications.

In [122], the process of calendar aging is described for a lithium/thionyl chloride cell. The variation of all circuit elements (passive electric circuit is reported in fig.2.18(b))

depends on storage temperature, time and SOC (i.e. voltage). It is assumed that all the parameters (e.g. resistances, inductance, capacity) follow the same aging trends here expressed as:

$$L_{cal}(t,T,V) = L_{cal}(t0,T,V) \cdot [1 + B(T,V)F(t)] \qquad F(t) = c_a \cdot t^{\beta} \tag{2.29}$$

Lcal is used for the evolution in time of any battery parameter. F(t) describes time dependence and it can have different shapes according to the dominant aging process. Once more, it is stated that if SEI formation is a predominant aspect in the degradation process, $\beta = 0.5$

$$\begin{aligned} B(T,V) &= c_T^{\frac{T-T_0}{\Delta T}} \cdot c_v^{\frac{V-V_0}{\Delta V}} \\ B(T,V) &= c_T^{\frac{T-T_0}{\Delta T}} \cdot (c_v \cdot (\frac{V-V_0}{\Delta V})^2 + 1) \end{aligned} \tag{2.30}$$

Eq. 2.30 (a) is the best fitting trend for all components except for ohmic resistance (Rser) where eq. 2.30 (b) holds.
Measurements for calculating equations constants of each circuital element are done through EIS technique.
To predict lifetime of the battery, the value of each parameter is updated at each time step.

Stochastic models

Stochastic models described in section 2.2 were mainly focused on non rechargeable batteries. The adaptation of the models in order to describe rechargeable batteries needs to take into account also degradation phenomena. Markov chains can express the evolution of batteries' health indicator SOH as a non deterministic process similarly to SOC estimation described in the previous section. The evolutionary process of the state of health is a function of charge/discharge process, SOC and SOH at the previous time step, with a certain transition probability of passing from one to another state of the Markov chain.
Michelusi et al in various works used this approach for wireless sensors' network applications, where battery degradation is an important issue [32].

Michelusi model
Michelusi et al. [123], described the degradation process of a battery as a Markov chain. They define the battery health state Hk at time k, taking values from 0 to Hmax, with $Hmax > 0$. Hmax is the health state at the beginning of life. The maximum battery capacity at time k, is

$$Q_{max}(k) = [\frac{H_k}{H_{max}} q_{max}] \tag{2.31}$$

being q_{max} the initial amount of available charge units. The battery degradation process is discretized and this introduces an approximation. Battery degradation probability can be extracted by manufacturer's data as explained in [123]. The probability is really low when compared to the probability of changing SOC, to represent the slow phenomena of degradation when compared to cycling, and it is higher the more the battery is already degraded.
Charge transfer process, described as a stochastic process, is hence dependent on state of health of the battery: the amount of charge providable by battery decreases with time. This model has been proposed for the optimal management of harvesting-based wireless sensors devices, accounting for battery lifetime while guaranteeing a minimum quality of service.

Summary

A recapitulatory table is here reported in order to sum up the main characteristics of each modeling approach.
Each modeling approach entails different degrees of accuracy and difficulties in implementation that make it suitable for particular applications. Before entering in details in the next chapters into BESS modeling for sizing tool applications, a brief

	Electrochemical	**Analytical**		**Electrical**			**Stochastic**
		Empirical	**KiBam, Diffusion**	**Single resistance**	**1 or 2 RC groups**	**Many circuital elements, EIS based**	
Accuracy	High	Low	Medium	Low	Medium	High	Low
Comput. time	Very long	Very short	Medium	Short	Medium	Long	Short
Applications	Battery design & optimization	Sizing tools		Online monitoring of EV,HEV Real time BMS			BMS
I-V	x			x	x	x	
Rate discharge effect	x	x	x	x	x	x	
Recovery effect	x	x	x		x	x	x
Self discharge	x					x	
Charge transfer resistance	x			x	x	x	
Double layer capacity	x				x	x	
Diffusion	x		x			x	
Ohmic reistance	x			x	x	x	

Table 2.1: Comparison among modeling approaches

summary of possibilities of applications of the various methodologies it is reported in the following.

1. **Online applications**: battery models are required to optimize battery performance during operation.

    - Battery Management Systems (BMS): these are systems aimed to monitor, control and optimize batteries during operation. They find application especially in EVs and HEVs. BMS monitor state of the batteries by measuring characteristic physical quantities, such as voltage, current and temperature. From real time measures, thanks to battery models (especially adaptive models), they are able to calculate secondary quantities, such as SOC and SOH. BMS control logic works in order to protect batteries from operating outside their safe operating area and to optimize load profile so to prolong batteries' lifetime, and reduce maintenance costs.
      Electric models are the most diffuse approach for this kind of application, as long as they can relate I-V battery characteristic to SOC and SOH with a quite high level of accuracy. Combining OCV measurements with Coulomb Counting method in closed loop-algorithms, can give good estimation of SOC.
      Stochastic models are able to characterize the stochastic nature of battery-powered systems as a whole, taking into consideration both battery behavior and usage profile. They could be used in BMS, in order to optimize battery performance by properly shaping the load profile, so to maximize charge recovery effect of each cell, e.g. by switching between the cells during discharge or balancing the load between multiple batteries. As stated in [32], studies are being done to implement stochastic models in smart scheduling schemes, for the exploitation of pulsed charge and discharge.

2. **Offline applications**: batteries' offline simulations require accurate models able to predict their performance.

    - Battery design and optimization: detailed microscopic models are used to assess change in battery performance with the change of physical quantities: different chemistry, activities, diffusion coefficients, material properties and thicknesses. Identification and understanding of degradation mechanisms is one of the major issues of today's batteries' research. The final goal is to reduce costs and improve operational performance by increasing batteries' energy density and useful life. In order to deeply investigate electrochemical cells, the focus is on great precision instead of short computational time. Electrochemical models, with systems of partial differential equations to be solved, are required in this kind of application.

- Sizing of Stand Alone systems: several softwares are commercially available for the simulation of off-grid energy systems. The scope of the simulation tools is the optimal sizing of the system, taking into account Loss of Load Probability (LLP), Net Present Cost (NPC) and the Levelized cost of Energy (LCoE). They entail mathematical models to represent system components (PV, Wind, Loads, Batteries). Each tool addresses particular issues and is suited to certain applications. The focus of design softwares is not on the accuracy of battery performances estimation but on the optimization of the hybrid system as a whole. For this reason, the battery model present in the tool, needs to find a good compromise between computational time and accuracy. Battery models need to accurately simulate battery behavior under a given load profile estimating SOC, to predict energy not providable to the load, and SOH, to compute replacement costs. Nowadays, the widespread category of models is analytical models that can represent in a good way energetic battery behavior while neglecting its physical background. Electrical models have not been used yet for this application, although the most simple ones could match the required characteristics of short computational time and accuracy, while maintaining a physical basis. This motivates the proposal discussed in chapter 4, to adopt a battery electric model in a tool devoted to design a microgrid.

Thanks to the results found in scientific literature, in the following part of the thesis work, after an insight into the off-grid design methodologies present in literature, a novel procedure for battery modeling in sizing tools is proposed.

Chapter 3

Off grid systems sizing methodologies

In the previous chapter, the different methodologies present in literature for modeling batteries have been reported. It has resulted that each approach is suitable for different applications and in order to choose the proper one it is necessary to deeply understand which characteristics are needed in the desired application context.
The scope of the present work is to develop a novel procedure for modeling battery systems in dimensioning tools for off-grid plants; off-grid systems play an important role to ensure diffuse electricity access in developing countries, in all the contexts where the national grid is not available or unreliable. Literature provides many different methodologies that thanks to accurate simulations of life-time performance of stand alone systems can help investors and donor's agencies in choosing the best plant solution in terms of size of components and control strategies. The majority of the sizing methods, whatever techniques are employed, ultimately search for an optimal combination of system reliability and cost. Actually, system reliability is proportional to system costs, and hence the greater the reliability the higher will be the costs and vice-versa [124]. System reliability can be identified with the Loss of Load Probability (LLP) which is the share of the electricity demand not fulfilled by the power system over a certain period while the cost is often represented by the Net Present Cost (NPC).
However, most of the tools and methodologies present in literature don't take into account important aspects typical of rural areas. These are for instance uncertainties related to final users' electricity needs and to energy production from RES, the important role played by storage systems and the consequent need for an accurate BESS model and the forecast of load evolution. Comprehensive stochastic procedures that look at the atypical features of rural contexts and include estimation errors into the design phase are strongly required into a robust design of off grid systems [125]. Moreover, it is necessary to stress the importance of BESS modeling in robust design of off-grid systems, as long as they play an important role in defin-

ing reliability and cost of a plant: the correct estimation of their SOC is related to the capacity of the plant in providing the requested load, while the increase in SOH and consequent need for replacement are related to plant costs.
Once having reported in the chapter an insight into the principal sizing methodologies for stand alone systems present in literature, a detailed description is reserved to Poli.NRG, a new methodology developed by Energy Department of Politecnico of Milan, adopted as a simulation tool for the thesis project.

3.1 State of the art

Within scientific literature, different sizing methodologies are used to design off-grid systems [126]:

- Intuitive methods: they use simplified algebraic relationships between load requirements and energy sources availability. They utilize average values of solar irradiation and load demand. Due to their simplicity, they can be used just to have a rough evaluation of the system size.
- Analytical methods: the components of the system are characterized by computational mathematical models as a function of reliability so as to determine system's feasibility. The system performance can be estimated for different set of feasible size of system components. They oppose to the simplicity in sizing calculations, the difficulty in estimating coefficients of the mathematical equations.
- Numerical methods: simulations are carried out at each time step (usually 1 hour or 1 day), to compute energy balances and evaluate yearly performance of the system. Load and generation profiles can be deterministic or probabilistic.

When systems taken into consideration are hybrid systems composed of more than one generation source, or including dispatchable loads, the optimal choice has to take into account also the optimal energy dispatch strategy, in addition to size and types of components [127]. The conventional used optimization methods are based on: heuristic algorithms, linear programming model (LPM); dynamic programming (DP); non-linear programming(NLP); multi-objective programming (MOP); multi-objective evolutionary algorithms (MOEA); multi-objective goal programming and multi-input linear programming (MILP) [128].
Many softwares that utilize mainly analytical and numerical methods for the optimal sizing of off grid systems, from small stand alone systems to bigger hybrid mini grids, are commercially available. Some of them are listed in the following:

- HOMER [5]: it was developed in 1993 by National Renewable Energy Laboratory (NREL) USA, for the design of both on-grid and off-grid systems.

Simulations are based on 1 hour time step during which all of the parameters (e.g. load, input and output power from the components) remain constant. The objective function is the minimization of the Net Present Cost. Battery model is a simplification of KiBam model.

- HYBRID2 [7]: it was developed in 1996 by Renewable Energy Research Laboratory (RERL) of the University of Massachussetts, USA, with the support from NREL. It uses statistical methods to predict the long term performances of various hybrid systems. Battery model used is KiBam model. The simulation is accurate, as it can define time intervals from 10 min to 1 h.

- HOGA [8]: it was developed by the University of Zaragoza, Spain. It is a C++ based software that allows the multi or mono objective optimization of hybrid power systems utilizing Genetic Algorithms. Simulations are performed in intervals of 1 hour. Different options are proposed to users for modeling lead-acid batteries: KiBaM, Sheperd model with modifications proposed by Copetti and Schiffer model [25], moreover it includes also three models for Li-ion batteries, with particular attention to LFP and LCO chemistries.

- TRNSYS [9]: it was created in 1975 by the University of Winsconsin and University of Colorado. It was originally created to study passive solar heating systems, nowadays it has been revised and can be used for simulations of photovoltaic systems as well as low energy buildings and renewable energy systems. It is a quasi steady state performance simulation tool based on FORTRAN code; it does not provide optimization facilities but it carries out simulations with great precision. It uses Shepherd model for lead acid batteries.

- HYBSIM [6]: it was developed by Sandia National Laboratory analyzing off grid systems composed by renewable as well as fossil fueled generation sources. It carries out financial analysis computing cost comparisons between different configurations. The battery model utilized is a modification of Shepherd model.

Commercial softwares lack in modeling important features typical of electrification process in rural areas [125],[129]; in such applications the problem has some critical peculiarities.

- *Load consumption uncertainties*: data regarding electricity consumption in rural areas are typically not available either because the consumption does not exist (e.g. not electrified) or because the area is not monitored. Consequently load consumption has to be estimated based on local surveys and assumptions that are prone to significant uncertainties. For this reason it is necessary to use a stochastic approach to evaluate the distribution of different load patterns that the users could require.

- *Load evolution scenarios*: off−grid electrification would require a long term approach to properly evaluate return on investment, life cycle of technologies, architecture of the transmission/distribution systems and the impact evaluation. The basic pillar in this approach is that the load forecasting would require long-term evaluation, in order to avoid unreliable system design (oversizing or undersizing). Moreover, unreliable system design can entail a social, economic and environmental impact [130]. Load evolution forecasting is particularly important in developing countries context, where the energy consumption is growing very fast.
  The forecast of load evolution for creating a lifetime load profile can be grouped into different approaches [130].

  – Assumed function: exploiting costumers' questionnaire or expert's opinions some growth trends can be assumed. Some examples are a linear function, presuming that load increases linearly during the years; logarithmic function, assuming the consumption stabilizes after a while; step function, if it is presumed that consumption faces sudden changes due to future connections.

  – Extrapolation from data: load evolution scenarios can be estimated by extrapolating growth trends from historical data. However, in the case of rural communities, data about past consumption trends are often not available; moreover, the extrapolation of past trends can give inaccurate results when the development of new activities has to be taken into account.

  – Scenarios driven models: different evolution scenarios in rural communities can be assumed. These could be for instance, household electrification, the development of electrically powered income generating activities or the improvement of public services such as street lighting [4].

  – System dynamics: it is an approach that allows to understand the nonlinear behavior of complex systems over time using stocks and flows, internal feedback loops and time delays. It is and advanced method, able to tackle techno-economic and social complex dynamics.

  – Other approaches: input/output analysis, time-series, regression techniques are among the other possible approaches found in literature to forecast load consumption [131].

- *Unpredictable energy sources*: off grid power systems typically rely on renewable energy sources which are by nature unreliable and unpredictable. It is necessary to collect data regarding energy resource availability, which in rural areas of developing countries have to be estimated on the basis of weather

stations located in the main cities. Several databases and models are available that can facilitate the computation

- *BESS modeling*: storage systems are a fundamental part of off-grid plants, contributing to the costs and reliability of the system. Sizing methodologies should implement accurate BESS models in order to embrace the unconventional working conditions in DCs scenarios and provide accurate results. In the commercial softwares previously described, the most common used battery models result to be the analytical models (KiBam or Shepherd): their strength stands in the short computational time that makes them suitable for robust design of off-grid systems. On the other side, they use analogies and equations to represent batteries which are far from the real battery physics. No commercial software has been found that adopt different BESS modeling approaches: electric, stochastic or electrochemical have not been investigated yet.

Starting from these considerations, E4G ([132]) research group of Energy Department of Politecnico of Milan developed the dimensioning tool Poli.NRG: it is a Matlab based tool aimed to the optimal design of a PV+BESS systems for off grid applications. It is a comprehensive procedure that allows for a robust dimensioning of the off grid plant: it couples the atypical features of rural contexts (i.e. resources and loads) by including estimation errors into the design phase with proper component models. Its strengths, with respect to the previously mentioned tools, stay in the short time-step duration of just 1 minute, in the accurate stochastic forecasting of load demand that deals with load consumption uncertainties, and in the opportunity to provide optimal output for different load evolution scenarios.

In the following section a description of the software is reported.

3.2 Poli.NRG

Poli.NRG (POLItecnico di Milano-Network Robust desiGn) is a novel software package for the robust design of off-grid electric power systems [125]. Today, the software allows for the simulation of PV+BESS system, but it is open to future improvements. The software is composed of four building blocks (fig. 3.1), related to different phases of the design procedure.

Data inputs gathering

In this block the information regarding electricity consumption and power generation are collected: users' electric needs, fixed and variable equipment costs and weather data.

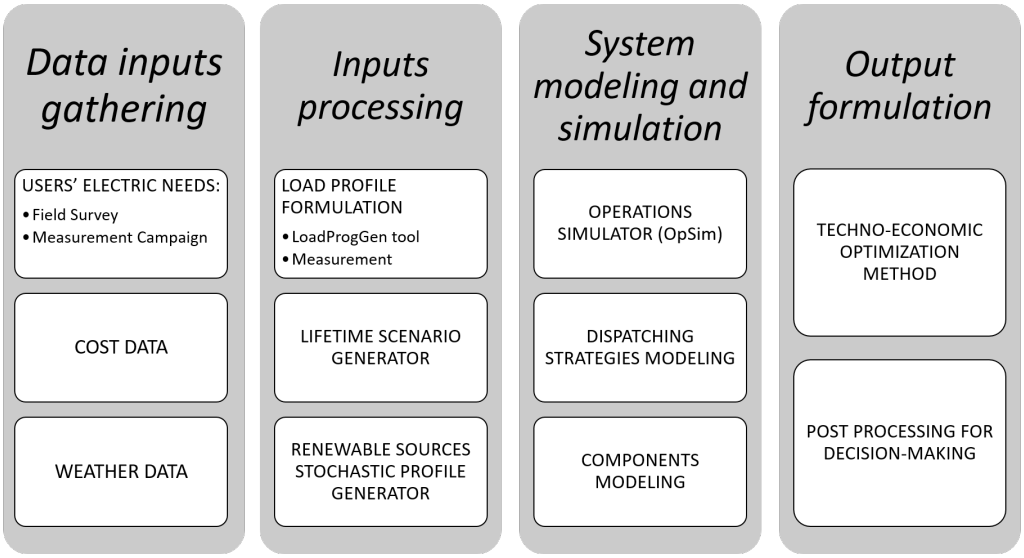

Figure 3.1: POLInRG building structure

- **Field Survey/Measurement campaign**: in order to compute the load profile of a given group of consumers in rural areas, a set of parameters is needed. Users are grouped into different user classes (j), each of them owning several appliances (i). For each appliance data regarding nominal power, overall daily functioning time, functioning window and functioning cycles are collected.
  Alternatively to field survey, a measurement campaign could be carried out, when direct consumption data are available. This is though often not the case in rural contexts.
- **Cost data and weather data**: specific costs of each component as well as weather data for estimating RES power production are collected.

Inputs processing

- **LoadProGen tool**: it is a procedure to formulate daily load profiles, that considers uncertainty related to users' energy consumption.
  Load profile is formulated for each of the users' class defined in the Field Survey. Uncertainties on the values of functioning times and functioning windows are introduced. The following steps are followed in order to compute the daily load profile:
  - Total daily electric need of the user class, the possible theoretical maximum power peak and the peak time are computed. A coincidence factor is computed thanks to the empirical correlation between the amount of users, the load factor and the coincidence factor.
  - The functioning schedule of each appliance is defined randomly by taking into account the functioning time, functioning cycle and functioning win-

dows predefined. The user class daily load profile is found by aggregating profiles of each appliances. The process is iteratively repeated until the resulting class power peak matches the reference power peak, within a predetermined error.

– The profiles of the different classes are aggregated in order to compute the total daily load profile, based on one minute time-step.

Each time the algorithm is run, it gives as output a different daily load profile, thanks its stochastic nature.

- **Lifetime scenario generator**: daily load profiles are generated until they represent all the range of profile variations for the given input setting. A convergence criterion allows to define the number n of profiles to be formulated.

$$\frac{\overline{y}(k)_n - \overline{y}(k)_{n+1}}{\overline{y}(k)_n} \leq 0.5\% \quad k \geq 95\% \text{ of time steps} \tag{3.1}$$

$$\frac{std[y(k)_n] - std[y(k)_{n+1}]}{std[y(k)_n]} \leq 0.5\% \quad k \geq 95\% \text{ of time steps} \tag{3.2}$$

where k corresponds to the profile time-steps, in this case of one minute; $\overline{y}(k)_n$ is the average load profile value of n generated profiles at the time step k; $std[y(k)_n]$ is the standard deviation of the load value of n generated profiles at time step k.

Daily load profiles can then be randomly aggregated in order to obtain an yearly profile. Yearly loads profile have to be projected over the entire lifetime of the plant according to specific load evolution scenarios (e.g. linear increase of the load).

- **Renewable sources stochastic profile generator**: photovoltaic power production during the year is reproduced exploiting specific algorithms.

System modeling and simulation

- **Components modeling**: this block includes mathematical models of system's components. Equation for PV power production at each time step k is the following:

$$E_{PV}(k) = P_{nom} \cdot (1 - \rho_T \cdot (T_{cell}(k) - T_{ref})) \cdot \frac{H_\beta(k)}{h} \cdot \eta_{BOS} \tag{3.3}$$

where P_{nom} is the rated panels power at an irradiance h of $1kW/m^2$, temperature of 25°C and air mass value of 1.5; ρ_T is the temperature coefficient provided by the manufacturer; $H_\beta(k)$ is the specific solar irradiation on tilted surface at time step k and η_{BOS} is the balance of system efficiency, related to losses not directly connected to sun energy conversion process.

- **OpSim tool** simulates the off-grid power system lifetime operations. At each time step, the amount of energy flowing through the BESS is given by the balance between PV power production and load consumption. At each time step k, the energy required or provided to the batteries is given by an energy balance between load consumption and photovoltaic power generation:

$$E_{user} = E_{PV}(k) - LC_{ns}(k)/\eta_{inv} \tag{3.4}$$

Where $LC_{ns}(k)$ is the load consumption and η_{inv} is the inverter efficiency.
Battery SOC is updated in order to evaluate the Loss of Load according to the specific modeling approach, see chapter 4. For each combination of PV and BESS size, OpSim provides techno-economic performance parameters: Loss of Load Probability (LLP), Net Present Cost (NPC) and Levelized Cost of Energy (LCoE).
LLP is the amount of energy not provided to the load during the plant lifetime over the total energy required.

$$LLP = \frac{\sum_{k=1}^{LT} LL(k)}{\sum_{k=1}^{LT} LC_{ns}(k)} \tag{3.5}$$

NPC is the present value of all the costs of installing and operating the system over the project lifetime.

$$NPC = \sum_{y=1}^{LT} \frac{Inv(y) + O\&M(y)}{(1+r)^y} \quad [\$] \tag{3.6}$$

LCOE is an indicator that measures lifetime costs divided by energy production. It represents the final cost of electricity required for the overall system to break even over the plant's lifetime. It is useful to compare the unit costs of different technologies over their life and it is a reference value for the electricity cost that rural consumers would face [125]

$$LCOE = \frac{r \cdot (1+r)^{LT}}{(1+r)^{LT} - 1} \cdot \frac{NPC}{(1 - LLP) \cdot \sum_{k=1}^{LT} LC_{ns}(k)} \quad [\$/kWh] \tag{3.7}$$

where LL(k) is the Loss of Load at time k, r is the discount rate, Inv(y) is the investment and replacement cost at year y and O&M are the Operation and Maintenance cost at year y.

- **BESS modeling**: Poli.NRG was based on a very simplified model for BESS. One of the main goal of this thesis work is to propose a novel methodology for developing BESS models in off-grid dimensioning tools applications, given that in the current state of art mainly approximated analytical models are adopted

(as it has been aforementioned in this chapter). The authors propose two different methodologies: a simple empirical model (with two different versions) and the more detailed and novel electric model. Details and implementation of the models are reported in chapter 4.

Output formulation

Heuristic and mathematical optimization methods are used to find the most robust design of the systems.

- **Techno-economic optimization method**. Optimal combination of PV and

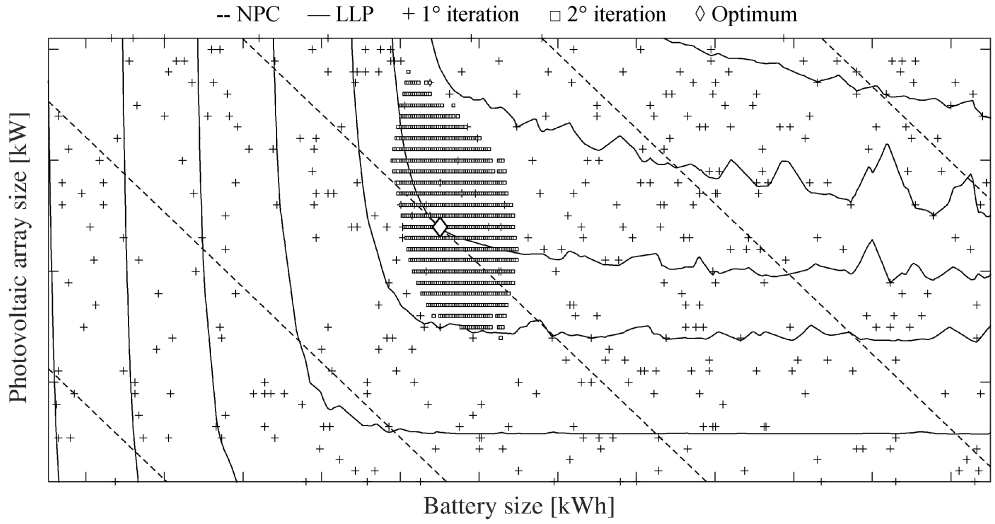

Figure 3.2: Searching space of the Poli.NRG optimization procedure [129]

BESS size is found inside the defined research space: this is the combination that minimizes the NPC while respecting the wanted system reliability, namely a constraint on the maximum LLP. An iterative procedure is implemented in order to find the most robust solution for each lifetime load profile.
The optimization algorithm is divided in two steps. Firstly, the searching space is defined, i.e. the ranges of PV and BESS to be investigated; secondly, the optimal combination of PV and BESS is found within the searching space. As regards the first step, constraints about minimum and maximum sizes of PV and BESS are set: PV minimum size has to be sufficient to produce the load consumption including an acceptable loss of load, the maximum size could be set as a multiple of the maximum power required by the load. BESS minimum size is set equal to a reasonable value while maximum size is considered as a multiple of daily energy consumption. For more details about the equations see [125].
The second step utilizes an heuristic procedure to find the optimal plant size.

The adopted algorithm is based on the imperialistic competitive algorithm: it is an iterative process that progressively explores the searching space, synthesized in figure 3.2. When considering the first load profile, the algorithm tries randomly a fixed number of PV+BESS combinations within the research space (the crosses in figure 3.2); for each of them OpSim provides the LLP and NPC. A first scattered matrix of LLP and NPC values is created and an estimation of the probable solutions can be done. In the graph, the curves represent the point with the same values of NPC and LLP: NPC decreases as PV and BESS size reduces while the opposite holds for LLP. A second iteration is computed, trying only combinations surrounding the supposed optimum solution: in the graph they are represented by the small squares. The optimal solution is found when a new iteration confirms the results of the previous one, given a predefined tolerance. In the graph the diamond shows the optimal solution which is the point with minimum NPC that respects the maximum LLP constraint.
New load profiles are simulated until a convergence criterion is fulfilled: the new iteration confirms the results of the previous one given a predefined tolerance.

$$\frac{std[PV_{rbt}(n-1,s)] - std[PV_{rbt}(n,s)]}{std[PV_{rbt}(n-1,s)]} \leq 0.25\% \tag{3.8}$$

$$\frac{std[BESS_{rbt}(n-1,s)] - std[BESS_{rbt}(n,s)]}{std[BESS_{rbt}(n-1,s)]} \leq 0.25\% \tag{3.9}$$

where n is the number of profiles simulated; s is the number of scenarios; $std[PV_{rbt}(n,s)]$ and $std[BESS_{rbt}(n,s)]$ are the standard deviations of the robust solution. Finally, given the area of optimal solutions, one for each profile, the optimal solution is considered to be the most frequent solution. When more than one evolution scenarios are considered, different areas of solutions are computed in parallel, and a map of solutions is shown.

- **Results**. Size of PV and Batteries that minimize the NPC while fulfilling the desired level of LLP are the outputs of the software; LCOE of each robust solution is also computed. Different evolution scenarios show different results.

Each block of Poli.NRG methodology is well structured and designed to give in output reliable and robust solutions; the stochastic load profile generator, the iterative optimization process and one-minute time step simulations contribute to the accuracy of the modeling tool. For this reason, it is important that even the system modeling block, (comprising PV panel and BESS), respects the characteristics of precision and accuracy without introducing errors given by excessive simplifications. It is worthwhile to stress the meaningful difference in the length of the simulation time-step between Poli.NRG package and the other off-grid dimensioning tools found in literature: Poli.NRG simulates every minute of the system lifetime

in order to highlight the variations in load consumption and the dynamic behavior of the battery. The results allow to:

- obtain a precise and correct definition of the BESS requirements;
- precisely estimate BESS efficiency or equivalently the electrical response (OCV and voltage)

A simulation time–step of 15 minutes or 1 hour is not able to represent the transient characteristic that is specific of the electrochemical energy storage, as it has been shown in chapter 1 and chapter 2.
On the other side, each block has to be optimized in terms of computational time, in order to allow simulations over the whole plant lifetime. This is particularly relevant when thinking about future improvements of the method, for instance to take into account dispatching strategies or the possibility of grid integration, that could enhance the complexity and hence the computational effort.

Taking into account the previous considerations, in the following chapters two methodologies are proposed and compared in order to model battery system: a more simple but faster empirical model and an accurate electrical model.

Chapter 4

Proposed battery models

The foremost goal of the present thesis work is to develop a battery model, suitable to applications in sizing softwares such as Poli.NRG, described in the previous chapter. Two aspects have to be considered when simulating a BESS system in a design tool:

1. The proper modeling approach has to be chosen, in order to estimate both SOC and SOH of the battery. As described in chapter 2, according to the actual scientific literature the possibilities are electrochemical, stochastic, analytical and electrical models.

2. The modeling approach has to be set for a specific battery technology as long as each one has its peculiar features. As explained in chapter 1, the choice in the case of off-grid applications falls mainly on lead acid or lithium ion batteries.

As regards the first point, it has been found in literature that the most common approach in battery modeling for robust design application is the empirical/analytical (KiBam,Shepherd (sec. 2.2)).
The contribution of the authors was to introduce and compare two other different BESS modeling approaches, after having deeply analyzed the current state of art of the battery modeling in the chapter 2. The choice of the authors has been dictated by the search of a good compromise between accuracy and feasible computational time.

- Empirical model with variable efficiency and degradation: this represents a classic approach, with an easy parametrization; moreover, it does take into account the dependence of battery behavior on operational conditions.

- Electric model: the battery is modeled through an equivalent electric circuit, able to represent in an accurate way battery current-voltage characteristics. It is a novel approach in sizing tools application; the idea is to utilize a model as bounded as possible to the real battery physics without compromising computational time.

Electrochemical models have not been taken into account due to their complexity. They need a wide range of parameters to be determined and require long computational time: these are compensated by a high accuracy, which is not needed in design tools, where many approximations and long time steps are used. Stochastic models, instead, are too bounded to specific battery phenomena (e.g. recovery effect) and cannot represent in a good way battery as a whole.

With respect to the second point, the technological choice of BESS for off-grid systems in developing countries is determined by cost-effectiveness and availability of materials on site, not on the best available technology. Thus, lead acid batteries still represent the most used technology in this field [133]. However, lithium ion technology faced a steep costs reduction in recent years and this trend is forecasted to continue in the next future[134]. Therefore, it is likely that lithium ion batteries will soon enter in competition for off-grid market with lead acid batteries. For this reasons, the authors applied the modeling approaches described before both to lithium and lead batteries, to compare advantages and disadvantages of each technology.

In this chapter, at first it is given an insight on the battery modeling approaches proposed by the authors; secondly it is described their implementation in Poli.NRG package.

4.1 Empirical battery model proposed

Simplified empirical model. The model is the simplest empirical model present in scientific literature and described in chap 2. The goal is to have a term of reference for the perfomances evaluation. It considers the charge/discharge battery efficiency as a constant value, non dependent on E-rate. Moreover, a model for battery lifetime is not present and the change in SOH is not considered. To account for degradation a fixed maximum number of cycles and a maximum number of years are given as input. Other key features are constraints on the minimum SOC and on the maximum power-to-energy ratio. The parametrization of this simple model can be done by considering literature reference values. The choice has been driven by the willingness to compare the novel approaches proposed by the authors to the simplest and less time consuming model found in literature.
Empirical model. The main empirical model proposed considers the battery as a black box that can store energy with an efficiency representing energy losses during charge and discharge. Efficiency value is not constant, but it depends on the operating conditions and it decreases as power increases. Efficiencies during charge and discharge are considered equal for the sake of simplicity.

The graph in figure 4.1 shows the roundtrip efficiency as function of E_{rate}:

$$E_{rate} = P/E_{BESS,rated} \quad [1/h] \tag{4.1}$$

$$\eta_{charge} = \eta_{discharge} = \sqrt{\eta_{roundtrip}} \tag{4.2}$$

The efficiency equation can be written as:

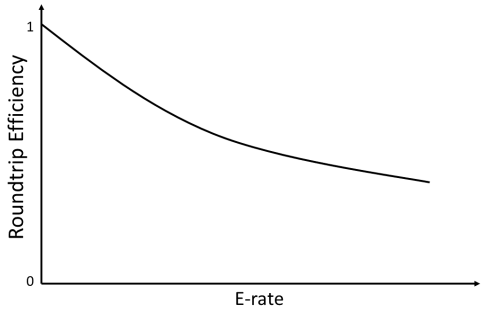

Figure 4.1: Roundtrip efficiency for a generic battery as a function of E-rate

$$\eta_{roundtrip} = a \cdot E_{rate}^3 + b \cdot E_{rate}^2 + c \cdot E_{rate} + d \tag{4.3}$$

where *a,b,c,d* are coefficients empirically fitted depending on the battery technology. This model can be applied both to lithium ion and lead acid battery, by simply changing the input parameters that can be selected from datasheet.
State of charge indicator is computed as the sum of the energy previously accumulated by the battery and the energy charged or discharged over the effective capacity [Wh] of the BESS:

$$SOC(t) = \begin{cases} SOC(0) - \frac{E(t)_{charge} \cdot \eta_{charge}}{E_{BESS,rated}} & \text{Charge} \\ SOC(0) - \frac{E(t)_{discharge}/\eta_{discharge}}{E_{BESS,rated}} & \text{Discharge} \end{cases} \tag{4.4}$$

Describing battery behavior by simply using an efficiency allows to estimate energy providable by the battery only utilizing data given in battery datasheet; no complex experimental parameters evaluations are necessarily required. Nevertheless, testing procedures on a cell is a more accurate way to derive empirical model parameters. This model can adequately describe rate charge effect.

Lifetime modeling

Battery lifetime degradation has to be taken into account in order to have a model that follows real behavior of batteries as precisely as possible. Indeed, in real operation batteries tend to degrade at a faster rate then the off-grid system itself, meaning that during lifetime batteries must be replaced. Replacement strongly influences the overall cost of the system, hence degradation model is fundamental.

The estimation of battery SOH in the model proposed by the authors is based on the equivalent full cycles to failure method (see chapter 2). As described in the section 1.3, degradation mechanisms are strictly dependent on the chemistry of the cell. Hence, it is necessary to distinguish lifetime degradation model for lithium ion cell and lead acid cell.

Lead acid degradation model
Battery lifetime decreases with increasing number of cycles and the decline is more rapid the higher DOD is. Indeed, lead acid battery cycle aging is strongly affected by DOD. Calendar aging is modeled by considering a maximum number of years after which battery is considered permanently damaged and it must be replaced.
Capacity fade cf(t), which is the rate of battery capacity loss per cycle, is evaluated considering the maximum number of cycles to failure for the battery and the maximum value of capacity loss.
The curve that represents the maximum number of cycles as function of DOD is derived from curves showing the variation of remaining effective capacity with the number of cycles at different DOD, that can be derived from literature [135] or manufacturers' data. Therefore, capacity fade is computed as the maximum acceptable capacity loss $C_{loss,max}$ over the maximum number of cycles at that specific DOD(t) (cyc_{max}).

$$cf(t) = \frac{C_{loss,max}(t)}{cyc_{max}(t)} \tag{4.5}$$

For instance, if the maximum capacity loss is 40% and the maximum number of cycles are 2000, cf(t) is $0.02\frac{\%}{cycle}$. A comprehensive diagram that shows capacity fade index as a function of DOD is depicted in fig. 4.2(a).
Lithium ion degradation model

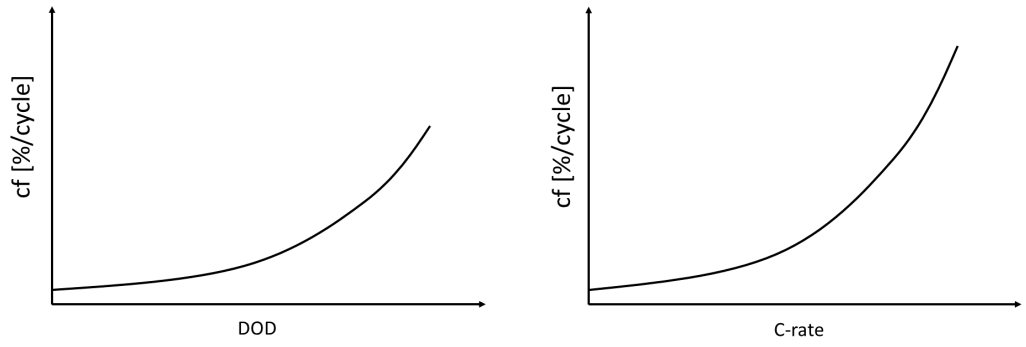

Figure 4.2: Capacity fade index as a function of DOD for a generic lead acid battery(a) Capacity fade index as a function of C-rate for a generic lithium ion battery(b)

A model for cycle aging is developed as seen for lead acid battery: battery lifetime

decreases with increasing number of cycles and the decline is more rapid the higher the current is. Indeed, lithium ion battery cycle aging is strongly affected by C-rate. Calendar aging is modeled by considering a maximum number of years. The example reported in figure 4.2(b) shows the generic trend of the capacity fade index cf(t) as a function of C-rate, that can be derived following the same procedure as for lead acid degradation model (eq. 4.5).

Independently from battery technology, the state of health indicator is calculated using capacity fade per cycles multiplied by the equivalent cycles the battery has passed through.
Equivalent cycles are defined for two different instants of time as:

$$Eq_{cycles}(t) = \left| \frac{SOC(t) - SOC(t-1)}{2} \right| \tag{4.6}$$

If Eq_{cycles} is equal to 1, it means the battery has completed a full discharge and charge cycle.
Finally, SOH indicator is defined as

$$SOH(t) = SOH(t-1) - Eq_{cycles}(t) \cdot cf(t) \tag{4.7}$$

SOH is used to change the capacity of the battery for each time step, until a minimum value of SOH or the maximum number of years is reached. Typically battery is considered dead and hence needs to be replaced when SOH=0.8 (see chapter 2).
The major drawback of empirical model is that battery dynamic response, as well as voltage characteristics are totally ignored. Real battery physical limits are represented by a maximum and minimum voltage acceptable by the cell: to compute the amount of charge not providable by the battery it is hence important to have an accurate estimation of the OCV and voltage. In order to accomplish that, a suitable solution could be the electrical battery model, proposed in the following section.

4.2 Electrical battery model proposed

A simplified equivalent circuit model is proposed as a valid alternative to the more diffuse analytical models: it has in fact been shown multiple times that electrical models can be a good compromise between electrochemical and analytical models in terms of accuracy and short computational time.
Many sophisticated electrical models are present in literature (section 2.2) able to accurately describe the dynamic behavior of the battery: for example, the EIS-based passive models with many parallel impedance groups (figure 2.12, figure 2.13) are able to precisely approximate both the electrochemical processes happening inside the cell, as electrode kinetics phenomena and diffusion phenomena, and the battery

external effects seen in section 1.4. However, the main problem lays in the computational time: the conclusions in chapter 2 underline the very high accuracy level of EIS-based model but also the very long simulation time. The implementation of this kind of electrical models in sizing tools like Poli.NRG software is not feasible, since robust design of off-grid system presents some other time consuming activities besides BESS modeling, like optimization tool, heuristic approach to load profile, evolutions scenario (see chapter 3). Hence, there is a need for compromise between accuracy and short simulation time, between precise electrochemical description and inevitable simplifications.

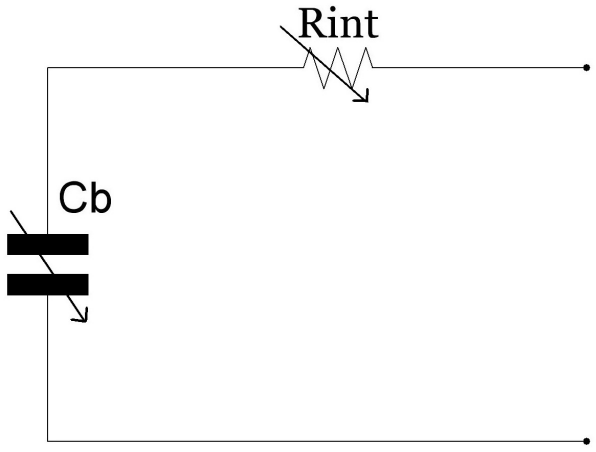

Figure 4.3: Equivalent electric circuit of the proposed model

Starting from all the previous considerations, the authors chose the simplest passive "R int model" (shown in chap. 2, fig 2.7). The proposed equivalent electric circuit is composed of a capacitance, Cb in series with a resistance, Rint as it is shown in figure 4.3. The choice of both of the parts of the equivalent circuit have precise reasons: as explained in chapter 2, the capacitance is aimed to represent the cell equilibrium condition while the resistance accounts for the losses.
Overpotential (and ohmic loss) of the cell during operation is taken into account by a single resistance Rint[Ohm] (i.e., power performances), so that the simplicity of the model allows to shorten computational effort at most. Moreover this allows for an easy parametrization of the cell, with the need of just a few experimental measurements. Transient behavior of the cell is neglected because most of the effects are fast and expire in few seconds (see chapter 2 and annex A) and in the context of dimensioning tools, where the time steps vary from minutes to hours, battery can be imagined to work in steady state condition.
Internal resistance can be determined in many ways according to the assumptions. One option is to use the Electrochemical Impedance Spectroscopy (see annex A) and to define the resistance as the real part of impedance at a specific frequency, dependent on the load input profile. In the case of unknown characteristic frequency of the

load profile, the equivalent resistance is evaluated at a frequency of 16mHz(1/60s): considering a minute time step in the simulation, the battery will never be subjected to frequency higher than 1/60 Hz. Moreover, most of the transient effects occurring in the cell have expired after one minute (double layer and diffusion inside porous electrodes have a short time constant, see figure A.1 in annex A).
Resistance values at different state of charge can be evaluated through eletcrochemical impedance spectroscopy applied to the battery at different SOC (for further details, see annex A); hence, laboratory testing is necessary. The measurements collected with EIS can be shown on the Nyquist plot (figure 4.4 (a)), from which it is possible to select the real part of the impedance corresponding to the desired frequency. Rint as a function of SOC for a generic cell is reported in figure 4.4 (b). Missing values of Rint(SOC) are interpolated from Rint-SOC curve.

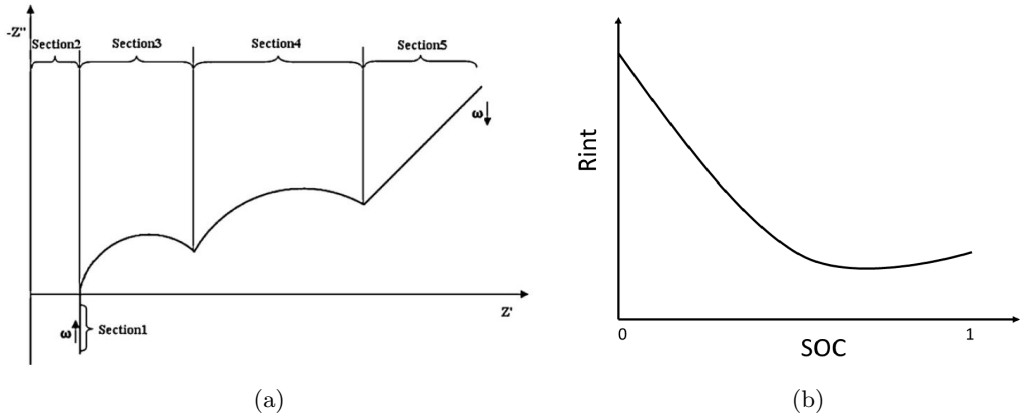

(a) (b)

Figure 4.4: Typical battery Nyquist plot(a) and variation with SOC of the parameter Rint(b)

Passive model has been preferred to active ones because it represents in a better way battery physical characteristic: battery cannot provide an infinite quantity of energy as a controlled voltage source, it is instead better represented by a capacitor which can release only the amount of charge accumulated. Moreover, the commonly used Rint model with an ideal voltage generator, has often to be coupled to Coulomb Counting methods (see eq. 2.4) to account for SOC and hence OCV. This introduces errors due to the indeterminations on current values that sum up when computing the integral of current over time. With the proposed passive battery model, it is sufficient to know the constitutive capacitor's law together with look up tables, without having to integrate the current.
The capacitance Cb[F] represents the total capacity of cell (i.e. energy performances) in regime conditions and it varies with the open circuit voltage. Sometimes it is called intercalation capacitance to underline the relation with accumulation and depletion of ions [136]. OCV is directly related to the SOC through discharge curve

(figure4.5 (b)), hence Cb is a function of SOC. The voltage at its terminals is the open circuit voltage (Equilibrium Potential Difference eq. 1.7) of the cell. Cb has been determined applying the capacitor's constituent equation:

$$I(t) = C(t)\frac{dOCV}{dt} \tag{4.8}$$

This capacity can also be called Incremental Capacity (IC) since it is calculated by taking the derivative of the OCV profile: it can be represented in a graph as a function of OCV (see figure4.5 (a)). The trend of the curve reflects the evolution of electrochemical processes during charge and discharge: peaks in the IC curve are associated to specific phase transition phenomena in the cell [61]. The integral of the curve corresponds to the total charge storable in the cell [Ah]. After the

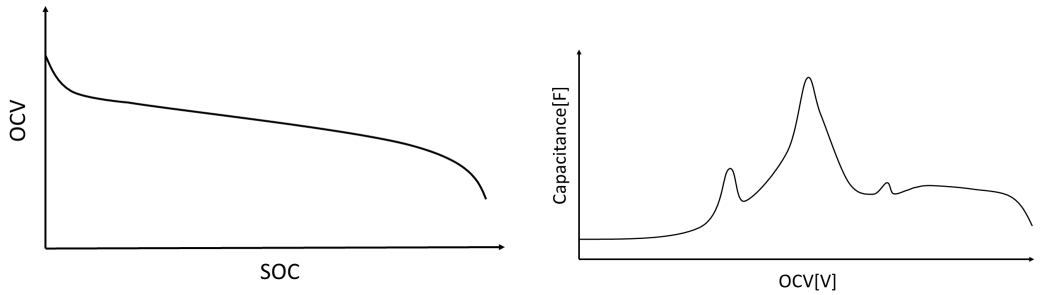

(a) (b)

Figure 4.5: OCV as a function of SOC(a) and the derived incremental capacitance as a function of OCV(b) for a generic battery

presentation of the key parameters, it is necessary to formalize the characteristic equations of the model.
The fundamental assumptions on which this model is based are:

- Temperature dependence of battery behavior is not considered: the parameters of the model are not dependent on temperature. This is a strong assumption as long as the working temperature of a cell strongly affects its performances and its degradation processes (as stated out in chapter 2). However, a thermodynamic model for the cell would be needed to estimate temperature during operation and to take into account variations of parameters; this would be too complex and not viable in off-grid design applications.

- The battery is composed of a certain number of electrochemical cells connected in series or in parallel, but the model is developed at the cell level. The loss related to the connections between cells are considered negligible.

- Electrochemical cell has the physical limits of maximum and minimum voltage, given by manufacturers or experimental tests.

Considering that the scope of this chapter is to develop battery models for Poli.NRG software, which has been implemented in Matlab, the system of equations that characterizes the battery needs to be solved numerically.
Assuming to know the power input of the battery, the following system of equations holds:

$$\begin{cases} I = P/V \\ I = C(OCV)\frac{dOCV}{dt} \\ V = OCV(SOC) + R(SOC) \cdot I \end{cases} \tag{4.9}$$

This is a system of differential algebraic equations (DAE) that needs to be solved numerically to give as output the value of voltage and SOC at each time step. SOC is directly derived from the OCV curve.
Different numerical methods have been implemented by the authors in Matlab in order to find the optimal solution in terms of computational time and accuracy; these are, with increasing complexity: Euler, Euler modified, Runge Kutta with adaptive step size (Matlab solver ODE15s has been chosen to solve DAE problem), as shortly reported in the following.

Explicit Euler method. This method is used to numerically solve a Cauchy problem as

$$\begin{cases} y' = f(t, y) \\ y(t_0) = y_0 \end{cases} \tag{4.10}$$

where $y(t_0) = y_0$ is the initial condition or boundary condition.
The numerical solution in the time step n over a generic time interval [t_0;t_0+T] is represented by

$$y_{n+1} = y_n + h \cdot f(x_n, y_n) \tag{4.11}$$

where h=T/N is the numerical step, N is the number of intervals in which subdivide [t_0;t_0+T].

Modified Euler method. With this method, the numerical solution to Cauchy problem becomes

$$y_{n+1} = y_n + h \cdot f(x_n + \frac{h}{2}, y_n + \frac{h}{2} \cdot f(x_n, y_n)) \tag{4.12}$$

Runge Kutta method with adaptive step size. In adaptive step size methods, a certain accuracy criterion is fixed and if the estimation of the local truncation error does not satisfy that criterion, the the step size is decreased, otherwise it is kept fixed. Many RK methods of different orders are merged to obtain the estimation of the truncation error. In general, the numerical solution can be written as:

$$y_{n+1} = y_n + h \cdot \varphi(x_n, y_n; h) \tag{4.13}$$

where $\varphi(x_n, y_n; h)$ is an incremental function; its approximations are computed in x_n points not necessarily evenly spaced.

In conclusion, the Euler method is the simplest and also the most approximate method for solving differential equation whilst Runge Kutta with adaptive step size is the most accurate. However, given that a DAE system entails a high degree of complexity when solved with RK methods, the Euler and Euler modified are more computationally affordable in off-grid system dimensioning tools; the different methods are eventually compared in terms of trade off between performance and computational effort.

Lifetime modeling

Modeling degradation in electrical model accounts for both capacity and power fade (for further details look section 2.3).
As far as capacity fade is concerned, the approach to the estimation of the SOH is equivalent to the one proposed in the empirical model; capacity fade cf(t) is different in lithium ion technology and lead acid technology.
In addition, an indicator for power fade is computed and it is called State Of Resistance (SOR), which represents the increase in the internal resistance of the cell due to degradation. SOR depends on the Power Fade factor pf(t), that is calculated differently according to technology; pf(t) represents the percentage of resistance increase due to cycle aging.

Lithium ion degradation model
For lithium ion cell, the method of the number of cycles to failure is applied in the same way to determine both SOH and SOR. The increasing factor pf(t) for the internal resistance depends on C-rate (example is reported in figure 4.6).

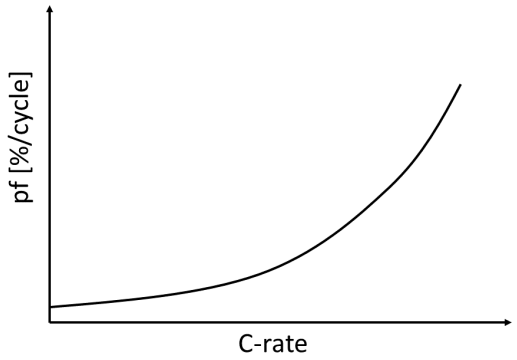

Figure 4.6: Power fade as a function of C-rate for a generic Li-ion battery

Lead acid degradation model
For lead acid cell, resistance increases with number of cycles at constant rate, independent from DOD or C-rate. This approach is followed also in literature [15]. Hence, pf(t) has a constant value during simulation.
For both the technologies, SOR is evaluated as:

$$SOR(t) = SOR(t-1) + Eq_{cycles} \cdot pk(t) \tag{4.14}$$

Again, calendar aging is modeled only considering a maximum number of years for battery lifetime.
The model parameters are then updated to take into account degradation.
In the following section the implementation of both empirical and electrical models in Poli.NRG is detailed.

4.3 Models implementation

In this section, we deal with the implementation of the aforementioned battery models (i.e. empircal and electrical) within Poli.NRG procedure. As presented in chapter 2, the parameters of each battery model are tailored to the technology. Therefore, two set of parameters have to be found for each battery model: one for the lead acid case and another one for the Li-ion case. Two different sources of data have been used to complete the parametrization of the models:

- Manufacturers' datasheets detailed in annex E.
- Available measurements on electrochemical cells collected at the Energy Storage Research Center (ESReC) located in Nidau(CH) with cutting edge machines. The measurement were carried out within the framework of the collaboration between Politecnico di Milano (DoE) and CSEM-PV Center (Swiss Center for Electronics and Microtechnology) and are detailed in [129].

Experimental tests and datasheets refer to the following electrochemical cells: (i) Lithium Nickel Cobalt Oxide(LNCO) cell BostonPower-Swing5300E; (ii) Lead-acid VRLA cell Sonnenschein A502/10S, Exide TechnologiesE. The experimental test used in the present thesis are listed in the following.

- **OCV test**: OCV curves of the two cells have been determined by discharging the cells with very small currents: 1/100C. Due to the low current value, voltage of the cell corresponds to the open circuit voltage.
- **Efficiency test**: efficiency curve (i.e. efficiency as function of the operating current) has been experimentally measured for the only Li-ion cell by applying several charge-discharge cycles at different C-rates. Whilst for the lead-acid

cell efficiency curve has been derived from data about charge-discharge cycles given by the manufacturers.

- **Square current tests**: square current profiles at different C-rates (0.1C, 0.5C, 1C and 2C) have been applied to the cell at different SOC (20%, 50% and 80%).

- **EIS tests**: impedance characterization has been performed for both the technologies. Frequency range moves from 10 kHz to 3 mHz. EIS were performed at different SOC (0%, 20%, 50%, 80%, 100%) for the Li-ion ion cell, while at only 50% SOC for the lead-acid cell.

- **Aging tests**: Li-ion cells have been cycled with different conditions (i.e. different C-rates with fix DOD 100%) to compute capacity fade and resistance increase. Whilst, lead acid cells capacity fade has been computed using manufacturers' data.

Empirical model

The model parametrization for lead acid battery has been done with the datasheet of the Sonnenschein A502/10S. It has been used to create the roundtrip efficiency and capacity factor index. No laboratory measurements were needed.
On the other side, lithium ion model efficiency has been determined through the laboratory tests explained above.
In figure 4.7(a) and 4.7(b) are reported respectively the roundtrip efficiency of the lead acid cell and of the lithium ion cell. The difference is strongly marked: the lithium ion cell can withstand higher E-rate before having strong decrease in energy performance.
Capacity fade index for lithium ion cell derives from experimental measurements in the laboratory previously cited. It is plotted as a function of C-rate in figure 4.8(a). Capacity fade index for Sonnenschein derives from datasheet because experimental measurements were not available. It is plotted as a function of DOD in figure 4.8(b).
In the approach adopted, load profiles and power production are given as input. The power is assumed constant for 1 minute (i.e., the time step k). At each time step, the energy respectively entering or exiting the battery is computed as the following:

$$\begin{aligned} E_{charge(k)} &= E_{user} \cdot \eta(E_{rate}) \\ E_{discharge(k)} &= E_{user} / \eta(E_{rate}) \end{aligned} \tag{4.15}$$

where $E_{user} = E_{PV} - E_{load}/\eta_{inv}$ is the energy balance between energy production and consumption, i.e. the energy withdrawn or injected in the battery by users. It is lower than zero when the battery is discharging and viceversa when it is charging.

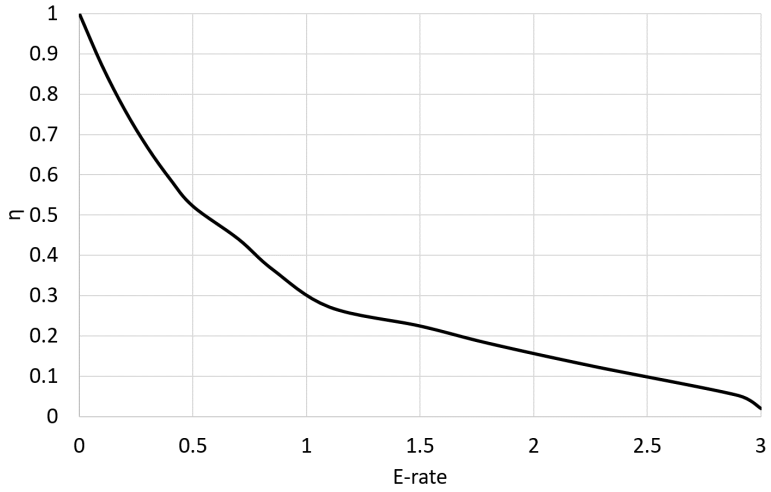

(a)

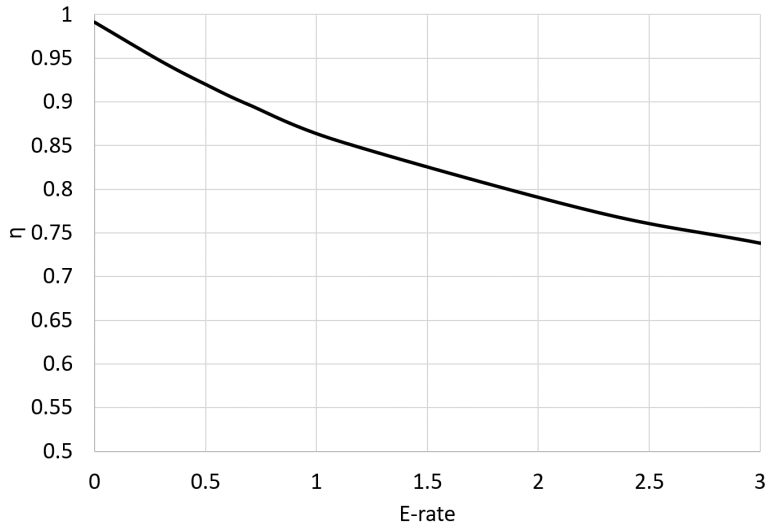

(b)

Figure 4.7: Roundtrip efficiency for lead acid cell(a) and Li-ion cell(b)

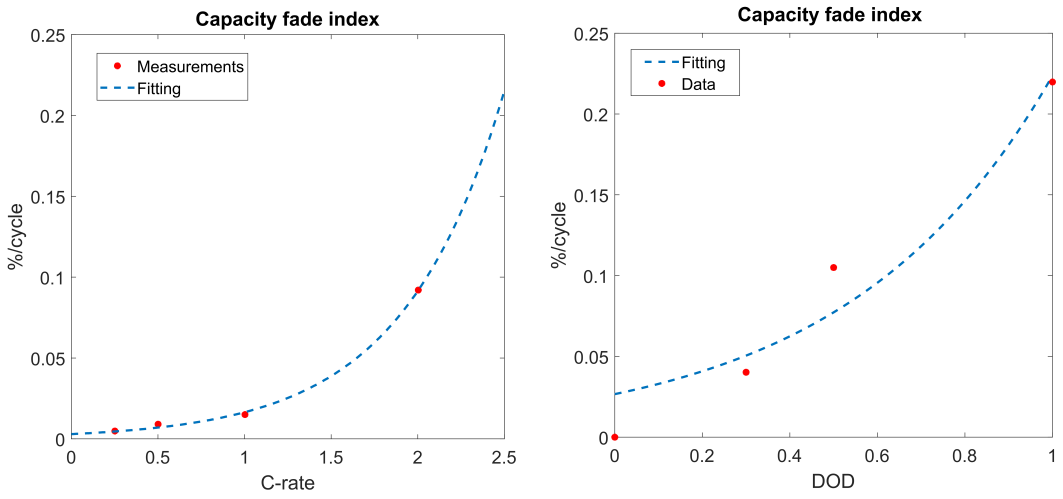

Figure 4.8: Capacity fade as a function of DOD for a the lead acid cell(a) Capacity fade as a function of C-rate for the lithium ion cell(b)

SOC(k) is updated at every time step[1]:

$$SOC(k) = SOC(k-1) + \frac{E_{charge(k)/discharge(k)}}{E_{BESS} \cdot SOH(k)} \tag{4.16}$$

E_{BESS} is the battery nominal capacity [KWh].
The model is subject to constraints that limit the storable energy:

- a maximum value for the power to energy ratio PE_{ratio}, which is the maximum power output with respect to the rated capacity of the batteries; E_{max} is defined as

$$E_{max} = PE_{ratio} \cdot \Delta k \cdot E_{BESS} \tag{4.17}$$

- a minimum and maximum value for SOC that will prevent permanent damage to battery;

Effective capacity of the battery is limited due to degradation mechanisms and it is estimated through SOH (eq.4.7).
As a consequence, the eventual loss of energy required by the loads that the system is not able to supply is evaluated as a loss of load LL:

$$LL(k) = \begin{cases} LL(k-1) + (E_{max} - E_{user}(k))\eta_{inv} & \text{if } E_{user}(k) \leq -E_{max} \\ LL(k-1) + (SOC_{min} - SOC(k))E_{BESS}(k)\eta_{inv}\eta_{disch} & \text{if } SOC(k) \leq SOC_{min} \end{cases} \tag{4.18}$$

[1]An approximation is introduced by the variable denominator in the fraction. However, as long as time steps are short, SOH doesn't change much from one to another and the error is negligible.

Electrical model

Equally to what has been done for empirical model implementation, electrical battery model has been parametrized for lithium ion technology (BostonPower cell) and lead acid technology (Sonnenschein cell).

BostonPower and Sonneschein cells OCV-SOC characteristic are reported in the figure 4.9(a) and figure 4.9(b) and they are used for the parametrization of the model. SOC has been calculated starting from unit (fully charged) and subtracting

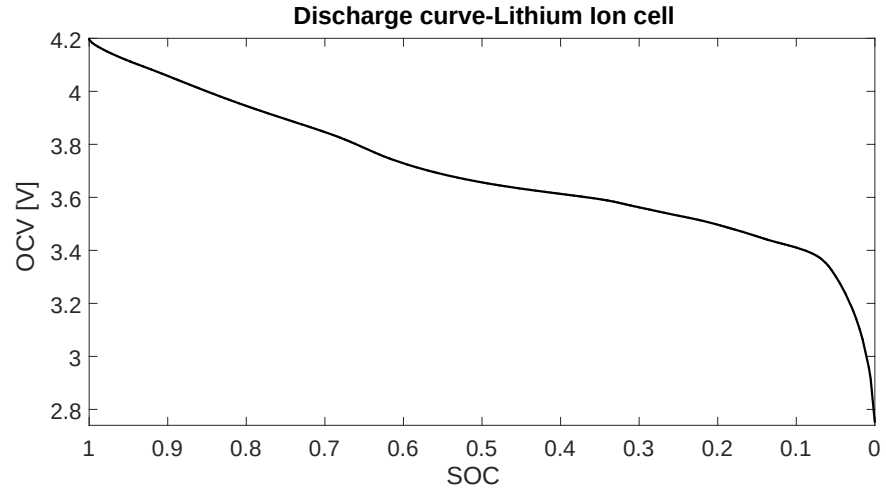

(a)

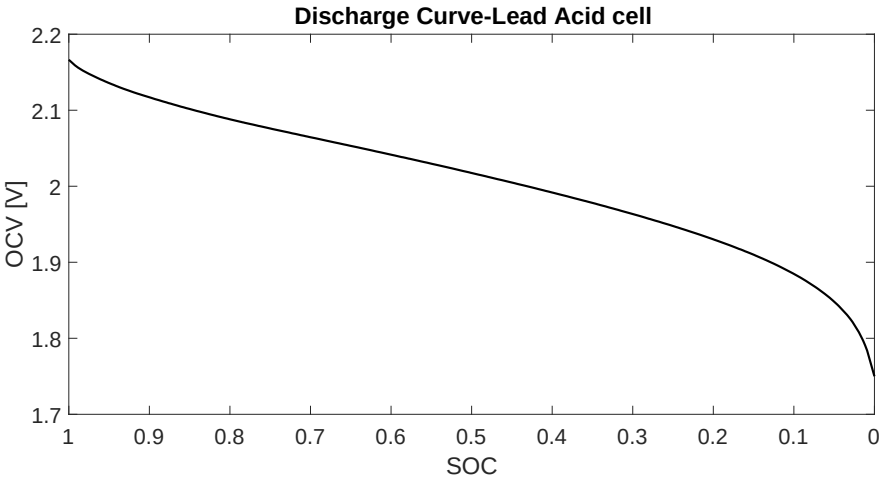

(b)

Figure 4.9: Discharge curve @1/100C of:Li-ion cell(a) and lead acid cell(b)

the ratio between the measured discharged capacity in each instant of time and the rated capacity of the battery. The parameter Cb is calculated as a function of the OCV using the constituent equation of the capacitor; the numerical solution of this differential equation has been found applying the central finite difference method for the derivative of the OCV. Cb-OCV diagrams of the cells are reported in figure

4.10(a) and figure 4.10(b). The fitting curve is simply a look-up table that utilizes first order interpolant matlab function. Since the integral of this curve correspond to the storable charge in the cell, the error was calculated between the integral of the fitting curve and the rated capacity of the cell. This fitting is very accurate, indeed the errors are equal to 0.033% and 0.035%.
It is possible to notice that IC curves differ according to technology (figure 4.10(a), figure 4.10(b)). The smoother trend of the lead acid battery is directly related to its linear OCV characteristic. The discharge curve of lithium ion cell shows instead a stronger non linearity, and this difference is the cause of the sharp peaks in its IC curve. As far as the internal resistance is concerned, the complete characterization

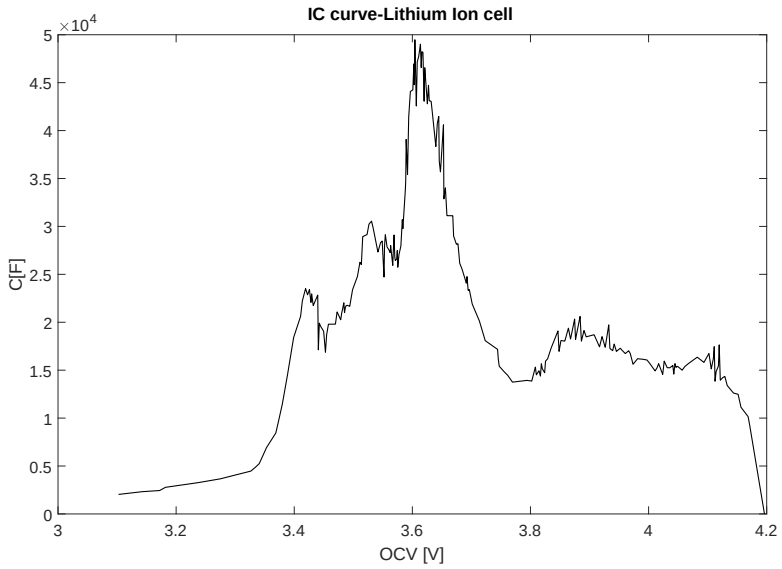

(a)

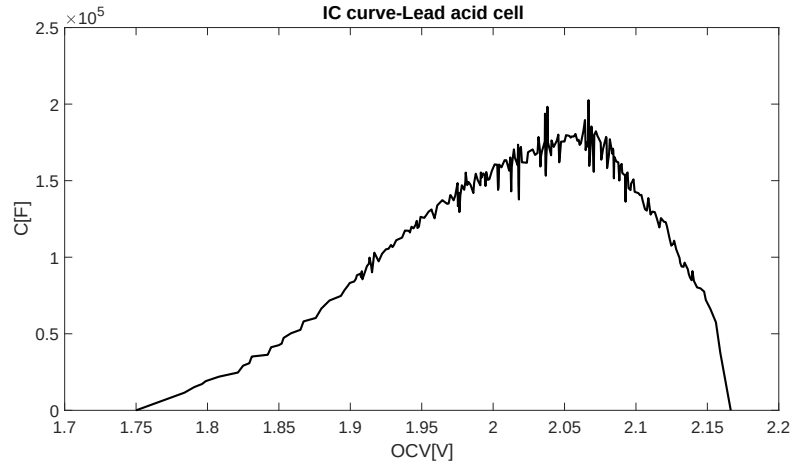

(b)

Figure 4.10: Cb as function of SOC of the Li-ion cell(a) and of lead acid cell(b)

of Rint with SOC was possible only for the lithium ion cell, due to lack of EIS mea-

surements for the lead acid cell. Nyquist plot for BostonPower is reported in figure 4.11. For the Sonnenschein only measurements at SOC=50 % were available: curve of resistance vs SOC was determined adapting trends found in literature [137]. Comparing figure 4.12(a) and figure 4.12(b), it is evident that the specific trend depends on the examined technology, but in both cases resistance tends to be very high for low SOC with a decreasing trend in the middle range and an increasing trend for SOC values in the range 80-100%. The selected fitting curve for Rint(SOC) is a a look-up table with first order interpolant.
Capacity fade index for the electrical model is equal to the one reported in parametrization of empirical model. Power fade index for BostonPower cell has been determined from laboratory measurements and it is reported in figure 4.13.

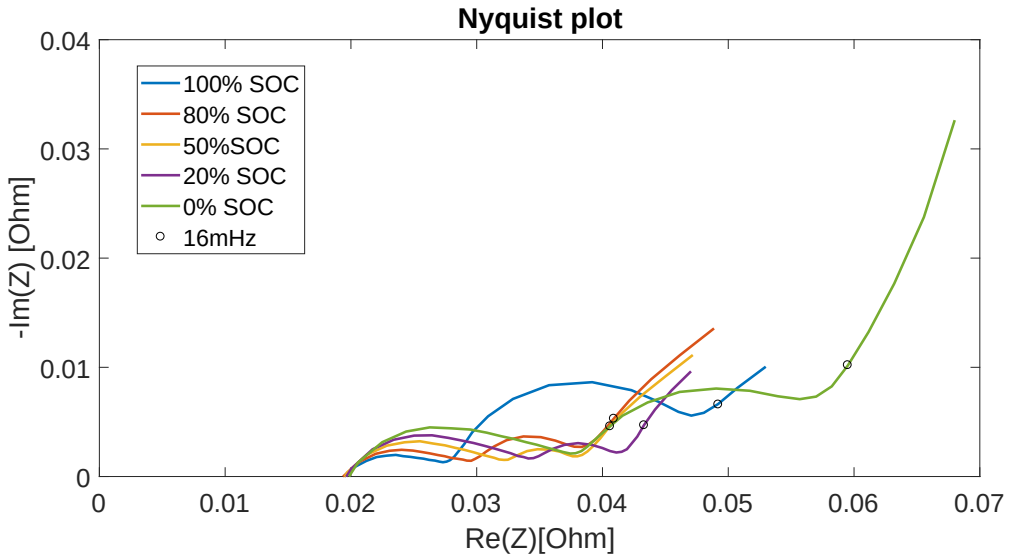

Figure 4.11: Nyquist plot of BostonPower-Swing5300

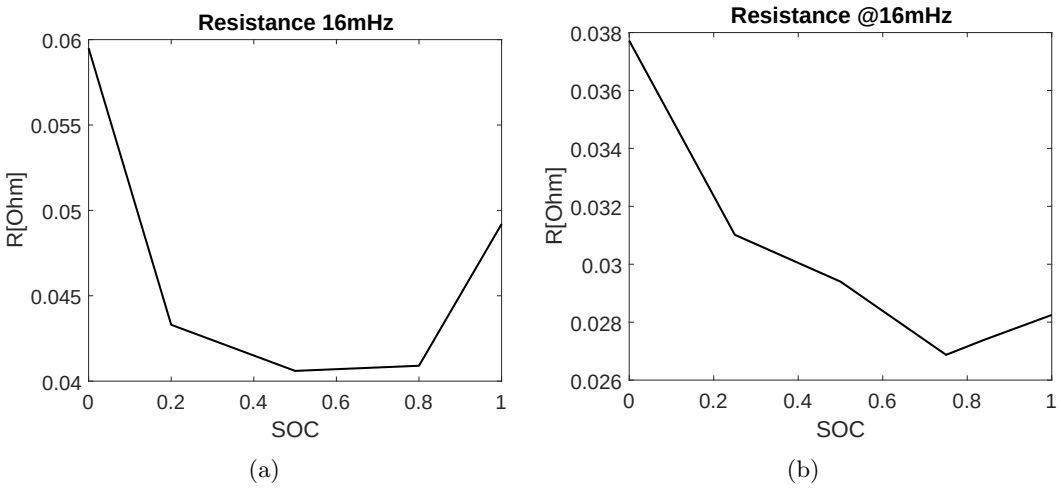

(a) (b)

Figure 4.12: Internal resistance variation with SOC for lithium ion cell(a) and lead acid cell(a)

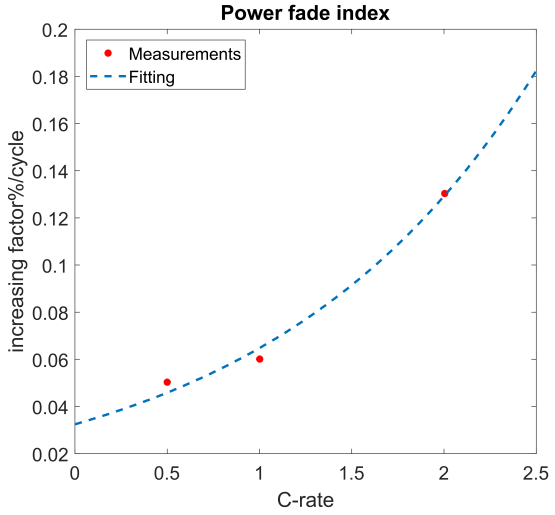

Figure 4.13: Increasing factor for internal resistance as a function of C-rate

In the following, the proposed models have been validated with the three numerical solving procedures previously described: Euler, Euler modified and Runge kutta. A comparison between the results is reported in order to select the appropriate solving method.

Solving method selection

The model has been tested with lithium ion parameters. Voltage output has been measured and used in this section to select the solving method for electrical model system of equations. The parameter Rint(SOC) has been taken from the Nyquist plot at the frequency correspondent to 5 minutes, which is the frequency of the applied square current profile.

Figure 4.14 shows experimental voltage measures (V_{exp}) versus simulated voltage during constant current profile at 50% SOC. Similar trends has been obtained for 20% and 80% SOC, thus figures are note reported. This simple model is not able to follow the transient period during current variations, but it can accurately model the voltage during steady-state conditions and accurately estimate OCV, i.e. SOC. Actually, it is worth to notice that the higher the current the higher the discrepancy between model and experimental voltage is: this means that the main error in this model is due to the evaluation of the resistance. In figure 4.15 are reported the simulated voltage values for Euler method, but with two different resistance function: in one cases the Rint is taken at 16mHz frequency, while in the other is taken at 3.33 mHz which is the specific frequency of the load input. It is possible to notice that in the first case the simulated voltage is less accurate than in the second case. The root mean square error (RMSE) is a frequently used measure of the differences between values predicted by a model and the values actually measured. It is cal-

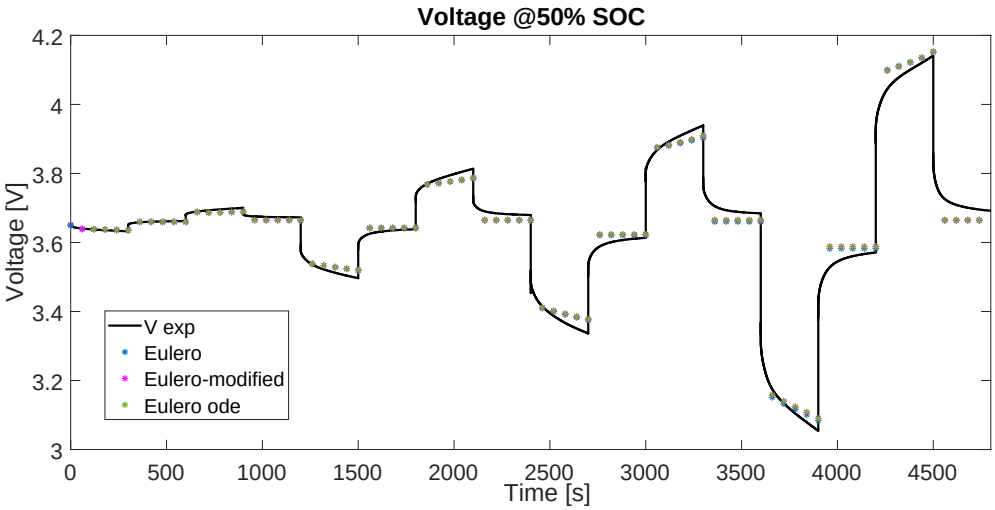

Figure 4.14: Simulated and measured voltage of BOSTON POWER SWING 5300 cell at 50% SOC

culated as the square root of the mean of the squares of the deviations (between predicted value and observed value):

$$RMSE = \sqrt{\frac{\sum_{t=1}^{n}(\hat{y}_t - y_t)^2}{n}} \tag{4.19}$$

RMSE of the three different method are (the values for 80% SOC has been excluded[2]):

- Euler RMSE for 20% SOC=0.0424V; RMSE for 50% SOC=0.08V
- Eluer modified RMSE for 20% SOC=0.0855V; RMSE for 50% SOC=0.083V
- Euler ODE RMSE for 20% SOC=0.0825V; RMSE for 50% SOC=0.0831V

In addition, the simulation time for the model is doubled for Euler modified with respect to Euler, and it is around 20 times higher for ODE. Considering that:

- the rmse values are quite similar between all the methods, since the main cause for the error lays in the assumptions of the model and not on the solving method; moreover, the rmse values are sufficiently low (considering the application context) even for Euler method: this method, in fact, does not lead to relevant approximation errors since the iteration time-step is short enough (1 minute);
- the simulation time for Euler is the lowest and, in robust design of off grid system, simulations are very time-consuming processes;

[2]The assumed maximum voltage limit of the cell was infinitesimally different from the maximum voltage reached during testing, causing a misleading high RMSE value.

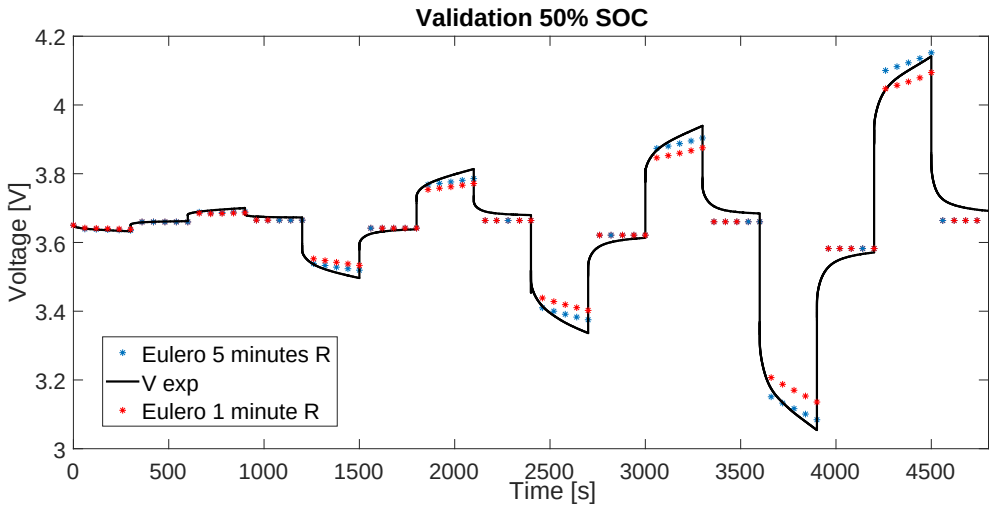

Figure 4.15: Simulated and measured voltage of BOSTON POWER SWING 5300 cell at 80% SOC

consequently, the electrical model is implemented using the Euler method. This electrical model can be applied both for a lithium ion cell and a lead acid cell, since the modeling approach is suited for both (see chapter2).

In the approach adopted, load profiles and power production are given as input. The power is assumed constant for 1 minute (i.e., the time step k). The energy actually entering or exiting the battery is dependent on the SOC. During each time step, the energy that could be provided or required to the battery for users is known (E_{user}); power flowing in the cell is assumed constant and it is scaled down from total energy batteries pack have to fulfill:

$$P(k) = \frac{E_{user}}{\Delta t \cdot N_{cells}} \tag{4.20}$$

The number of cells N_{cells} is equal to the size of the BESS divided by the capacity [Wh] of the cell.
Therefore, the current I(k) can be computed as:

$$I(k) = P(k)/V(k-1) \tag{4.21}$$

OCV(k) and V(k) are updated accounting for Cb and Rint at the previous time step.

$$OCV(k) = OCV(k-1) + \frac{I(k)}{C(k, OCV(k-1))}\Delta t \tag{4.22}$$

$$V(k) = OCV(k) + R(k, SOC(k-1))I(k) \tag{4.23}$$

Moreover it is relevant to point out that, at each time step, a control on the voltage value is performed: when voltage is outside the limits, the assumption is that the battery is not able neither to accept nor to provide power for the whole time step;

thus, in case of voltage higher of maximum voltage or lower than the minimum one, OCV(k)=OCV(k-1) and V(k)=OCV(k). This is an approximation that does not lead to big mistakes as long the time step is no longer than 1 minute while it would not have been a correct assumption in the case of iteration time-step lasting 15 minutes or 1 hour. When 1 hour time step is considered, voltage limits could be reached after several minutes: it would hence be a big approximation, in terms of energy provided or received, to consider the battery fully charged or discharged for the whole time step.
SOC(k) indicator is directly derived from the OCV look-up table.
The capacity Cb and the resistance Rint are updated every day to take into account degradation :

$$Cb(k) = Cb(0) \cdot SOH(k) \tag{4.24}$$

$$Rint(k) = Rint(0) \cdot SOR(k) \tag{4.25}$$

where Cb(0) and Rint(0) correspond to a new cell. At this point the loss of load of the system is computed as

$$LL(k) = \begin{cases} LL(k-1) + (E_{max} - E_{user}(k))\eta_{inv} & \text{if } E_{user}(k) \leq -E_{max} \\ LL(k-1) - E_{user}(k)\eta_{inv} & \text{if } V(k) \leq V_{min} \end{cases} \tag{4.26}$$

Summary

The table 4.1 is a summary of the main characteristics of each BESS model developed.
The methodology and BESS model presented in section 4.1 and 4.2 have been implemented in section 4.3 for the enhancement of BESS modeling in robust design of off-grid tools.

Model (code)	**SOC estimation**	**SOH estimation**	
		Calendar aging	**Cycle aging**
Empirical simplified (M1)	SOC limits $\eta_{roundtrip}$ const	Max n. years	Max n cycles
Empirical (M2)	SOC limits $\eta_{roundtrip}$ f(E-rate)	Max n. years	Min SOH Lead acid: SOH f(n cycles, DOD) Lithium ion: SOH f(n cycles, E-rate)
Electrical (M3)	Voltage limits R f(SOC,SOR) C f(SOC,SOH)	Max n. years	Min SOH Lead acid: SOH f(n cycles,DOD), SOR f(n cycles) Lithium ion: SOH f(n cycles, C-rate) SOR f(n cycles, C-rate)

Table 4.1: Main characteristics of the BESS models proposed

Chapter 5

Case study: E4G project

The BESS modeling methodologies presented in the previous chapters are suited to be implemented in the dimensioning tool Poli.NRG, in order to elaborate the robust design of a real case study.
The study case taken into consideration is Ngarenanyuki secondary school, in Tanzania, were the authors spent one month from September 19th until October 17th 2017. Politecnico of Milan has been collaborating for some years with the secondary school, where it contributed to install a hybrid micro-grid system. During the years after the installation, load consumption rose considerably, and the system is now subject to relevant stresses: in particular the installed storage system must tolerate continuous cycles at high power. The school has been recently connected to Tanzania national grid Tanesco, which helps in supplying the requested power; however Tanesco is highly unreliable (and costly) and cannot be the sustainable solution for the constantly growing load consumption. Moreover the microgrid in place is a single phase system, while in the school several three-phase loads have been deployed (e.g. fire protection system, as detailed in the following).
In this context, it makes sense to dimension a possible new alternative for the school: Poli.NRG methodology allows to find the optimal size for a combined photovoltaic (PV) and energy storage system (BESS). During the period spent in the school the authors monitored and collected data about load consumption; the field survey was useful to accurately determine school consumption patterns, so to dimension the off-grid system starting from reliable inputs. Using data collected and the different BESS modeling methodologies presented in the previous chapter, some simulations were performed. It is worthwhile noting that in rural areas the real load consumption profile cannot be determined with high precision; even after an accurate field survey many uncertainties remain and just statistical information can be obtained. In this context, it is not easy to define which is the best approach to model BESS performances. Even accurate BESS models would not provide very reliable results when data in input are affected by many uncertainties. From these considerations derives the choice of the authors of comparing the three modeling methodologies

of growing complexity presented in the previous chapter. The different modeling approaches have been compared in terms of output results and computational time. Moreover, the off-grid plant has been dimensioned with lead acid and lithium ion batteries, in order to compare and find eventual advantages of one technology with respect to the other.
In this chapter, the case study and the simulations set-up are explained .

5.1 Case study: Ngarenanyuki secondary school

Tanzania is one of the countries mostly experiencing the problem of poverty related to lack of energy access. It is a low income country, with the majority of the population living in rural areas. Electricity deficit is experienced by the majority of population as shown in figure 5.1

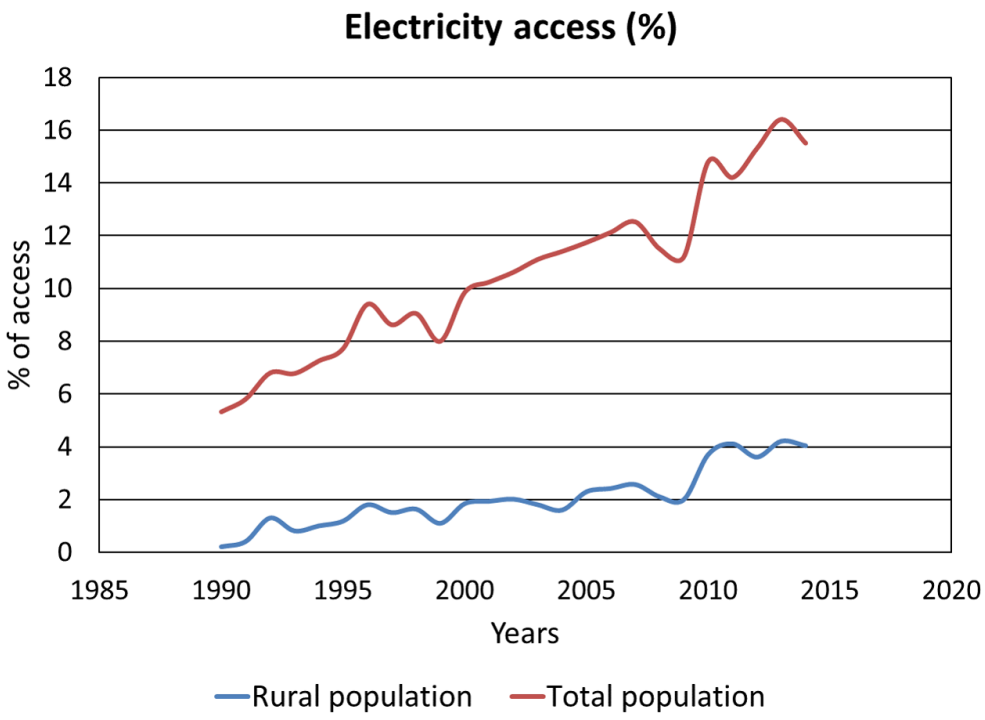

Figure 5.1: Development of electricity access in Tanzania [2]

From 1975, Tanzanian power sector is controlled by the single vertically integrated national company Tanesco. It owns a total of ca 1500 megawatts of installed generation capacity, 5 per cent of which composed by off grid systems. Tanesco aims to expand transmission and generation capacity (over 1000MW) by 2020. Moreover, the company has short and long term plans to extend the national main grid to isolated mini-grid areas [138].

Energy4Growing is an initiative of a research group of the Energy Department of

Politecnico of Milan. It was activated in 2013, with the aim of providing on grid and off-grid solutions in developing countries. Since 2015 it has been collaborating with Ngarenanyuki secondary school, in Tanzania, focusing on improving energy access in the school. The school is situated near to the small village of Ngarenanyuki, in a rural area of Arusha region, in the NorthEastern part of the country. The pilot

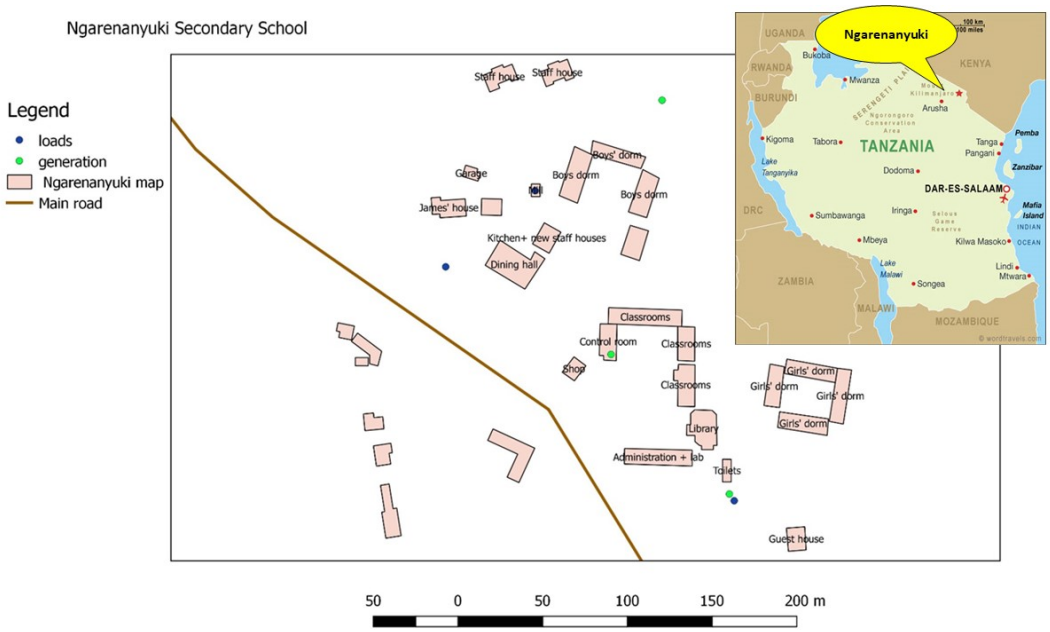

Figure 5.2: Location of Ngarenanyuki secondary school

project launched in Ngarenanyuki school in 2015 represents a significant case study for bottom-up implementations via micro grids. A hybrid micro-grid system was installed in the school, combining power systems already available on site and new installations. The system, to date still working and providing to the majority of school's electricity needs, is composed of generation units, a storage system, control units and conversion systems (see fig. 5.3).

Generation units and storage system are:

- 2 Photovoltaic panels of 1.5kW of nominal power each.
- 30 VRLA batteries Gaston GT 12 200, connected in series. Nominal characteristics: 30x200Ah, 72kWh.
- Hydro turbine: variable output between 800W and 3.2kW.
- Three phase diesel generator, 20kW nominal.
- Single phase diesel generator, 4.3kW nominal.

Generation units and load units are connected by means of an interface converter (IC) with specific control units. The micro-grid comprises a dc energy sources aggregation (Q1) and an ac double bus-bar system (Q2). In particular, Q1 is a dc/ac

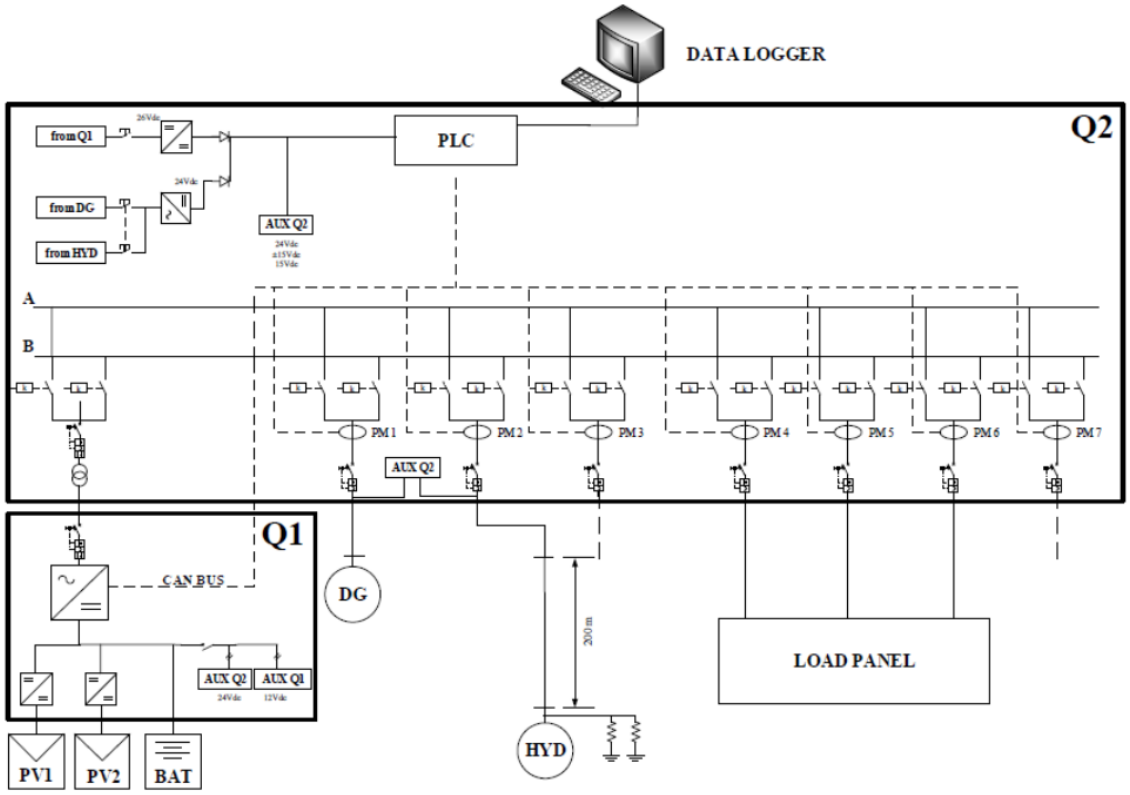

Figure 5.3: Micro-grid architecture for Ngarenanyuki school

control board connecting PV panels and the battery pack to the IC. The loads, the hydro turbine and diesel generator are connected to the ac double bus-bar board. Finally, an industrial PLC measures and controls the micro-grid, acting on the switchers of each line while calculating proper power set points for the IC [139]. The school energy consumption has been monitored by Politecnico of Milan since 2015, when the stand alone system was installed. During the last two years, school conditions further improved, thanks to the connection to the national grid Tanesco. The new power availability lead the school to develop, increasing number of loads and power consumption.

The authors spent one month in the school with the following purposes:

1. Help in the installation of a new monitoring system for Tanesco national grid. The instruments where donated by the company Energy Team S.p.A. in the framework of a long term collaboration with Politecnico of Milan. The Data Logger installed measures voltage and current of the national grid every second: from the direct measures, all the necessary derivative quantities are computed, such as active and reactive power of lines and frequency. The whole school consumption can in this way be monitored, merging data coming from the previously installed PLC, regarding generation units and the newly measured consumption from national grid.

Figure 5.4: Picture of the students reunited in the school yard, near classrooms

Moreover, data collected will be utilized in further studies, in order to analyze the quality of the grid, in terms of voltage and frequency oscillations, as well as interruptions. The quantitative investigation will help in promoting new projects for the school as for instance the integration of a new *minigrid* system with the national grid; the new hybrid power plant would be composed of PV panels and BESS, and could provide ancillary services to the highly unstable grid, such as primary regulation.

2. Perform a field survey in order to assess the new school power consumption and the eventual load evolution scenario, in terms of loads and generation units. Data collected have been utilized to dimension an hypothetical new plant for the school, composed of PV and BESS systems, that could supply to the overall energy needs.

3. Characterize batteries storage system. Lead acid batteries installed in Ngarenanyuki are subject to high stresses typical of applications in off-grid systems: long periods at low SOC, high current levels and almost never complete charges. The scope of the authors was to measure batteries' actual capacity and resistance in order to assess their state of health: parameters' value could be used for the parametrization of lead acid battery model in Poli.NRG.

As concerns the first goal, details regarding installed instrumentation, monitoring results and Elettra project are reported in annexD.

With respect to the second goal, the authors performed a survey with the local

head of technicians, including an "on situ" reading of the nominal characteristic of the machines. Quantitative and qualitative data regarding school loads and usage patterns were collected during the field survey. Loads are classified into daily and occasional:

- Most of the school loads are used every day. The most relevant daily loads are:
    1. Water pump: 2.4 kW, used every day for a total of ca 1hour, at different moments according to the needs.
    2. Farm: incubator and warming lights for chicks, total of ca. 1 kW. Used 24hours 7 days a week.
    3. Classrooms lights: ca.800 W. Used in the evening hours.
    4. Dormitory lights: ca.1.5 kW. Used in the evening and morning hours. Some of them are left on during all the night.
    5. Private buildings: mainly lights (estimated ca.800 W) and some appliances of ca.1 kW each (iron, toaster...) seldom used.
- Occasional loads are big three phase loads or single phase loads that are used only in case of need:
    1. Mill machine, 15 kW nominal. It is used to prepare flour for students twice a week for some hours.
    2. 2 Bricks machines, 11 kW and 8 kW nominal power. Used only for selling purposes.
    3. Fire-system pump, 2.4 kW nominal.
    4. Other single phase machines (drilling, welding), less then 1 kW nominal. Their consumption is very oscillating and they could create disturbances to the system lines; usually they are supplied from Tanesco or diesel generator.

Concerning the third goal, on field batteries characterization was performed. The scope was to parametrize BESS models for the specific case of Ngarenanyuki, where Gaston GT 12 200 batteries were previously installed, in the context of setting-up simulations for PoliNRG. Description of procedure and results of on field battery characterization is reported in annex B. Battery experimental characterization was divided into three phases: charge with PV, discharge with almost constant loads and resistance measurements with power pulses. The final scope was to determine the OCV discharge curve and values of resistances at different SOC for charge and discharge. However, data were affected by many errors and uncertainties due to non controllable external conditions: this is typical of measures that are not taken in the controlled laboratory environment. The main problems occurred are listed in the following.

- Non complete battery charge: due to system auto consumption, and the control system regulation, the complete charge would have required a really high number of days.
- Non complete discharge due to the impossibility of isolating the batteries for a significant period of time because of school needs.
- Discharge (for OCV curve) at non constant and sometimes high current due to primary electrical needs of the school that could not be excluded from the system.
- Not accurate resistance measurements. The dispersion of the measures was very high and the measurement uncertainty of every device was unknown.

For these reasons, measures do not have the necessary characteristics of repeatability and reproducibility and they have not been used as inputs parameters for the following simulations, where laboratory data and manufacturer's data were preferred.

5.2 Simulations' set up

After having performed a detailed field survey and having determined loads and usage patterns of the school, 3 different pools of daily load profiles have been generated with Poli.NRG-LoadProGen tool.

- Ordinary day: a normal school day, all the daily loads are taken into account.
- Mill day: 2 times a week, in addition to the normal loads, the grinding machine is utilized. This daily profile substitutes the ordinary day once every 4 days.
- Holiday: during Christmas, Easter and summer holidays, students go home. Normal classes do not take place and the power consumption is only related to teachers living in the school.

Notice that due to the high indeterminacy regarding usage patterns of occasional loads, they have not been considered into the load profiles' generation process. Occasional loads are seldom used during the year and for this reason, when a statistical approach is followed, there is no commitment of a big error when they are neglected. The only exception is constituted by the triphases grinding machine, which has been considered as long as it is used twice a week.
The inputs given to LoadProGen in order to generate the 3 pools of daily load profiles, in terms of users' classes, appliances, functioning times and windows, are reported in annex C. In figure 5.5 it is shown the user interface of LoadProGen with the set-up for the generation of the *ordinary day profile*. A convergence criterion has been used in order to define the number of daily load profile per each type to

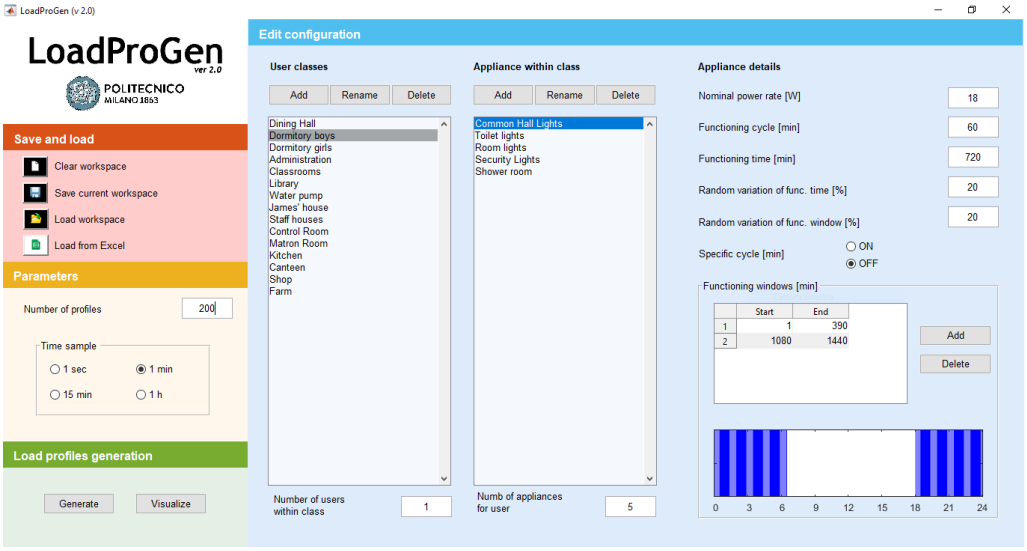

Figure 5.5: LoadProGen user interface. User classes of the ordinary day

generate, so that they could represent all the possible stochastic load variations. The yearly load profiles for Poli.NRG are obtained by randomly drawing from the above described pools. In this way, it is possible to define a finite number (200) of equiprobable yearly load profiles.

As explained in chapter 3, when considering electricity consumption in rural areas, it is important to take into account an eventual increase in load consumption during the years. The different methodologies reported in the chapter were anyway difficult to implement for Ngarenanyuki case study. Power consumption in the school started being monitored in 2015, when the micro-grid was installed; data regarding previous years are not available and it is therefore difficult to estimate the historical consumption growth trend. Moreover, increase in load consumption has not been gradual as long as the school has experienced two relevant improvements so far: after the installation of the micro-grid and after the connection with Tanzania electric grid, load consumption faced a sudden increase. The three phase machines bought after the connection with the national grid, require a total power of 36 kW, which is almost six times the whole school single phase consumption. In this context, it is difficult to quantify the step increase of power consumption and to predict when other major changes will occur. Other reasons that make it difficult to take into account a load evolution scenario are listed in the following. The survey to local inhabitants of the school has shown unreliable information about prevision of future electrical needs; simple load evolution function present in literature does not perfectly fit to the specific case of a single school; moreover, more advanced system dynamic tools were not feasible to be implemented in Poli.NRG due to their complexity entailing long simulation time. Hence, lifetime load profile has been generated without considering a load evolution scenario meaning that every year the load profile is exactly

the same. Despite being an unrealistic assumption, about 68% of 77 local energy planning studies found in literature considers a constant energy demand [130].

PV power profile given as input to Poli.NRG derives from data regarding annual mean irradiation in Tanzania [140], [141].

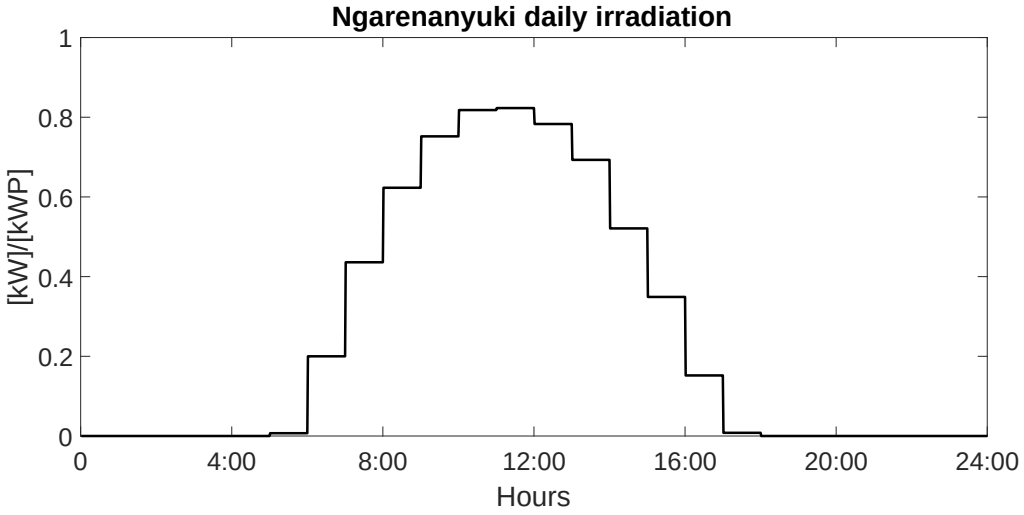

Figure 5.6: Solar irradiation hourly profile in January in Ngarenanyuki

Cost information about PV modules, batteries, and off-grid inverters are the result of a survey among Tanzanian local suppliers, while O&M, other investment costs and modeling parameters (efficiencies mostly) have been estimated based on experience. They are reported in table 5.1.

Various simulations have been carried out changing the battery model and tech-

Parameter	Value	Unit
Plant lifetime	20	years
Balance of system efficiency	85	%
Inverter efficiency	90	%
Discount rate	6	%
Lead acid battery cost	150	$/kWh
Lithium ion battery cost	400	$/kWh
Off-grid inverter cost	900	$/kW
PV module cost	2500	$/kW
O&M cost	100	$/kW/year
Other investment costs	20	% (of the main component cost)
LLP maximum	5	%

Table 5.1: Technical and economical assumptions

	Lead acid			*Lithium ion*		
	M1	**M2**	**M3**	**M1**	**M2**	**M3**
SOC initial	1	1	1	1	1	1
SOC min	0.5	0.5	-	0	0	-
PE ratio [kW/kWh]	0.25	0.25	0.25	2	2	2
SOH min	-	0.8	0.8	-	0.8	0.8
Calendar life [years]	8	8	8	12	10	10
Cycle life [n cycles]	1500	f(DOD)	f(DOD)	2000	f(E-rate)	f(C-rate)
Charge efficiency %	90	f(E-rate)	-	97.5	f(E-rate)	-
Discharge efficiency %	90	f(E-rate)	-	97.5	f(E-rate)	-
Cell capacity [Ah]	-	-	10	-	-	5.3
Max voltage [V]	-	-	2.17	-	-	4.2
Min voltage [V]	-	-	2	-	-	2.75

Table 5.2: Lead acid and lithium ion battery specifications

nology in order to make a comparison between different approaches. In particular constant efficiency, empirical and electrical battery models are compared in terms of results and simulation times. The models are those proposed in chapter 4. Moreover, BESS system is sized with the two different technologies of lithium ion and lead acid batteries, in order to analyze costs and differences. The simulations are classified according to BESS model and battery technology:

- **Simplified empirical model (M1)−lead acid**. Charge and discharge efficiency are 0.975; maximum number of cycles is 2000 and the maximum number of years to replacement are 8. Values are taken from last updated reference literature [134].
- **Simplified empirical model (M1)−lithium ion**. Charge and discharge efficiency values are 0.9; maximum number of cycles is 1500 and the maximum number of years to replacement is 12 Values are taken from last updated reference literature [134].
- **Empirical model (M2)−lead acid**. A limit to the maximum value of power acceptable by the battery is set according to datasheet (annex E), E-rate max=0.25. In the simulations SOH min is set to 0.8 as found in literature [15].
- **Empirical model (M2)−lithium ion**. The maximum E-rate is equal to 2

according to laboratory measurements described in sec.4.3. In the simulations SOH min is set to 0.8 as found in literature [15].

- **Electrical model (M3)−lead acid**. The minimum and maximum voltage are set equal to 2 and 2.17 , the nominal capacity is 10 Ah, as reported in datasheet (annex E).
- **Electrical model (M3)−lithium ion**. The minimum and maximum voltage are set equal to 2.75 and 4.2 , the nominal capacity is 3.53 Ah, as reported in laboratory tests (sec. 4.3).

The table 5.2 summarizes the parameters for BESS model in input to Poli.NRG. The approach that more likely could be followed by software users is to select the input parameter from manufacturer's datasheet.
For each single lifetime profile LC, Poli.NRG tool has been used to simulate all the possible configuration of PV-BESS. Specifically, the simulations were performed by ranging PV array size from 2 to 50 kW with 50 W step and BESS size from 10 to 1000 kWh with 500 Wh step for lead acid batteries and 100 Wh step for lithium ion batteries. Then, the PV-BESS combination that results in having the minimum NPC while respecting a maximum LLP of 5% is identified as the optimum solution for the given LC by using eq.3.1 and eq.3.2.

Chapter 6

Simulations, Results and Discussion

In the present chapter, the results of simulations set in chapter 5 are presented.
At first, simulated load profiles obtained thanks to the procedure developed to properly evaluate Ngarenanyuki energy needs (i.e. the school's load profiles) are reported and compared to real consumption measurements, elaborating data collected with the new measurement system installed.
Secondly, a comparison of modeling approaches is reported: trends of SOC and SOH of batteries obtained during simulations with different BESS models are shown, in order to deeply analyze every approach explained in chapter 4.
In the third section, results of the procedure adopted to design a new microgrid, that could ideally be able to supply the whole school consumption, are presented and discussed.
Finally, the authors propose a comparison and discussion among the design of a different BESS based on different models and technologies, the most promising Li-ion and the most common in DCs off-grid system lead acid; the section is concluded with an economic analysis on investment costs to evaluate the most economic viable solution.

6.1 Simulated load profiles

In figure 6.1 the averaged *ordinary daily profile* simulated with Poli.NRG-LoadProGen subroutine, is compared with the average value over 20 days of measured data. The school consumption is constituted of single phase and three phase loads, as explained in chapter 5. At first, only single phase loads have been considered in order to compare the 2 average profiles.
The simulated profile follows correctly the average real consumption trend: there are two power peaks, during morning and evening, while during the rest of the day the profile is flat. Percentage error between total kWh really consumed and the

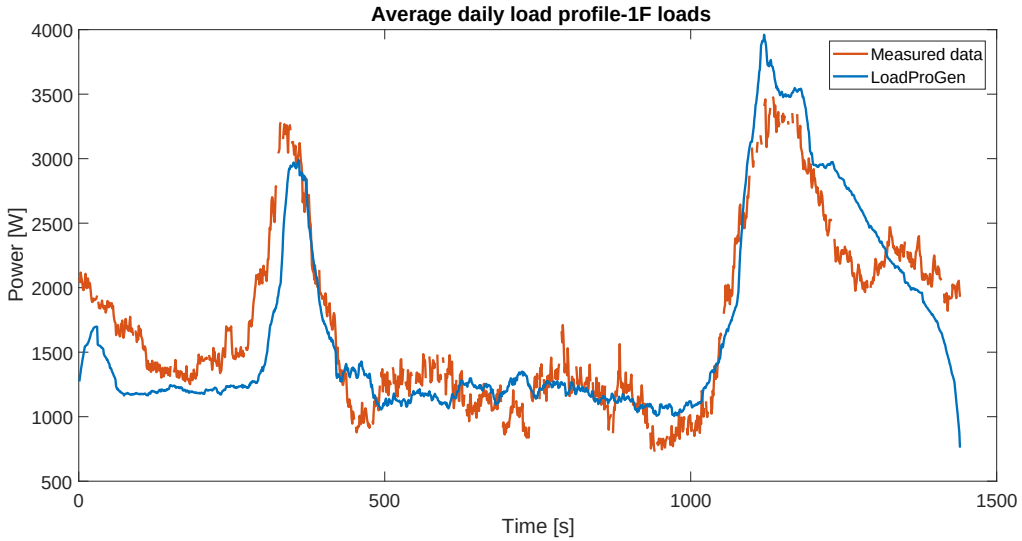

Figure 6.1: Comparison among single phase loads consumption mean measures and the average of simulated ordinary day profiles

simulated one is 3.5%, with simulated energy consumption slightly lower than the real one.

In figure 6.2, Tukey plot of the ordinary daily profile is compared to the one of measured profile. On each box, the central mark indicates the median, and the bottom and top edges of the box indicate the 25th and 75th percentiles, respectively. The whiskers extend to the most extreme data points not considered outliers, and the outliers are plotted individually using the '+' symbol. Simulated profiles have

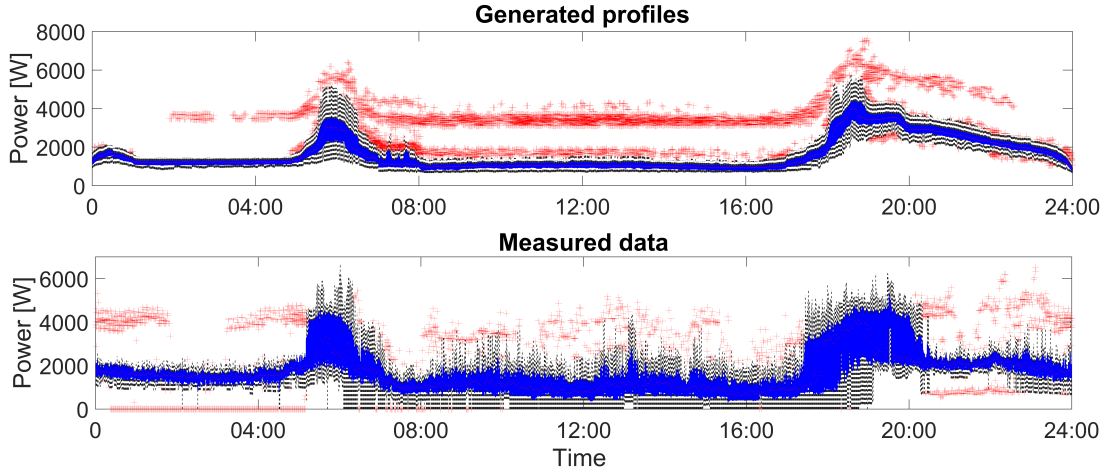

Figure 6.2: Data dispersion of measured single phase load consumption and of simulated profiles

a much smaller data dispersion with respect to measured ones. This represents a limit of the procedure for simulating load profiles. The tool takes into account load uncertainties and stochastic variations but it requires in input an accurate Field Survey. Indeed, during on field data collection campaign, it is complicated to ac-

curately assess all the specific parameters of load consumption (e.g. functioning period of appliances and functioning cycles); thus, the resulting simulated load profiles does not exhibit the typical high dispersion of real load profiles. Consequently, data regarding amount of loads and total power requirement have been taken correctly with respect to single phase consumption, while there is likely a bigger error related to functioning times and windows. Nevertheless, this specific case study of

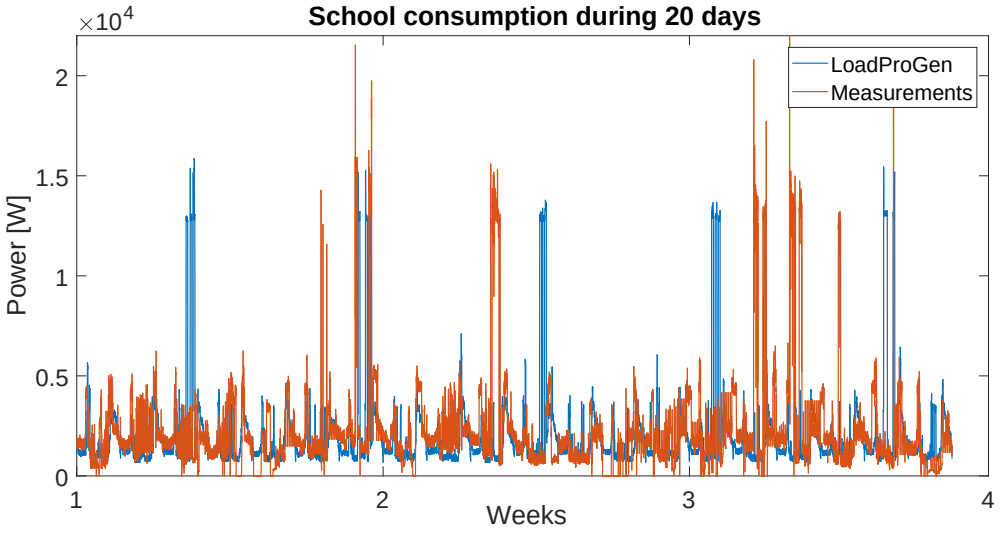

Figure 6.3: Trends of measured and simulated load profiles, including three phase loads, over 20 days

Ngarenanyuki school represents a positive anomaly with respect to the totality of DCs-based case study: typically, the data about energy habits (when the lights are turned on, when the water pump is activated etc...) and energy consumption is much less detailed, due to difficulties in gathering information from local inhabitants and in spending locally a sufficient period of time to report an accurate energy assessment. The authors have been able to reproduce as best as possible the load profile of the school. It is possible to state that this specific case study represents one of the best case scenario obtainable in DCs context.
In addition to the *ordinary day profile*, a *Mill day profile* has been generated to take into account the likely usage of three phase loads every 4 days. Profiles are aggregated randomly to create a yearly profile. In figure 6.3, 20 days of a generic simulated month are compared to the real 20 days' measures. It can be noticed that the real usage pattern of the big three phase loads (from the graphs the peaks at 15 kW) is not as regular as the one of the simulated profiles: there were consecutive days with three phase consumption and long periods without. On the 20 day periods, three phase loads have been used for a total of 7 days, which is not substantially different from the 5 simulated *Mill daily profiles*. Finally, real profiles show some peaks at markedly high power (20 kW), correspondent to the starting of the mill machine that could not be taken into account into the procedure for load

profile generation. The average daily profile considering both triphase and single phase loads over 20 days, is compared to 20 days' average of the simulated annual profile in fig. 6.4.

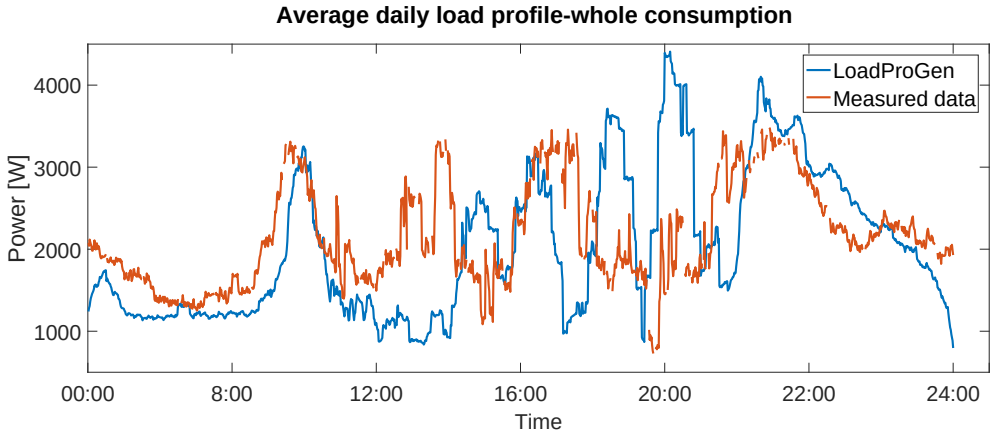

Figure 6.4: Comparison among measured average loads consumption and average simulated profiles (with three phase loads)

It can be noticed that the trend is much more complex than when considering only single phase consumption due to the high aleatority of big loads usage. It is difficult to exactly reproduce the daily consumption profile with a simulation tool solely based on data collected on field. Moreover, the comparison here reported is just a qualitative example as long as to make a really accurate analysis, data of more months would be needed: one year measurements would be necessary to reproduce an accurate load profile. Percentage error between energy really consumed and the one simulated is 5.8%, which is an acceptable value in the context of off-grid system design for DCs. Moreover, the procedure properly evaluates both the load peaks and the minimum load of the school. In figure 6.5 it is represented the probability density function of measured and simulated load consumption, considering both single phase and three phase loads. Once more, the general trend between simulations and real profiles is similar; the highest power probability is in the range of 1-2 kW, and there is a non null probability of power peaks at 13 kW, due to the three phase consumption.

In view of the above, the input load profiles LC that have been chosen for Poli.NRG simulations correspond to the simulated load profiles with Poli.NRG-LoadProGEN subroutine.

In the following section, the results of several simulations run with fixed PV+BESS size are reported in order to analyze the output of different BESS models.

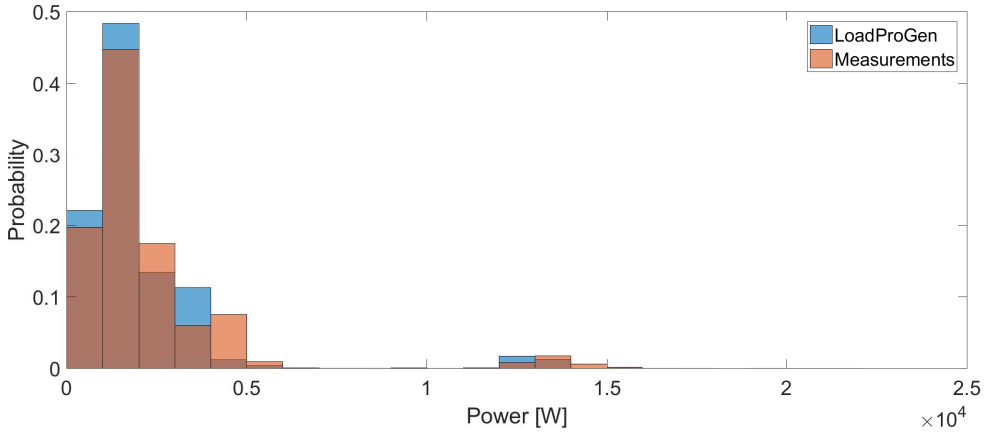

Figure 6.5: Probability distribution of measured three phase load consumption compared to the simulated profile

6.2 Simulations: comparison of different BESS models

Simulations are based on the load profiles of the school presented in the previous section.

In order to assess the differences among batteries' modeling approaches, some simulations with fixed BESS and PV sizes were run. In particular trends of SOC and SOH were compared for three increasing different size of batteries in order to evaluate BESS models output variations. PV size is kept constant. The specific BESS sizes are 25, 50 and 100 kWh and PV size of 13 kW, i.e. a reasonable nominal power for the input load profile. SOC trends are shown for a typical simulated school week, with both *Ordinary day* and *Mill day* load profiles; SOH is plotted instead over 20 years, i.e. the plant lifetime. Simulations are performed with Li-ion battery technology. The trends of batteries' SOC with different modeling approaches and BESS sizes are shown in figure 6.6. It is easy to notice that batteries' SOC follows an almost constant pattern during the days of the week. BESS discharges during the night and charges during the day. It reaches the maximum charge level almost everyday while it arrives at complete discharge only when the big threephase load is present (once every 4 days). Figure 6.6(a) reports the trend for a 25 kWh battery: the battery is quite small for the system and SOC limits are reached at each cycle. There are no big differences among the 3 modeling approaches. However, is noticeable that at high SOC levels, electric model shows a smoother SOC evolution with respect to the others; this can be due to the fact that battery has reached the terminal voltage limits and can charge only gradually with low currents. When battery sizes increases to 50 kWh in fig. 6.6(b) and 100 kWh 6.6(c), SOC variations are smaller and differences among the models become more evident. In particular, in the last graph, it is evident that when using electric model, battery seems to experience less deep cycles than with the other models. This could lead to an over

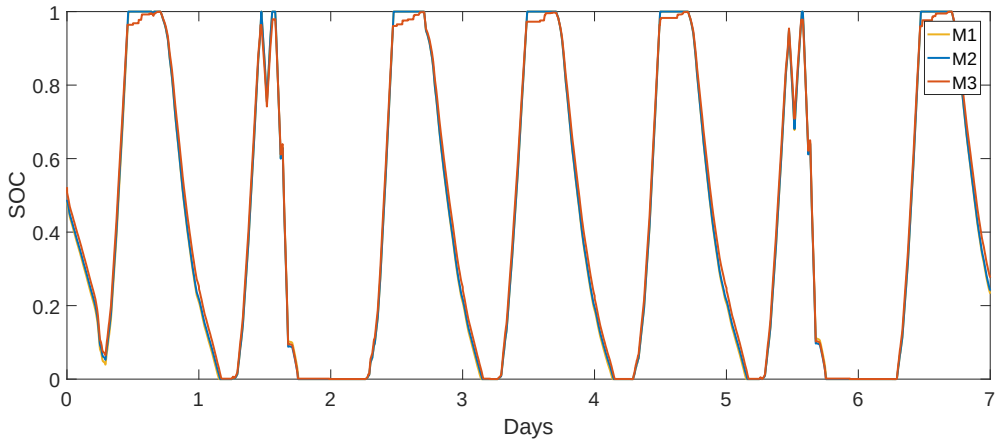

(a)

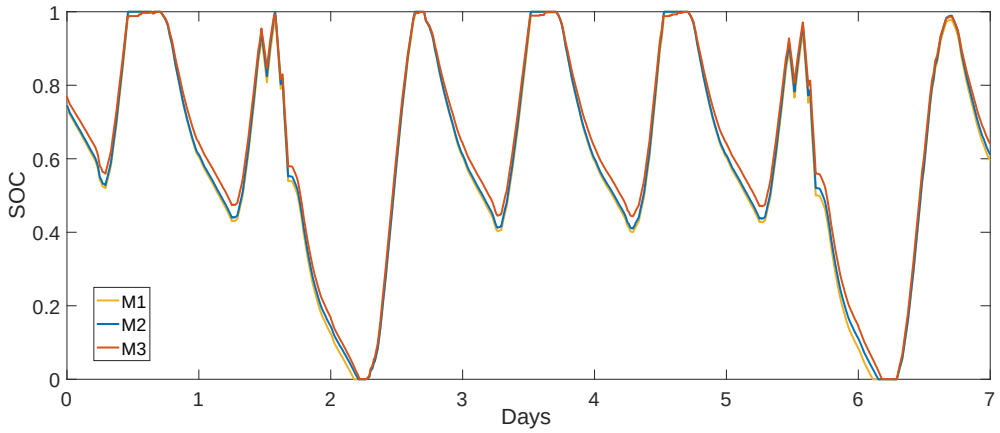

(b)

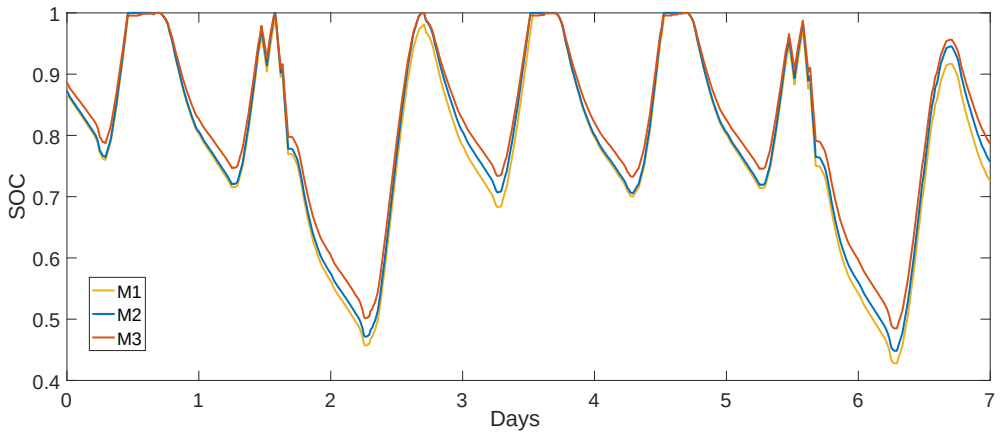

(c)

Figure 6.6: Comparison of SOC trends during simulations with different Li-ion modeling approaches and BESS sizes: 25kWh(a), 50kWh(b), 100kWh(c)

dimensioning of batteries when using simplified empirical models.

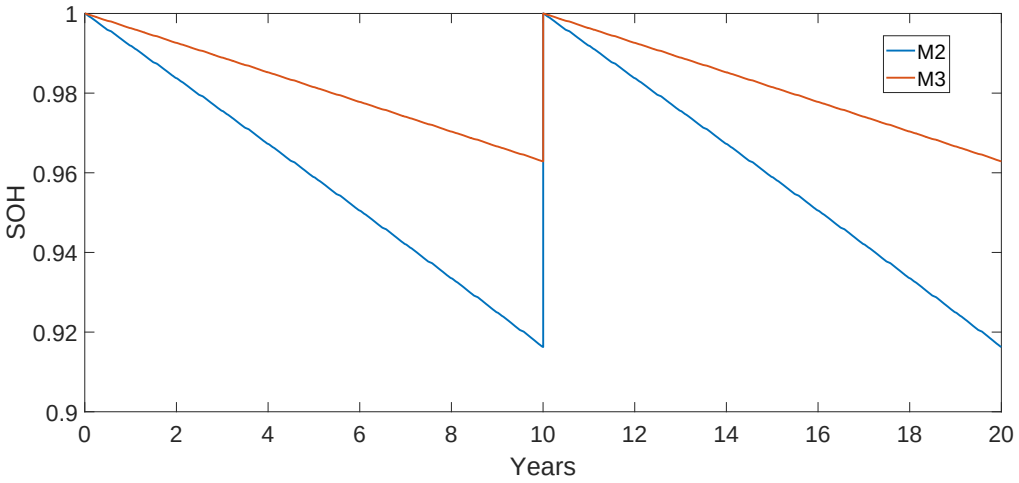

Figure 6.7: SOH simulations' trends for different Li-ion BESS models with BESS = 50kWh, PV=13kW

With respect to SOH, just one graph is reported (fig. 6.7), with simulations performed with BESS of 50 kWh and PV of 13 kW over 20 years. Simulations were run also with BESS of 25 kWh and 100 kWh but the graphs are not reported because they do not provide further elements to the discussion, since the combination with 50 kWh highlights at most the difference between models. The graph shows only empirical and electric model trends because the simplified empirical model does not account for lifetime modeling (i.e., SOH indicator).
Empirical model overestimates battery degradation when compared to the electrical one. However, with both models battery never reaches the minimum SOH level of 0.8 because after 10 years it is replaced due to calendar aging (SOH of new batteries is again initialized to 1) : for this reason, batteries' replacements costs will result the same in the two cases even if SOH changes in different way. A possible improvement of the model with respect to calendar aging could be taken into account. Finally, it is worth to point out that the differences among modeling approaches, that seemed minor when comparing SOC on a daily basis, are not negligible when simulations cover the entire plant lifetime. This can have an impact on the results of the simulations, as shown in the next section.

6.3 Results: micro-grid robust design

After having analyzed and compared how the different modeling approaches simulate battery performance, the different simulations described in detail in the previous chapter were run. Results are described in the following.
Figures 6.8 and 6.9 display the map of solutions of the simulations with the three BESS models (electrical, empirical, simplified empirical) for lead acid and lithium

ion technology. The map of solutions is composed of different areas of solutions that are related to the specific BESS model adopted in the simulation.

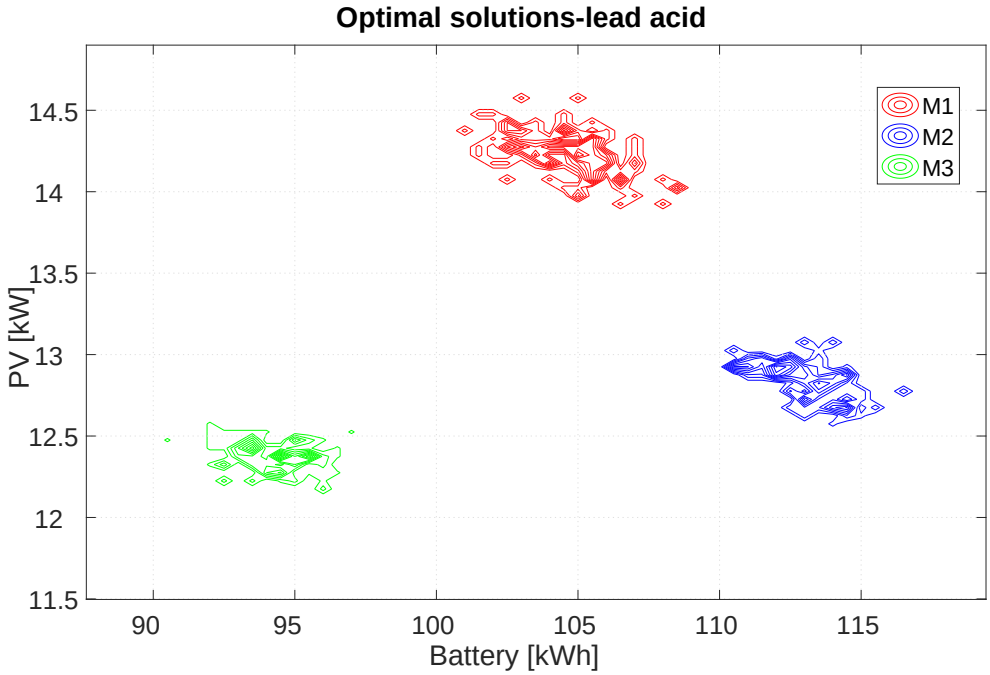

Figure 6.8: Sizing results of Poli.NRG with lead acid BESS systems

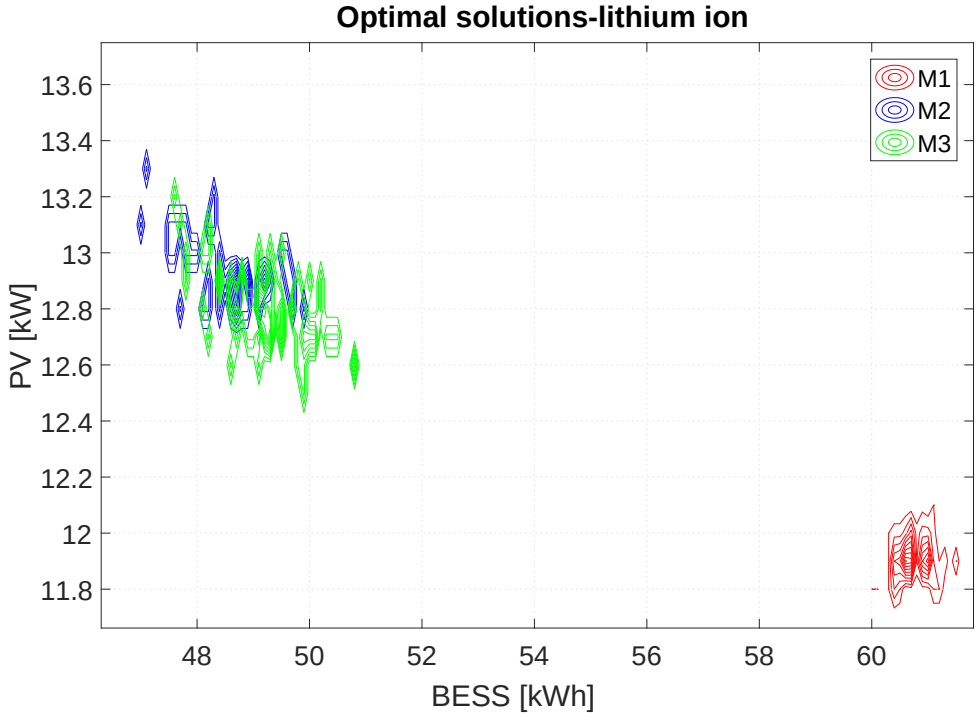

Figure 6.9: Sizing results of Poli.NRG with Li-ion BESS systems

Each area of solutions represents with contour lines the resulting optimal combina-

BESS technology	**BESS model**	PV_{opt} **[kW]**	$BESS_{opt}$ **[kWh]**	**NPC [k$]**	**LCOE [$/kWh]**	**LLP [%]**	**Single LC simulation time [min]**	LC_{opt}	F_{opt}
Lead acid	Empirical simplified	14.2	105	119.82	0.644	4.99	8	114	4
	Empirical	12.9	112	118.66	0.637	4.99	45	124	7
	Electric	12.35	94.5	114.85	0.617	4.99	67	114	8
Li-ion	Empirical simplified	11.9	60.6	120.50	0.648	4.90	7	101	12
	Empirical	12.9	48.6	116.28	0.625	4.99	45	108	5
	Electric	12.8	49.1	116.22	0.624	5	140	98	4

Table 6.1: Results of Poli.NRG simulations with different battery technologies and modeling approaches

tions of PV and BESS size among the N simulated lifetime profiles LC. The contour line of the optimal combinations is a curve along which specific combinations have appeared with the same frequency (i.e., it represents isolines). The frequency ranges between 0 and 1 since it has been normalized according to the most frequent combination in the considered BESS model. The isolines are concentric, the most external is the one with the lowest frequency of occurrence.
The table 6.1 has been derived from the map of solutions and it shows the robust design solutions referring to the previously described six simulations (chapter 5). The robust design ($BESS_{opt}$;PV_{opt}) is evaluated as the optimal combination result with the highest frequency (i.e, 1). The NPC, LCOE and LLP of the robust design are evaluated as the mean value of each solution in which appears $BESS_{opt}$ and PV_{opt}. Frequency of occurrence F_{opt} is the number of times the optimal solution appears in simulation's results. The parameter LC_{opt} represents the number of simulated load profiles until convergence. Single profile simulation time depends on the calculator processor (specifically, an "Intel i7 4700k-16 Gb)
Every simulation with different type of BESS modeling shows a robust solution, since the dispersion of the optimum around the identified design is very limited.
Regarding lead acid technology, the modeling approaches show relevant differences in the obtained optimal solutions. Optimal BESS and PV size according to electric battery model are respectively 94.5 kWh and 12.35 kW while they are 112 kWh and 12.9 kW according to the empirical model. In particular, empirical model tends to overestimate the size of the system: the percentage difference between the results is 18%. The overestimation with respect to the more accurate electrical model is likely caused by the parametrization of the variable battery efficiency, which has been computed using manufacturer's data. As a consequence, the NPC is 4000$ higher when sizing the system using empirical model.
The simulation based on the simplified empirical model has found the optimal size

equal to 14.2 kW for PV and 105 kWh for BESS. The BESS size is an intermediate value between the other two models. Even if the parameters in input (efficiency and maximum number of cycles) are correctly estimated, simulation results could not resemble the ones of more sophisticated approaches. PV system size is noticeably bigger with respect to the results obtained with the two other simulations, due to the fact that battery operates with a lower efficiency (90% charge and discharge) than the average efficiency in empirical model (see fig.6.13). Hence, the NPC is the highest among the results of the three approaches.
An important aspect to be taken into consideration is the simulations' time. As reported in the last column of the table 6.1, computational times strongly vary with the BESS modeling approach adopted. Simulation run with the most simple model needed only 8 minutes to simulate 20 years of plant lifetime with a specific load profile. When adopting empirical model the time rises up to 45 minutes to arrive to 1h 07 minutes with the most accurate electric model. Considering that at least 100 load profiles curves need to be simulated to arrive to convergence, the difference is quite important: from 13 hours of simulation to almost 5 days.

When considering results obtained with lithium ion battery technology, the outcome is different. With the electric model, optimal PV and BESS size are respectively 12.8 kW 49.1 kWh, with empirical are 12.9 kW 48.6 kWh and with simplified empirical model 11.9 kW and 60.6 kWh. Only the simplified empirical model shows a non negligible difference for PV and BESS size. For this last model, the same consideration made for lead acid technologies can be done: it does not succeeds in giving the accurate results like electrical model even if input parameters are adequately estimated. The resulting NPC is very similar between electric and empirical methodologies while it is 4000 $ higher when using the more simplified approach.
It is noticeable the similarity among results with empirical and electric model, not encountered in the case of lead acid batteries. This could be explained by the different parametrization methods adopted for the two technologies: the values of the variable parameters of the different BESS models (efficiency in empirical model and R and OCV curve in the electrical), as well as degradation curves, have been obtained by laboratory measurement on the same cell. This was not the case for lead acid where laboratory measurement could be used just for the determination of $Rint@50\%SOC$ and for OCV discharge curve in the electric model: other data where taken from literature or datasheet. Empirical and electrical models are hence directly comparable for Li-ion.
Computational times of simulations with simplified empirical model and empirical one are the same as for lead acid. Electric model instead, results even slower, with 140 min required to simulate 20 years of a single load profile. The difference with respect to lead acid can be explained by two factors: look−up tables for the de-

termination of Li-ion cell capacity, resistance and open circuit voltage have more elements because it can experience greater voltage variations with respect to lead acid; moreover Li-ion model considers a variable resistance degradation rate that increases the complexity. Once more, it can be stated that accuracy works at the expense of higher computational effort.

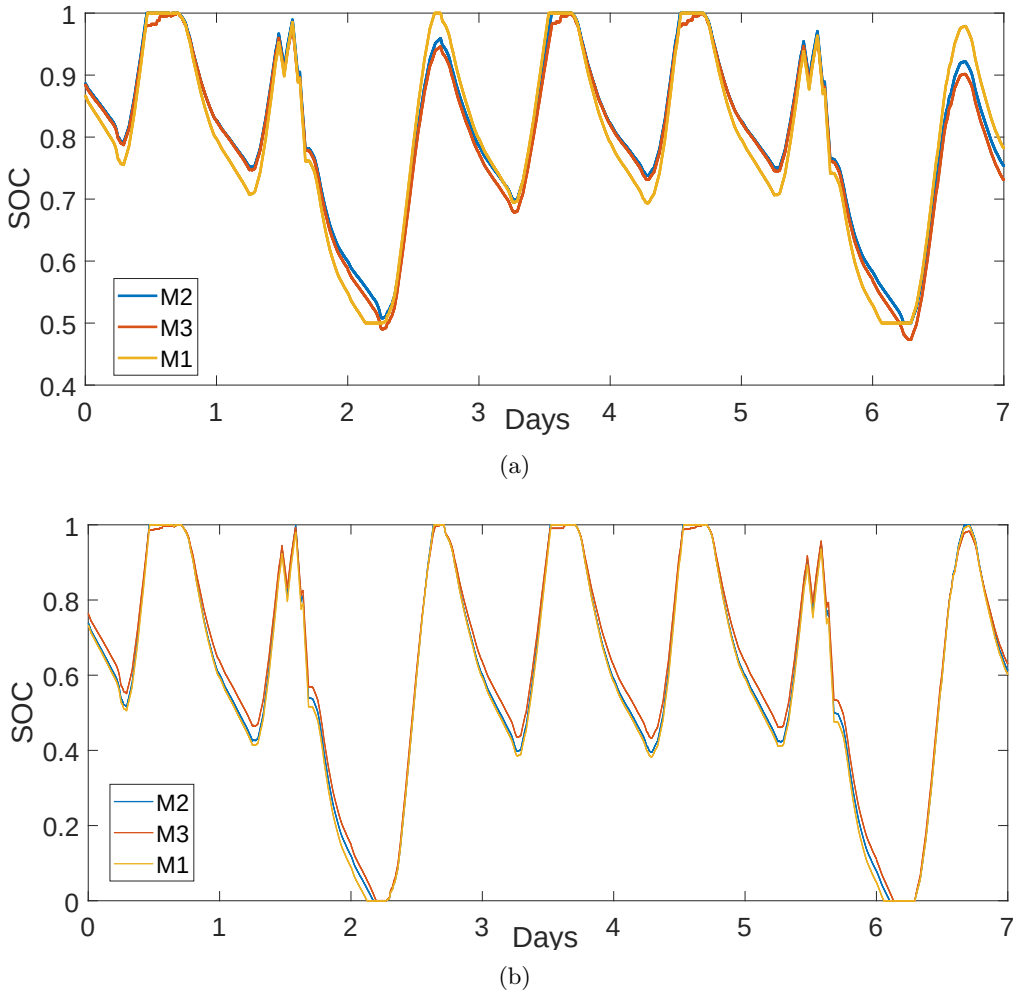

Figure 6.10: Comparison of SOC variation of the three battery models during one week of simulation: lead acid (a) and Li-ion (b)

A detail on the SOC variations over a week obtained with the three modeling approaches for the most robust solution both of lead and lithium acid are reported in figures 6.10(a) and 6.10(b). The week taken into consideration is the second week of the year, in which both *ordinary days* and *Mill days* are present. At first lead acid SOC pattern is considered. The same trend is present with the three modeling approaches: it means that in all the cases the battery is quite big with respect to the load required and optimized to work at high SOC. There are anyway some differences: the minimum SOC value for empirical and simplified empirical models was set to be 0.5, while the electrical, following the imposed voltage limit, can reach

slightly lower values of SOC according to OCV-SOC curve.
SOC cycles are deeper for the simplified empirical model when compared to the empirical due to the fact that the optimal battery size is smaller. Electric model however, which gives as a result the smaller BESS size, experiences shallower cycles: this is thanks to the fact that the electrical model better estimates the state of charge of the battery. Similar considerations can be done when looking at the graph for lithium ion batteries, noticing that SOC can vary between 1 and 0, not having a limitation on a minimum value. Batteries, which are smaller than lead acid, experience deeper cycles and the electric model is once more the one that shows the less steep SOC variations, reaching more gradually the limits.

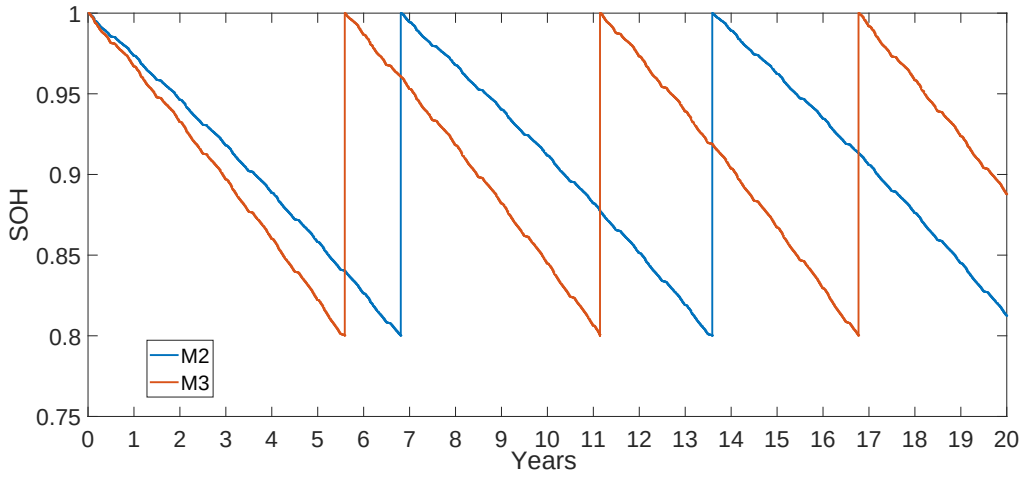

(a)

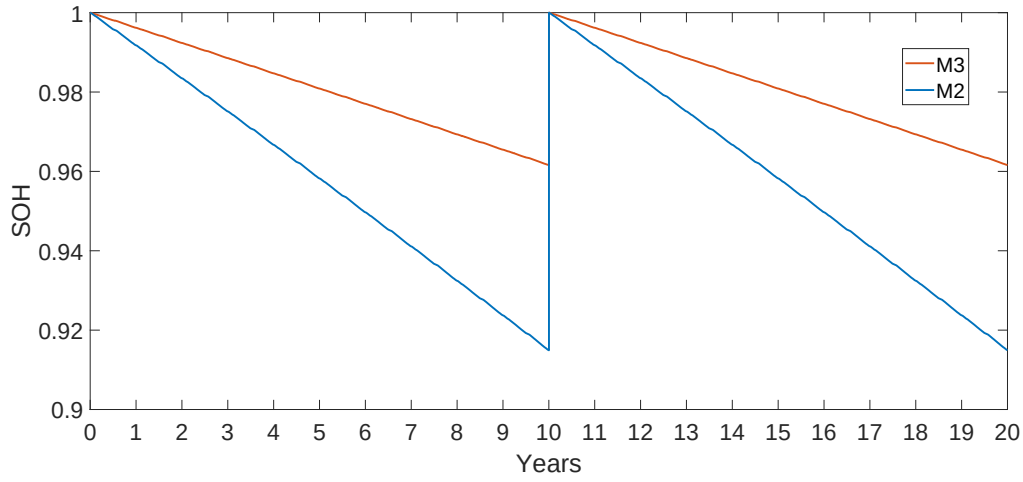

(b)

Figure 6.11: Comparison of SOH variation of empirical and electrical models during 20 years of simulation: lead acid(a) and Li-ion (b)

In conclusion, whichever model is utilized, the optimal BESS+PV system is found

so that batteries experience always more or less the same amount of cycles during the lifetime (according to each model). This can be related to the way in which degradation in computed: degradation and consequent replacement's costs is in fact proportional to the number of cycles; hence, number of cycles have to be reduced at most to allow for a minimization of the costs.

In figure 6.11(a), SOH variation over the 20 years of plant life of lead acid battery is shown. Battery degradation modeled with the electric approach is much faster than with the empirical: in the first case batteries need to be replaced 3 times while in the second only 2, differently to what has been shown in figure 6.7 for Li-ion; it is likely due to the different assumptions in the models: SOC minimum value for the empirical model and voltage limits for the electrical. When imposing a limit on the voltage the battery tends to work at lower SOC with respect to the assumed minimum SOC of the empirical model, influencing the degradation rate. When considering SOH trend for lithium ion batteries, shown in figure 6.11(b), the same consideration as for 6.7 can be done, as long batteries and PV sizes are similar. Empirical model overestimates battery degradation. All these results have an impact on the evaluation of LCOE of the plant as explained later with more details.

6.4 Discussion: comparison of lead-acid and Li-ion options in micro-grid design

The table 6.1 shows a significant difference in BESS size between lithium ion and lead acid technology, being BESS_{opt} of lead acid about the double of lithium ion. Each implemented battery model is able to represent the typically better performances of lithium ion technology, as explained in section 1.1: generally speaking, a smaller battery capacity is needed in order to fulfill the same load input.

In the following paragraphs, an analysis about the variation in time of the principal characteristics of each model for lithium and lead acid batteries is presented. The comparison is carried out accounting for the parameters of the two technologies during one typical week of the school (e.g., with daily loads and mill machine). An exception is made for SOH and SOR indicators which are represented for the whole lifetime of the system. The PV+BESS size of the simulated systems is the solution of the robust design. For each modeling approach, the variation of the most important parameters is shown: equivalent cycles for simplified empirical model, variable roundtrip efficiency for empirical model and electrical output (i.e. current and voltage) for electrical model; moreover for the latter model, a direct comparison of SOC variation between lead acid and Li-ion is shown.

Simplified battery model

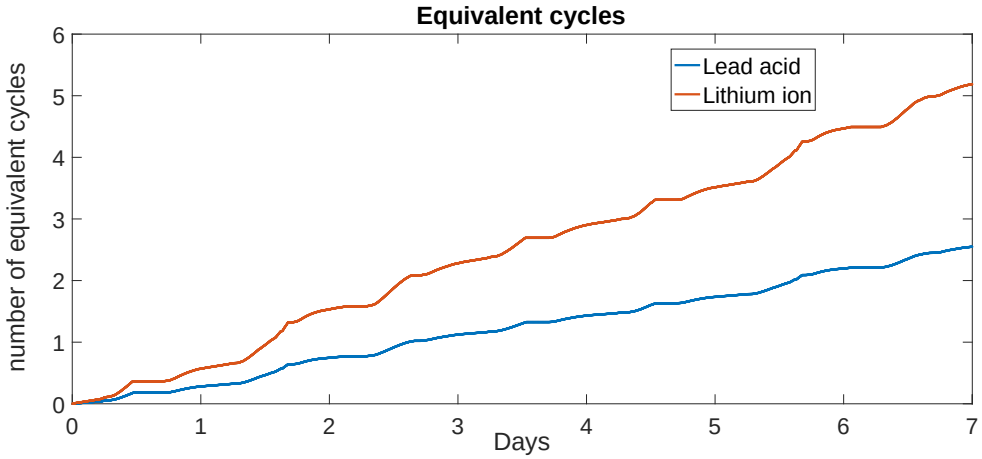

Figure 6.12: Equivalent cycles' increasing trends of Li-ion and lead acid simplified empirical models

Parameters of this simple model are constant, i.e. they do not vary with time. For this reason, the only relevant comparison between the two technologies can be made on the basis of the equivalent cycles experienced by the battery during lifetime. It is possible to notice from figure 6.12 that the equivalent cycles the lithium ion batteries pass through are constantly higher than the ones of the lead acid batteries, with a higher slope. Their behavior is coherent with the general trend of SOC in figures 6.10(a) and 6.10(b), as equivalents cycles are related to SOC variations (eq. 4.6). Lithium ion battery experiences a higher number of equivalent cycles because the optimal size of the BESS is half of the lead acid one: lithium ion batteries can withstand harsher cycling conditions without being compromised, and the maximum number of allowable cycles is higher than lead acid.

Empirical model

Despite the double BESS size, lead acid battery model performs much worse than lithium ion model (see fig. 6.13): lithium ion efficiency remains very often around a high value, while the lead acid efficiency varies more during cycling, reaching worse performances. Once again, this behavior is coherent to what has been reported about battery technologies in section 1.1. Values of obtained efficiencies are higher than the reference average values given as input to the simplified empirical battery models (respectively 0.95 and 0.8 for lithium and lead acid batteries), and, in a more accurate version of the model, should decrease with lifetime.

Electrical model

The variation of current, voltage and OCV with time are reported in figure 6.14(a) and 6.14(b) for both lead acid and lithium ion technologies. They refer to the cell level, thus it represents the simulated voltage of the cell.

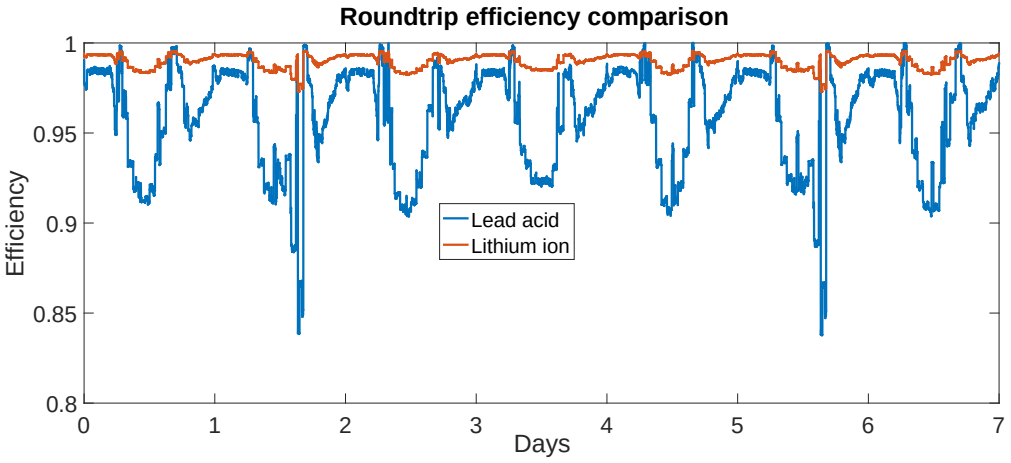

Figure 6.13: Comparison of roundtrip efficiency variation of lead acid and Li-ion empirical models during one week of simulation

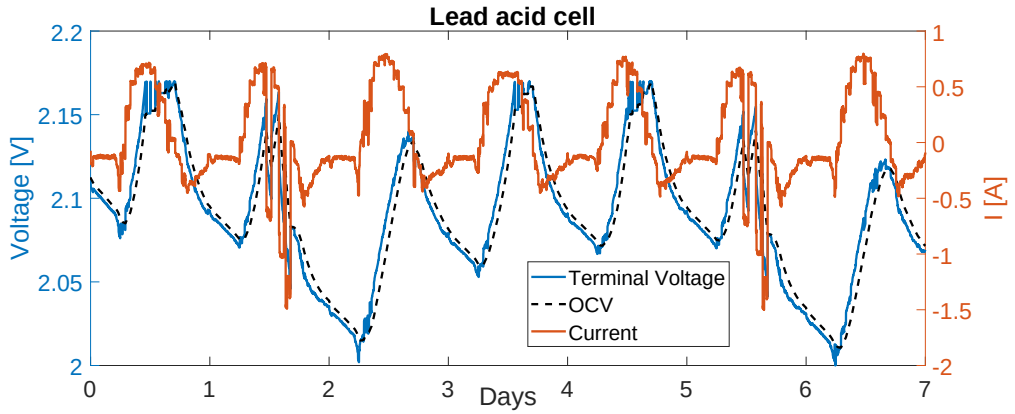

(a)

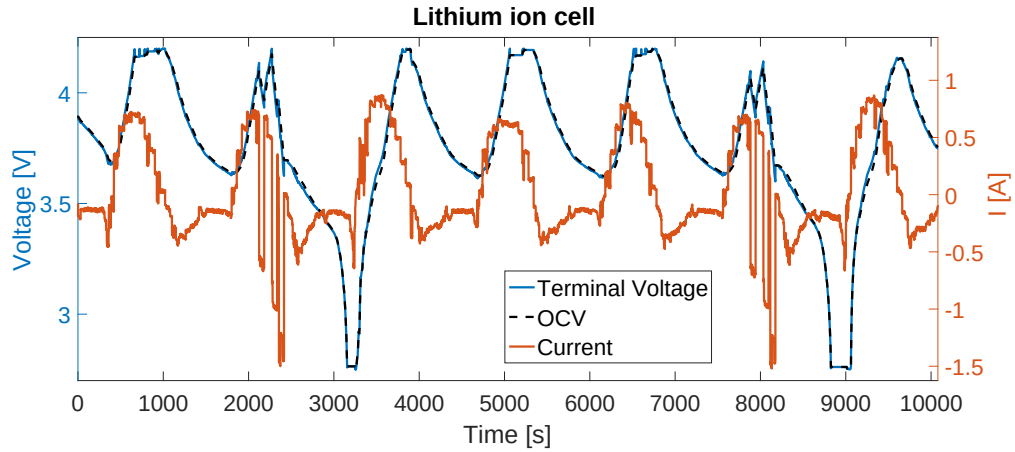

(b)

Figure 6.14: Voltage and current characteristics during one week of simulation: lead acid cell(a) and Li-ion cell (b)

Given that lithium ion and lead acid BESS model have the same input current but different cell capacity, in the simulation lead acid cell operates at much lower C-rate with respect to lithium ion. This is caused by the minimum voltage limit imposed to the lead acid cell, which is set to a value corresponding to about 50% of the SOC in order not to prematurely destroy it. The effective dischargeable or chargeable capacity is halved with respect to nominal capacity: thus, to supply a certain load demand it is necessary to increase the number of batteries, while for lithium ion cell the minimum voltage can be lowered as much as possible according to physical limits of the battery, and the whole capacity can be exploited.
The very short distance among OCV curve and simulated voltage curve is related to the low value of the internal resistance of the cell. It is likely to happen that at the end of the cell life (thus, at the end of the simulation), the distance between curves would be higher due to the power fade effect and the voltage limits would be reached for a longer period of time, increasing the loss of load.

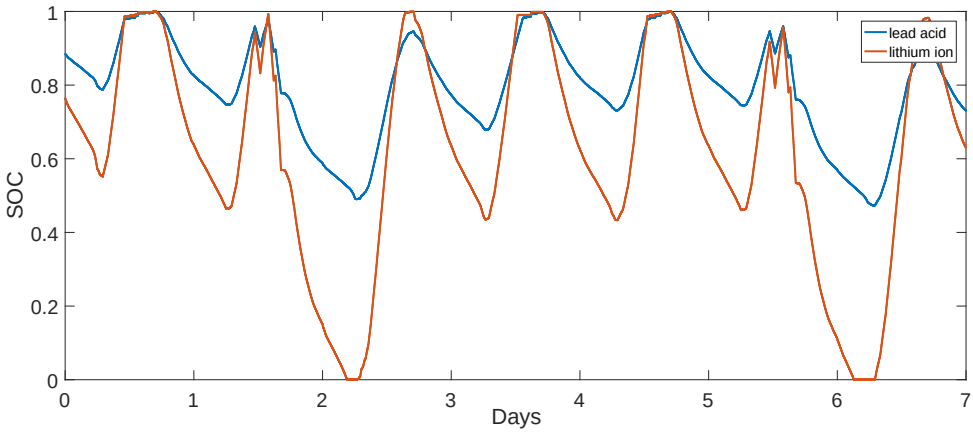

Figure 6.15: Comparison of SOC variation of Li-ion and lead acid during one week of simulation

The trend of the SOC in figure 6.15 is a direct consequence of the minimum voltage limit of the cell as aforementioned in the simulated voltage comparison.

In the figure 6.16(a) SOH decreasing trend during system lifetime is reported. As already mentioned, lead acid batteries degrade at a much faster rate than lithium ion batteries even if their optimum size is bigger. In fact, they reach the minimum value of SOH in almost six years of operation, after which batteries pack must be replaced with a new one (and SOH is initialized at 1): it is noticeable from this graph that BESS sizing with lead acid batteries forecasts that the replacement should happen 3 times along 20 years. On the other side, lithium ion BESS never reaches 80% SOH and it is replaced every 10 years, which is the maximum lifetime of the battery set in input to represent its calendar aging. The same considerations are reflected in figure 6.16(b) for SOR trend during lifetime: the lead acid resistance increases

at a much faster rate than lithium ion resistance, even though the power fade rate of pf(k) is a constant value for the lead acid batteries. Again, the faster increase in internal resistance assumed in the model reproduces the worse characteristics of lead acid batteries.

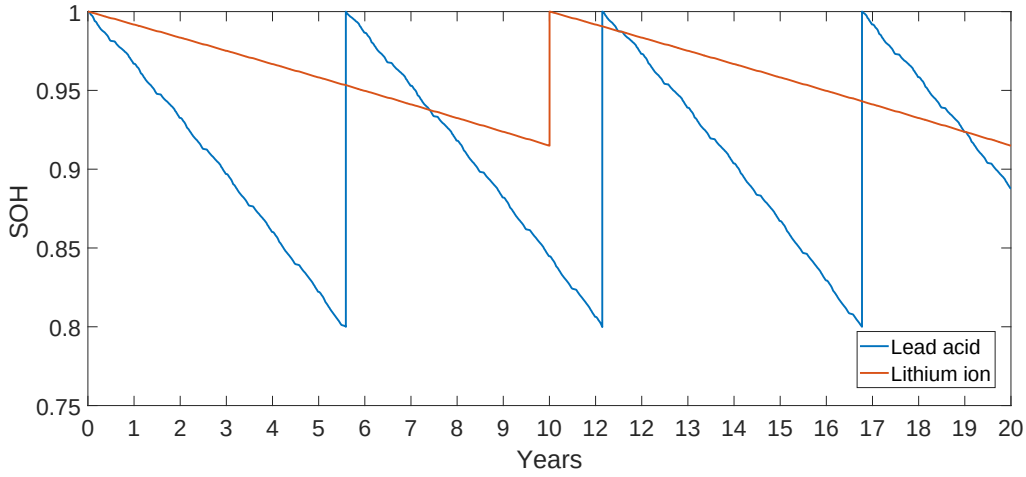

(a)

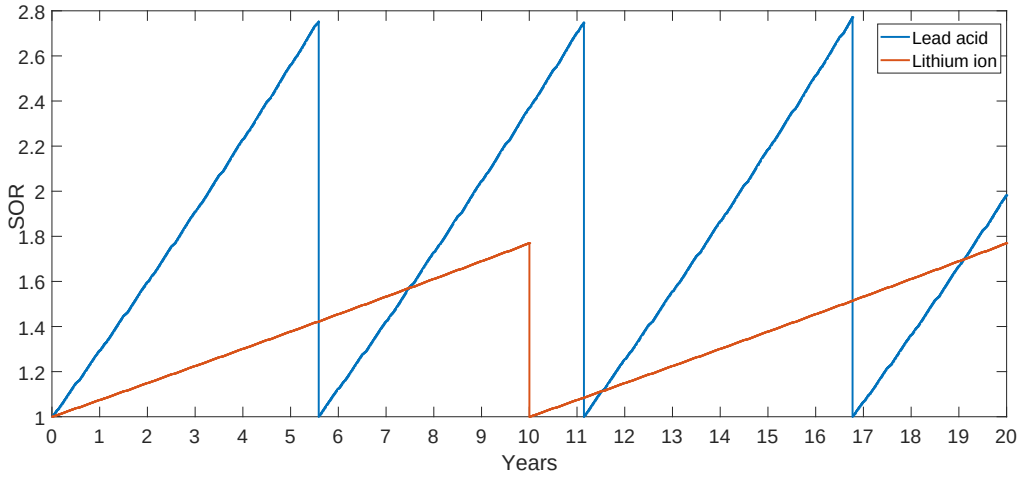

(b)

Figure 6.16: Comparison of SOH (a) and SOR (b) variation of Li-ion and lead acid during 20 years of simulations

Considering what previously mentioned, a more careful calendar aging model seems to be particularly necessary for lithium ion battery.
The pie charts depicted in figure 6.17 represent the investment cost breakdown share for lead acid and lithium ion technologies; it gives decision makers a comprehensive instrument to compare and decide between the two technologies.
Costs' share shown in the graphs is similar to those reported in figure 2, related to real projects developed around the world: PV module constitutes the largest percentage of investment cost with a cost almost double to that of batteries. BESS investment costs are different among lithium and lead acid technology: even if size

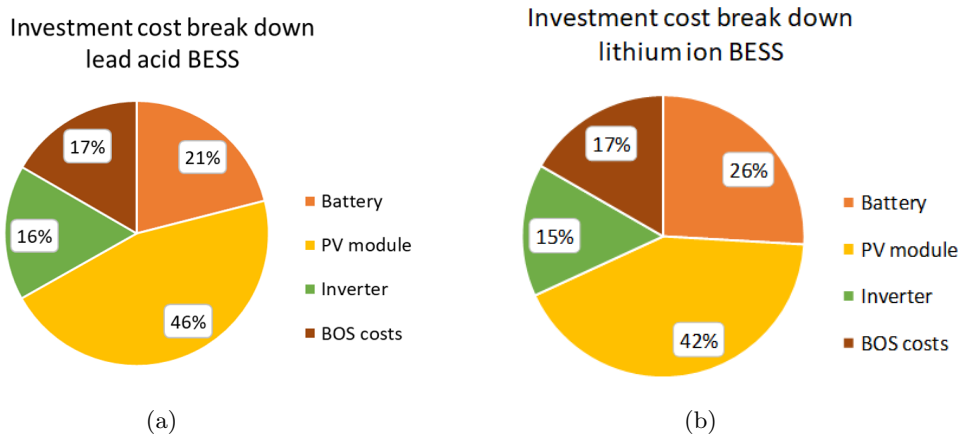

Figure 6.17: System cost breakdown shares: lead acid battery(a) and Li-ion battery(b)

of lithium batteries is almost half that of lead acid batteries, their cost has a larger impact on the total expenditure. Lithium batteries constitute the 26 % of the total initial investment cost while lead acid batteries only the 21%, which is comparable to results of fig. 2, where BESS system represented not more than 20% of the project value. Investing in a plant with lead acid batteries seems more convenient, when looking only at the upfront payment: the initial investment cost of the system is 67 k\$ while with lithium ion batteries it rises up to 76k\$. However, when analyzing properly the costs associated to each technology, it is necessary to account also for batteries' replacement costs which are different for lithium and lead acid. As shown in fig. 6.16, lead acid batteries need to be replaced three times during plant lifetime while lithium ion batteries only one. For this reason NPC of the plant with lithium ion batteries is only 2000 \$ higher than with lead and LCOE value is comparable.
It is not trivial to draw conclusion over which modeling approach is the most suited to be utilized in Poli.NRG as long as each one has shown advantages and disadvantages. The simplified empirical model requires very short computational time but does not evaluate properly the size of the system: it could be used by investors for a first rough dimensioning of the plant. The empirical model computational effort places in the middle among the simplified and the electric model. Its accuracy strongly depends on its parametrization; when data are taken from laboratory measurements and battery technology does not suffer of strong degradation, the output results are accurate. Empirical model represents a good compromise for modeling lithium batteries, while it is not the case of lead acid; for the second technology however, data from experimental measurements would be needed to better analyze results. Electric model requires very long computational time but, though still simple, is the one that mostly resemble batteries' real physics; it would be better for investors to opt for this more accurate model when the solution impacts on the project implementation costs.

Concerning BESS technologies, the results have shown similarities among NPC of plant with lead acid and lithium ion batteries; even the values of LCOE are considerably similar between the two technologies. It is possible to conclude that Li-ion batteries are nowadays competitive with lead acid batteries and they can be even a better solution for off grid systems.

Conclusions

The scope of the present thesis is to develop a new methodology for modeling battery storage systems, to be integrated in tools for sizing off-grid plants. The authors started from a rigorous literature review to find modeling approaches that could represent a good compromise between accuracy and simplicity. A BESS model implemented in off-grid simulation tools needs to accurately evaluate both battery SOC and SOH to account for system reliability and costs. Loss of load probability and replacement's costs are the most common adopted performance indexes. However,the model must be simple enough to allow for viable computational effort. From the literature research, it resulted that BESS modeling approaches can be divided in four categories, each of them suited for particular applications. In the context of stand alone systems sizing tools, analytical models are preferred; battery is represented with hydraulic analogies or empirical equations, simple to parametrize and requiring little computational effort.
The authors looked for a novel approach, able to represent more accurately battery physics, such as the electric characteristics of voltage and current. The chosen model represents the battery as an equivalent electric circuit, in particular as a capacitance is series with a resistance. Parameters values depend on SOC and SOH. This approach for BESS modeling is commonly found in literature for online applications, such as BMS in HEV but no examples of implementation in sizing softwares have been found. In addition to the novel approach, 2 empirical models have been proposed, a basic one with constant parameters and a more advanced which takes into account the change of battery parameters with operational conditions and degradation. The proposed methodologies have been implemented in the dimensioning tool Poli.NRG, developed by Politecnico of Milan, to dimension a theoretical new PV+BESS system for Ngarenanyuki school in Tanzania. Data regarding school consumption have been collected with an on field survey performed by the authors during one month spent in the country. The models have been parametrized with data of both lead acid and lithium ion batteries as far as they are the two technologies that will likely compete in the future in off-grid application; results can help investors in finding the most convenient solution. The three modeling approaches have been compared in terms of results and computational time. The simulations' results lead to the following conclusions.

- The methodologies differ greatly in terms of computational time: the empirical simplified approach is the fastest and requires only some hours to converge. Empirical and electrical approaches require instead more than one day of simulation. In particular, the electrical approach for lithium ion cell is the more complex model, with big look-up tables and the increasing coefficient of SOR depending on C-rate: it requires a total of more than 9 days of simulations. The long computational time and big differences among the modeling approaches are caused by the short simulation time step of 1 minute: the iterations are repeated for the whole 20 years of plant lifetime and a small increase in model complexity leads to a noticeably growth of the computational effort.

- Concerning the optimal solution, the empirical simplified model leads to an oversizing of the plant with consequent overestimation of investment costs. Empirical and electric model are instead comparable when data are taken from laboratory measurements, as it is the case of lithium batteries. Empirical model tends however to overestimate battery degradation, and this leads to different conclusions in terms of optimal plant size in the case of lead acid batteries. Finally, it is necessary to stress the importance of correct models' parametrization: data taken from batteries' datasheets are enough to characterize empirical models but do not lead to accurate results. The differences in results between empirical and electrical model for lead acid batteries are likely caused by the non correct parametrization of the empirical model.

- Lead acid batteries result to be cheaper than lithium ion from investment cost point of view. Taking into account the whole lifetime costs, instead, lithium ion batteries results to be competitive due to the lower degradation; moreover, the LCOE of both options (Li-ion or lead acid technologies) is considerably similar. As found in literature, it is likely that, thanks to decreasing costs of lithium ion batteries, in the near future they will replace lead acid for off grid applications.

Investors will be given the opportunity, using the proposed procedure to size off-grid plants, to choose between simplified faster approaches for BESS modeling, or the more accurate one. The choice will be dictated by the needs of the users; for a first rough dimensioning of the plant, the empirical approaches can be used. It is instead better to opt for the more accurate model when the solution impacts on the project implementation costs. Finally, the output of the tool can help investors make up their minds whether to invest in lead acid of lithium ion battery technologies; however, Li-ion battery costs are nowadays competitive with respect to lead acid and they have better performances.

In literature, there is a lack of adequate tools to dimension microgrids: there is a

variety of expensive tools that perform simulations with hourly time steps that are not able to properly represent batteries' transient behavior and fast variations in load consumption.
The thesis work and further possible developments insert in the framework of the research of E4G group, are devoted to improve the procedure for sizing off-grid plants, in order to have a reliable and freely available instrument, able to take into account all the typical features of developing countries. The main difficulties related to start an off-grid system project in DCs concern uncertainties related to load consumption and load evolution, unpredictability of energy sources and characterization of BESS performances. Simulations' time step of one minute helps in determining an accurate load profile, able to resemble the real pattern of variation in load consumption and in resembling real battery behavior. However, simulations result to be very slow and it would hence be advisable to take into account an optimization of the computational process: new algorithms or programming environments could be used to enhance simulation speed. This could allow for the implementation of the more accurate BESS model without compromising computational efficiency. However, it is difficult to correctly simulate BESS performances in off-grid systems due to the non controlled working environment. The electric model proposed helps in modeling some aspects of battery operation but it still does not take into account important characteristics typical of off-grid applications. Batteries, in particular lead acid technology, experience a different behavior during charge and discharge, that would be advisable to take into account adopting a variable resistance in a future development of BESS model. Eventually, it is strongly recommended the implementation of a model to accurately represent calendar aging, since BESS in off-grid systems is widely stressed during its working lifetime, especially in DVs environment.
Regarding the adopted tool, it would be interesting to simulate hybrid systems, with more than one energy source and the consequent need for dispatching strategies optimization. Moreover, the reported case study of Ngarenanyuki, demonstrates the need of integration of micro grids with national electricity grid. BESS systems could provide ancillary services to national grids, such as primary and secondary control reserve, contributing to improve reliability and security.
In conclusion, this thesis highlights the necessity of a proper and smart BESS modeling when facing the design of off-grid systems. The dimensioning tool would need to take into account also the possibility of system grid integration to be at pace with future trends and to help investors in the decision making process. This would require further studies for modeling control strategies and costs.

Appendix A

Fundamentals of Electrochemical Impedance Spectroscopy

Electrochemical impedance spectroscopy is a non disruptive technique that allows to describe the response of a electrochemical cell to a sinusoidal signal. It can be applied to the cell as a whole or to single components, such as electrolyte or electrodes.
The input signal could be an *ac* current (Galvanostatic EIS) and the voltage response of the battery is measured, or on the contrary a sinusoidal voltage (Potentiostatic EIS) and the current is measured. The electric response of the cell depends on its equivalent impedance that is computed at each frequency as the ratio of voltage over current.
EIS measurements can be taken at various temperatures and SOC in order to assess variation of battery characteristics. Moreover a dc current can be superimposed to the low ac signal to evaluate cell response at different C-rates.
Results of EIS can be reported in graphs, in order to visualize cell characteristics. The most popular plot format are Nyquist plot and Bode plot.

Nyquist plot

The opposite of the imaginary part of the impedance is plotted on the y axis against the real part of impedance. Impedance imaginary part is reported with a minus sign because electrochemical cells typically have a capacitive behavior and hence a negative imaginary impedance. The expedient is hence taken in order to represent the graph mostly in the first quarter. Each part of the graph corresponds to a different value of frequency. In figure A.1 are reported a general Nyquist plot for a cell and the characteristic time length of phenomena occurring inside the cell. The frequency of each section of the Nyquist plot can be related to the characteristic frequency of phenomena happening inside the cell:

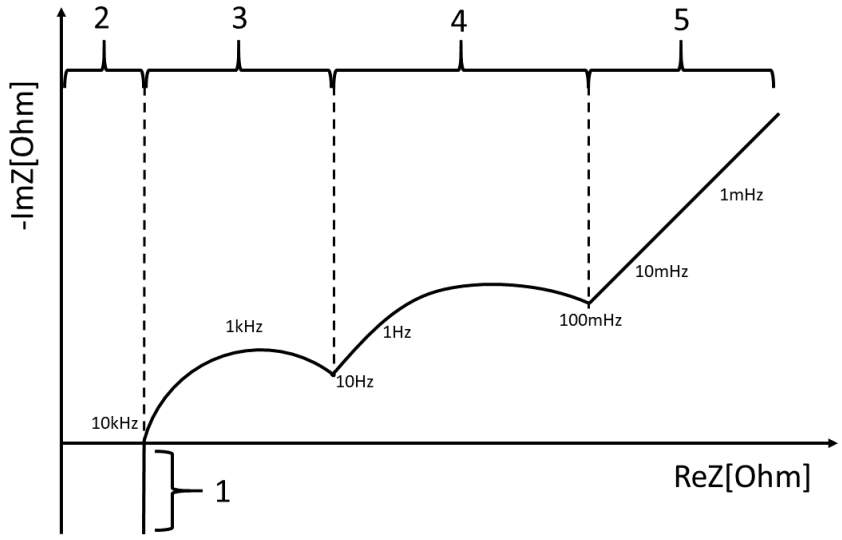

(a)

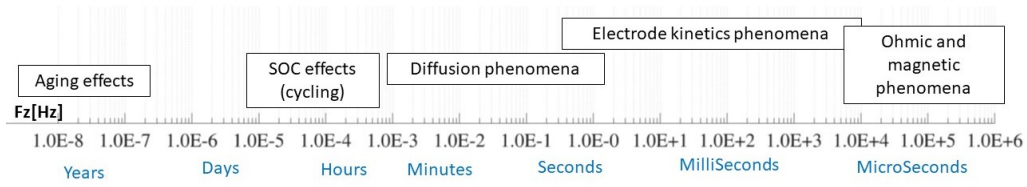

(b)

Figure A.1: Typical battery Nyquist plot with sections for different phenomena(a) and Characteristic time length of phenomena occurring in the cell(b)

1. High frequency inductive reactances of metallic elements in the cell and wires.
2. Ohmic resistance due to voltage drops at current collectors, electrolyte, active material and separator.
3. Charge transfer resistance of the electrodes in parallel with the double layer capacitance [14].
4. Diffusion inside porous electrodes [14].
5. Diffusion processes in or outside the electrodes.

In the case of Li-Ion batteries, a second interpretation for the last three sections of the diagram is present in literature [15], [16]:

3. Impedance related to Solid Electrolyte Interface (SEI).
4. Charge transfer resistance in parallel with double layer capacitance.
5. Diffusion phenomena occurring inside and outside electrodes.

From the shape of the diagram, it is possible to extrapolate the correspondent circuital elements.

- **Resistor**: Z=R. It appears in the graph as a point on the x-axis as long as its value does not depend on the frequency.
- **Resistor in parallel with capacitance (RC group)**: $Z = \frac{1}{R+1/j\omega C}$. It can be demonstrated that, when represented on the diagram, it corresponds to a semi-circumference with center on the horizontal axis. The maximum of the circumference relates to the frequency $f = 1/\tau$, where τ is the time constant equal to R*C. Often, Nyquist plot of real electrochemical systems, presents

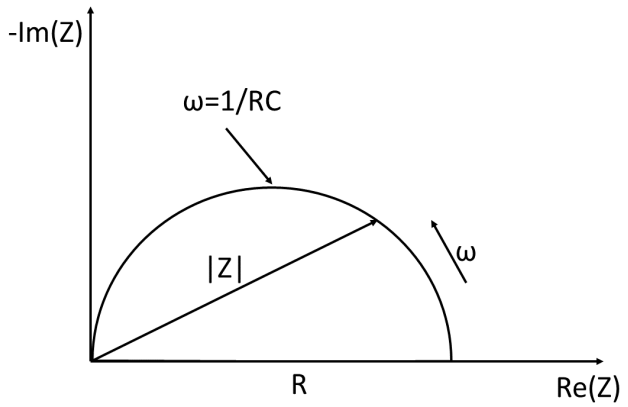

Figure A.2: RC group

shapes that are not directly conductible to the classic circuital elements described before. To associate the plot to an equivalent electric circuit, some

other elements, that does not present a Laplacian anti-transform and remain hence expressed in the frequency domain, have to be utilized.

- **Constant Phase Element**: $Z_{CPE} = \frac{1}{(j\omega)^{\psi}\theta}$. ψ is the depression factor and its value is comprised between 0 and 1. θ is a generalized capacity. The element represents a non ideal capacitor, with a non homogenous surface and porosity effects. If ψ is equal to one, CPE becomes an ideal capacity, with θ=C. The phase angle of the CPE impedance is independent on the frequency and has a value of $(-90 * \psi)$ degrees.

- **ZARC element**: ZARC impedance corresponds to the parallel connection of a CPE with a resistance: $Z_{ZARC} = \frac{1}{1/R+(j\omega)^{\psi}\theta}$. In the Nyquist plot it appears as a depressed semicircle, with the center below the x-axis. The angle that the

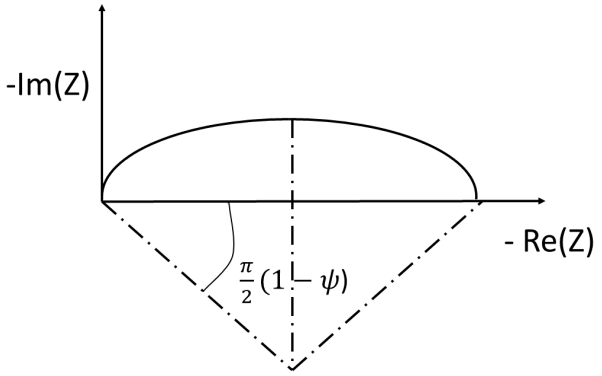

Figure A.3: ZARC element

real axis forms with the straight line connecting the center of the circumference, is related to the depression factor ψ as shown in the picture.

- **Warburg Element**: Warburg impedance was developed to model the diffusion of ionic species. Several expressions, based on different assumptions can be used to describe this impedance.

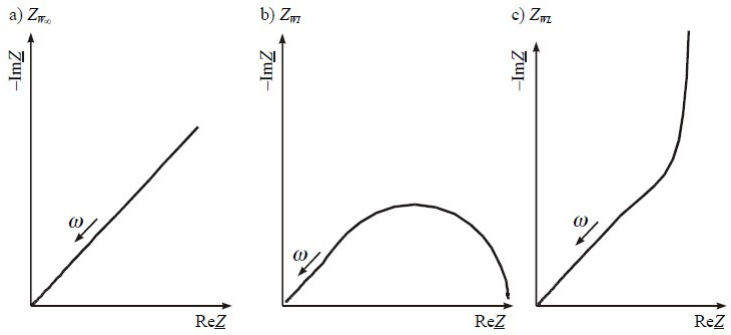

Figure A.4: Warburg Impedances

a) Semi-infinite linear diffusion:$Z_W = \frac{1}{1/Y_0\sqrt{(j\omega)}}$. Phase angle is constant and equal to -45^o.

b) Finite diffusion layer with ideal reservoir at the boundary $Z_W = \frac{tanh(B\sqrt{j\omega})}{Y_0\sqrt{(j\omega)}}$

c) Finite length diffusion with reflexive boundary $Z_W = \frac{AW}{\sqrt{(j\omega)}}coth(B\sqrt{(j\omega)}$

The three impedances appear similar at high frequencies but differ in the diagram at low frequencies.

As stated before, the last three elements previously described can be represented in the time domain only accepting some approximations. Warburg diffusion impedance and ZARC element can be transformed into a finite series of RC circuit elements [65],[90]. The greater the number of RC groups, the higher the accuracy.

The main disadvantage of Nyquist plot is that frequency does not appear explicitly. When one wants to understand the cell frequency behavior Bode plot is preferable.

Bode plot

The absolute value of impedance and the phase shift are plotted as a function of frequency. It uses a logarithmic scale. In the picture, the bode plot of a simple electrochemical system is reported. The graph is also preferable, when data scatter

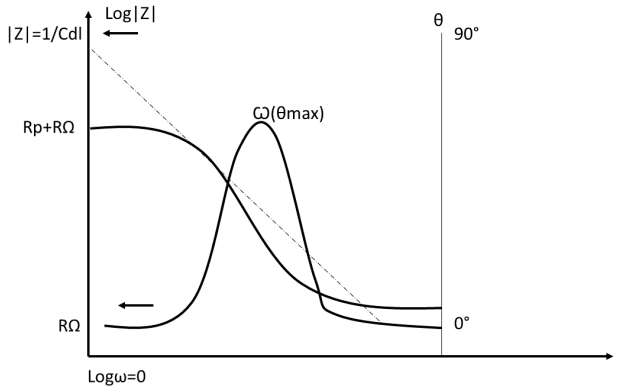

Figure A.5: Bode plot

prevents a good fitting in Nyquist plot. A disadvantage of the plot is that, the shape of the curve changes, changing the value of circuital elements [142].

Appendix B

Batteries' on field characterization

Some of the time spent at Ngarenanyuki school has been devoted to the monitoring and checking the battery storage system with a double purpose.

- Understand the way in which the BESS system is used, assess state of health of batteries and provide suggestions for an efficient battery use.
- Find the values of the parameters of lead acid model in place. The accurate parametrization of BESS models with on field measures would allow to have an accurate dimensioning of the PV+BESS system suited for the school.

BESS system plays an important role for the satisfaction of the school energy needs. School is provided with 30 VRLA batteries Gaston GT 12 200. Each battery has a nominal voltage of 12V and a nominal capacity of 200Ah when discharged at constant current C_{20}. Batteries are connected in series to provide a total nominal energy of 72 kWh.
In the graph B.1, are reported voltage and current of batteries measured during a whole day, from midnight (0s) to midnight (86400s). The trends are representative of what happens during a typical day, in which batteries are charged by PV panels. During the night batteries are discharged by autoconsumption of control switchboards and by the lights equipment. At sun rise, around 6 a.m., batteries start to be charged by the PV panels and they arrive to their maximum voltage level at around 2p.m.. After that, sun power slowly decreases together with increasing load consumption. At around 5 p.m. batteries start to being discharged, and go back to a low SOC value late in the evening. When hydro turbine is present during the day, it contributes to battery charging process. Data collected by Politecnico of Milan Team, from 2015, depict a low SOC level during most of the year. This is an important issue when speaking of lead acid batteries, whose degradation is strongly affected by low SOC levels and not complete charge.
In order to characterize batteries, procedures described in the following have been adopted. The final goal was to determine the OCV discharge curve and values of resistances at different SOC for charge and discharge.

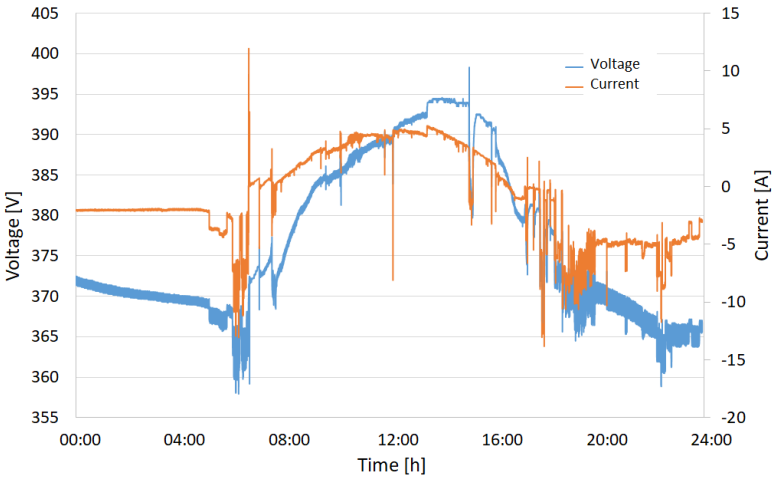

Figure B.1: Batteries voltage current characteristic during a typical day in Ngarenanyuki

Charge characterization

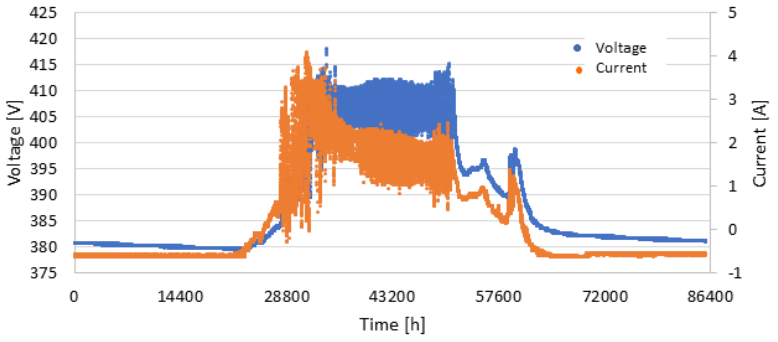

(a)

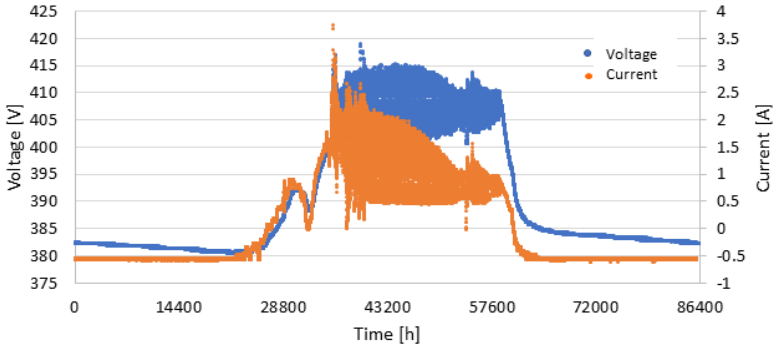

(b)

Figure B.2: BESS voltage and current characteristic during the first charging day(a), and the last charging day(b)

PV and batteries have been isolated from school loads for six days, in order to charge batteries with solar power. Voltage current characteristic of batteries at the beginning and end of discharge process are reported in the graphs B.2a and B.2b, VOC value increased from 372V to 384.5V. It has not been possible to obtain a

complete charge (VOC ca. 396V from manufacturer's datasheet reported in E) due to different reasons.

- System auto consumption: control switchboard require ca. 200 W from the batteries in order to work continuously. For this reason, even though batteries were isolated from the school, they discharged during night with an almost constant current of 0.5A (C_{400}).
- Voltage saturation: when voltage of dc bus reaches 410 V, the control system lowers the current coming from PV in order to maintain voltage under that limit. Therefore, at the beginning of the charging process, when SOC was low the current was quite high (ca 4A) and the charge fast; at higher SOC were instead charged with a current of less than 1A. So as days went by charge became slower and the complete battery charge could not be reached in a reasonable amount of days.

Discharge characterization & Resistance Measurements

In order to allow batteries to be discharged with almost constant current, PV panel has been disconnected from batteries for 4 days. Batteries were completely isolated during night, so to discharge with the constant autoconsumption current of 0.5A and connected only to few school loads during the day (max discharge power ca 500 W). During the discharge process, some pulsed power tests were made on the batteries to measure resistance value. The obtained discharge curve is the one shown in the graph B.3.

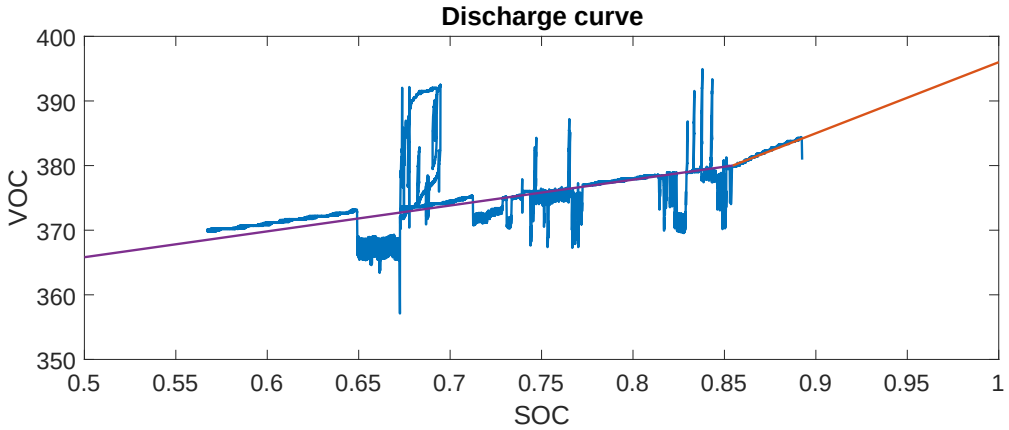

Figure B.3: Discharge curve

Peaks are caused by power pulses for resistance characterization (see later in the section). Due to school needs and shortage of time, it has not been possible to completely discharge batteries. The curve can be approximated with 2 straight lines, corresponding to the two different slopes at beginning and end of discharge. At low levels of SOC, measured voltage is quite distant from the fitting line: this could be

caused by the fact that batteries were discharged by a non negligible current and so the measured voltage does not correspond exactly to the OCV. Moreover, as seen in chapter 1 and 4, lead acid batteries discharge curve is not exactly approximable with straight lines and this simplification introduces errors.

As already introduced, tests where performed on batteries during the discharge period so as to assess the value of their internal resistance at different SOC levels and different C-rates. As long as lead acid battery resistance has different values during charge and discharge, charge and discharge pulses of constant power have been applied. $R = \Delta V/\Delta I$, where ΔV and ΔI are computed measuring voltage and current at the beginning and end of the pulse.

- Discharge resistance: power pulses of one minute length and some of longer duration have been imposed to batteries.
  - High power: 2650W, Current ca. -7A
  - Low power: 1250W/1400W, Current ca. -4A

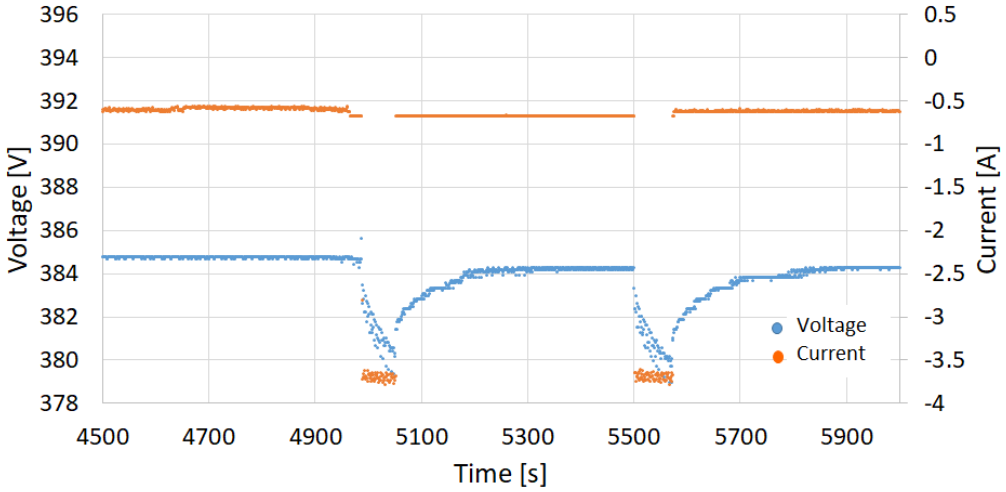

Figure B.4: Discharge power pulse, 1min

Comparing figure B.4 and B.5, it can be noticed that transient effects seem to expire in one minute. After that, voltage remains constant. From the second graph it can be noticed though, that measures are affected by a great degree of uncertainty. In figure B.6, computed resistance values as function of OCV are reported. R seems to have a slowly decreasing linear trend with respect to OCV, in accordance with theory. At higher C-rate, resistance is lower.

$\text{Rmean}_{lowpower}$=1.6Ω $\text{Std}_{lowpower}$=0.1Ω; data are related to 20 samples.

- Charge resistance: PV panel has been connected to batteries in order to give charge power pulses. However, power from PV panels is not controllable and

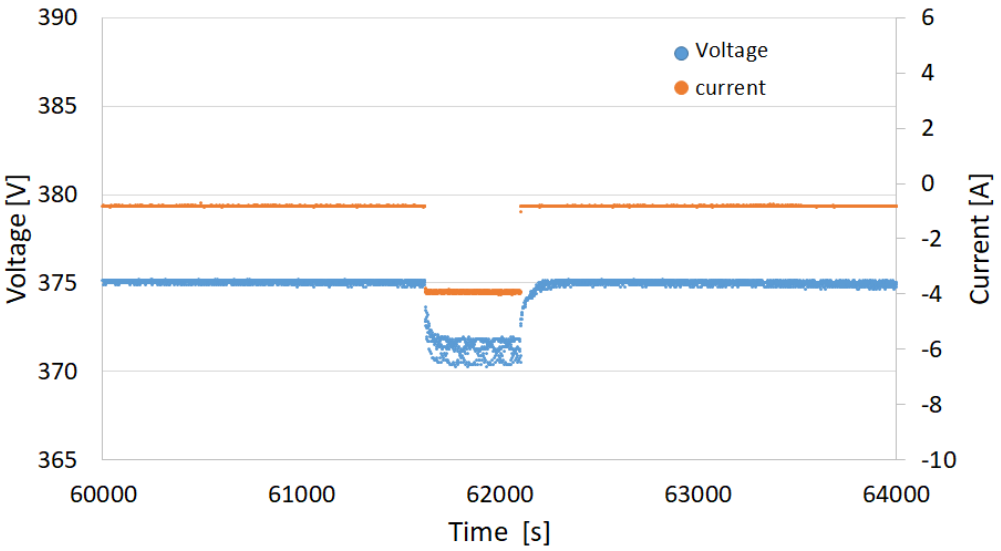

Figure B.5: Discharge power pulse, 10 min

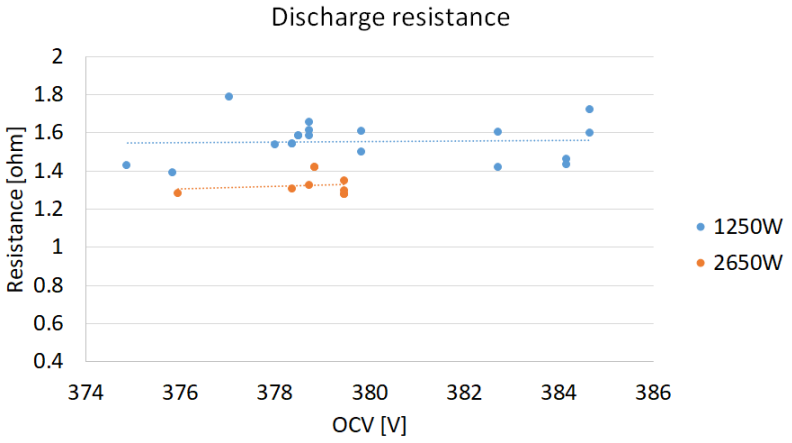

Figure B.6: Discharge resistance @1 minute power pulse

constant during the time step. Max power ca. 3000W. but variable. Pulses of different length were applied because current increases slowly when the panel is connected.

As it can be noticed from the graph B.7, charge behavior is markedly different

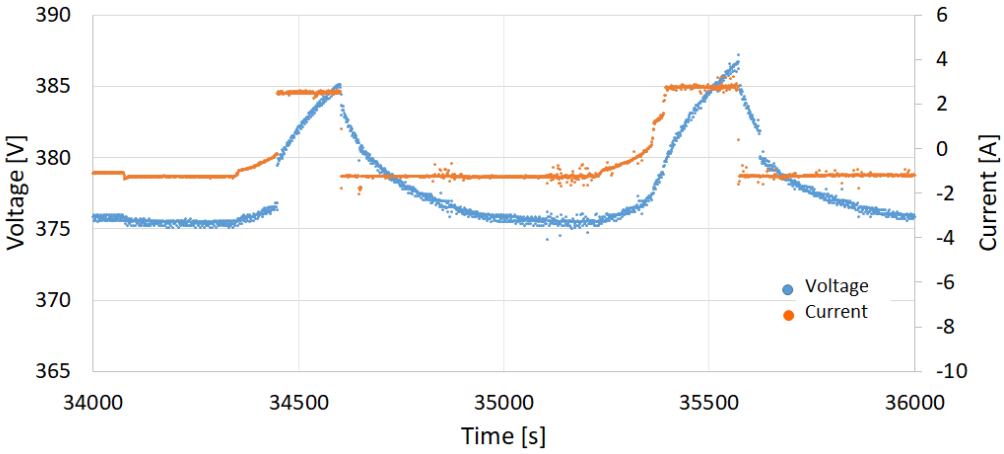

Figure B.7: Charge power pulse, 20min

from discharge. It is more difficult to approximate behavior with a resistance as long as transient periods time length seems longer either during power pulse and during the following relaxation period. Values of resistance computed after two minutes power pulse versus OCV are reported in the figure B.8

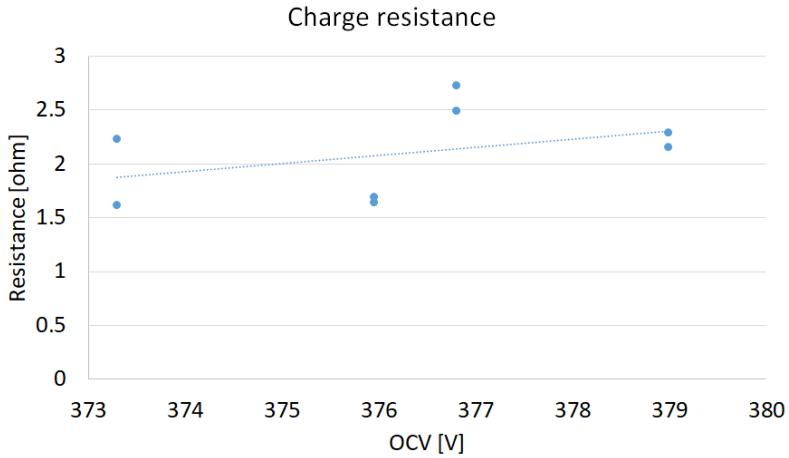

Figure B.8: Charge resistance @2minutes power pulse

It is noticeable the great dispersion of measures. Even in a charging status, a slowly increasing trend with OCV value and hence SOC is present. Generally speaking charge resistance value is higher in the charging status. This is not due to the fact that it has been computed with power pulses of longer duration: it is in fact shown in graph B.5 that during discharge, even when the power pulse is of 10 minutes, the value of the resistance does not change. The reason

of the difference among charge and discharge can be found in the different transient behavior of the battery.
Due to the high variability of measures and the non well defined trend with respect to OCV, it was not possible to get reliable information about resistance value.

The data, gathered during the period spent in Ngarenanyuki school, have been used to develop an "on-line" SOC indicator available for the local technician in charge of controlling the microgrid system. Data are affected by many uncertainties, however the necessity was to replace the already present commercial on line SOC indicator that was highly unreliable and consequently misleading for a correct management of the microgrid. Two different approaches have been chosen to evaluate SOC of the batteries: (i) Coulomb counting method and (ii) the equivalent electric circuit model, using OCV-SOC relation(see chapter 2 for further details).

Instead, manufacturer's data and laboratory measurements have been preferred to perform simulations in Poli.NRG software, given that there were many external factors that made on field measures unrepeatable and non reproducible; data collected were affected by too many errors and uncertainties and could not be used to assess parameters of battery models.

Appendix C

LoadProGen input data

Table C.1: School loads, as input to LoadProGen

Users' class	**Appliance**	**units**	**Nom P [W]**	**func. cycle(min)**	**func. time (h)**	**func window**
Boys' dorm	Common lights	24	18	60	12	all the night
	Room lights	20	18	60	2	morning and evening
Girls' dorm	Common lights	22	18	60	12	all the night
	Room lights	31	18	60	2	morning and evening
Classrooms	Lights	30	15	60	4	evening
Library	Lights	9	18	60	5	evening
Administration	Computer headmst.	1	90	30	3	8 am; 3pm
	Computer secretary	2	90	30	4	7.30 am; 6pm
	Printer	1	600	3	10 min	7.30 am; 6pm
	Outside lights	2	14	30	4	all the night
	Inside lights	3	11	30	3	7.30 am; 6pm
Control Room	Light	1	11	10	0.5	evening
	Computer	1	80	all day	all day	all day
	Desktop	1	50	5	20 min	7 am 10 pm
Matron Room	Light	1	11	30	2	evening
Kitchen	Light	1	11	60	1.5	evening
Canteen	Light	2	11	60	2	evening
Dining Hall	Lights	9	50	80	1.5	evening
Shop	Light	1	11	30	1.5	evening
Farm	Warming lights	6	100	all day	all day	all day
	Incubator	1	300	all day	all day	all day
	Lights	3	13	60	11	all the night
Water pump	Pump	1	2400	20	1	6 am 7 pm
Staff apartments	Lights	45	15	30	12	all day
	Iron	1	1000	20	1	morning and evening
Headmst apartment	Lights	10	15	10	13	all day
	TV	1	30	30	4	all day
	Toaster	1	900	5	20 min	morning
Mill	Grinding machine	1	12000	60	3	10 am 5 pm

Appendix D

Tanesco monitoring and Elettra project

Within the thesis project a cooperation with EnergyTeam has been activated with the goal of developing an advanced monitoring system devoted to operate as a meter for Ngarenanyuki secondary school and, at the same time, to collect data on the Tanzania's power grid. Such a monitoring system has been deployed and activated during the residence period at Ngarenanyuki.
The grid, as it is the case of national grids in developing countries, suffers from many instability and unreliability problems. Having accurate quantitative data regarding frequency and voltage oscillations, as well as electricity interruptions, is the first step towards the promotion of possible solutions. The system installed at Ngarenanyuki secondary school, is conceived as part of a possible wider pilot project, where decentralized mini grids could offer information and services to national electricity provider. A future development for the school has been proposed by Politecnico of Milan Energy Department in the frame of Elettra project.
In the following sections, after a brief description of the installed system hardware components', the status of Tanesco grid over a 20 days time window is reported. Finally, motivations and contents of Elettra project are discussed.

D.1 Tanesco Grid monitoring

Monitoring system

The monitoring system donated by the company Energy Team S.p.A. measures voltages and currents of each phase of Tanesco line with a frequency of 1Hz. ICT and TLC equipment are designed to locally store the samples and to send (share) them with the operational center, sited in Milan.
Samples are relevant to:

- 3 Current Transformers (CT); they measure the current of the 3 Tanesco

phases. Output in voltage. Transformation ratio: 100A/1V.

- 3 Voltage Transformers (VT).
- Multifunction network analyzer, X-Meter; it receives signals from the 3 CT and 3 VT. Accuracy: +/- 0.25 % of full scale (V,I measures).
- XM2-B BRIDGE USB-RS485. The module enables the conversion of the 485 signal going from the X-Meter to the PC's USB port.
- PC box; it is a small computer provided with the software Energy Sentinel Web, accessible by users.

The whole monitoring system, including data transfer procedure, has been tested in the laboratory of Energy Department of Politecnico of Milan. The picture D.1 illustrates the experimental set-up, with three phase load simulator.

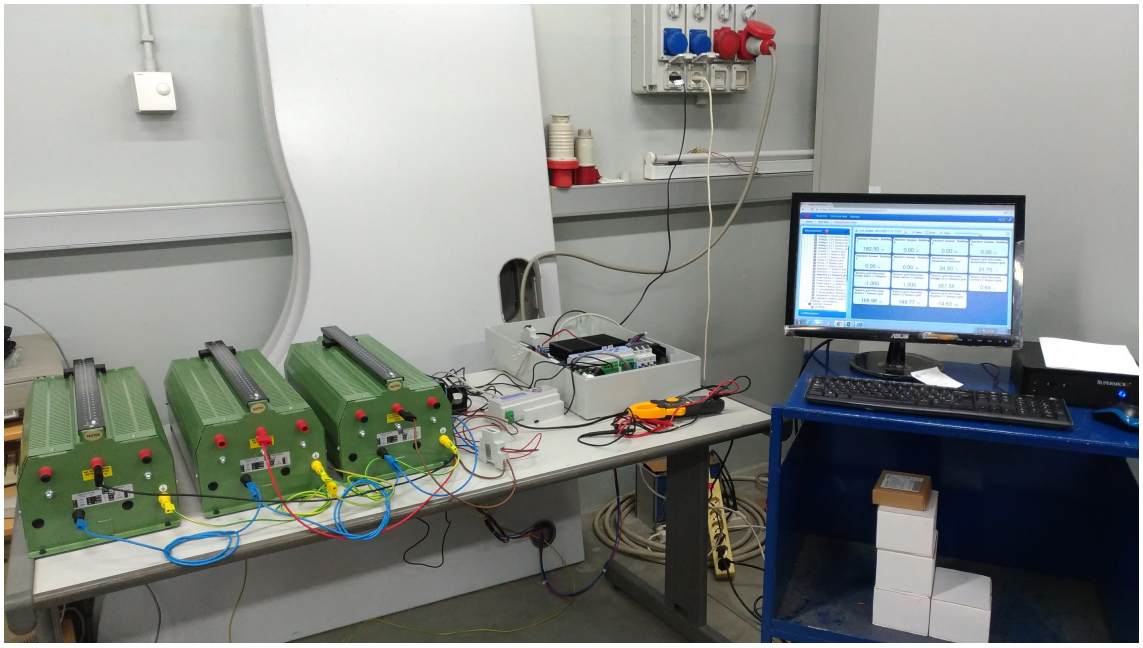

Figure D.1: Testing set-up of monitoring system: on the left, three phase load simulator, in the middle the monitoring system and on the right a PC with software Energy Sentinel Web

Figures D.2 and D.3 show respectively the X-Meter connection scheme, the components of the system and the panel once installed in Ngarenanyuki.

Monitoring status

In the following graphs it is reported Tanzania's grid status during the first 20 days after system installation. Data are still few to make an accurate statistical analysis and so they are devoted to provide just a first outlook on the principle issues.
Figure D.4 shows the oscillation of the voltage of the three phases during all the period, blank spaces correspond to missing data. Voltage oscillates between 220 and

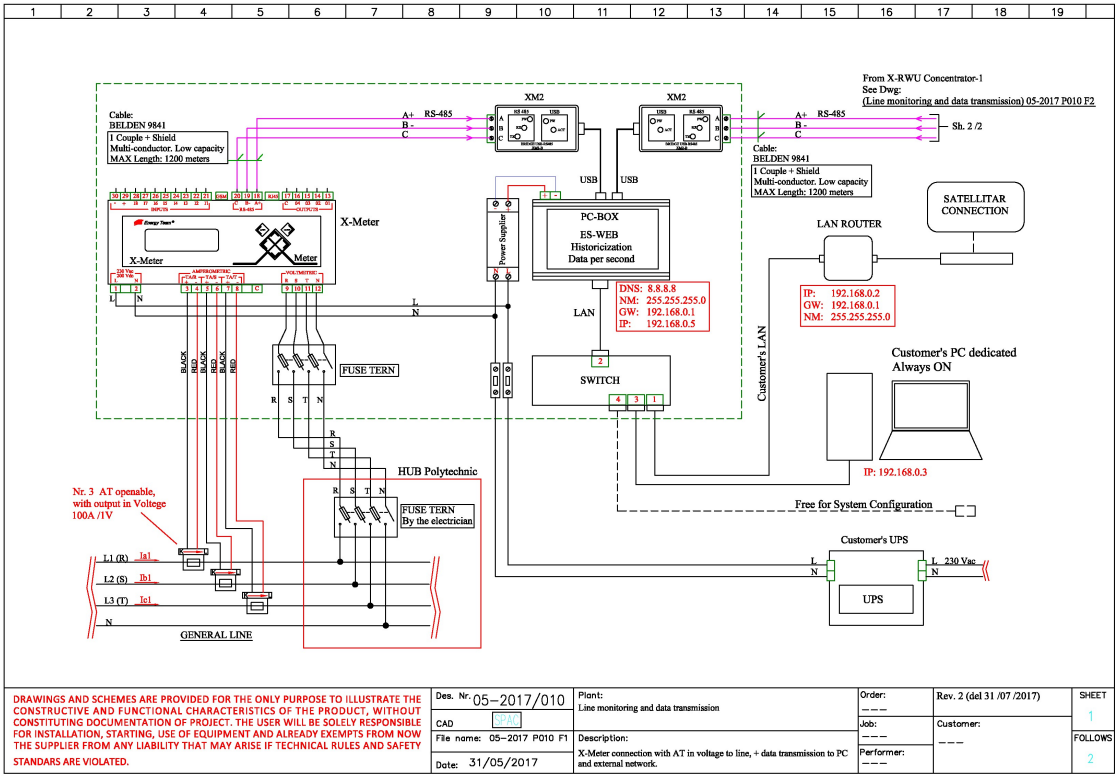

Figure D.2: Electric diagram of X-meter connections

240 V and many voltage drops are evident. The graph D.5 displays the voltage value dispersion of the three phases. On each box, the central mark indicates the median, and the bottom and top edges of the box indicate the 25th and 75th percentiles, respectively. The whiskers extend to the most extreme data points not considered outliers, and the outliers are plotted individually using the '+' symbol. Voltage is asymmetric on the three phases, being the median value of phase 1 and 3 higher than 230V and of phase 2 slightly lower; moreover, data dispersion is really high, from peaks of 300V to power outages at 0V. The carpet plot of figure D.6, represents with different colors the value of voltage during the considered days. White spaces correspond to missing data while blue bars are related to voltage equal to zero volts, i.e. to black out occurrences. Half of the days experienced some minutes of black out; the total duration of power outages represents the 10% of the measured period. The shortest outages lasted some minutes while the longest almost 8 hours.
Concerning frequency, the graph D.7, represents the trend over the 20 days period: frequency oscillates in a spectrum of $50Hz \pm 0.5Hz$. It is clear that the national grid, when compared to any European standard, is highly unstable and unreliable. To report an example, in Italy normal frequency variation are in the range of $\pm 15mHz$, when frequency is higher or lower than $50Hz \pm 0.1$, the system in in emergency status [143]. The histogram of figure D.8 compares frequency distribution of Italian and Tanzanian national grid; the gaussian of italian grid is centered on 50Hz while that of

Figure D.3: Picture of the complete electric panel

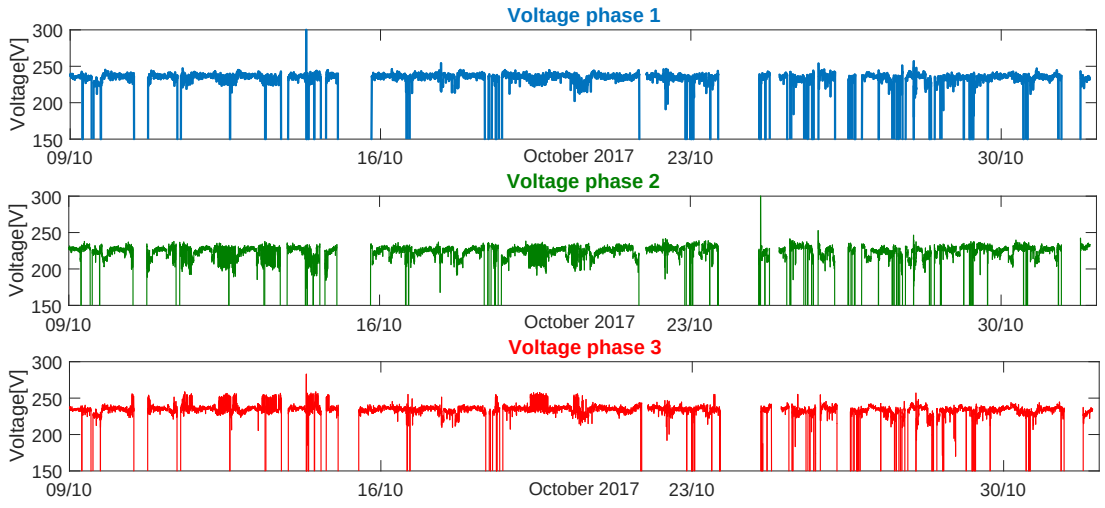

Figure D.4: Voltage of the three phases along 20 days

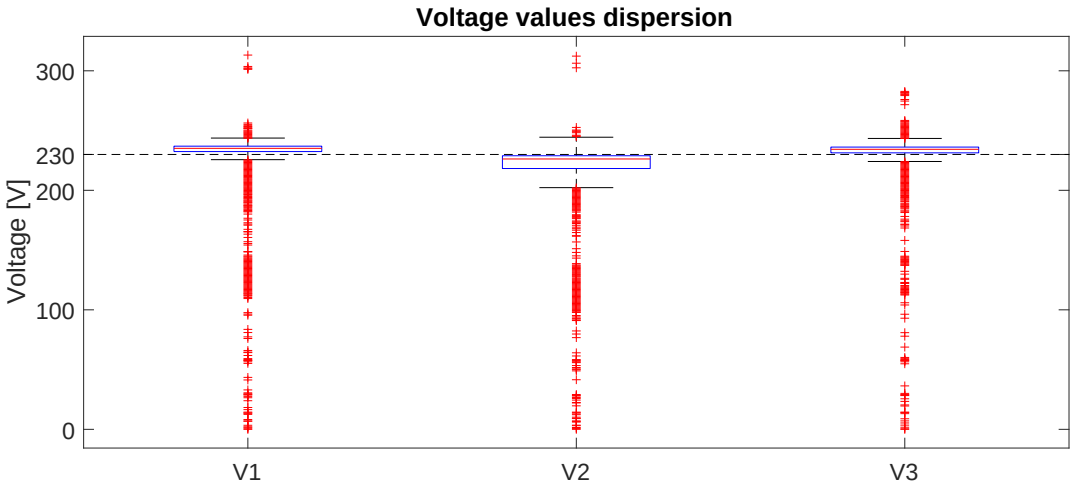

Figure D.5: Boxplot of voltage of three phases during 20 days

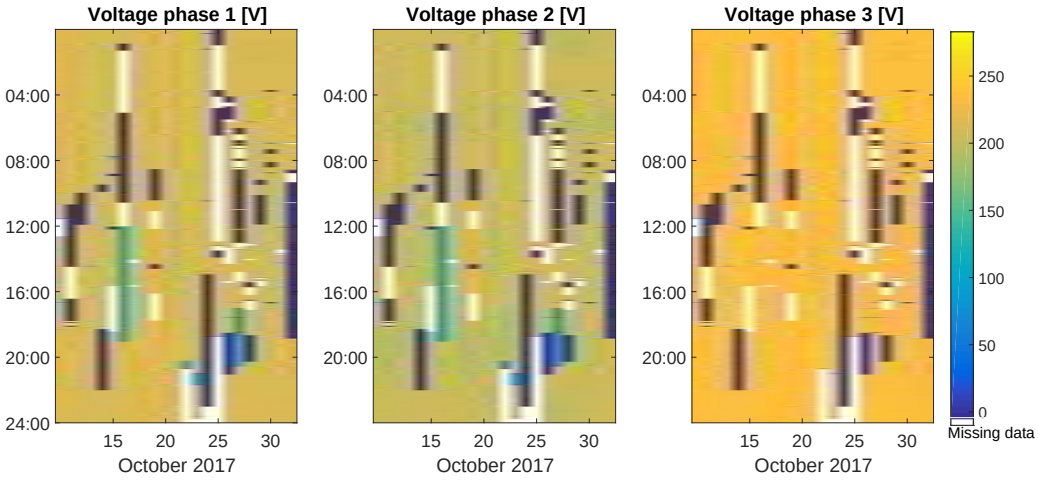

Figure D.6: Blackout occurrencies

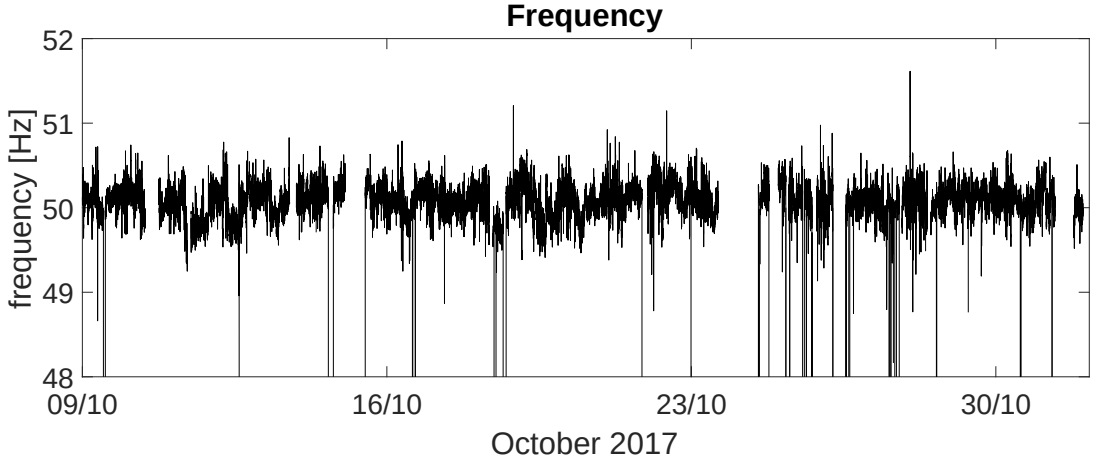

Figure D.7: Frequency along 20 days

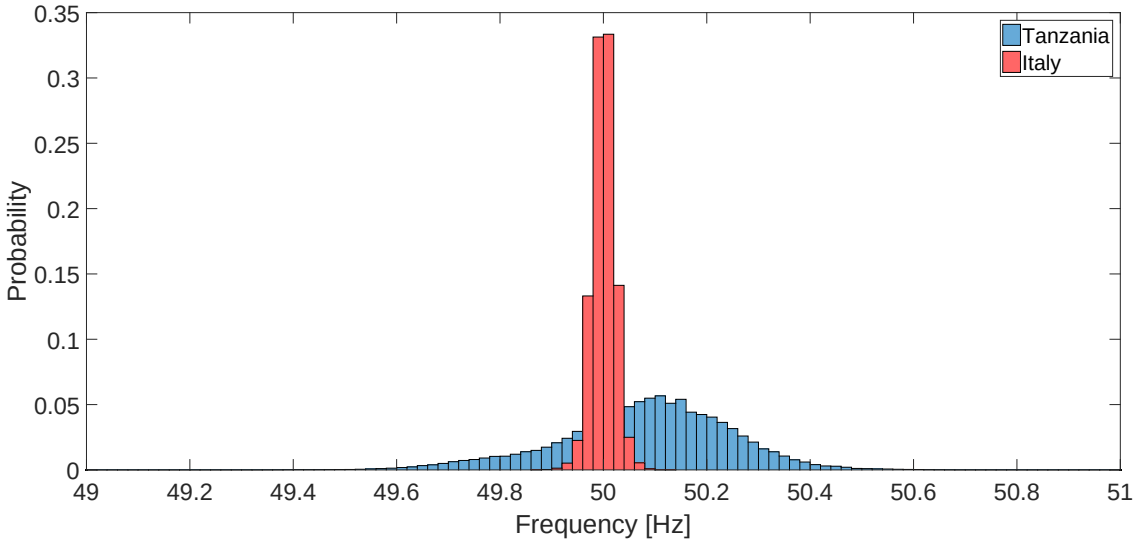

Figure D.8: Probability distribution of frequency during 20 days

Tanzania is shifted at 50.1 Hz and the dispersion is much higher. In this framework it appears with evidence the importance of projects aimed to the improvement of grid quality, like Elettra.

D.2 Elettra project proposal

Energy Department of Politecnico of Milan, in collaboration with EPS Elvi Energy S.r.l., and the o.n.g. Istituto Oikos, prepared a project proposal, to be submitted to international calls for sustainable development. The technical and economic proposal is related to installation of an Hybrid Power Plant at Ngarenanyuki secondary school, Tanzania, in the frame of the ELETTRA project.
The proposed solution, consist in the installation of a Hybrid Power Plant (HPP), composed of two PV plants (31.36 kW), a BESS composed of two Li-ion battery racks (137 kWh) and two Power Conversion System (PCS) (transformers, inverters, converters); the Li-ion batteries are directly connected to the main dc busbar, whereas the PV plants are connected through dc/dc converters, allowing for maximum power point tracking, independently from battery voltage and state of charge. The electric scheme of the plant is reported in figure D.9.
The micro grid can work in island mode or connected to Tanesco grid. It is provided with a control system that operates in order to maintain the microgrid stability, by maximizing the employment of renewable energy sources and optimizing the lifecycle of the storage systems included into the system. The HPP control can provide ancillary services to the grid: among which active and reactive power regulation. The successful installation of Tanesco metering system plays an important role in this framework: a quantitative detailed analysis of grid quality can have an important

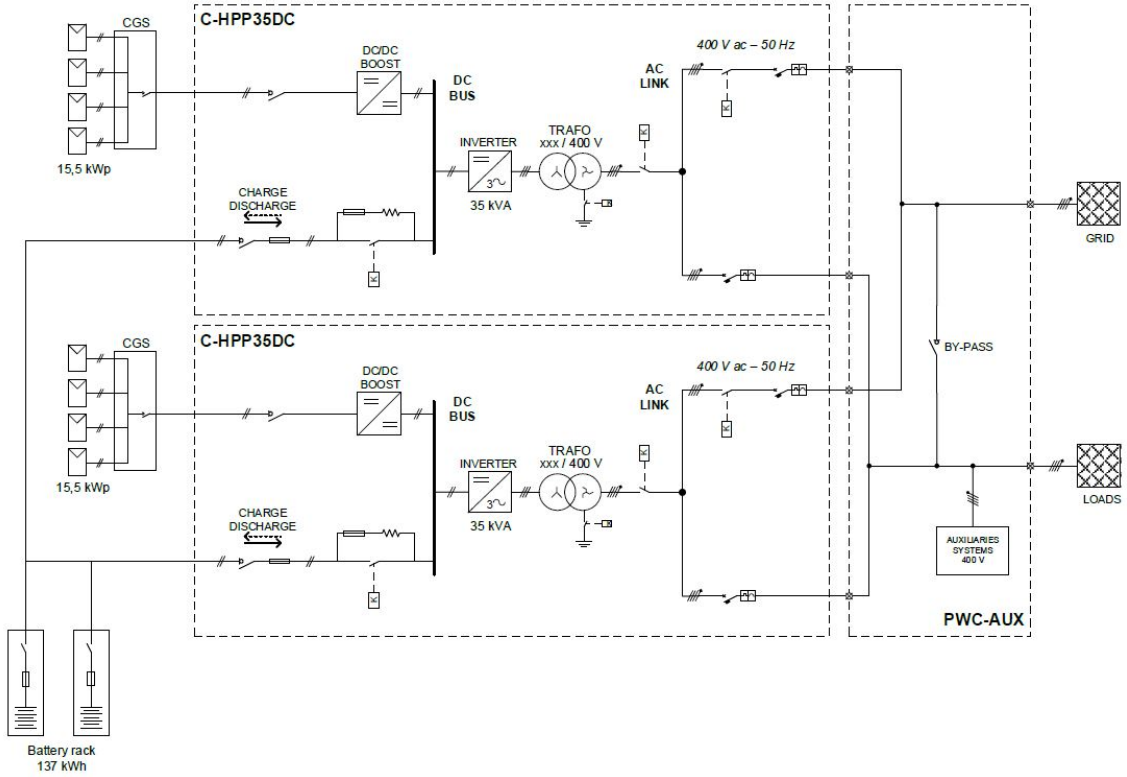

Figure D.9: Single line diagram of the HPP

impact on the correct management of integrated system.

Appendix E

Datasheets of tested cells

Table E.1: Boston Power Swing 5300 datasheet

Quantity	Value	Unit
Nominal capacity	5.3	Ah
Nominal energy	19.3	Wh
Nominal voltage	3.65	V
Max voltage	4.2	V
Energy density	207	Wh/Kg
Nominal cell impedance	15.5	mohm
Cycle life	100% DOD >1000	cycles
	90% DOD >2000	cycles
	80%DOD >3000	cycles
Max continuous disc. rate	13	A
Max continuous charge rate	10.6	A
Weight	93.5	g
Operating temp	charge -20 to +60	°C
	discharge -40 to 70	°C
Storage temp	-40 to 60	°C

Table E.2: Sonneschein A502-10S datasheet

Nom. voltage	Nom. capacity C20 1.75 Vpc 20 Â°C	Max. load	Length (l)	Width (b/w)	Height up to top of cover (h1)	Height over terminals (h2)	Weight	Internal resistance	Short circuit current
V	Ah	approx. A	max. mm	max. mm	max. mm	max. mm	approx. kg	mOhm	A
2	10	80	52.9	50.5	94.5	98.4	0.7	11.2	189

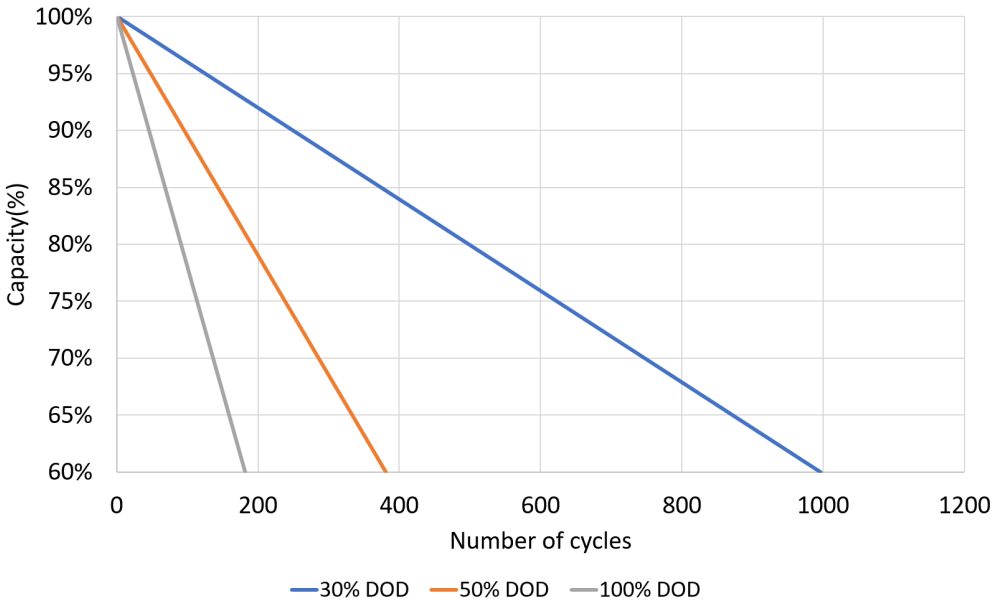

Figure E.1: Cycle life service at different DOD at ambient temperature of Sonnenschein A502-10S

Table E.3: Gaston GT12-200 datasheet

Quantity	Value	Unit
Nominal capacity	200	Ah
Nominal energy	2400	Wh
Nominal voltage	12	V
Max voltage	13.8	V
Internal resistance	4	mohm
Designed floating life	8	years
Weight	61	Kg
Capacity affected by temperature	102% 100% 85% 65%	40° C 25° C 0° C -15° C

Bibliography

[1] United Nations Development Programme. Sustainable Development Goals-Goal 7: Affordable and Clean Energy. http://www.undp.org, 2017.

[2] World Bank Group. The World Bank. http://www.worldbank.org.

[3] Emanuela Colombo, Stefano Bologna, and Diego Masera. *Renewable energy for unleashing sustainable development*. 2013.

[4] S. M. Mustonen. Rural energy survey and scenario analysis of village energy consumption: A case study in Lao People's Democratic Republic. *Energy Policy*, 38(2):1040–1048, 2010.

[5] HOMER Energy LLC. HOMER Pro - Microgrid Software for Designing Optimized Hybrid Microgrids. http://www.homerenergy.com/.

[6] David Trujillo. Hybrid Generation Simulator Hybrid Generation Simulator HybSim 3.3 HybSim 3.3.

[7] University of Massachussets. Hybrid2. http://www.umass.edu/, 2014.

[8] University of Zaragoza. iHOGA software. https://ihoga-software.com/.

[9] TRNSYS : Transient System Simulation Tool. http://www.trnsys.com/.

[10] Energy Storage Association. Energy Storage Facts & Figures. http://energystorage.org/, 2017.

[11] International Renewable Energy Agency. *Electricity storage and renewables: Costs and markets to 2030*. Number October. 2017.

[12] Martin Winter and Ralph J. Brodd. What are batteries, fuel cells, and supercapacitors? *Chemical Reviews*, 104(10):4245–4269, 2004.

[13] John Warner. *The Handbook of Lithium-Ion Battery Pack Design*. 2015.

[14] Xing Luo, Jihong Wang, Mark Dooner, and Jonathan Clarke. Overview of current development in electrical energy storage technologies and the application potential in power system operation. *Applied Energy*, 137:511–536, 2015.

[15] Elena M. Krieger, John Cannarella, and Craig B. Arnold. A comparison of lead-acid and lithium-based battery behavior and capacity fade in off-grid renewable charging applications. *Energy*, 60:492–500, 2013.

[16] Greg Albright, Jake Edie, and Said Al-Hallaj. A Comparison of Lead Acid to Lithium-ion in Stationary Storage Applications. *AllCell Technologies LLC*, (March):1–14, 2012.

[17] Boucar Diouf and Ramchandra Pode. Potential of lithium-ion batteries in renewable energy. *Renewable Energy*, 76:375–380, 2015.

[18] Andrea Casalegno. Slides of the course "Eletrochemical energy conversion and storage", Politecnico di Milano. pages 1–13.

[19] Paul Ruetschi. Aging mechanisms and service life of lead-acid batteries. *Journal of Power Sources*, 127(1-2):33–44, 2004.

[20] Kais Brik and Faouzi Ben Ammar. Causal tree analysis of depth degradation of the lead acid battery. *Journal of Power Sources*, 228:39–46, 2013.

[21] F. Beguin, E. Flahaut, A. Linares-Solano, and Jean Pinson. Surface properties, porosity, chemical and electrochemical applications. *Lecture Notes in Physics*, 677:495–549, 2006.

[22] The Boston Consulting Group. Batteries for Electric Cars: challenges, opportunities, and outlook to 2020. http://www.bcg.com/documents/file36615.pdf., 2010.

[23] Ana-Irina Stan, Maciej Swierczynski, Daniel-Ioan Stroe, Remus Teodorescu, and Soren Juhl Andreasen. Lithium ion battery chemistries from renewable energy storage to automotive and back-up power applications â An overview. *2014 International Conference on Optimization of Electrical and Electronic Equipment (OPTIM)*, pages 713–720, 2014.

[24] J. Vetter, P. Novák, M. R. Wagner, C. Veit, K. C. Möller, J. O. Besenhard, M. Winter, M. Wohlfahrt-Mehrens, C. Vogler, and A. Hammouche. Ageing mechanisms in lithium-ion batteries. *Journal of Power Sources*, 147(1-2):269–281, 2005.

[25] Julia Schiffer, Dirk Uwe Sauer, Henrik Bindner, Tom Cronin, Per Lundsager, and Rudi Kaiser. Model prediction for ranking lead-acid batteries according to expected lifetime in renewable energy systems and autonomous power-supply systems. *Journal of Power Sources*, 168(1 SPEC. ISS.):66–78, 2007.

[26] Isidor Buchmann. Battery University-Battery Definitions. http://batteryuniversity.com/, 2017.

[27] Mr Jongerden and Br Haverkort. Battery modeling. *Thecnical Report in Faculty Electrical Engineering, Mathematics and Computer Science*, page 18, 2008.

[28] Giovanni Viganò. *Master thesis: Modellazione elettrica e termica di una batteria agli ioni di litio con stimatore dello stato di carica.* 2014.

[29] David Linden and Thomas B. Reddy. *Handbook of batteries*, volume 17. Third edit edition, 2001.

[30] Dennis W. Dees, Vincent S. Battaglia, and André Bélanger. Electrochemical modeling of lithium polymer batteries. *Journal of Power Sources*, 110(2):310–320, 2002.

[31] M.R. Jongerden and B.R. Haverkort. Which battery model to use? *IET Software*, 3(6):445, 2009.

[32] Laifa Tao, Jian Ma, Yujie Cheng, Azadeh Noktehdan, Jin Chong, and Chen Lu. A review of stochastic battery models and health management. *Renewable and Sustainable Energy Reviews*, 80(July 2016):716–732, 2017.

[33] CF Chiasserini and R.R. Rao. Pulsed Battery Discharge in Communication Devices. 1999.

[34] M Doyle, T.F Fuller, and John Newman. Modeling of Galvanostatic Charge and Discharge of the Lithium/Polymer/Insertion Cell. *Journal of Hydrology*, 139(1):79–96, 1992.

[35] John Newman. Fortran Programs for the Simulation of Electrochemical Systems. http://www.cchem.berkeley.edu/jsngrp/fortran.html, 1998.

[36] Shriram Santhanagopalan, Qingzhi Guo, Premanand Ramadass, and Ralph E. White. Review of models for predicting the cycling performance of lithium ion batteries. *Journal of Power Sources*, 156(2):620–628, 2006.

[37] Cheng Lin and Aihua Tang. Simplification and Efficient Simulation of Electrochemical Model for Li-ion Battery in EVs. *Energy Procedia*, 104:68–73, 2016.

[38] V. Ramadesigan, P. W. C. Northrop, S. De, S. Santhanagopalan, R. D. Braatz, and V. R. Subramanian. Modeling and Simulation of Lithium-Ion Batteries from a Systems Engineering Perspective. *Journal of the Electrochemical Society*, 159(3):R31–R45, 2012.

[39] Long Cai and Ralph E. White. Mathematical modeling of a lithium ion battery with thermal effects in COMSOL Inc. Multiphysics (MP) software. *Journal of Power Sources*, 196(14):5985–5989, 2011.

[40] COMSOL Inc. COMSOL Multiphysics® Modeling Software. https://www.comsol.it.

[41] PDE Solutions Inc. FlexPDE finite element model builder for Partial Differential Equations. http://www.pdesolutions.com/.

[42] Linda Petzold. A description of DASSL : A differential/algebraic system solver. 1982.

[43] Parthasarathy M. Gomadam, John W. Weidner, Roger A. Dougal, and Ralph E. White. Mathematical modeling of lithium-ion and nickel battery systems. *Journal of Power Sources*, 110(2):267–284, 2002.

[44] Sven West, Keld; Jacobsen, Torben; Atlung. Modeling of Porous Insertion Electrodes with Liquid Electrolyte. *Electrochemical Society. Journal*, 129:1480–1485, 1982.

[45] Mark Verbrugge and H Gu. Finite difference routines for one and twodimensional problems utilizing a functional programming style. In *J. Newman, R. White (Eds.), Proceedings of the Douglass N. Bennion Memorial Symposium, The Electrochemical Society, Vol. 94/22, Pennington, NJ*, page 153. 1994.

[46] Rodolfo Dufo-López, Juan M. Lujano-Rojas, and José L. Bernal-Agustín. Comparison of different lead-acid battery lifetime prediction models for use in simulation of stand-alone photovoltaic systems. *Applied Energy*, 115:242–253, 2014.

[47] Rodolfo Dufo-Lòpez and Josè L. Bernal-Agustìn. Design and control strategies of PV-diesel systems using genetic algorithms. *Solar Energy*, 79(1):33–46, 2005.

[48] Nicholas Etherden and Math H J Bollen. Dimensioning of energy storage for increased integration of wind power. *IEEE Transactions on Sustainable Energy*, 4(3):546–553, 2013.

[49] Massoud Pedram and Qing Wu. Battery-powered digital CMOS design. *Proceedings -Design, Automation and Test in Europe, DATE*, 10(5):72–76, 1999.

[50] Ala Al Haj Hussein and Issa Batarseh. An overview of generic battery models. *IEEE Power and Energy Society General Meeting*, (4):4–9, 2011.

[51] A. Cherif, M. Jraidi, and A. Dhouib. A battery ageing model used in stand alone PV systems. *Journal of Power Sources*, 112(1):49–53, 2002.

[52] Gregory L. Plett. Extended Kalman filtering for battery management systems of LiPB-based HEV battery packs - Part 3. State and parameter estimation. *Journal of Power Sources*, 134(2):277–292, 2004.

[53] J. B. Copetti, E. Lorenzo, and F. Chenlo. A general battery model for PV system simulation. *Progress in Photovoltaics: Research and Applications*, 1(4):283–292, 1993.

[54] Michael M D Ross. A Simple but Comprehensive Lead-Acid Battery Model for Hybrid System Simulation.

[55] O. Tremblay, L.-a. Dessaint, and A.-I. Dekkiche. A Generic Battery Model for the Dynamic Simulation of Hybrid Electric Vehicles. *2007 IEEE Vehicle Power and Propulsion Conference*, (V):284–289, 2007.

[56] James F. Manwell and Jon G. McGowan. Lead acid battery storage model for hybrid energy systems. *Solar Energy*, 50(5):399–405, 1993.

[57] Daler Rakhmatov, Sarma Vrudhula, and Deborah A. Wallach. A model for battery lifetime analysis for organizing applications on a pocket computer. *IEEE Transactions on Very Large Scale Integration (VLSI) Systems*, 11(6):1019–1030, 2003.

[58] Venkat Rao, Gaurav Singhal, Anshul Kumar, and Nicolas Navet. Battery model for embedded systems. *VLSI Design, 2005. 18th International Conference on*, pages 105–110, 2005.

[59] Tingshu Hu and Hoeguk Jung. Simple algorithms for determining parameters of circuit models for charging/discharging batteries. *Journal of Power Sources*, 233(March):14–22, 2013.

[60] Simone Barcellona. A novel lithium ion battery model: A step towards the electrochemical storage systems unification. *Clean Electrical Power (ICCEP), 2017 6th International Conference on*, pages 416–421, 2017.

[61] Yang Gao, Jiuchun Jiang, Caiping Zhang, Weige Zhang, Zeyu Ma, and Yan Jiang. Lithium-ion battery aging mechanisms and life model under different charging stresses. *Journal of Power Sources*, 356:103–114, 2017.

[62] Jamie Gomez, Ruben Nelson, Egwu E. Kalu, Mark H. Weatherspoon, and Jim P. Zheng. Equivalent circuit model parameters of a high-power Li-ion battery: Thermal and state of charge effects. *Journal of Power Sources*, 196(10):4826–4831, 2011.

[63] S M G Mousavi and M Nikdel. Various battery models for various simulation studies and applications. *Renewable and Sustainable Energy Reviews*, 32:477–485, 2014.

[64] Nagham El Ghossein, Jack P. Salameh, Nabil Karami, Moustapha El Hassan, and Maged B. Najjar. Survey on electrical modeling methods applied

on different battery types. *2015 3rd International Conference on Technological Advances in Electrical, Electronics and Computer Engineering, TAEECE 2015*, pages 39–44, 2015.

[65] Nathalie Devillers, Marie Cècile Pèra, Samir Jemei, Frèdèric Gustin, and Daniel Bienaimè. Complementary characterization methods for Lithium-ion Polymer secondary battery modeling. *International Journal of Electrical Power and Energy Systems*, 67:168–178, 2015.

[66] Eckhard Karden. Using low-frequency impedance spectroscopy for characterization, monitoring, and modeling of industrial batteries. (May), 2002.

[67] Abbas Fotouhi, Daniel J. Auger, Karsten Propp, Stefano Longo, and Mark Wild. A review on electric vehicle battery modelling: From Lithium-ion toward Lithium-Sulphur. *Renewable and Sustainable Energy Reviews*, 56:1008–1021, 2016.

[68] Markus Einhorn, Fiorentino Valerio Conte, Christian Kral, and Senior Member. Comparison , Selection , and Parameterization of Electrical Battery Models for Automotive Applications. *IEEE Transactions on Power Electronics*, 28(3):1429–1437, 2013.

[69] Jana Kalawoun, Patrick Pamphile, Gilles Celeux, Biletska Krystyna, and Maxime Montaru. Estimation of the Battery State of Charge: a Switching Markov State-Space Model. *23rd European Signal Processing Conference (EUSIPCO)*, 77:1950–1954, 2015.

[70] Jana Kalawoun and Krystyna Biletska. From a novel classification of the battery state of charge estimators toward a conception of an ideal one. *Journal of Power Sources*, 279:694–706, 2015.

[71] Kai Sun and Qifang Shu. Overview of the types of battery models. *Proceedings of the 30th Chinese Control Conference*, pages 3644–3648, 2011.

[72] Grzegorz Pilatowicz, Andrea Marongiu, Julia Drillkens, Philipp Sinhuber, and Dirk Uwe Sauer. A critical overview of definitions and determination techniques of the internal resistance using lithium-ion, lead-acid, nickel metal-hydride batteries and electrochemical double-layer ca[1] G. Pilatowicz, A. Marongiu, J. Drillkens, P. Sinhuber, and D. U. *Journal of Power Sources*, 296:365–376, 2015.

[73] S. M. Mousavi G. and M. Nikdel. Various battery models for various simulation studies and applications. *Renewable and Sustainable Energy Reviews*, 32:477–485, 2014.

[74] Valerie H Johnson. Temperature-Dependent Battery Models for High-Power Lithium-Ion Batteries. (January), 2001.

[75] Lijun Gao, Shengyi Liu, Roger A Dougal, and Senior Member. Dynamic Lithium-Ion Battery Model for System Simulation. *IEEE Transactions on Components and Packaging Technologies*, 25(3):495–505, 2002.

[76] Hongwen He, Rui Xiong, and Jinxin Fan. Evaluation of lithium-ion battery equivalent circuit models for state of charge estimation by an experimental approach. *Energies*, 4(4):582–598, 2011.

[77] Jaemoon Lee Jaemoon Lee, Jaeho Lee Jaeho Lee, Onyong Nam Onyong Nam, Jonghun Kim Jonghun Kim, Bo Hyung Cho Bo Hyung Cho, Han-Seok Yun Han-Seok Yun, Soo-Seok Choi Soo-Seok Choi, Kiho Kim Kiho Kim, J.H. Kim, and Sonu Jun Sonu Jun. Modeling and Real Time Estimation of Lumped Equivalent Circuit Model of a Lithium Ion Battery. *2006 12th International Power Electronics and Motion Control Conference*, pages 1536–1540, 2006.

[78] Stephan Buller, Marc Thele, Eckhard Karden, and Rik W. De Doncker. Impedance-based non-linear dynamic battery modeling for automotive applications. *Journal of Power Sources*, 113(2):422–430, 2003.

[79] Ehsan Samadani, Siamak Farhad, William Scott, Mehrdad Mastali, Leonardo E Gimenez, Michael Fowler, and Roydon A Fraser. Empirical Modeling of Lithium-ion Batteries Based on Electrochemical Impedance Spectroscopy Tests. *Electrochimica Acta*, 160:169–177, 2015.

[80] Matthieu Dubarry, Cyril Truchot, and Bor Yann Liaw. Cell degradation in commercial LiFePO4 cells with high-power and high-energy designs. *Journal of Power Sources*, 258:408–419, 2014.

[81] Matthieu Dubarry, Bor Yann Liaw, Mao Sung Chen, Sain Syan Chyan, Kuo Chang Han, Wun Tong Sie, and She Huang Wu. Identifying battery aging mechanisms in large format Li ion cells. *Journal of Power Sources*, 196(7):3420–3425, 2011.

[82] Matthieu Dubarry and Bor Yann Liaw. Identify capacity fading mechanism in a commercial LiFePO4 cell. *Journal of Power Sources*, 194(1):541–549, 2009.

[83] K M Tsang, L Sun, and W L Chan. Identification and modelling of Lithium ion battery. *Energy Conversion and Management*, 51:2857–2862, 2010.

[84] Matthias Dürr, Andrew Cruden, Sinclair Gair, and J. R. McDonald. Dynamic model of a lead acid battery for use in a domestic fuel cell system. *Journal of Power Sources*, 161(2):1400–1411, 2006.

[85] V Johnson. Battery performance models in ADVISOR. *Journal of Power Sources*, 110(2):321–329, 2002.

[86] Valerie H Johnson, Ahmad A Pesaran, and Thomas Sack. Temperature-Dependent Battery Models for High-Power Lithium-Ion Batteries. 2000.

[87] Luiz Carlos Stevanatto, Valner Joao Brusamarello, and Stanislav Tairov. Parameter identification and analysis of uncertainties in measurements of lead-acid batteries. *IEEE Transactions on Instrumentation and Measurement*, 63(4):761–768, 2014.

[88] Shengbo Eben Li, Baojin Wang, Huei Peng, and Xiaosong Hu. An electrochemistry-based impedance model for lithium-ion batteries. *Journal of Power Sources*, 258:9–18, 2014.

[89] Salim Erol and Mark E Orazem. The influence of anomalous diffusion on the impedance response of LiCoO2—C batteries. *Journal of Power Sources*, 293:57–64, 2015.

[90] D Andre, M Meiler, K Steiner, H Walz, T Soczka-guth, and D U Sauer. Characterization of high-power lithium-ion batteries by electrochemical impedance spectroscopy . II : Modelling. *Journal of Power Sources*, 196:5349–5356, 2011.

[91] D Andre, M Meiler, K Steiner, Ch Wimmer, T. Soczka-Guth, and D U Sauer. Characterization of high-power lithium-ion batteries by electrochemical impedance spectroscopy. I. Experimental investigation. *Journal of Power Sources*, 196(12):5334–5341, 2011.

[92] Matthieu Urbain, Melika Hinaje, Stphane Rael, Bernard Davat, and Philippe Desprez. Energetical modeling of lithium-ion batteries including electrode porosity effects. *IEEE Transactions on Energy Conversion*, 25(3):862–872, 2010.

[93] C.-F. Chiasserini and R.R. Rao. Energy efficient battery management. *IEEE Journal on Selected Areas in Communications*, 19(7):1235–1245, 2001.

[94] Peng Rong and Massoud Pedram. Battery-aware power management based on markovian decision processes. *IEEE Transactions on Computer-Aided Design of Integrated Circuits and Systems*, 25(7):1337–1349, 2006.

[95] Christian Schlasza, Peter Ostertag, Daniela Chrenko, Reiner Kriesten, and David Bouquain. Review on the aging mechanisms in Li-ion batteries for electric vehicles based on the FMEA method. *2014 IEEE Transportation Electrification Conference and Expo (ITEC)*, pages 1–6, 2014.

[96] Anthony Barre, Benjamin Deguilhem, Sebastien Grolleau, Mathias Gerard, Frederic Suard, and Delphine Riu. A review on lithium-ion battery ageing mechanisms and estimations for automotive applications. *Journal of Power Sources*, 241:680–689, 2013.

[97] V Marano, S Onori, Y Guezennec, G Rizzoni, and N Madella. Lithium-ion batteries life estimation for plug-in hybrid electric vehicles. *Vehicle Power and Propulsion Conference, 2009. VPPC '09. IEEE*, pages 536–543, 2009.

[98] Martin Ebner, Federica Marone, Marco Stampanoni, and Vanessa Wood. Visualization and Quantification of Electrochemical and Mechanical Degradation in Li Ion Batteries. *Science*, 342(November):716–721, 2013.

[99] Simon Tippmann, Daniel Walper, Luis Balboa, Bernd Spier, and Wolfgang G. Bessler. Low-temperature charging of lithium-ion cells part I: Electrochemical modeling and experimental investigation of degradation behavior. *Journal of Power Sources*, 252:305–316, 2014.

[100] M. Broussely, S. Herreyre, P. Biensan, P. Kasztejna, K. Nechev, and R. J. Staniewicz. Aging mechanism in Li ion cells and calendar life predictions. *Journal of Power Sources*, 97-98:13–21, 2001.

[101] Alexander P. Schmidt, Matthias Bitzer, Árpád W. Imre, and Lino Guzzella. Model-based distinction and quantification of capacity loss and rate capability fade in Li-ion batteries. *Journal of Power Sources*, 195(22):7634–7638, 2010.

[102] P. Ramadass, Bala Haran, Parthasarathy M. Gomadam, Ralph White, and Branko N. Popov. Development of First Principles Capacity Fade Model for Li-Ion Cells. *Journal of The Electrochemical Society*, 151(2):A196, 2004.

[103] FEMLAB 3: Multiphysics Modeling.

[104] José L. Bernal-Agustín and Rodolfo Dufo-López. Simulation and optimization of stand-alone hybrid renewable energy systems. *Renewable and Sustainable Energy Reviews*, 13:2111–2118, 2009.

[105] Andreas Aichhorn, Michael Greenleaf, H. Li, and J. Zheng. A cost effective battery sizing strategy based on a detailed battery lifetime model and an economic energy management strategy. *IEEE Power and Energy Society General Meeting*, pages 1–8, 2012.

[106] Noshin Omar, Mohamed Abdel Monem, Yousef Firouz, Justin Salminen, Jelle Smekens, Omar Hegazy, Hamid Gaulous, Grietus Mulder, Peter Van den Bossche, Thierry Coosemans, and Others. Lithium iron phosphate based batteryâAssessment of the aging parameters and development of cycle life model. *Applied Energy*, 113:1575–1585, 2014.

[107] E. V. Thomas, H. L. Case, D. H. Doughty, R. G. Jungst, G. Nagasubramanian, and E. P. Roth. Accelerated power degradation of Li-ion cells. *Journal of Power Sources*, 124(1):254–260, 2003.

[108] Maciej Swierczynski, Daniel Ioan Stroe, Ana Irina Stan, and Remus Teodorescu. Lifetime Estimation of the Nanophosphate LiFePO4/C Battery Chemistry Used in Fully Electric Vehicles. *IEEE Transactions on Industry Applications*, 51(4):3453–3461, 2015.

[109] Daniel Ioan Stroe, Maciej Swierczynski, Ana Irina Stan, Remus Teodorescu, and Soren Juhl Andreasen. Accelerated lifetime testing methodology for lifetime estimation of lithium-ion batteries used in augmented wind power plants. *IEEE Transactions on Industry Applications*, 50(6):4006–4017, 2014.

[110] John Wang, Ping Liu, Jocelyn Hicks-Garner, Elena Sherman, Souren Soukiazian, Mark Verbrugge, Harshad Tataria, James Musser, and Peter Finamore. Cycle-life model for graphite-LiFePO4 cells. *Journal of Power Sources*, 196(8):3942–3948, 2011.

[111] Justin Purewal, John Wang, Jason Graetz, Souren Soukiazian, Harshad Tataria, and Mark W. Verbrugge. Degradation of lithium ion batteries employing graphite negatives and nickel-cobalt-manganese oxide + spinel manganese oxide positives: Part 1, aging mechanisms and life estimation. *Journal of Power Sources*, 269:937–948, 2014.

[112] Bolun Xu, Alexandre Oudalov, Andreas Ulbig, Goran Andersson, and Daniel Kirschen. Modeling of Lithium-Ion Battery Degradation for Cell Life Assessment. *IEEE Transactions on Smart Grid*, 3053(c):1–1, 2016.

[113] Alan Millner. Modeling Lithium Ion Battery Degradation in Electric Vehicles. *Massachusetts Institute of Technology Lincoln Laboratory*, pages 349–356, 2010.

[114] Daniel Ioan Stroe, Maciej Swierczynski, Soren Knudsen Kar, and Remus Teodorescu. A comprehensive study on the degradation of lithium-ion batteries during calendar ageing: The internal resistance increase. *ECCE 2016 - IEEE Energy Conversion Congress and Exposition, Proceedings*, 2017.

[115] S. S. Zhang, K. Xu, and T. R. Jow. EIS study on the formation of solid electrolyte interface in Li-ion battery. *Electrochimica Acta*, 51(8-9):1636–1640, 2006.

[116] RB Wright, CG Motloch, and JR Belt. Calendar-and cycle-life studies of advanced technology development program generation 1 lithium-ion batteries. *Journal of power*, 110:445–470, 2002.

[117] I. Bloom, B. W. Cole, J. J. Sohn, S. A. Jones, E. G. Polzin, V. S. Battaglia, G. L. Henriksen, C. Motloch, R. Richardson, T. Unkelhaeuser, D. Ingersoll, and H. L. Case. An accelerated calendar and cycle life study of Li-ion cells. *Journal of Power Sources*, 101(2):238–247, 2001.

[118] Bor Yann Liaw, Rudolph G. Jungst, Ganesan Nagasubramanian, Herbert L. Case, and Daniel H. Doughty. Modeling capacity fade in lithium-ion cells. *Journal of Power Sources*, 140(1):157–161, 2005.

[119] M Einhorn, V F Conte, C Kral, J Fleig, and R Permann. Parameterization of an electrical battery model for dynamic system simulation in electric vehicles. 2010.

[120] R. Lazzari, E. Micolano, and L. Pellegrino. Sviluppo di un sistema per la stima dello stato di carica(SOC) e dello stato di salute (SOH) di una batteria litio-ioni, procedura di gestione ottimanle delle batterie litio-ioni. Technical report, Ricerca Sistema Energetico, 2015.

[121] A. Eddahech, O. Briat, E. Woirgard, and J. M. Vinassa. Remaining useful life prediction of lithium batteries in calendar ageing for automotive applications. *Microelectronics Reliability*, 52(9-10):2438–2442, 2012.

[122] Sijie Cheng, Bimei Li, Zhongzhi Yuan, Fuyi Zhang, and Jincheng Liu. Development of a lifetime prediction model for lithium thionyl chloride batteries based on an accelerated degradation test. *Microelectronics Reliability*, 65:274–279, 2016.

[123] Nicolo Michelusi, Leonardo Badia, Ruggero Carli, Luca Corradini, and Michele Zorzi. Energy management policies for harvesting-based wireless sensor devices with battery degradation. *IEEE Transactions on Communications*, 61(12):4934–4947, 2013.

[124] Stefano Mandelli. *Strategies for access to energy in developing countries: methods and models for off-grid power systems design.* PhD thesis, Politecnico di Milano, 2015.

[125] Claudio Brivio, Matteo Moncecchi, Stefano Mandelli, and Marco Merlo. A novel software package for the robust design of off-grid power systems. *Journal of Cleaner Production*, 166:668–679, 2017.

[126] Tamer Khatib, Ibrahim A. Ibrahim, and Azah Mohamed. A review on sizing methodologies of photovoltaic array and storage battery in a standalone photovoltaic system. *Energy Conversion and Management*, 120:430–448, 2016.

[127] Simone Mazzola, Marco Astolfi, and Ennio Macchi. A detailed model for the optimal management of a multigood microgrid. *Applied Energy*, 154:862–873, 2015.

[128] A review on planning, configurations, modeling and optimization techniques of hybrid renewable energy systems for off grid applications. *Renewable and Sustainable Energy Reviews*, 58:376–396, may 2016.

[129] Claudio Brivio. *Battery Energy Storage Systems: Modelling, Applications and Design Criteria*. PhD thesis, Politecnico di Milano, 2017.

[130] Matteo Moncecchi, Fabio Riva, and Emanuela Colombo. Load Demand and long-term electric load forecasting in Rural Electrification. Technical report, Politecnico di Milano, Energy Department, 2016.

[131] Subhes C. Bhattacharyya and Govinda R. Timilsina. Modelling energy demand of developing countries: Are the specific features adequately captured? *Energy Policy*, 38(4):1979–1990, 2010.

[132] Politecnico of Milan. E4G. https://www.facebook.com/energy4growing2014/, 2014.

[133] International Renewable Energy Agency. *Solar Pv in Africa: Costs and Markets*. Number September. 2016.

[134] International Renewable Energy Agency. *Electricity storage and renewables: Costs and markets to 2030*. Number October. 2017.

[135] Dirk Uwe Sauer and Heinz Wenzl. Comparison of different approaches for lifetime prediction of electrochemical systems-Using lead-acid batteries as example. *Journal of Power Sources*, 176(2):534–546, 2008.

[136] D Aurbach, B Markovsky, M.D Levi, E Levi, A Schechter, M Moshkovich, and Y Cohen. New insights into the interactions between electrode materials and electrolyte solutions for advanced nonaqueous batteries. *Journal of Power Sources*, 81-82:95–111, 1999.

[137] F Huet. A review of impedance measurements for determination of the state-of-charge or state-of-health of secondary batteries. *Journal of Power Sources*, 70:59–69, 1998.

[138] Eng Patrice Tsakhara. Presentation on the Tanzanian solar PV-Hybrid workshop held in Berlin, Germany. Technical report, Tanzania Electric Supply Company LTD (Tanesco), 2015.

[139] Stefano Mandelli, Claudio Brivio, Matteo Leonardi, Emanuela Colombo, Marta Molinas, Eugene Park, and Marco Merlo. The role of electrical energy storage in sub-Saharan Africa. *Journal of Energy Storage*, 8:–, 2015.

[140] Stefan Pfenninger and Iain Staffell. Renewables.ninja. https://www.renewables.ninja/.

[141] Stefan Pfenninger and Iain Staffell. Long-term patterns of European PV output using 30 years of validated hourly reanalysis and satellite data. *Energy*, 114:1251–1265, 2016.

[142] Princeton Applied Research. Application Note AC-1 Subject : Basics of Electrochemical Impedance Spectroscopy Overview.

[143] Terna. Qualità del servizio di trasmissione. Livelli attesi della qualità della tensione per l'anno 2017. Technical report, 2017.